DISS. ETH NO. 21257

Comonomer Effects in Radiation Grafted Membranes for Polymer Electrolyte Fuel Cells

A dissertation submitted to

ETH ZURICH

for the degree of

Doctor of Sciences

presented by

Kaewta Jetsrisuparb

MSc in Chemical Engineering

TU Delft

born February 15th 1984

citizen of Thailand

accepted on the recommendation of

Prof. Dr. A. Wokaun, examiner

Prof. Dr. T. J. Schmidt, co-examiner

Dr. L. Gubler, co-examiner

2013

≪*If I have seen further it is by standing on the shoulders of giants.*≫

Bernardus Carnotensis

Philosopher, scholar, and administrator, 1124

Synopsis

High stability and low cost proton conducting membranes are a prerequisite for the commercialization of the polymer electrolyte fuel cell (PEFC). The state-of-the-art PEFC has achieved a durability of several thousands of hours under operating conditions using perfluorosulfonic acid (PFSA) membrane. Nevertheless, the PFSA membrane places a high burden on the cost of the PEFC. This drives the need for alternative materials to lower the cost of the proton conducting membrane while maintaining or improving the performance and durability of the PEFC.

Radiation grafting is an attractive way to modify a polymer film to serve as polymer electrolyte membrane (PEM). Such membranes are commonly prepared by grafting of styrene or its derivatives into a polymer matrix and subsequent sulfonation to introduce proton conductivity. The use of styrene based membranes has been motivated by the easy polymerization and sulfonation of styrene. However, such membranes are prone to radical attack in the fuel cell environment, which leads to premature failure of the fuel cell. Membrane properties can be tuned and durability enhanced by introducing a comonomer that is incorporated in the grafts by covalent attachment and is thus not washed out by water present in the fuel cell.

To understand the effects of comonomers on the membrane properties and stability, several co-grafted membranes containing styrene (as a primary monomer) and various comonomers were prepared. Methacrylonitrile (MAN), acrylonitrile (AN), methyl methacrylate (MMA) and methacrylic acid (MAA) were chosen to be grafted with styrene as they are commercially available and can be polymerized with styrene by radical polymerization. The graft composition is carefully controlled by changing the styrene to comonomer ratio in the grafting solution, which was done to investigate the effect of the graft composition and comonomer functionality on the membrane properties. Compatibility of the monomer and base film facilitates monomer transport to the grafting sites, allowing grafting to occur by a reaction front mechanism. The grafting kinetics and degree of sulfonation of the styrene units are affected by the nature and chemical structure of the comonomer. Complete sulfonation of styrene is obtained in styrene grafted membranes, styrene / MAN and styrene / AN co-grafted membranes.

The chemical composition of the grafted films and membranes was characterized by FTIR analysis. Some of the nitrile groups of MAN and AN underwent acid catalyzed hydrolysis during

membrane preparation and fuel cell operation, converting nitrile into amide and carboxylic acid. Under the same conditions, AN is more susceptible to hydrolysis than MAN, because the latter contains a methyl substituent at the α-position and its electron donating nature inhibits the nucleophilic attack by water molecules. The resistance to hydrolysis of the nitrile-containing membranes is reduced with increasing styrene to comonomer ratio in the grafts. For MMA, partial hydrolysis takes place during sulfonation by substituting the ester groups with carboxylic acids, whereas styrene / MAA membranes undergo an internal Friedel-Crafts acylation, leading to a cyclic ketone structure.

The influence of the comonomer functionality was further investigated by evaluating the key properties affecting proton conductivity, such as ion exchange capacity (IEC), water uptake and nanoscale structure. The proton conductivity is strongly influenced by the relative humidity and IEC. In water swollen state, proton conductivity of grafted membranes with similar IEC are comparable. At reduced relative humidity (10-80%), however, the co-grafted membranes exhibit lower proton conductivity compared to a styrene grafted membrane at the same IEC. It is proposed that the proton conductivity at low water content is dominated by the structure and morphology of the membranes, which is changed upon varying the graft composition. When the IEC and styrene molar fraction are kept constant, the proton conductivities of all co-grafted membranes are comparable, irrespective of the comonomer type. The presence of a comonomer reduces the proximity of acid groups and decreases the connectivity within the hydrophilic domain, thereby hampering the proton transport. The nanostructure of the membranes was studied by small angle X-ray scattering (SAXS). In comparison with Nafion, the distribution of hydrophilic domains in the grafted membranes is less homogeneous. This increases the percolation threshold of the aqueous phase in the membrane, thereby hindering proton transport. The proton conductivity of the grafted membranes at reduced humidity is limited by the presence of the crystalline phase in the base film, serving as a barrier of the aqueous pathway. Yet, this crystalline phase is required for mechanical stability. The insight gained from the structural investigation is critical and should enable optimization of membrane design for fuel cell applications.

Although the comonomer functionality does not lead to any considerable effect on proton conductivity, an appropriate comonomer should be selected for oxidative stabilization. The preliminary accelerated stress tests carried out under open circuit voltage (OCV) conditions showed that the styrene / MAN co-grafted membrane has a superior durability compared to styrene / AN, styrene / MAA and pure styrene grafted membranes. The nitrile functionality results in effective chemical stabilization by reducing hydrogen crossover. Loss of this functional group by hydrolysis leads to accelerated membrane degradation.

Zusammenfassung

Kostengünstige protonenleitende Membranen von hoher Stabilität sind eine der Anforderungen für die Kommerzialisierung der Polymerelektrolyt Brennstoffzelle (PEFC, polymer electrolyte fuel cell). Derzeit verwendete PEFC Systeme haben eine Lebensdauer von mehreren tausend Stunden unter Betriebsbedingungen mit der Verwendung von perfluorierten Sulfonsäure (PFSA, perfluorosulfonic acid) Membranen. Die hohen Kosten dieses Typs Membran erschweren jedoch die Erlangung der Marktreife von PEFC Systemen. Dies nährt die Suche nach alternativen, kostengünstigen Materialien mit gleichzeitig gleicher oder verbesserter Leistungsfähigkeit und Langzeitstabilität.

Die Methode des Strahlenpfropfens bietet die Möglichkeit, vorgefertigte Polymerfilme derart zu modifizieren, dass protonenleitende Membranen für die PEFCs hergestellt werden können. Styrol ist ein gebräuchliches Monomer, um Fluorpolymerfilme durch Propfkopolymerisation zu funktionalisieren, da es sich einfach polymerisieren und sulfonieren lässt. Jedoch zeigen Styrol gepfropfte Membranen eine geringe chemische Stabilität in Brennstoffzellenversuchen. Durch eine geeignete Wahl eines Comonomers, das zusammen mit Styrol in den Basisfilm gepfropft wird, können die Stabilität und Eigenschaften von Membranen verbessert werden. Da die gepfropften Monomere kovalent an das Basispolymer gebunden ist, findet kein Auswaschen der Pfropfkomponente statt.

Methacrylnitril (MAN), Acrylnitril (AN), Methylmethacrylat (MMA) and Methacrylsäure (MAA) sind günstig und kommerziell erhältlich und wurden als Comonomere des Styrols untersucht. Das Verhältnis von Styrol zu Comonomer in der gepfrropften Polymerkette kann über die Zusammensetzung der Propflösung gesteuert werden, wobei der Einfluss des Comonomer Typs und dessen funktionellen Gruppen auf die Membraneigenschaften untersucht wurde. Typischerweise erfolgt die Pfropfreaktion nach dem Frontmechanismuns, wobei die Polymerisation an der Filmoberfläche startet und langsam ins Innere des Basisfilmes vordringt. Die Propfkinetik und der Sulfonierungsgrad werden durch die Art und chemischen Eigenschaften des Comonomers beeinflusst. Eine vollständige Sulfonierung der aromatischen Einheiten des gepfropften Styrols wurde in Styrol, Styrol / MAN und Styrol / AN gepfropften Membranen erhalten.

Die chemische Zusammensetzung der gepfropften Filme und Membranen wurde mittels FTIR Spektroskopie analysiert. Die Hydrolyse der Nitrilgruppen des MAN und AN wird durch die säurehaltige Umgebung während der Membransynthese und im Brennstoffzellbetrieb begünstigt. Durch Hydrolyse wird das Nitril ins entsprechende Amid und die Carbonsäure überführt. Unter identischen Bedingungen zeigt AN eine grössere Hydrolyseanfälligkeit als MAN. Im MAN stabilisiert die Methylgruppe das Monomer aufgrund seiner elektronenspendenden Eigenschaft gegen Hydrolyse. Die Hydrolysebeständigkeit der nitrilhaltigen Gruppen sinkt mit zunehmendem Comonomergehalt in der Propfkomponente. Bei MMA findet während der Sulfonierung eine partielle Hydrolyse der Estergruppe zur Carbonsäure statt, während in den Membranen mit MAA eine interne Friedel-Crafts-Acylierung mit Styrol beobachtet wurde, wobei eine zyklische Keton-Struktur gebildet wird.

Der Einfluss der Comonomerfunktionalität auf die Ionenaustauschkapazität (IEC, ion exchange capacity), die Quellung und die Nanostruktur der Membranen wurde eingehend untersucht. Die Protonleitfähigkeit ist von der relativen Feuchte und der IEC beinflusst. Hingegen ist die Protonleitfähigkeit von gequollenen Membranen mit verschiedenen Comonomeren bei konstanter IEC vergleichbar. Bei reduzierter relativer Feuchte (10-80%) zeigen alle co-gepfropften Membranen jedoch eine geringere Protonenleitfähigkeit als vergleichbare, nur mit Styrol gepfropften Membranen mit identischer IEC. Die Nanostruktur der Membranen wurde durch Kleinwinkelstreuung mit Röntgenstrahlen (SAXS, small-angle X-ray scattering) untersucht. Im Vergleich zu Nafion ist bei den gepfropften Membranen die Verteilung der hydrophilen Domänen weniger homogen. Dies führt zu einer höheren Perkolationsgrenze der wässrigen Phase in der Membran, bei tiefer relativer Feuchte und dem damit verbundenen geringen Wassergehalt ist dadurch der Protonentransport behindert. Der kristalline Anteil im Basispolymer wirkt offenbar als Barriere für die Transportwege des Protons in der wässrigen Phase und limitiert daher die Leitfähigkeit der gepfropften Membranen bei geringerer relativer Feuchte. Andererseits ist der kristalline Anteil massgeblich für die mechanische Stabilität der Membran verantwortlich.

Obwohl die Art des Comonomers keine wesentlichen Auswirkungen auf die Protonenleitfähigkeit aufweist, ist die Wahl des Comonomers hinsichtlich der Stabilisierung des Pfropfcopolymers gegen oxidative Schädigung von hoher Wichtigkeit. Die oxidative Stabilität von Membranen wurde in der Zelle unter Bedingungen beschleunigter Alterung bei Leerlaufspannung untersucht. Im Vergleich zu Styrol, co-gepfropften Styrol / AN und Styrol / MAA Membranen zeigen co-gepfropfte Styrol / MAN Membranen die höchste Stabilität. Die Nitril-Funktionalität führt zu einer chemischen Stabilisierung durch eine Verringerung des Durchtritts von Reaktanden (H_2, O_2) durch die Membran. Ein Verlust dieser funktionellen Gruppe durch Hydrolyse führt zu beschleunigter Membranalterung.

Acknowledgements

It gives me a great pleasure to acknowledge those who contributed their dedicated efforts to this work. First of all, I am deeply grafteful to my supervisor, Dr. Lorenz Gubler, who guided me, and whose kindness and infinite patience helped me throughout my PhD. I also want to thank Dr. Hicham Ben youcef, my first year mentor and friend, who taught me 'to swim' so that I 'can swim' on my own.

I wish to express my sincere gratitude to Prof. Dr. Alexander Wokaun, head of the General Energy Department for giving me the opportunity to carry out this PhD and showing his immense interest in my work. Further appreciations go to Dr. Günther Scherer and Prof. Dr. Thomas J. Schmidt, for their time and expertise to guide me from a broader perspective.

I also give credit of many fuel cell experiments to Zhuoxiang Zhang. I am extremely grateful to him for his care to my membranes, his expertise and generosity. I owe fruitful discussions, help, and continuous support to Yves Buchmüller and Tom Engl. Special thanks go to the current and former members of the membrane team, Sandro Lüscher, Dr. Frank Wallasch, Mini mol Menamparambath, Lukas Bonorand, Albert Albert and Pia Reichel for helping me in innumerable ways. I particularly want to thank our kindhearted technician Jürg Thut for his practical help. I kindly thank Christian A. Marmy for taking care of the safety issues. I thank my students, Adrian Weibel, Friederike Lindner, Joanna Conder and Benjamin Miserere-Janssens for their commitment, contribution to my thesis and helping me to learn.

I also thank Dr. Sandor Balog from the Adolphe Merkle Insitute, University of Fribourg and Dr. Urs Gasser from the Laboratory for Neutron Scattering (LNS), PSI, for the successful collaboration and discussions on the nanoscale structure of styrene / MAN membranes. Prof. Dr. Corine Bas and Dr. Lara Perrin from the University of Savoie, France, are thanked for the study on styrene / methacrylic acid membranes by the magic angle NMR spectroscopy.

I wish to express my gratitude to the electrochemistry members for their help, advices and discussions. I thank Dr. Pierre Boillat, Johannes Biesdorf, Felix Bernauer-Neuschütz, Dr. Bernhard Schwanitz, Daniel Weingarth, Dr. Nicolas Linse, Patrick Lanz and Annett Rabis for all their friendship and humor. I particularly thank Dr. Pierre Oberholzer for his continuous help,

Contents

1

Introduction

1.1 Motivation

Since the beginning of mankind, we have been aware of the importance of energy. We burned wood for cooking and heating and later we learned to harvest energy and convert it into desired forms. Due to worldwide economic growth, there is a rising demand for energy and the global economy depends on the continuous availability and affordability of energy sources. The most abundant energy sources nowadays are fossil fuels, namely coal, natural gas and crude oil. Although these fossil fuels are rather cheap and are of high energy density, they are limited in supply and will be depleted. Moreover, combustion of fossil fuels emits green house gases (CO_2), which significantly contribute to the global climate change [1]. The Earth's near surface temperature has increased by 0.8°C over the past century [2]. This change seems to be small, yet it profoundly affects every life on Earth. The solution to mitigate climate change and satisfy growing energy demands is to deploy renewable energy technologies on a large scale.

Alternative energy sources are essential to replace fossil fuels [3]. Water for instance can be a renewable source of hydrogen through electrolysis, where electricity is generated from renewable resources (i.e., wind power, geothermal power, photovoltaic power or biomass) without CO_2 emissions. In addition, the move from fossil fuel dependency to hydrogen could improve access to energy around the world because a wide range of feedstocks can be used to produce hydrogen. Chemical energy stored in hydrogen can be converted to electrical energy by fuel cells to generate pollution-free power. If fuel cell technology is implemented, the widespread use of this clean energy technology can contribute to alleviate global warming.

The operation of a fuel cell is environmentally friendly, since its only by product is water (vapor). In addition to its low (if not zero) emission, the efficiency of fuel cells is generally higher than that of combustion engines [4]. The advantages of fuel cells also include its simplicity with no or few moving parts, which can lead to low maintenance and high reliability and durability [5].

1. INTRODUCTION

A number of different types of fuel cells have been developed for particular applications and they are classified by the electrolyte employed. The electrolyte determines the operating temperature, catalyst and fuel that can be used.

The *alkaline fuel cell (AFC)* was developed for space application to provide power and water for astronauts. It uses an aqueous solution of potassium hydroxide as electrolyte and operates at 60-250°C. The advantages of the AFC include high efficiency, low oxygen reduction reaction (ORR) losses and robust operation. However, commercial application has not been achieved, primarily due to the intolerance to CO_2 contamination. Purification of reactant gases before being supplied to the AFCs has proven to be too costly for practical use.

The *polymer electrolyte fuel cell (PEFC)* is also a low temperature fuel cell, utilizing a solid polymer as electrolyte. The conventional PEFC operates at the temperature around 30-100°C. Primary advantages of this type of fuel cell are high efficiency and rapid start-up. It is particularly suitable for automotive and portable application. Technical challenges include water and heat management, durability and freeze start. In addition to the conventional PEFC, high temperature fuel cell (HT-PEFC) has been developed. Such fuel cell is characterized by its high operating temperature of 160-180°C, in which mobile acid such as phosphoric acid assists the proton conduction in the polymer electrolyte.

The *phosphoric acid fuel cell (PAFC)* operates at the temperature range between 160 and 220°C with phosphoric acid as electrolyte. The acid is contained in a matrix, e.g., a porous ceramic. Since the electrolyte is in a liquid phase, the PAFC suffers from acid loss during operation. Due to its higher operation temperature, this type of fuel cell can tolerate 1-2% of CO contamination, yet it requires a longer start-up time compared to the low temperature fuel cells. In addition, the efficiency of the PAFC is lower than that of the PEFC and AFC. A promising application for this type of fuel cell is stationary power generation.

The *molten carbonate fuel cell (MCFC)* utilizes an electrolyte consisting of molten alkali metal carbonates in a porous matrix. The operating temperature is 600-800°C. At such high temperature, inexpensive catalysts and a broad choice of fuels can be used. The waste heat can be used to generate additional electricity. But the high temperature operation also leads to a very long start-up time and requires extensive electrolyte maintenance. This fuel cell is suitable for stationary application.

The *solid oxide fuel cell (SOFC)* operates at high temperature (600-1000°C). The electrolyte is a solid phase ceramic. The advantages and promising application of the SOFC are similar to those of the MCFC. The drawback of the SOFC is its lack of redox cycle ability.

Although fuel cells offer potential applications from stationary to mobile, it should not be seen as the solution for every power generating application needed in the world [4]. Different types of fuel cells possess individual differences, advantages and limitations. Besides the presented fuel

cell types, other types of fuel cell such as the direct methanol fuel cell (DMFC) exist, which operates using methanol as fuel, and biologically based fuel cells. Further details can be found in [4] and references therein.

In spite of the progress being made in fuel cell research and development, the transition from conventional combustion engines to fuel cells will not occur unless we can overcome the technical barriers. The common factors that limit the use of fuel cells today are as follows [4]:

- Cost. At present, fuel cells are economically not very attractive due to the high cost of the materials and manufacturing involved. PEFCs were applied in small stationary power units. The development of more cost-effective materials and processing methods is therefore of prime importance to compete with the existing technology such as combined heat and power (CHP) engines and combustion engines [4].

- Reliability and durability. In real life the fuel cell performance gradually deteriorates and the power output steadily drops with time [6]. The major reason for this performance drop is aging of fuel cell components, e.g., electrolyte and catalyst [7].

- Hydrogen production, storage and delivery. This is a difficult challenge because the energy density of hydrogen is low compared to gasoline. The fuel cell tank size should ideally be the same as in cars with internal combustion engine. For hydrogen based mobility, this also includes the overall hydrogen infrastructure.

Clearly, to overcome these challenges, major advances are to be made to promote the use of fuel cells. Despite continuing progress in fuel cell technologies, the current understanding is not sufficient to describe many phenomena occurring in fuel cell [8]. It is therefore of utmost importance to improve understanding and create innovations in fuel cell technologies.

1.2   Working principle

The fuel cell is a device designed to convert chemical energy to electrical energy. A schematic representation of the polymer electrolyte fuel cell (PEFC) is illustrated in Figure 1.1.

Hydrogen and oxygen enter the flow channels, separated by the membrane electrode assembly (MEA) consisting of proton conducting membrane, catalyst layers and gas diffusion layers (GDL). Delivery of reactant gases from the flow field plate to the catalyst layer is accomplished by the GDL, which is usually made of carbon cloth or paper with a homogenous dispersed catalyst on the surface. Gases are transported through the GDL by diffusion and convection and distributed over the catalyst surface.

The electrochemical reactions occur on the catalyst surface, known as the triple-phase boundary, where the reactant gas, catalyst and electrolyte meet. Therefore, the catalyst layer must be
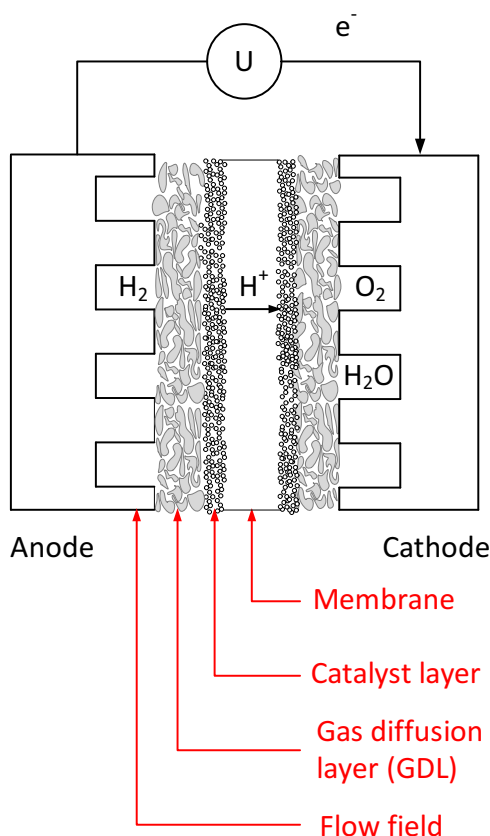
Figure 1.1: Working principle and components of a PEFC.

able to conduct electrons and protons, and enable transport of reactants and products. Since the PEFC is operated at low to moderate temperature (30-100°C), the use of catalyst such as Pt or Pt-alloy nanoparticles is necessary to accelerate and increase the efficiency of the electrochemical reactions on the electrodes. The membrane is a polymer material which is in direct contact with the catalyst layer and serves as a) Electrolyte to provide a pathway for the proton to flow, b) Electronic insulator to prevent electron transport and c) H_2 / O_2 separator.

In case undesirable mixing of reactants occurs, direct chemical reaction of the reactants will take place, generating heat and decreasing or stopping the production of electrical energy [6]. To allow operation of the fuel cell, continuous supply of reactants and removal of product water is required to provide reactants access to the electrodes. This emphasizes the main difference between a fuel cell and a battery, since a fuel cell does not undergo depletion and can generate electricity as long as the fuel and oxidant are supplied. In practice, several single fuel cells are connected in series to form a fuel cell stack, e.g., for automotive applications, over 200 single fuel cells are coupled for high power output [4].

1.3   Fundamentals of the PEFC

1.3.1   Thermodynamics of fuel cell operation

The electrochemical reactions between hydrogen and oxygen occur independently and simultaneously at the electrodes, and directly generate current, heat and water. The overall reaction is expressed as follows

$$H_2 + \frac{1}{2}O_2 \rightarrow H_2O \tag{1.1}$$

At the anode, the hydrogen oxidation reaction (HOR) takes place, releasing protons and electrons.

$$H_2 \rightarrow 2H^+ + 2e^- \tag{1.2}$$

At the cathode, the oxygen reduction reaction (ORR) takes place, where oxygen is combined with electrons from the electrode and protons that migrate through the electrolyte to produce water.

$$\frac{1}{2}O_2 + 2H^+ + 2e^- \rightarrow H_2O \tag{1.3}$$

Although the HOR and ORR occur independently at different electrodes, they are coupled by the exchange of electrons and protons. The amount of the electron flow through the circuit is equivalent to the flow of protons. When no electrons are exchanged between the two electrodes, no current is generated and the forward and backward reactions of the HOR and ORR are in equilibrium.

The measure of the potential to generate electrical work is the voltage. If all the chemical energy for a reaction is converted into electrochemical work (i.e., without heat transfer or change in entropy), the theoretical voltage (also known as the thermal voltage) can be determined based on the standard enthalpy of reaction (ΔH^o).

Under standard conditions (298 K and 1 bar), the theoretical voltage (based on liquid product water) corresponds to

$$U_{theo}^o = -\frac{\Delta H^o}{zF} = 1.48V \tag{1.4}$$

where ΔH^o=-286 kJ mol^{-1}, z is the number of electrons transferred in the reaction and F is the Faraday constant. The thermal voltage is however not a realistic value since all reaction processes are associated with entropy change. Therefore, the maximum output voltage should be corrected with the entropy change. If the fuel cell has no losses, the maximum output voltage, so called reversible voltage (U_{rev}^o) can be derived from the Gibbs free energy of the reaction (ΔG^o=-237 kJ mol^{-1}).

$$U_{rev}^o = -\frac{\Delta G^o}{zF} = 1.23V \tag{1.5}$$

The thermodynamic efficiency of the fuel cell is given by

$$\eta_{th} = -\frac{\Delta G^o}{\Delta H^o} = 0.83 \tag{1.6}$$

In reality, the voltage of an operating fuel cell is determined by the potential difference between the two electrodes.

$$U = E_C - E_A \tag{1.7}$$

in which E_C and E_A are the electrode potentials at the cathode and anode, respectively. The working conditions of a fuel cell however differ from the standard conditions, which results in the change in the Gibbs free energy and hence the reversible voltage. Since dG=Vdp-SdT, it follows that

$$\left[\frac{\partial \Delta G}{\partial T}\right]_p = -\Delta S \tag{1.8}$$

and the change of the reversible cell voltage with temperature is determined by the entropy change (ΔS):

$$\left[\frac{\partial U_{rev}}{\partial T}\right]_p = \frac{\Delta S}{zF} \tag{1.9}$$

If the temperature changes, U_{rev} will change according to the sign of ΔS. Considering the hydrogen fuel cell, ΔS is negative. An increase in temperature will therefore lower U_{rev}.

The Nernst equation is used to predict U_{rev} as function of temperature and activity of the reactants and products:

$$U_{rev} = E_C^0 - E_A^0 + \frac{RT}{zF}\ln\left(\frac{a_{\text{ox}}}{a_{\text{red}}}\right) \tag{1.10}$$

where E_C^0 and E_A^0 are the standard potential of the cathode and anode, T is the temperature in Kelvin, R is the ideal gas constants, and a_{ox} and a_{red} are the activities of the oxidized and reduced species, respectively.

It is important to note that the reversible voltage is not the operational cell voltage but it represents the theoretical value when no current is generated. When current flows, the potential of the electrodes will be shifted depending on the current density and the nature of the reaction. The decrease in the operating cell voltage compared to the open circuit voltage is generally termed as overpotential or polarization. The reasons of this loss will be discussed in detail in the following section (subsection 1.3.2).

1.3.2 Voltage loss mechanisms

Upon drawing current, the electrochemical reactions associated with the electrodes of the fuel cell are not in equilibrium. The actual cell voltage departs from from the open circuit voltage (OCV) and depends strongly on the current density. The operating cell voltage is given as

$$U_{cell} = U_{rev} - \Sigma \mid \eta_i \mid \tag{1.11}$$

in which $\Sigma \mid \eta_i \mid$ is the sum of all overpotentials occurring in the cell. The combination of different voltage loss mechanisms results in the total overpotential at a given current density. As can be observed in Figure 1.2, the voltage decreases with increasing current density. The characteristic shape of the polarization plot can be divided into three different regimes to distinguish dominant effects caused by different voltage loss mechanisms.
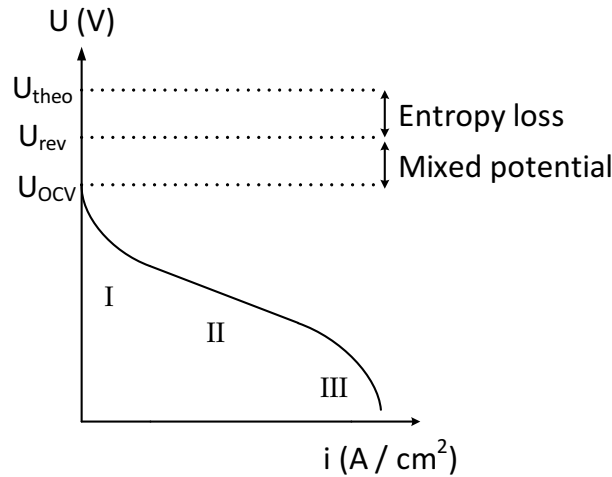
Figure 1.2: Polarization curve showing different contributions of the overpotentials in the fuel cell. The voltage losses in regions I, II and III are dominated by the activation losses, ohmic losses and mass transport losses, respectively.

1.3.2.1 Mixed potential and internal short circuit at open circuit voltage (OCV)

The reduction of measured OCV from the reversible voltage indicates the voltage loss associated with two phenomena, namely the mixed potential and the internal electrical short. The mixed potential is caused by parasitic reactions, when oxidation and reduction reactions are taking place simultaneously at the same electrode with no net current. This can be seen as an internal closed circuit at the electrode surface. The apparent electrode potential can be determined from the potential where the current of the anodic reaction is equal to that of the cathodic ORR. Current due to crossover of reactants, particularly hydrogen, significantly contributes to loss of OCV. Possible side reactions were previously reviewed in literature [9].

Internal electrical short across the membrane is caused by electron leakage through the membrane. This occurs when the MEA is damaged. In comparison with the mixed potential, an electrical short is a minor contributor to the loss of OCV in a PEFC.

1.3.2.2 Activation losses in the low current density regime (Region I)

The sharp initial voltage drop is dominated by the activation of reactions occurring at each electrode in the low current density region. To enable charge transfer, charges are

building up along the surface of the catalyst forming the double layer structure at the electrolyte / electrode interface. This leads to a potential drop across the double layer. With increasing current density, the loss of voltage increases logarithmically. The activation overpotential at each electrode is expressed in the Tafel equation (Equation 1.12),

$$\eta_{CT} = b \cdot log \frac{j}{j_0} \qquad (1.12)$$

where η_{CT} is the charge transfer overpotential, j and j_0 are the current density and the exchange current density, respectively, and b is the Tafel slope, which provides information about the reaction kinetics. It can be obtained from the linear fit of a plot of the log of j versus η_{CT}. In the PEFC, the HOR kinetics are facile compared to that of the ORR, hence the η_{CT} of the HOR is considered to be negligible. Thus, the activation loss occurs mainly at the cathode, where the ORR takes place.

1.3.2.3 Ohmic losses in the moderate current density regime (Region II)

The voltage loss in the moderate current density regime is dominated by ohmic losses due to the electrical and ionic resistance of the cell components, e.g., electrodes and electrolyte. The extent of the ohmic losses depends on the current drawn from the cell. A nearly linear behavior of the polarization curve at moderate current density is reflected by Ohm's law. In a well assembled cell, significant ohmic loss is caused by the ionic resistance of the membrane. A membrane that can easily conduct protons will result in lower ohmic losses. Therefore, to minimize the overpotential and increase the fuel cell efficiency, membranes with high proton conductivity are desired. In addition, to facilitate proton transport, the membrane should always be hydrated. This suggests that water plays an important role in the performance of a fuel cell. The ohmic overpotential can be expressed as

$$\eta_\Omega = j \cdot R \qquad (1.13)$$

where R is the area specific resistance in $\Omega \cdot cm^2$.

1.3.2.4 Mass transport losses in the high current density regime (Region III)

Since the reactant consumption rate is determined by the current, more reactants are required at high current density. The major contribution of voltage loss in the high current density region is due to depletion of reactants at the catalyst surface, which leads to a reduction of reactant activity. The factors that limit reactant availability are gas diffusion limitation and build up of inert gas when air is used. In addition, water accumulation in the porous diffusion layer (electrode flooding) will restrict the gas access to the catalyst surface [4]. To avoid reactant depletion at high current density, an excess amount of gas should be fed to the fuel cell. Moreover,

water should be effectively transported away from the catalyst to prevent pore blockage. The limiting current (j_{lim}) at high current density is defined as

$$j_{lim} = \frac{zFDc_r}{\delta}$$ (1.14)

in which z is the charge of the charge carrier, D is the diffusion coefficient, c_r is the reactant concentration in the bulk and δ is the diffusion distance. From the limiting current, the mass transport overpotential (η_{tx})can be calculated using the Nernst equation.

$$\eta_{tx} = -\frac{RT}{zF}ln\left(1 - \frac{j}{j_{lim}}\right)$$ (1.15)

1.4   Proton exchange membrane (PEM)

1.4.1   Historical perspective

Proton conducting membranes are polymer materials, which contain negatively charged groups to accommodate protons [10]. The use of a proton conducting membrane was first proposed in the 1950s by Grubb at the General Electric (GE) company [11]. This membrane contained formaldehyde sulfonic acid, which was brittle and readily hydrolyzed in the fuel cell. Lifetime of only 100 hours at 50-60°C was reported [12].

The second generation of membranes prepared by the Rohm and Haas company consisted of polystyrene sulfonic acid (PSSA) mixed with polyethylene, designated as Amberplex membranes. However, the physical properties were rather poor. Fuel cells based on this type of membrane suffered greatly from premature failure and only survived for 200 hours at 60°C under fuel cell operation [4, 13].

Improvement in physical strength was achieved with the "D"membrane manufactured by the American Machine Foundry (AMF) through copolymerization of styrene and divinylbenzene (DVB, serving as a crosslinker) into a copolymer matrix of CTFE and VDF (Aclar 22A) followed by sulfonation. The useful operating life was extended to 1000 hours at 60°C [13]. The series "D"membranes were the first membranes employed in the Gemini space program in 1965. Yet, the membranes suffered from fast dry out and low power density (0.038 W cm^{-2} at 0.83 V per cell). In addition, the lifetime was still considered to be limited. These are critical factors that moved the application towards to alkaline fuel cell (AFC) instead of PEFC in the later Apollo program [14].

The premature failure of the PSSA membrane is due to an alpha C-H bond, which is a weak link towards oxidative degradation in the fuel cell environment (subsubsection 1.4.3.2). This leads to the loss of protogenic sites by chain scission, resulting in inferior mechanical strength and ultimately fuel cell failure. Further improvement was achieved with a fluorinated analog of

1. INTRODUCTION

PSSA, poly(trifluorostyrene sulfonic acid) (PTFSSA) to eliminate the weak C-H bond, blended or grafted into an inert fluorocarbon matrix, known as "S" membrane. The membranes outlasted 10000 hours at 80°C [13]. Unfortunately, limiting factors in the serie "S" membranes included poor mechanical properties. To resolve these problems, Ballard Advanced Materials developed BAM3G membranes by incorporating TFS derivatives to the PTFSSA based membrane [15]. The BAM3G membrane has been shown to be stable in H_2 / air fuel cell for over 14000 hours at 80°C [13]. The chemical structures of the membranes are shown in Figure 1.3.

Poly(styrene sulfonic acid)

Poly(trifluorostyrene sulfonic acid)

R=OR, CN, OH, No$_2$, CF=CF$_2$
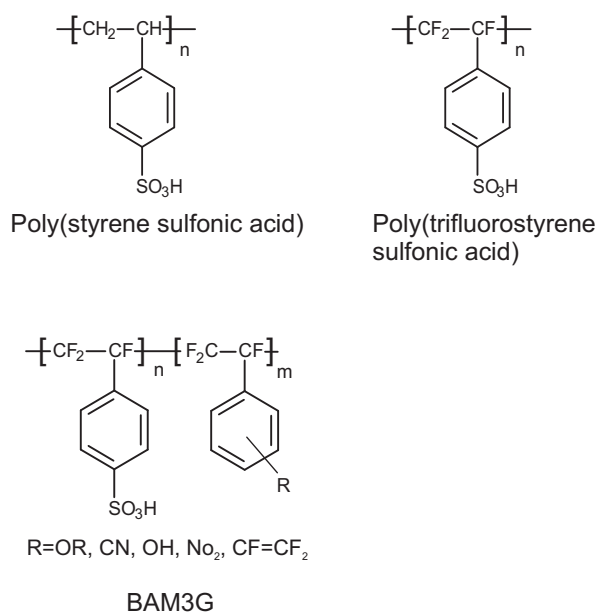
BAM3G

Figure 1.3: Chemical structures of polystyrene sulfonic acid (PSSA), poly(trifluorostyrene sulfonic acid) (PTFSSA) and BAM3G (Ballard Power Systems) membranes.

A major breakthrough in PEMs came with the introduction of the Nafion membrane, developed by E. I. Dupont de Nemours and Company [4]. Initial attention was paid to Nafion because of its high chemical stability, mechanical strength, high ionic conductivity in water swollen state and electrical insulation [16], which are prerequisites for a membrane in the PEFC. Nafion is a perfluorinated ionomer consisting of side chains with a sulfonic acid group covalently bound to the backbone of a polytetrafluoroethylene (PTFE) structure (Figure 1.4). The hydrophilic sulfonic acid groups enable proton conductivity while the hydrophobic PTFE structure provides chemical and mechanical strength, which contributes to inherently more stable membranes compare to the hydrocarbon-based membranes. The PFSA membranes have achieved a durability of 60000 hours in operation at 43-82°C [17] and reached a conductivity of about 0.1 S cm^{-1} at 80°C [6]. The stability of Nafion is believed to be due to the inert fluorine chemistry. This marks a significant milestone in the membrane development and is nowadays considered as the most promising membrane for fuel cell applications.

x= 5-15
y= 1000
m= 0-1
n = 2-5
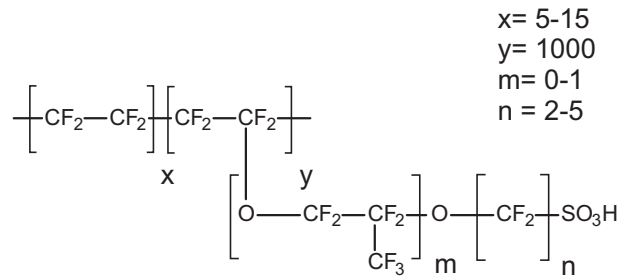
Figure 1.4: Molecular structure of PFSA.

The major drawback of Nafion is its high cost and poor proton conductivity at low relative humidity and at high temperature [10]. This raises the need for alternative membrane materials, which can sustain the durability of Nafion and high performance while reducing the cost. Different types of membranes based on polyaromatic or polyheterocyclic repeating units have been developed, such as sulfonated poly(ether ether ketone) (SPEEK) [18], polybenzimidazole (PBI) [19] and polysulfone (PSU) [20]. The hydrocarbon polymers are relatively inexpensive [10], however, their common drawback lies in the inferior durability compared to Nafion. Extensive research of different types of membranes has been carried out by many groups [10, 21, 22]. Among different approaches, membranes prepared by radiation induced grafting have been presented as a promising alternative to Nafion. The membranes prepared by this method will be discussed in the following section.

1.4.2   History of radiation grafted membranes for PEFC

Radiation chemistry has been used as a synthetic tool to prepare new materials or modify polymer materials. It opens up opportunities to numerous potential applications, such as to enhance the biocompatibility of materials used in medical applications, substrates for cell tissue growth, surfaces modification of glass, semi-permeable membranes and non-woven fabrics and modification of bulk properties of materials [23]. Moreover, radiation techniques have proven to be suitable for membrane processing, e.g., synthesis of ion exchange membranes for fuel cell, electrolyzer [24], chloro alkali industry, electrodialysis [25] and various separation applications [26, 27].

Despite the potential of radiation grafted materials in various applications, only few are commercially available including PE-*g*-acrylic acid (AA) as battery separator, ion exchange non-woven fabric for air and water purification, functional fabrics and cell culturing dishes [28].

Development of radiation grafted membranes owes largely to the discoveries of Chapiró and Chen. The former established the concept of radiation grafting and the latter is considered to be the first to prepare cation exchange membrane using this technique. Chen grafted styrene

11

and styrene / DVB into polyethylene film with subsequent sulfonation for battery separator and dialysis applications [29, 30].

In the late 1980s, cation exchange membranes were prepared by simultaneous [31] or pre-irradiation grafting [32–35] of TFS into various polymer films such as FEP, LDPE, ETFE, PFA and PTFE. Permion® membrane manufactured by RAI Co. made it through to commercialization [28] and was used as a battery separator [27]. This membrane consisted of PTFE backbone grafted with styrene sulfonic acid. Unfortunately, such membranes heavily degraded at 80°C (1 A cm^{-2}) in the electrolyzer, while a membrane consisting of ETFE backbone with PTFSSA grafts (Raymion® by Chlorine Engineers Co., CEC) showed a better performance and durability comparable to that of Nafion® 117 membrane, as shown in Figure 1.5 [35].
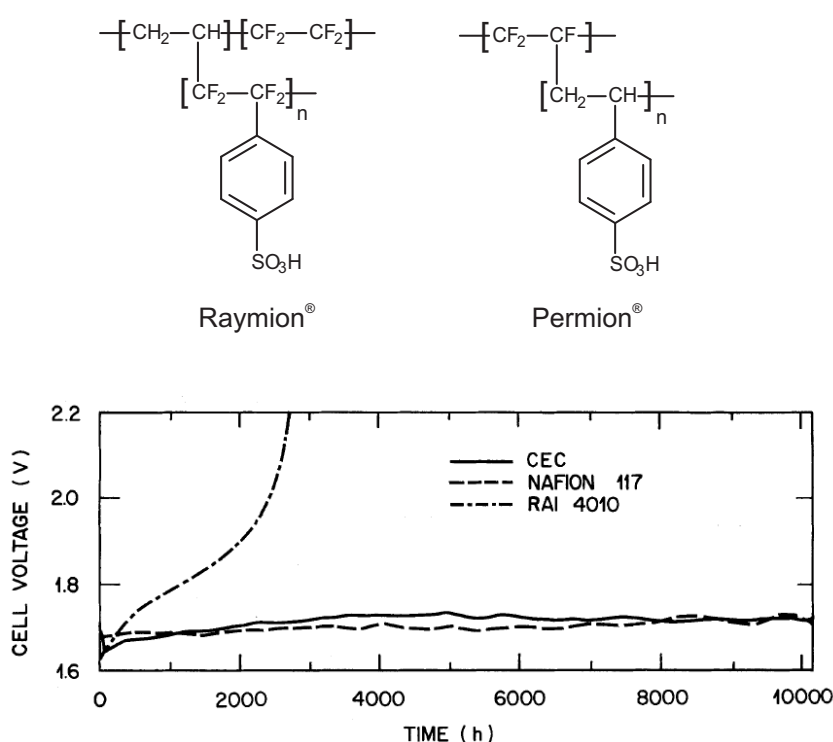

Figure 1.5: Chemical structures and durability of Raymion® type membrane (RAI 4010) and Permion® type membrane (CEC) at 80°C in an electrolyzer compared to that of Nafion® 117 [35].

In 1990, radiation grafting started to be developed for fuel cell application. The development of this type of PEM was initiated by Scherer at the Paul Scherrer Institut (PSI). The first generation of radiation grafted membranes consisted of a FEP polymer and styrene sulfonic acid grafts prepared by simultaneous γ-irradiation grafting. A power density of 125 mW cm^{-2} (H$_2$ / O$_2$, 1 bar, 60°C, 0.5 mA cm^{-2} and 0.8 mg cm^{-2} Pt loading electrode) was obtained with this membrane type and a long term stability of 500 hours was achieved [36, 37].

Improvements in membrane performance and lifetime have been achieved by changing key parameters during the grafting process, e.g., change of the irradiation source and base films [38],

incorporation of crosslinking comonomers [38–40], reducing membrane thickness, change of the sulfonation process and improved membrane / electrode interface [36, 41]. The useful operating life was extended to 2500 hours at 60-80°C by incorporation of a crosslinker, divinylbenzene (DVB) [42].

Major progress has been achieved in the last decade concerning improved performance and durability by going from styrene based membranes to α-methyl styrene (AMS) based membranes with incorporation of methacrylonitrile (MAN) [43]. This is known as a second generation of radiation grafted membranes prepared at PSI (Figure 1.6). Under fuel cell operation, the lifetime of an AMS / MAN co-grafted membrane reached 550 hours, which is about 10 times longer than that of the styrene grafted membrane. This improvement in durability is rather impressive, considering that this membrane is not crosslinked. To further improve the MEA lifetime, DVB is used as crosslinker. A power density of 340 mW cm^{-2} (H$_2$ / O$_2$, 1 bar, 80°C, ELAT® BASF electrode) was achieved with FEP-g-AMS / MAN / DVB membrane.
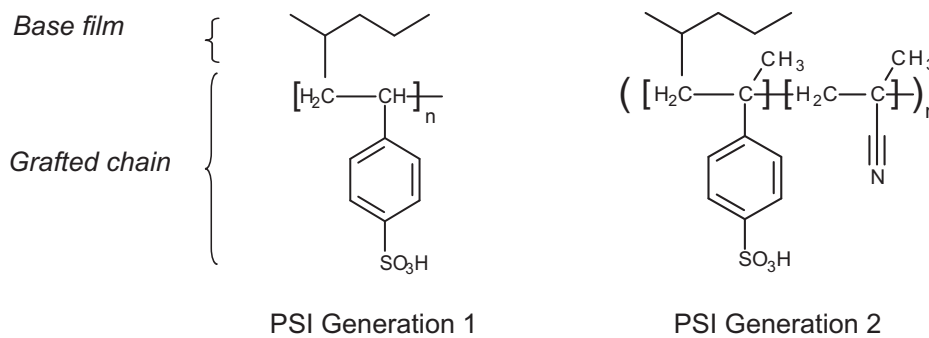
Figure 1.6: Radiation grafted membranes with PSSA grafts (PSI Generation 1) and AMS / MAN grafts (PSI Generation 2) [38, 43].
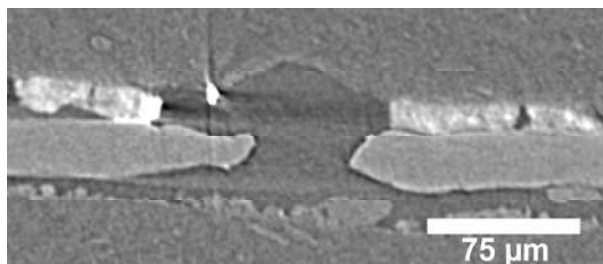
1.4.3   Membrane degradation

Membrane degradation can cause a catastrophic failure of the fuel cell. This phenomenon is influenced in part by the mechanical failure, chemical degradation and thermal degradation, which eventually leads to voltage loss and premature failure of the MEA.

The mechanical failure is commonly found in the form of pinholes, blister formation, creep deformation and crack formation [13, 44]. Mechanical decay can occur during membrane processing or MEA fabrication, fuel cell operation or from material defects. The mechanical degradation is commonly developed at the area of increased stress, such as the reactant inlets, edges, and the borders between lands and channels [45], resulting in reactant crossover through the membrane. Since the recombination of reactant gases is highly exothermic, generation of hotspots can take place and thereby promoting further membrane degradation. An example of pinhole formation is shown in Figure 1.7.

Figure 1.7: Direct observation of pinhole in degraded MEA using synchrotron based X-ray tomographic microscopy [46].

The chemical degradation of membranes is caused by chemical attack of radicals (HO·, HO$_2$· and H·) and can be observed in the form of increased crossover, membrane thinning, development of electrical short-circuits and emission of membrane materials in the effluent water. Mechanical and chemical degradation cannot be completely separated and both degradation mechanisms are mutually influential. Chemical degradation of the membrane leads to reduced mechanical strength, whereas reactant crossover through mechanical defects also accelerates chemical degradation by increasing radical formation, yielding progressive membrane decay [7].

Thermal degradation is likely to occur at high temperature, where chain scission of the membrane takes place. This phenomenon generally involves changes in the molecular weight of the polymer and consequently leads to changes in the membrane properties, such as lowering membrane mechanical strength. Thermal degradation can be avoided by using a membrane material that is thermally stable at the fuel cell operating temperature.

As a basis to design chemically stable membranes for fuel cells, understanding the chemical degradation mechanisms and the origin of reactive intermediates and aggressive radicals are of prime importance. Possible reaction pathways for the formation of H$_2$O$_2$, HO·, HO$_2$· and H· will be discussed.

1.4.3.1   Formation of oxidative species

HO· in particular is the primary source of membrane degradation in an operating fuel cell. Besides HO·, HO$_2$· and H· are also capable of breaking polymer constituent bonds, leading to polymer chain scission [47]. As a consequence, the membrane loses its ionic content and the mechanical properties deteriorate.

H$_2$O$_2$ is not directly involved with membrane degradation due to its inertness but it is a precursors for radicals and was termed as a 'carrier of disaster' [48]. The major amount of H$_2$O$_2$ is formed by gas crossover. Therefore, crossover is a decisive factor in the formation of reactive intermediates. It is noteworthy that formation of radicals is not necessarily restricted to the reaction of H$_2$O$_2$ with its reaction partners. The location of the H$_2$O$_2$ formation is

controversial and under debate [49]. At the anode, hydrogen peroxide is formed as a result of oxygen permeation by the following steps [13].

$$H_2 \xrightarrow{Pt} 2H^{\cdot} \tag{1.16}$$

$$H^{\cdot} + O_2 \rightarrow HO_2^{\cdot} \tag{1.17}$$

$$HO_2^{\cdot} + H^{\cdot} \rightarrow H_2O_2 \tag{1.18}$$

At the cathode, a small amount of hydrogen peroxide can be formed via two electron oxygen reduction reaction (E_0=0.672 V) [48].

$$O_2 + 2H^+ + 2e^- \rightarrow H_2O_2 \tag{1.19}$$

In addition, hydrogen peroxide can be formed chemically as a result of hydrogen permeation.

$$H_2 + O_2 \xrightarrow{Pt} H_2O_2 \tag{1.20}$$

The diffusion length of hydrogen peroxide at fuel cell relevant temperature is in the millimeter range and therefore hydrogen peroxide can diffuse through the membrane [48]. The presence of hydrogen peroxide and metal ion contaminants, such as Fe^{2+} and Cu^{2+}, is detrimental to the membrane [50–52]. These metal ions originating from fuel contamination, corrosion of components or fabrication are embedded in the membrane and only trace amounts of these transition metals (ppm level) is enough to catalyze the decomposition of hydrogen peroxides to intermediate radical species as described by the Fenton reactions [53].

$$H_2O_2 + M^{2+} \rightarrow M^{3+} + HO^{\cdot} + OH^- \tag{1.21}$$

$$HO^{\cdot} + H_2O_2 \rightarrow H_2O + HO_2^{\cdot} \tag{1.22}$$

In addition to the Fenton reactions, radicals can be generated from homolysis of H_2O_2.

$$H_2O_2 \rightarrow 2HO^{\cdot} \tag{1.23}$$

Direct formation of radical species on the catalyst can also occur at the cathode, assuming that PtO is present [54].

$$PtO + H_2O_2 \rightarrow HO^{\cdot} + PtO_2 + H^+ + e^- \tag{1.24}$$
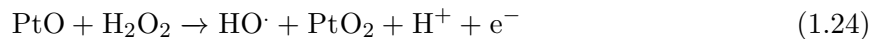
The hydrogen radical is found on the cathode by the reaction of H_2 crossover with $HO^{\cdot}$.

$$HO^{\cdot} + H_2 \rightarrow H_2O + H^{\cdot} \tag{1.25}$$

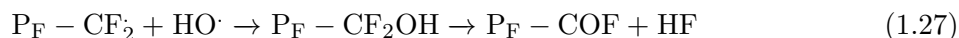An overview of reactions involving radical formation in the fuel cell can be found in literature [47, 48].

1. INTRODUCTION

1.4.3.2 Degradation mechanism of PFSA versus PSSA membranes

The mechanism of membrane degradation depends on the membrane type. The most studied system is the PFSA membranes, which degrades according to a combination of multiple mechanisms. Here, three degradation pathways of PFSA membrane will be discussed.

In the first pathway, degradation is initiated via weak carboxylic end groups and proceeds further via a series of steps. This mechanism is also known as the end group unzipping mechanism [44].

$$P_F - CF_2 - COOH + HO\cdot \rightarrow P_F - CF_2^{\cdot} + CO_2 + H_2O \tag{1.26}$$

$$P_F - CF_2^{\cdot} + HO\cdot \rightarrow P_F - CF_2OH \rightarrow P_F - COF + HF \tag{1.27}$$

$$P_F - COF + H_2O \rightarrow P_F - COOH + HF \tag{1.28}$$

Upon radical attack, hydrogen is abstracted from the carboxylic acid end group, yielding a perfluorocarbon radical, CO_2 and water. The perfluorocarbon radical reacts further with the hydroxyl radical, resulting in formation of HF. The amount of F^- release is determined by the fluoride emission rate (FER), which is generally used as a measure for membrane degradation [7, 50, 55, 56]. This mechanism leads to a carboxylate product, which will continue to be decomposed by the radicals. Improvements in membrane lifetime under accelerated test are achieved by removing the carboxylate end groups of the PFSA membranes by e.g., post-fluorination [57, 58].

The second degradation pathway is initiated by the presence of hydrogen radicals. The hydrogen radical is a very reactive species capable of F-abstraction from the PFSA backbone. The driving force of this reaction is the formation of the very strong H-F bond (136 kcal mol^{-1}). F-abstraction subsequently leads to radical formation on the main chain, which ultimately results in chain scission [59].

The third degradation pathway occurs in dry conditions. It is proposed that the proton is abstracted from SO_3H, resulting in $SO_3^{\cdot}$ [59]. The presence of $SO_3^{\cdot}$ weakens the C-S bond and eventually leads to chain fragmentation to form fluorocarbon radical [44]. By exchanging proton with metal ions, degradation by this pathway is suppressed [60]. Additionally, many research groups also proposed alternative side chain degradation mechanisms, in which the C-S bond is capable of being attacked by hydroxyl radicals. More detail can be found in literature [44] and the references therein.

Degradation of PSSA membranes proceeds via an entirely different pathway. The attack of HO· at the sulfonic acid group in PSSA membranes is highly unlikely [48]. In fact, the product
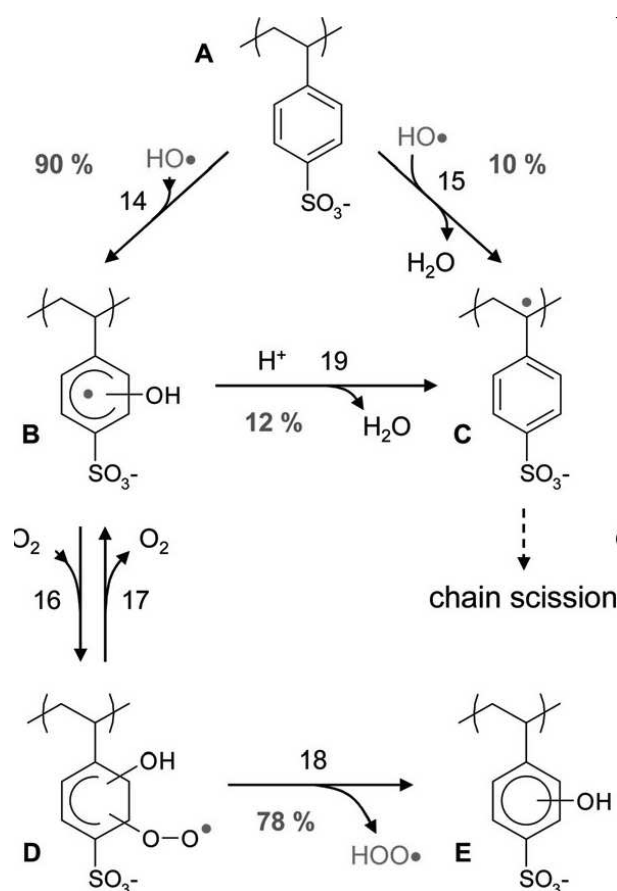
Figure 1.8: Proposed mechanism for hydroxyl radical attack on poly(styrene sulfonate) [48].

water analysis of PSSA based membranes reported by Büchi *et al.* indicates that the sulfonic acid always remained attached to the aromatic ring [48, 61].

Studies of PSSA have been conducted to identify the degradation mechanism of the PSSA membrane. In the early studies, Hübner *et al.* used *p*-toluene sulfonic acid as a model compound to investigate the chemical degradation caused by the attack of radicals generated from hydrogen peroxide [62]. Electron paramagnetic resonance (EPR) spectroscopy was used as a tool to follow the sequential degradation mechanism of the polymer. They proposed that in acidic conditions, addition of HO· to the aromatic ring occurs. This step is followed by acid catalyzed water elimination, which leads to formation of benzyl radicals. The attack of HO· on *p*-toluene sulfonic acid is proposed to be similar to pathway 14 followed by 19, as depicted in Figure 1.8. Once the radical is formed on the α-position, intramolecular hydrogen abstraction in the back-biting reaction or β-scission takes place [63].

More recently, a kinetic study of the reaction of HO· with poly(sodium styrene sulfonate) oligomer (PSSS) has been carried out by Dockheer *et al.* [64]. Their results agree well with the proposed mechanism of Hübner *et al.* [62]. They demonstrated that 90% of the OH· attacks

by addition to the aromatic ring of styrene, whereas only 10% leads to α-H abstraction. In the absence of α-H, the aromatic ring may serve as a radical scavenger [48, 64]. Although the nature of both types of membrane are completely different, degradation of PSSA membranes involves similar phenomena as observed in PFSA membranes, including the loss of sulfonated groups and chain scission through radical attack.

To improve the durability of PSSA membranes, α-H abstraction should be prevented since the benzyl radical can react further to form fragmented products. Substitution of a suitable group at the α-position of styrene, e.g., SO_3^- substituent, has been proposed to improve the stability of PSSA with an additional benefit to improve proton conductivity [62]. Furthermore, incorporating OH$\cdot$ scavengers such as catechol-like compounds may further improve membrane stability [64].

1.4.4   Membrane requirements

Radiation grafted membranes are a worthy candidate for PEMs in the PEFCs [65]. One of the key questions concerning the use of the radiation grafted membrane is whether the membrane is durable enough under fuel cell operation. The requirements the PEMs should meet are listed below [66, 67]

- Impermeable to H_2 and O_2

- Non electrical conducting

- High proton conductivity (approximately 100 mS cm^{-1})

- High chemical stability under the fuel cell environment

- High mechanical strength

- Good thermal stability

- Compatibility to other fuel cell components

- Inexpensive

1.5   Radiation grafted membranes

In recent years, there has been growing interest in radiation grafted membranes. The advantages of using radiation grafting over the conventional wet chemical processes are as follows:

- Simplicity and ease of preparation. Radiation grafting allows tailoring of polymer properties, in which elaborate chemistry can be avoided [68]. This technique includes a straightforward synthesis approach and therefore can be potentially cost effective compared to PFSA membranes.

- Wide range of reaction temperatures. Conventional polymerization needs to be carried out in a limited temperature range that suits the working of the initiators or catalysts, while in radiation grafting low to moderate temperature can be applied to initiate copolymerization reactions.

- No residual from initiators. While the conventional polymerization method involves the initiation by chemical means, radiation grafting is free from contamination caused by initiators since radiation plays the role of initiator [69].

- Designability. Radiation grafting allows a variety of materials to be grafted into base polymer [39, 61, 70]. In addition, the graft level can be easily controlled by the reaction conditions and parameter [71].

- No film formation. This is mostly advantageous in thin film application where shaping of the membrane into desired physical shape may be difficult [72].

- Suitable for industrial scale production and can be potentially cost effective [65, 73].

- No dissolution problems. Radiation grafted membranes offer high hydrolytic stability compared to hydrocarbon-based or PFSA membranes.

Disadvantages of grafting also exist [68]

- Secondary processes under radiation treatment such as crosslinking or degradation of the polymer base material due to chain scission may occur, leading to the change in polymer structure.

- Processing. The process requires optimization for high throughput and monomer utilization.

- Sensitivity to through-plane distribution of monomer. Grafting proceeds via the grafting front mechanism, therefore enough grafting time should be allowed to obtain homogeneous grafting throughout the film.

1. INTRODUCTION

1.5.1   Radiation grafting process and materials

Radiation induced polymerization proceeds through radical or ionic mechanisms (Figure 1.9). The formation of active sites in the base film occurs by high energy radiation, plasma treatment, ultraviolet (UV) light radiation or decomposition of a chemical initiator [72]. The active sites, in the form of radicals or ionic groups, enable initiation of polymerization and allow the base film to be grafted with monomers to form a branched copolymer. The base films is composed of crystalline and amorphous domains, in which the latter accommodate the grafted chains. Grafting into the crystalline domains of the base film is not likely since monomer cannot easily permeate through the crystalline phase. On the other hand, grafting onto the surface of the crystalline domains seems to be more probable. The amount of grafted polymer is quantified
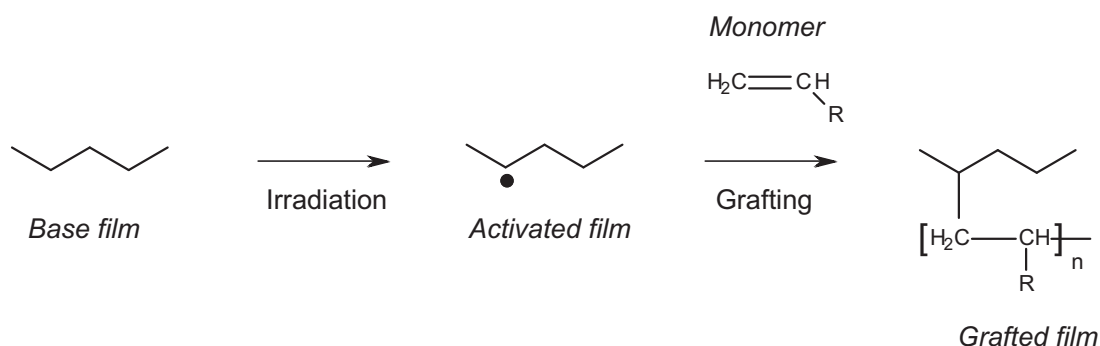
Figure 1.9:   Illustration of the pre-irradiation method to prepare grafted film.

by the graft level (GL), which is defined as the percentage of mass increase compared to that of the base film.

$$GL = \frac{m_g - m_0}{m_0} \times 100\% \tag{1.29}$$

where m_0 and m_g are the weight of the film before and after grafting, respectively.

The most recent research in radiation induced graft copolymerization has been devoted to two main methods, in particular simultaneous irradiation and pre-irradiation [72]. Both methods are similar since upon contact of the exposed radicals with monomers, graft polymers can be formed. However, the former applies γ-rays while the latter uses electron beam to generate radicals. Gupta and coworkers showed that the graft level is based solely on the dose applied and the reaction time, and the generated radicals are identical irrespective of the nature of radiation employed [74].

1.5.1.1   Simultaneous irradiation method

During simultaneous irradiation, the polymer substrate and monomer are exposed to γ-radiation at the same time (single step method), leading to the formation of active free radicals on both polymer substrate (P·) and monomer (M·). Polymerization occurs on the surface, in the polymer

substrate (both covalently and non-covalently bonded) as well as in the grafting solution. Non-covalently bound polymers can also be leached out by dissolution, which could lead to severe loss of grafts and ionic properties during fuel cell operation [12]. In principle, simultaneous irradiation should be the most efficient method to radiation induced graft copolymerization, however, it suffers from a high level of polymerization in the grafting solution. In addition, there is a high possibility of mutual recombination which deactivates primary radicals of the polymer backbone (P·).

$$P· + P· \rightarrow PP \tag{1.30}$$

To suppress extensive polymerization in the grafting solution and to improve the grafting efficiency, addition of inhibitors such as Fe^{2+} and Cu^{2+} can be applied [69]. This approach is however not favorable in membrane synthesis for fuel cell applications since contamination of the metal ions can lead to severe membrane degradation in the fuel cell by catalyzing the Fenton reactions (subsubsection 1.4.3.1). The use of monomers in a different phase than the polymer substrate may also render serious polymer formation in the solution and increase the graft level. Detailed studies are explained elsewhere [72, 75].

1.5.1.2 Pre-irradiation method

The pre-irradiation method differs from simultaneous irradiation because it is a two-step process [76]. First, the polymer substrate is irradiated to generate active sites, such as trapped radicals. In the second step, monomers are grafted into the substrate. Typically, the pre-irradiation process is carried out in air using high energy electron beam (EB) radiation. This pre-irradiation condition is most likely to be the chosen method for industrial scale because its effectiveness [72] and cost since the films experience a shorter exposure time to radiation compared to those prepared by simultaneous irradiation. In addition, pre-irradiation is considered superior to simultaneous irradiation method because less polymer is formed in the solution. Moreover, storage of the pre-irradiated film is possible, meaning that grafting can be performed away from the radiation source [69]. To evaluate irradiation methods for the purpose of membrane preparation, different factors such as material compatibility and exposure time to radiation must be considered.

1.5.2 Radiation grafting mechanisms

Radiation induced grafting comprises three steps: initiation, propagation and termination [77]. Initiation involves the formation of hydroperoxides and peroxides from the reaction of radicals with oxygen (Equation 1.31 and Equation 1.34). The initiator concentration is determined from the rate of adsorbed dose on the polymer substrate expressed in Grays (J kg^{-1}).

$$P \xrightarrow{EB} P· \tag{1.31}$$

$$P\cdot + O_2 \rightleftharpoons POO\cdot \tag{1.32}$$

$$POO\cdot + PH \rightarrow POOH \tag{1.33}$$

$$P\cdot + POO\cdot \rightarrow POOP \tag{1.34}$$

P represents the polymer backbone and POOH is the hydroperoxide. In radiation induced grafting, radicals are formed in the polymer backbone and capable of chain initiation so the products are free from contamination of initiators. Whereas in the chemical initiation method, the free radical first forms on the initiator before it transfers to the monomer [78]. At elevated temperature, hydroperoxide and peroxide are degraded by thermal dissociation of the O-O bond to form the initiation active radicals.

$$POOH \xrightarrow{\triangle} PO\cdot + HO\cdot \tag{1.35}$$

$$POOP \xrightarrow{\triangle} 2PO\cdot \tag{1.36}$$

The trapped radicals (P· and PO·) of the irradiated polymer can react with the monomer forming a covalent bond between the monomer and the polymer substrate [79–81], known as "grafting from" mechanism.

$$PO\cdot + M \rightarrow POM\cdot \tag{1.37}$$

$$P\cdot + M \rightarrow PM\cdot \tag{1.38}$$

However, it should be emphasized that the precise chemical structure of the ether linkages between the polymer base film and the grafted chain has not yet been proven. The grafted chain can further propagate to form the grafted moiety as side chain.

$$POM\cdot + M_n \rightarrow POM\cdot_{n+1} \tag{1.39}$$

Termination takes place at some point when two radicals react with each other (combination).

$$POM\cdot_n + POM\cdot_m \rightarrow dead - polymer \tag{1.40}$$
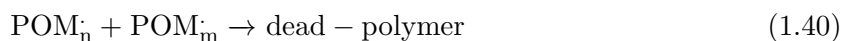
Termination can also occur by disproportionation. Furthermore, possible reactions such as chain transfer to solvent may also take place [72].

$$POM\cdot_n + S_x \rightarrow POM_{nx} + S\cdot \tag{1.41}$$

$$M_n^. + S_x \rightarrow M_{nx} + S^. \tag{1.42}$$

Here, POM_n is the graft growing chain of the copolymer, S is the solvent molecule, POM_{nx} is the dead polymer as a result of termination and $S^.$ is the solvent radical. $M_n^.$ is the growing chain of polymer in the solution and M_{nx} is the terminated chain.

1.5.3   Grafting front mechanism

Although the concept of radiation induced graft copolymerization is similar to conventional polymerization, it should be emphasized that radiation induced grafting also includes monomer transport into the base film, which is often the rate determining step [71]. Therefore, the properties of processed products such as reactivity ratios prepared by radiation induced grafting can differ from that prepared by conventional polymerization.

Monomer transport is made possible by swelling of the base film and diffusion of the monomer solution into the swollen base film. Grafting of monomer into the base film proceeds by the grafting front mechanism [71, 82]. The chain initiation occurs at the surface (Equation 1.37 and Equation 1.38), acting as the grafting front. The grafted layer swells in the monomer solution and polymerization continues in the swollen layer, resulting in chain growth. As a result of progressive diffusion of monomer through the swelling layer, the grafting front moves towards the middle of the film [71, 82, 83] (Figure 1.10). A homogeneous distribution of the grafted component across the film thickness can only be achieved when sufficient graft level is obtained.

1.5.4   Base films

Regarding the versatility of radiation grafting, a wide range of base films and monomers can be used. Common polymer films used to prepare ion exchange membranes are listed in Figure 1.11.

The chemical nature of the polymer base film also determines the sensitivity to radiation and the reactivity of the radicals formed. As described in subsection 1.5.2, radiation leads to formation of hydroperoxides and peroxides. Initiation by this path usually involves chain degradation and formation of crosslinks [72]. The most severe phenomenon owing to irradiation of base film is chain scission, yielding an unsaturated structure. This subsequently leads to the loss of molecular weight of the base polymer. The extent of these side effects depends on the chemical nature of the polymer base film, temperature of the irradiation and irradiation dose [83].
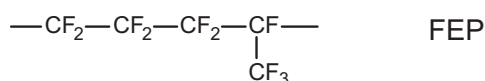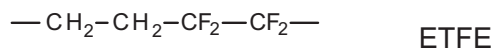
A number of researchers indicated that the use of a fluropolymer as base film is superior to the hydrocarbon type for fuel cell applications due to its low surface energy, ease of surface
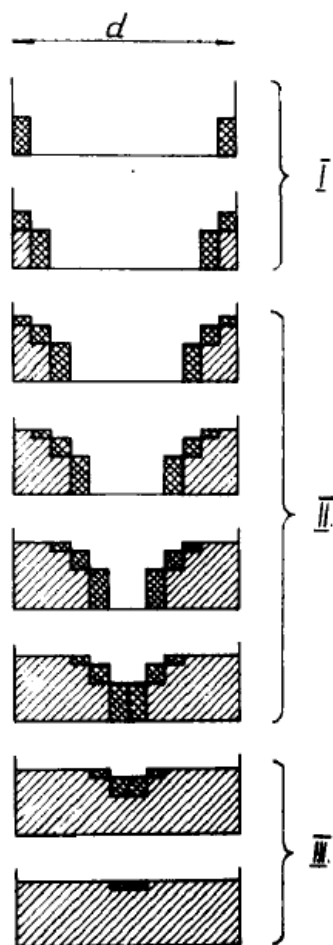
Figure 1.10: Grafting front mechanism through the film thickness (d). Regions I, II, III correspond to the induction period, linear period and flattening off period as described in literature [82].

modification by grafting, chemical-, mechanical- and thermal stability due to the C-F bond. [83, 84]. However, irradiation of perfluorinated base film can cause severe degradation due to chain scission [85, 86]. Here, only a selection of fluoropolymers will be discussed as potential base films for radiation grafted membranes for PEFCs. Comprehensive reviews on different base films can be found in literature [30].

To qualify the membrane for the fuel cell applications, chemical- and mechanical stability and ionic properties should be balanced. Different fluropolymers can be categorized into perfluorinated and partially fluorinated films. Perfluorinated films were found to be more chemically stable under the *ex situ* Fenton test compared to their partially fluorinated counterpart [85]. In spite of their chemical stability due to the fluorine chemistry, perfluorinated base films such as PTFE and FEP are prone to irradiation damage compared to the partially fluorinated ETFE, PVDF and PVF [85, 86]. The damage upon exposure to high energy radiation of the base film may lead to inadequate mechanical stabiliy of the membrane. The resistance to radical dam-

Perfluorinated films

$$-CF_2-CF_2-CF_2-CF- \qquad \text{FEP}$$
$$| \qquad\qquad\qquad$$
$$CF_3$$

$$-CH_2-CF_2- \qquad\qquad \text{PTFE}$$

Partially fluorinated films

$$-CH_2-CH_2-CF_2-CF_2- \qquad \text{ETFE}$$

$$-CH_2-CF_2- \qquad\qquad \text{PVDF}$$

$$-CH_2-CHF- \qquad\qquad \text{PVF}$$

Figure 1.11: Commonly used base films for radiation grafted membranes.

age is therefore a crucial requirement of the base film selection. Clearly, polymers with good radiation resistance allow the flexibility of irradiation dose applied.

In addition to radical resistance, ETFE also offers advantages over the perfluorinated FEP. Studies of Brack and coworkers suggested that ETFE is not only more robust towards radiation but also has superior mechanical properties compared to FEP [87, 88]. This could be a consequence of its higher molecular weight. The amount of radicals generated upon radiation in ETFE is higher than those in the FEP base films, resulting in lower radiation dose required to achieve the same graft level. Moreover, ETFE can be accessed easier by the graft components due to higher swelling in styrene and toluene, whereas the FEP does not swell. ETFE based membranes also show a higher water uptake than FEP based ones [85], indicating more hydrophilicity, which may promote the conductivity of crosslinked membranes.

Different partially fluorinated base films such as PVF and PVDF have been considered. The results found by Chen *et al.* indicate that PVF base film was chemically unstable and degrades upon sulfonation [66]. In addition, only surface grafting takes place when this base film is used [85]. The reason for this is not yet clear. This concludes that PVF is not suitable for the fuel cell application.

The radiation resistance and mechanical stability of PVDF based membranes are superior to those of ETFE based ones [85, 89, 90]. However, the PEFC performance of the grafted membrane based on PVDF is inferior to that based on ETFE [87]. ETFE is hence chosen as a base film for fuel cell application.

1.5.5 Monomers

In addition to the nature of the base films discussed previously, the grafted monomers also have a strong influence on the membrane properties. Ion exchange membranes can be prepared by grafting of monomers containing ion exchange groups such as SO_3^-, COO^-, PO_3H^- or NH_3^+. It is however not necessary that the monomer contains the ion exchange group if it can be post-functionalized either by sulfonation or phosphonation for cation exchange membranes or amination (quaternization) for anion exchange membranes. The ion exchange capacity (IEC) of the membrane is governed by the amount of ion exchange groups and is independent of the base film [85].

Styrene based radiation grafted membranes have been developed for more than two decades [37, 61, 91–94] and styrene is the most widely used monomer for preparation of PEM by radiation grafting. It allows easy polymerization, easy sulfonation and high proton conductivity at potentially low cost. Yet, membranes containing only styrene as a monomer are not suitable for fuel cell application due to its instability under fuel cell environment (subsubsection 1.4.3.2). This constitutes a serious threat to the lifetime of a fuel cell membrane based on sulfonated polystyrene. Therefore, membranes consisting of PSSA as protogenic constituent have to be well designed to enhance their longevity and fuel cell performance. A suitable comonomer can be employed together with styrene to improve membrane durability.

The use of styrene derivatives with a protected α-position, such as α,β,β trifluorostyrene (TFS) in BAM® membranes [95, 96] or α-methyl styrene (AMS) [43], leads to grafted membranes with improved durability over styrene grafted membranes [13, 97]. However, these monomers have low grafting rate [32–34, 43]. Enhanced grafting rate and membrane properties can be obtained by moving from single monomer grafted membranes to co-grafted ones containing two (or more) monomer types.

A widely used approach is to introduce a comonomer that serves as a crosslinker, e.g., divinylbenzene (DVB) or m-diisopropenylbenzene (DIPB), to further improve chemical and mechanical stability of the membrane [98–100]. The crosslinkers contain two (or more) vinyl functionalities which are available to copolymerize when exposed to radicals and thereby a three dimensional network can be formed in the grafted film. Once chain scission occurs, the network may hold the graft components together in the polymer matrix and avoid leaching out of chain fragments [101]. This approach shows significant improvement in membrane stability. A lifetime of 7900 hours was achieved with FEP-g-styrene / DVB membrane, whereas the uncrosslinked one failed within 50 hours [70].

However, the main drawback of such crosslinked membranes is the lower proton conductivity compared with the non-crosslinked ones at a given IEC. In addition, highly crosslinked

membranes are generally brittle. Recent trends in radiation grafted membranes involve the combination of styrene with non-crosslinking comonomers to optimize membrane durability, while maintaining low cost and easy sulfonation.

Non-crossliking comonomers such as AA, MAN and AN have been used with styrene for different purposes. The use of equimolar AA and styrene yields an alternating grafted chain. Sulfonation of this film leads to a condensed ring structure during sulfonation and the membrane has a pH-indicator property [102]. Becker *et al.* have modified base films (ETFE and FEP) with pendant chains consisting of styrene and acrylonitrile [103]. However, the fuel cell data of these membranes is lacking. MAN was initially applied as a comonomer to AMS to promote the grafting kinetics [70]. Ben youcef *et al.* have reported for the first time that the combination of styrene and MAN grafted onto ETFE can greatly improve the membrane durability compared to that consisting of styrene alone under fuel cell conditions [104]. MAN is susceptible to hydrolysis to some extent, resulting in formation of carboxylic acid and amide during fuel cell operation. This stimulated research into the understanding how a non-crosslinking comonomer influences in the stability and the fuel cell relevant properties of styrene based radiation grafted membranes.

Apart from styrene based membranes, proton conducting membranes based on glycidyl methacrylate (GMA) [105] or its derivatives [106] have also been synthesized by radiation grafting. The proton conducting site is introduced to the epoxy group of GMA by sulfonation. Incorporation of comonomers such as butylacrylate (BuA) and AN has been applied to GMA, in which membrane properties such as water uptake is positively affected, whereas the proton conductivity is negatively affected [105].

Furthermore, proton conducting membranes consisting of alkylsulfonic acid were synthesized from radiation grafting of methyl acrylate (MA) into an ETFE base film [107]. Subsequent sulfonation of the grafted films leads to partial ester substitution with sulfonic acid unit and carboxylic acid. Introduction of methyl methacrylate (MMA) as a comonomer to MA resulted in higher membrane durability in water (80°C) and oxidative environment (3% H_2O_2 solution at 60°C) [108]. This suggests that the absence of a hydrogen at the α-carbon leads to improvement in durability. Grafting of suitable comonomers is therefore a promising way to obtain membrane with required properties.

Alternative membranes include those grafted with comonomers containing carboxyl groups, such as AA [109]. However, the carboxylic acid group leads to lower cell performance because of its weak acidic properties resulting in only partial deprotonation.

Although there is a large variety of monomers which were radiation grafted into different based films in literature, only styrene based membranes for the application in fuel cell will be discussed throughout this thesis. The monomers shown in Figure 1.12 are a few examples illustrating the wide variety of grafting monomers used for PEMs. Since a large number of

comonomers can be used as crosslinker for PEMs, only the most plausible and common ones are presented here. On the contrary, there have been relatively few reports on modification of styrene based PEMs using radiation grafting of non-crosslinking comonomers. Potential non-crosslinking comonomers to be grafted with styrene by radiation grafting are also shown.
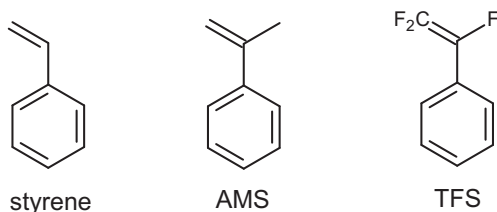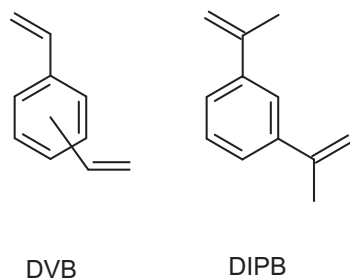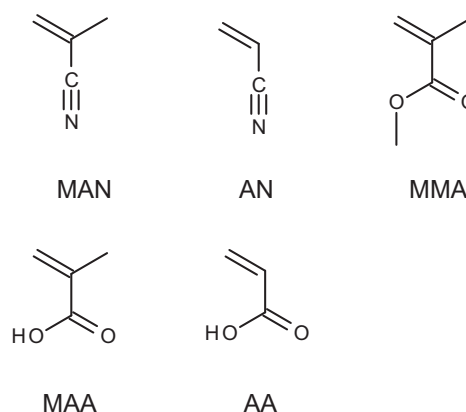
Figure 1.12: Common monomers used for the preparation of PEMs by radiation grafting.

It is beyond the scope of this thesis to summarize all possibilities. Different base films and graft monomers for radiation grafted membranes have been reported to which the reader is referred for more detail [72, 110].

1.6 Proton transport in the membrane

A key aspect responsible for the fuel cell performance is the proton transport. Sufficient proton transport corresponds to high fuel cell performance, while insufficient proton transport leads to ohmic losses. The ionic clusters are surrounded by the polymeric material of the membrane, forming aqueous domains upon hydration. In addition, water enables proton dissociation. Within such domains, water and proton transport occurs. The proton is carried away in the form of a hydronium ion (H_3O^+), Zundel ion ($H_5O_2^+$) or Eigen ion ($H_9O_4^+$). Continued moistening of the membrane is crucial to sustain high proton transport, and for that water vapor is

supplied to the cell by humidifying reactant gases.

The driving force for proton transport across the membrane is the electromotive force. The two principal mechanisms of proton transport in the membrane are the vehicle mechanism and the Grotthus mechanism [111, 112], depending on the nature and dynamics of the hydrogen bonding network of water.

The vehicle mechanism allows proton transport by diffusion through the aqueous regimes (Figure 1.13). The proton travels as one entity with water, therefore proton mobility is determined by the diffusion constant of water in the membrane. This proton transport mechanism is predominant in the membrane at low hydration level [4].
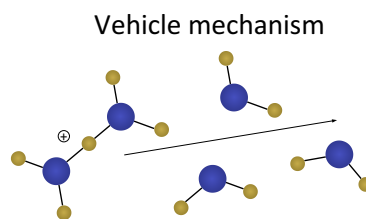
Figure 1.13: Proton transport in water by the vehicle mechanism (adapted from literature [113]). Large spheres represent oxygen atoms and small spheres represent hydrogen atoms.

In the Grotthuss mechanism, the proton 'hops' between adjacent water molecules through molecular orientation in the hydrogen bonding network by the formation or cleavage of the hydrogen bonding rather than by the movement of a single hydronium ion [114]. To form an extended hydrogen bonding network, water is required. Therefore, this mechanism generally predominates at high hydration level. A schematic plot of this mechanism is shown in Figure 1.14.
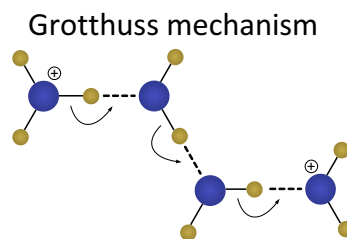
Figure 1.14: Proton transport in water by the Grotthus mechanism (adapted from [113]).

Proton conductivity (σ) in the membrane is determined by

$$\sigma = F\mu\,|z|\,a_{H^+} \tag{1.43}$$

where F is the Faraday constant, μ is the mobility, a_{H^+} is the activity of proton and z is the charge of the charge carrier (+1 for proton). The activity is defined as

$$a_{H^+} = f c_{H^+} \tag{1.44}$$

in which f is the activity coefficient and c_{H+} is the concentration of acidic group. The proton activity coefficient can change depending on the water content and degree of proton dissociation in water. If the membrane is insufficiently humidified, the protons may be immobile. Acidic functional groups with low pKa are required for complete proton dissociation.

The activity coefficient can not be practically obtained. Therefore, to correlate the experimentally measured proton conductivity with the proton mobility and acid concentration, the activity term of Equation 1.43 is substituted by the proton concentration (determined by titration). The effective mobility (μ_{eff}) can be determined. This parameter includes the uncertainties of the activity [115], tortuosity, diffusivity and the effects from the neighboring groups [116].

$$\sigma_{H+} = F\mu_{eff}\,|z|\,c_{H+} \tag{1.45}$$

In proton conducting membranes, optimization of the concentration of acidic functional groups is critical to ensure high proton conductivity. However, excessive proton conducting sites may lower the mechanical stability of the membrane and make it prone to dissolution. In addition, the membrane may become very hydrophilic associated with high water uptake, and hence resulting in proton dilution [117].

The membrane morphology is one of the main parameters to elucidate the proton transport. Over the years, considerable amount of research has been performed on PFSA membranes and several models have been proposed [118, 119]. It is established that the PFSA membranes are composed of a hydrophobic backbone and highly hydrophilic side chains of the sulfonic acid functional group. The difference between both phases provides separation at the nanoscale. Upon hydration the membrane swells, forming hydrophilic domains. Well connected hydrophilic domains create hydrophilic channels that are responsible for effective proton transport. The presence of hydrophobic backbone prevents the membrane from dissolving in water [120].

In comparison with Nafion, only a limited number of morphological studies has been carried out on radiation grafted membranes. The grafted membranes are semi-crystalline materials composed of crystalline domains and amorphous domains of the base film, which accommodate the grafted chains. The proton transport in radiation grafted membranes takes place exclusively in the amorphous phase that accommodates the ionic groups [78, 121–124]. Upon hydration, membranes absorb water due to the hydrophilic acid groups, forming water-rich domains. Similar to the PFSA membrane, these domains establish a water-rich network serving as proton pathway.

Structure and morphology of radiation grafted films and membranes can be examined by small-angle scattering of x-rays and neutrons (SAXS and SANS) and wide-angle X-ray scattering (WAXS). The results support the notion of phase separation of the crystalline base film and the ionic aggregate domains embedded in the amorphous phase [123–125]. Ding *et al.* carried out a study of different graft lengths of PSSA grafted onto a PS backbone. They reported that phase

separation of the grafted membranes is controlled by the graft length and the membranes with longer grafted chain shows a more pronounced phase separation than those with shorter chains [126].

The same group also demonstrated that the lack of phase separation and continuous hydrophilic phase leads to lower proton conductivity, even at a higher hydration level [127]. They compared the dry state morphologies of grafted polymer (PS-g-PSSNa) and random polymer (PS-r-PSSNa) using TEM micrographs and found that PS-g-PSSNa exhibits a more pronounced phase separated structure compared to the random copolymer.

In terms of proton transport, membrane structure and connectivity between hydrophilic domains have essential impact on the ion rich phase and proton conductivity accordingly. Phase separation can be tuned by, e.g., synthesis of block copolymer, polymer blend or graft polymerization. Random and alternating copolymers induce phase separation to a much lower extent and are therefore likely to exhibit a lower proton conductivity [128].

1.7   Aim of this work

As the use of PEFC holds promise in many applications [129–131], the study of fuel cell materials and their contribution to the overall cost and stability are of considerable practical importance [132]. One of the most important components that receives much research attention is the proton conducting membrane. Based on the recent and historical literature, perfluorosulfonic (PFSA) membranes such as Nafion are considered to be the current membrane technology for the PEFC. In spite of the significant progress that has been made in the 1960's due to the discovery of Nafion, the cost of this membrane type is still high (667 USD per m^2 [133]). Therefore, alternative materials are required. Many research groups devoted tremendous efforts to the synthesis of competitive alternatives to Nafion, with the primary concerns to lower cost and improve or sustain the durability of the membrane under fuel cell operating conditions [10, 21, 110, 129, 134].

While the cost factor may be eliminated by moving to different membrane materials, an understanding of how the materials affect the membrane properties and durability is essential. In this work, membranes were synthesized by the radiation grafting method, which allows fine tuning of membrane composition and properties. From a scientific point of view, this method does not only simplify the synthesis process but it can also be used as a tool to elucidate the complexities of the effects of the materials composed in the tailor-made membrane.

This thesis concerns the fundamental understanding of the comonomer effects in radiation grafted membranes and their potential applications in the PEFC. Based on the earlier study established by Ben youcef *et al.* [104], membrane stability is conferred by the presence of methacrylonitrile (MAN). Incorporation of a comonomer in a styrene based membrane may modify the membrane properties, leading to enhanced membrane durability. The present work composes

of two main contributions. The first parts of the thesis aim at understanding the role of MAN on fuel cell relevant properties and how it increases the membrane durability. The second part attempts to answer how various other comonomers affect membrane properties.

All experimental details and chemicals used in this thesis are summarized in the experimental chapter (Chapter 2). The basic experimental techniques needed to obtain relevant membrane properties are included.

Chapter 3 concerns the effect of the α-methyl group in MAN. Styrene / MAN and styrene / acrylonitrile (AN) co-grafted membranes were synthesized as model systems and characterized. The grafting kinetics and monomer distribution are presented and discussed. Fuel cell relevant properties of styrene / MAN and styrene / AN co-grafted membranes, such as ion exchange capacity (IEC), water uptake, proton conductivity, performance and durability under accelerated stress conditions were investigated in detail. In this chapter, the dependence of membrane stability on the presence of an α-methyl group is addressed.

Chapter 4 is an especially detailed study of MAN as styrene's comonomer. To assess the effect of MAN content in the graft, membranes were designed to have varying graft compositions, while keeping the IEC constant. The first part of this chapter presents the changes of the membrane properties brought about by the MAN content. The second part addresses the structural analysis of the co-grafted membranes in the dry state. The relationship between the microstructure of the membrane and its proton conductivity at reduced humidity is discussed.

Chapter 5 is devoted entirely to synthesis and characterization of styrene / methyl methacrylate (MMA) and styrene / methacrylic acid (MAA) co-grafted membranes. As a consequence of different chemical structures, a deeper understanding of the comonomer functionality on proton conductivity may be gained by examining proton mobility.

Chapter 6 summarizes the effect of the non-crosslinking comonomers (MAN, AN, MMA and MAA) on the fuel cell relevant properties and membrane structures. The conclusions and outlook are discussed in the last chapter (chapter 7).

2

Experimental

2.1 Membrane synthesis

2.1.1 Materials

The chemicals used during membrane preparation included styrene (99%, Aldrich), methacrylonitrile (MAN) (99%, Aldrich), acrylonitrile (AN) (99.5%, Fluka), methyl methacrylate (MMA) (99%Aldrich), methacrylic acid (99%, Aldrich) and chlorosulfonic acid (98%, Fluka). All monomers were grafted as received without removal of inhibitors. Analytical grade isopropanol and dichloromethane were purchased from Fisher Scientific, while analytical grade potassium chloride and potassium hydroxide were purchased from Merck. Analytical grade toluene was purchased from Empura. The base polymer is an ETFE (Tefzel® 100LZ) film with a thickness of 25 μm, purchased from DuPont (Circleville, USA).

2.1.2 Electron beam irradiation

The films were cut into appropriate sizes, washed in ethanol, dried in vacuum at 80°C and packed in zip-lock PE bags. The ETFE base films were electron beam irradiated in air at Leoni-Studer AG in ambient atmosphere (Däniken, Switzerland) to generate active sites, which enable grafting. A dose of 1.5-15 kGy were applied to the base films, depending on the monomer used. During irradiation allanine pellet dosimeters (Far West Technology Inc.) were placed together with the films as a reference to ensure the irradiation dose. The dose is determined by the time the sample is exposed to the electron beam which is controlled by the velocity of the conveyor belt. Immediately after the irradiation process, the pre-irradiated films were kept in dry ice for transportation to the laboratory and stored in a freezer at -80°C until use.

Grafting was carried out in glass tube reactor (60 ml) and in stainless steel reactor (600 ml), according to the experiment [67]. For kinetic study, grafting is carried out in glass tube reactor, in which a pre-irradiated film with 7.5 cm × 7.5 cm size is used. For fuel cell experiment,

2. EXPERIMENTAL

Table 2.1: Grafting conditions of different monomer systems used in this study (if not mentioned otherwise).

Monomers	Dose (kGy)	Grafting solvents	Washing solvents
styrene	1.5	7 isopropanol : 1 water (v/v)	toluene
styrene / MAN	1.5 and 3	7 isopropanol : 1 water (v/v)	toluene
styrene / AN	3	7 isopropanol : 1 water (v/v)	toluene
styrene / MMA	1.5	7 isopropanol : 1 water (v/v)	ethanol
styrene / MAA	15	ethanol	water (80°C) followed by toluene

grafting were carried out with 16 cm × 16 cm size films in the stainless steel reactor. Up to six pre-irradiated films were prepared in one batch. Prior to grafting, the pre-irradiated films were weighed to determine the initial mass. Then the films were immersed into the grafting solution and purged with nitrogen for 40-60 minutes to remove oxygen. The styrene molar fraction (styrene content with respect to total monomer content) was varied from $X_0=0$ to 1 in the grafting solution. X_0 and X refer to the styrene molar fraction in the grafting solution and in the grafted film, respectively. The reactors were subsequently sealed and placed in a preheated bath at 60°C (unless mentioned otherwise). After reaching the defined reaction time, the grafted films were removed from the grafting solution and washed in appropriate solvents overnight to remove excess monomers. The solvent used for washing were listed in Table 2.1.

After washing, the films were dried under vacuum at 80°C overnight and subsequently weighted. The grafted films were characterized by graft level (Equation 2.1), which is repeated here for clarity.

$$GL = \frac{m_g - m_0}{m_0} \cdot 100 \tag{2.1}$$

in which m_g and m_0 are the weight of pre-irradiated film and grafted film, respectively.

2.1.3 Sulfonation

Proton conducting membranes were obtained by sulfonation of the grafted films with 2% (v/v) chlorosulfonic acid in dichloromethane solution at room temperature for 5 hours. Then the sulfonated film was removed from the sulfonating solution and washed in deionized water several times to remove excess chlorosulfonic acid. Finally, the membranes were hydrolyzed in water at 80°C for 8 hours to ensure the formation of sulfonic acid groups. The membranes were stored in deionized water prior to carrying out *ex situ* experiments.

2.2   *Ex situ* characterization

2.2.1   Dimensional stability

The mechanical stability of the membrane was studied by the dimensional stability. First, the area and thickness of the membrane in fully hydrated state were measured. The membrane thickness was measured with a digital thickness gauge (MT12B Heidenhain, Germany) with a resolution of 0.5 μm. Then the membrane was dried at 60°C under vacuum for 2 hours and subsequently, the area and thickness were immediately remeasured. The dimensional stability was determined as the ratio of the area or volume change upon swelling and drying to that of the dry membrane.

$$S = \frac{x_{wet} - x_{dry}}{x_{dry}} \cdot 100 \tag{2.2}$$

where S is the dimensional stability and x indicates the mode of measurement in volume or area.

2.2.2   Compositional analysis by FTIR

The composition of the grafted films was determined qualitatively and quantitatively by FTIR spectroscopy, using a Perkin Elmer FTIR System 2000 spectrometer. The IR spectra were recorded at a 4 cm^{-1} resolution in the mid-IR spectral range (4000-400 cm^{-1}) and 10-32 scans were collected at room temperature. The spectra were evaluated using GRAMS / AI version 8.00 software (Thermo Electron Corporation, Waltham, USA) and the peaks were fitted assuming a mixed Gaussian and Lorentzian shape. Films can be measured directly in the dry state while the hygroscopic membranes were exchanged into potassium form by immersing into 0.5 M KCl solution overnight and dried at 60°C in vacuum overnight prior to the experiment to reduce the water uptake. The curve-fitting was performed using GRAMS / 386 software (version 7.01) from Galactic Industries. The relevant vibrational bands used for the quantification and the build up of calibration curves for the different monomers were discussed elsewhere [135].

To determine the extent of graft loss (L), a correlation between the change in the peak intensity of the pristine membrane and the tested membrane is established.

$$D = \frac{\widetilde{A}_0 - \widetilde{A}}{\widetilde{A}_0} \cdot 100 \tag{2.3}$$

where $\widetilde{A}$ is the area under the charateristic peak of the grafted monomer normalized with the ETFE relevant peak. The subscript 0 indicates the pristine membrane.

2. EXPERIMENTAL

2.2.3 Ion exchange capacity and degree of sulfonation

Six circular discs with 2 cm diameter were punched from the fully hydrated membrane. The membranes were equilibrated with 0.5 M KCl solution overnight and the number of protons released from the membrane by ion exchange with potassium ions is determined by titration using 0.05 M KOH to pH 7 (SM Titrino 702, Metrohm). After titration, the membrane discs were washed several times in water to remove excess salt from the membrane surface. The acidity of the membrane is determined by the ion exchange capacity (IEC), which is defined as

$$IEC = \frac{n(H^+)}{m_0} \tag{2.4}$$

where n indicates the number of mol of proton and m_0 is the corrected mass of dry membrane determined from titration as follows

$$n(H^+) = c_{KOH} \cdot V_{KOH} \tag{2.5}$$

$$m_0 = m_K - (M_K - M_H) \cdot n(H^+) \tag{2.6}$$

in which c_{KOH} and V_{KOH} are the concentration and volume of the standard KOH solution (0.05 M). M_K and M_H are the molar masses of potassium and hydrogen.

The degree of sulfonation (SF) can be determined from the difference between the experimental (IEC_{exp}) and theoretical IEC (IEC_{theo}) compared to the theoretical IEC, which is defined as

$$SF = \frac{IEC_{exp}}{IEC_{theo}} \cdot 100\% \tag{2.7}$$

$IEC_{th.}$ can be calculated by assuming that each styrene group is sulfonated and carries one sulfonic acid.

$$IEC_{theo} = \frac{GL}{M_S + \frac{M_C}{R_m} \cdot (100 + GL) + (M_{SO_3H} \cdot GL)} \tag{2.8}$$

where GL is the graft level and M is the molar mass. The subscript indicates the chemical species (S for styrene and C for comonomer). R_m indicates the molar ratio of styrene and comonomer, which is defined as

$$R_m = \frac{n(s)}{n(c)} \tag{2.9}$$

2.2.4 Swelling and hydration level

Swelling (Q), also known as water uptake, is the ability of a membrane to absorb water, which can be calculated from the mass difference of the membrane in wet (m_{wet}) and dry (m_{dry}) states.

The dry mass was obtained from the mass of the IEC samples dried at 80°C overnight under vacuum.

$$Q = \frac{m_{wet} - m_{dry}}{m_{dry}} \cdot 100\% \tag{2.10}$$

The water uptake is associated with the acidity of the membrane. The hydration number is the molar ratio between water and sulfonic acid.

$$\lambda = \frac{n(H_2O)}{n(SO_3H)} = \frac{Q}{IEC \cdot M_{H_2O}} \tag{2.11}$$

2.2.5 Through plane conductivity in water swollen membrane

The through plane conductivity of the membranes was measured by AC impedance spectroscopy (Zahner IM6 / IM6e) using a two-point probe conductivity cell prepared in house. A schematic representation of a two point probe measurement is shown in Figure 2.1. Two to six membrane discs with a diameter of 2 cm in water swollen state were stacked, assembled between two platinum disc electrodes and subsequently mounted into the conductivity cell. Using a torque wrench, the cell was tightened with 4.5 Nm to ensure good contact between the electrode and the membranes. The impedance was measured at room temperature in galvanostatic mode in the frequency range from 1-50 kHz at zero dc current with an amplitude of 5 mV. The measured impedance data were represented in a Nyquist plot. The resistance of the membrane stack is determined from the extrapolation of the linear regression at the high frequency end of the Nyquist plot. The resistance of the membrane stack can be determined and the average membrane resistance is obtained from the slope of the stack resistance as a function of the number of the membranes in the stack. The membrane conductivity (σ) can be calculated using the following equation.

$$\sigma = \frac{1}{R} \cdot \frac{l}{A} \tag{2.12}$$

in which, R is the membrane resistance (Ω) , l is the thickness of the membrane stack (cm) and A is the disc area (cm^2).
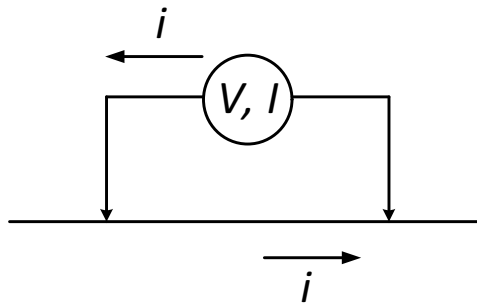
Figure 2.1: A representation of a two point probe measurement [4].

2.2.6 In-plane conductivity in water swollen membrane

A four point-probe conductivity cell (Bekktech BT-112) consisting of four Pt-electrode wires was used to evaluate the in-plane conductivity of the membrane in water swollen state (Figure 2.2). Rectangular sample of hydrated membrane in acidic form was cut using a punching tool (30 mm×12 mm) and mounted into the cell. All membranes were immersed in ionized water for at least 12 hour prior to use. During the measurement, the conductivity cell is immersed in deionized water at room temperature to ensure membrane hydration. Impedance and phase angle were measured at 1 kHz with 10 mV amplitude of the AC perturbation signal (Zahner IM6/IM6e). The ohmic resistance in fully swollen state was determined from the impedance when the measured phase angle is below 5 degree to ensure that the measured value is the true Ohmic resistance.
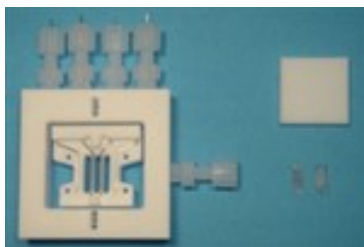
Figure 2.2: Four point-probe conductivity cell (Bekktech BT-112) used to measure the in-plane-conductivity of the membrane (picture taken from [136]).

2.2.7 In-plane conductivity under RH sweep

To measure membrane conductivity at different relative humidities, the same conductivity cell and membrane preparation procedure were used as described in subsection 2.2.6. In this case, the conductivity cell is connected to a relative humidity controlled fuel cell fixture at 70°C under air flow. The cell was sealed with a rubber gasket to ensure gas tightness during the experiment. The membrane resistance was measured at 1 Hz by an ac impedance measurement (four point-probe method, Zahner IM6/IM6e, Zahner-Elektrik, Kronach, Germany). The humidity probe (HMT330, Vaisala) was connected to the cell to monitor the dew point. The membranes were equilibrated for 2 hours at 70% RH before taking the first measurement. When changing the relative humidity from 70% to 20% and 70% to 95% ($\sim$10% per step), 15-30 min is needed for the membrane to equilibrate, during which the membrane resistance became stable. The phase shift of the measured impedance at 1 Hz was always below 5°, ensuring that the value can be taken as the ohmic resistance. The conductivity was subsequently calculated based on the dimensions of the wet membrane. The limitation of this measurement is that the change in RH

may influence the membrane dimensions. However, this information is not obtained during the measurement.

2.2.8 Water content analysis

Water vapor sorption isotherms were measured gravimetrically with a DVS HT sorption instrument (Surface Measurement Systems Ltd., UK). The measurements were carried out at 70°C unless specified otherwise. The membranes ($\sim$ 2 mg sample size) were initially dried in flowing air to establish the dry mass before exposure to a sequence of increasing relative humidity of 10% RH per step up to about 98% and subsequentially exposed to decreasing relative humidity with the same RH interval. The net percent change in mass based on the reference mass of dry membrane is used to determine the amount of water uptake at different relative humidities [1].

2.2.9 Thermal analysis

The thermal analysis of the membrane in potassium form was carried out in triplicate with differential scanning calorimetry (DSC, Perkin Elmer DSC7 instrument) under N_2 atmosphere. Prior to use, the DSC was first calibrated using indium (T_m=156.60°C, ΔH_f=28.5 J/g) and lead (T_m=327.50°C) as standards. The samples (1-2 mg) were accurately weighed and inserted into an aluminium pan and crimped. The heating endotherms were recorded over the temperature range of 25-320°C at a constant heating / cooling rate of 20 K min^{-1} and the baseline was collected and subtracted from the measured data. Single cooling curve was recorded with a cooling rate of 20 K min^{-1}. The melting temperature was determined from the peak maximum of the melting endotherm. To exclude the dilution effect caused by the grafted components, the intrinsic crystallinity of the membranes was determined as follows

$$C_i = \frac{\triangle H_f}{\triangle H_0} \cdot (1 + GL + \frac{GL_s \cdot M_{SO_3^-}}{M_s}) \tag{2.13}$$

where ΔH_f is the heat of fusion of the membrane and ΔH_0 is the heat of fusion of 100% crystalline ETFE (113.4 kJ/g). GL_S is the graft level of styrene which is determined by

$$GL_S = \frac{W_s}{W_0} \cdot 100 \tag{2.14}$$

where W_S and W_0 are the mass of styrene grafted film and pristine film, respectively.

---

[1]Measurement performed by Dr. Majid Naderi, Surface Measurement systems LTD, 5 Wharfside, Rosemont Road, Wembley HA0 4PE, UK

2.2.10 Elemental analysis

Elemental analyses of vacuum-dry samples were performed with LECO CHN-900 and LECO CHNS elemental analyzers to determine C, H, N and S fractions at the Laboratory for Organic Chemistry, ETH Zürich, Switzerland. 1-4 mg of the samples was used for this analysis. The temperature was ramped up to 1000°C for CHN analysis and 1000-1050°C for S determination.[1]

2.2.11 Small-angle X-ray scattering (SAXS)

Small-angle scattering of x-rays (SAXS) and neutrons (SANS) are characterization methods for structure investigations in various materials. The fundamental principles of SAXS and SANS techniques are identical. The main differences between SAXS and SANS are the probes that are used, i.e., X-rays and neutrons, respectively. Since X-rays interact with the electrons of an atom, SAXS allows us to discriminate inhomogeneities of the electron density [137], for instance, the phase separation in a polymer due to either crystalline and amorphous domains or large segments of different monomers. Unlike SAXS, the neutrons are scattered from the nuclei. The information that SANS provides can be similar or complementary to that of SAXS, because X-rays and neutrons are sensitive to different elements [138]. The structure information of the hydrated membranes may be obtained by the utilization of neutrons as probe.

An illustration of the small-angle scattering technique is shown in Figure 2.3. In the case of SAXS, a monochromatic X-ray beam with sub-nanometer wavelength is directed onto the sample, of which a small fraction is scattered by the atomic electron cloud due to the interaction of the X-ray with electrons. Since only a small fraction of the incoming beam (primary beam) interacts with the electrons in the sample, a beamstop is used to avoid damage of the detector and can be found in front of the detector in the same position as the incoming beam.

The scattered radiation is recorded by a 2D detector, resulting in an interference pattern. The information provided on the interference pattern includes the diffraction angle (2θ), azimuth angle (ϕ) and the sample orientation (anisotropy of the sample). When the sample exhibits random orientation such as in dilute dispersion, isotropic membrane or crystal powder, the scattering pattern shows circles around the primary beam with equal intensity. In case of a perfectly oriented sample such as single crystals, it will result in intensive spots due to reflections [140]. For partially oriented samples such as fibers or an anisotropic membrane, the scattering pattern will consist of circles around the primary beam with unequal intensity. The features of the scattering patterns of different materials are depicted in Figure 2.4.

From the 2D scattering pattern of an isotropic sample, the scattering profile is converted into a 1D azimuthal profile. The scattering vector modulus q is used to define the diffraction

---

[1]Measurement performed by Dr. Michael Schneider, Mikrolabor HCI E304, ETH Zürich, CH-8093 Zürich, Switzerland
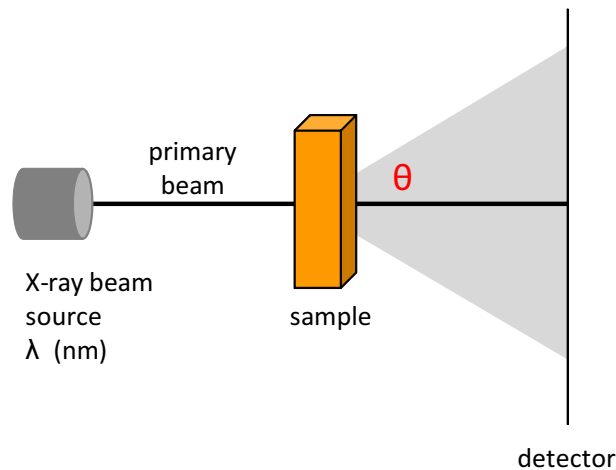
Figure 2.3: Schematic representation of small angle scattering. X-ray is represented here as a probe used in the SAXS technique (adapted from [139]).
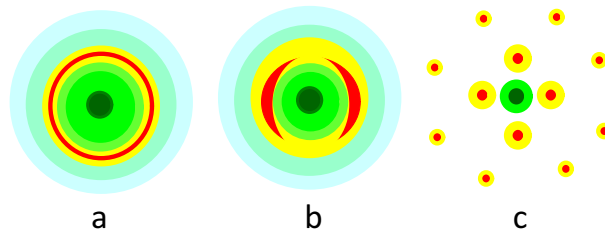
Figure 2.4: 2D scattering pattern of randomly oriented sample (a), partially oriented sample (b) and perfectly oriented sample (C) (adapted from [140]).

angle (2θ), is given as

$$q = \frac{4\pi sin\theta}{\lambda} \tag{2.15}$$

where θ is half of the diffraction angle and λ is the wavelength of the beam (nm). From this correlation, the unit of the scattering vector (q) is a reciprocal of length unit and is given in inverse nanometer (nm^{-1}). Therefore, an increase in q value corresponds to a decrease in length unit in real space. The characteristic length of the structure (d) is defined as

$$d = \frac{2\pi}{q} \tag{2.16}$$

The main challenge of SAXS is to extract the structural information of the 3D structure from the 1D scattering pattern. To evaluate the scattering data, inverse Fourier transform method is applied, from which the real space structure and morphology can be obtained. In addition, information based on SAXS measurement yields the spatial variation of the structural heterogeneities.

Structural analyses by small-angle X-ray scattering (SAXS) were carried out using a S-MAX3000 pinhole camera (Rigaku Innovative Technologies, Auburn Hills, USA). The wavelength of X-rays was 0.1524 nm. In the dry state, the sulfonic acid groups in the membrane form

ionic aggregates, which are phase separated from the other polymer domains. The difference in X-ray scattering length between these two phases creates the contrast that is visible by the SAXS measurement. In order to enhance this contrast, the membranes were exchanged to Cs^+ by immersion in 0.5 M CsCl solution overnight and dried under vacuum at 80°C. Therefore, the ion-rich phase has a higher electron density compared to the surrounding polymer and is responsible for the observable ionomer peak in the SAXS spectra. Experimental details were described elsewhere [141] [1].

2.3 *In situ* characterization

2.3.1 Preparation of MEA

Single cell experiments in this study were carried out using two types of cell configurations namely, the N1D and Q30 with a cell geometry of 16 and 29 cm^2, respectively. Besides the cell geometry, the flow field designs were different. The N1D and Q30 single cells are comprised of a parallel flow field and a three fold serpentine flow field, respectively, with 1 mm channel to land width machined into graphite plates. The membrane electrode assemblies (MEA) were prepared according to the cell configurations. Prior to MEA fabrication, the membranes were dried under vacuum at 60°C.

Cell design 1[2]: The MEA of the N1D cell fixture consists of 100 μm PTFE Gaskets, Pt-containing electrodes, polyethylene naphtalate (PEN) sub-gaskets (25 μm) and a membrane. Before assembling into the MEA, the membranes used for this cell design were impregnated with a 0.5% (v/v) Nafion / ethanol solution and dried at 60°C for 2 hours under vacuum to improve the adhesion of the membrane and the electrodes. Subsequently, the membranes were laminated with JM ELE162 gas diffusion electrodes (Johnson Matthey Fuel Cells, Swindon, UK) with a noble metal loading of 0.4 mg Pt cm^{-2} and sandwiched between the sub-gaskets by hot-pressing (110°C, 15 kN, 180 s) to form a membrane electrode assembly (MEA), which was subsequently assembled into the single cell fixture.

Cell design 2[3]: Using N1D cell fixture, the membranes were used as prepared without impregnation to investigate the chemical stability of the membranes under OCV conditions. The MEAs were fabricated by hot pressing using the same gas diffusion electrode and procedure as described in *Cell design 1.*

---

[1]Measurement performed by Dr. Sandor Balog, Adolphe Merkle Institute for Nanotechnology, University of Fribourg, CH-1723 Marly 1, Switzerland

[2]Measurement performed by Dr. Hicham Ben youcef, Paul Scherrer Institut, CH-5232 Villigen PSI, Switzerland

[3]Measurement performed by Zhouxiang Zhang, Paul Scherrer Institut, CH-5232 Villigen PSI, Switzerland

Cell design 3 : The Q30 cell fixture is used to investigate the effect of nitrile hydrolysis. In this case, the membrane was sandwiched between the electrodes and 100 μm Teflon gaskets (without subgaskets) to ensure the gas tightness and assembled into the cell fixture without lamination and hot pressing. The same type of gas diffusion electrode is applied.

2.3.2   Electrochemical characterization

2.3.2.1   Hydrogen permeation

The hydrogen crossover rate is an important parameter characterizing the membrane integrity. To determine the hydrogen crossover rate across the membrane, an *in situ* electrochemical measurement is used. Constant flows of 200 ml min^{-1} fully humidified H_2 and N_2 were applied at the anode and cathode, respectively. While the gases were fed to the electrode, the cell temperature and pressure were kept constant.

A concentration gradient of hydrogen is built up across the membrane due to the difference in gas partial pressure on the anode and cathode, which serves as a driving force for H_2 to permeate. After 1 hour, the cell is equilibrated and a cell voltage of approximately 0.1 V can be measured. The cathode supplied with N_2 serves as working electrode, and the anode side supplied with H_2 serves as counter electrode. When a voltage $\geq$ 0.2 V is applied on the cell, current is generated due to the oxidation reaction of permeated H_2. An Agilent potentiostat (Agilent E3633A) was used to apply a voltage scan to obtain limiting crossover current. The potential was applied stepwise from 200 to 800 mV in 100 mV steps and back with 200 mV step. The volumetric permeation rate of hydrogen can be calculated according to Faraday's law and the ideal gas law.

In principle, the permeation of hydrogen is governed by the concentration gradient and is independent of the applied voltage, yet an ohmic behavior can generally be observed, where the crossover current increases proportionally to the voltage. This indicates an electric short in the MEA [142]. To distinguish the hydrogen crossover rate from the electric short, the hydrogen crossover rate is estimated from the the extrapolation of the linear regression at 0 mV, which yields the limiting current density (Figure 2.5).

2.3.2.2   Polarization curve

Polarization curves are used to characterize the performance of fuel cells. It represents the relationship between the current and cell voltage and provides information about the overpotentials and degradation of the fuel cell components. To obtain the polarization curve, the voltage output is recorded as a function of current density, starting at open circuit voltage (OCV) and stopping when the voltage dropped below 0.3 V.
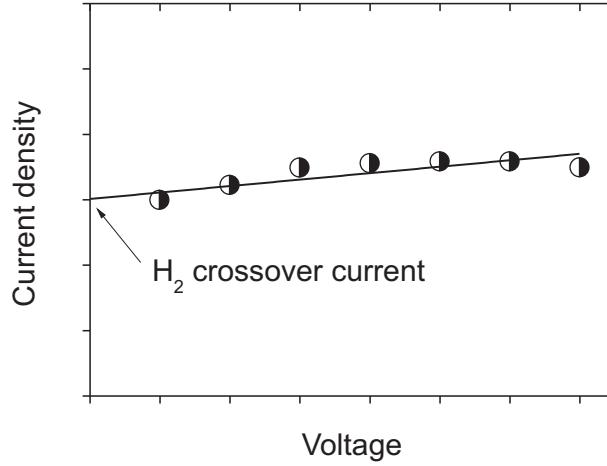
Figure 2.5: The influence of an internal electric short leads to a linear increase of the current density with increasing voltage. To eliminate the effects based on electronic conduction, the H_2 crossover current (j_{perm}) is determined from the y-intercept.

2.3.2.3 Electrochemical impedance spectroscopy (EIS)

The EIS technique is a diagnostic tool to distinguish processes occurring at different time constants during fuel cell operation. In fuel cells, the EIS is commonly used to study ORR, characterize transport losses and evaluate ohmic resistance, charge transfer resistance and double layer capacitance [143]. During the EIS measurement, a small ac potential or current perturbation is applied and the current or voltage response is measured along with the phase angle. In a (pseudo-) linear system, the current response of the ac potential is a sinusoidal function of the same frequency but shifted in phase [144]. The excitation potential (V) and current response (I) can be expressed as follows

$$V_t = V_0 \cos{(\omega t)} \tag{2.17}$$

$$I_t = I_0 \cos{(\omega t - \phi)} \tag{2.18}$$

The resulting impedance is

$$Z = \frac{V_t}{I_t} = Z_0(\cos\phi + j\sin\phi) \tag{2.19}$$

in which V_t is the is the potential at time t, V_0 is the amplitude of the voltage signal, ϕ is the phase shift and ω is the angular frequency (rad s^{-1}), which is expressed as

$$\omega = 2\pi f \tag{2.20}$$

where f is the frequency (Hz).

The impedance spectrum is represented in the Nyquist plot (Figure 2.6), which shows the real (Z_{Re}) and imaginary (Z_{im}) impedances. The interpretation of the spectra is performed

by means of equivalent circuit model. An ideal semi-circle is obtained with the Randles circuit model (Figure 2.7), under the assumption that HOR is negligible and the porous characteristic of the electrode is negligible [145]. The catalyst layers of the entire fuel cell are represented by a parallel circuit of a double layer capacitance (C_{DL}) and a charge transfer resistance ($R_{CT.}$).

The behavior of the double layer capacitor is frequency dependent. By varying frequency, the impedance contribution of individual components can be investigated. At high frequency, the double layer capacitor acts as an ideal conductor and the parallel circuit of the model can be suppressed. Therefore, the impedance measured at high frequency is attributed to the ohmic resistance. At low frequency, the capacitor represents an insulator behavior, and the measured impedance is a sum of the ohmic resistance and and the charge transfer resistance ($R_\Omega + R_{CT.}$).
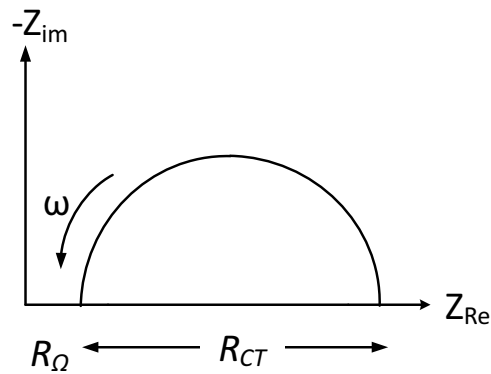
Figure 2.6: EIS spectrum represented in the Nyquist plot for the Randles cell.
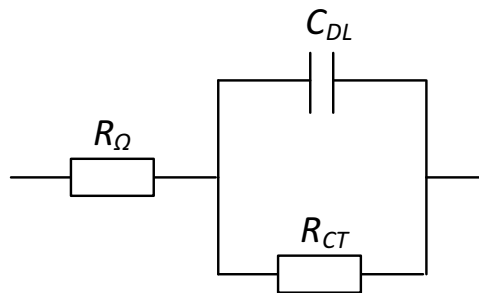
Figure 2.7: Randles equivalent circuit. C_{DL}=double layer capacitance of the electrode, R_Ω=ohmic resistance and R_{CT}=charge transfer resistance. The parallel circuit represents the entire catalyst layer in the fuel cell.

In the Nyquist diagram shown in Figure 2.6, the diameter of the semi-circle corresponds to the charge transfer resistance (R_{CT}) and the high frequency intercept is the membrane resistance R_Ω. The shortcoming of the Nyquist plot is that the frequency information is not visible. Another representation is the Bode plot, in which the absolute value of Z and the phase angle is plotted against the logarithm of frequency.

2. EXPERIMENTAL

In practice, interpretation of the impedance spectra is a complex issue. One or more depressed semi-circles can be found in a Nyquist plot of operating fuel cells. Therefore, applying the Randles equivalent circuit model would be inappropriate. Different effects govern the shape of the semi-circles and more complicated models are reviewed in [146].

All *in situ* EIS measurements have been performed using the four point probes configuration (Figure 2.8), in which two of the probes deliver current and the other two are used to measure voltage. The measurements were carried out by applying a sinusoidal current (amplitude 100 mA) in the frequency range between 100 mHz and 25 kHz (Zahner IM6).
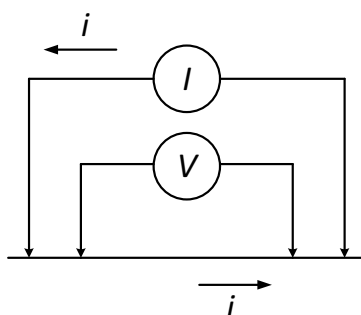
Figure 2.8: Illustration of a four point probe measurement (adapted from literature [4]).

2.3.2.4   CO stripping voltammetry

CO stripping voltammetry is an electrochemical method suited to study the electrochemical catalyst surface area (ECSA) of the electrodes. The principle of the technique is based on monolayer CO adsorption on the Pt particles and oxidation of CO. A cyclic potential is applied back and forth to the electrode of interest (with adsorbed CO) at a constant sweeping rate and the charge as a result of CO oxidation is measured, accordingly.

The CO stripping voltammetry was carried out at a cell temperature of 60°C with Zahner IM6. Prior to the measurement, fully humidified 5% H_2 / N_2 and N_2 were supplied (200 ml min^{-1}, 20 minutes) to the counter electrode and the working electrode (electrode of interest), respectively, until a stable equilibrium of around 0.1 V is reached. Then, preconditioning of the electrode was done in the potential range from 0.05 to 1 V at a sweep rate of 100 mV s^{-1} to remove impurities on the catalyst surface. CO was adsorbed by flowing 1% CO / N_2 for 20 minutes to the working electrode at a constant potential of 0.125 V. By holding the potential constant, excess CO in gas phase was removed by purging with N_2 (20 minutes, 600 ml min^{-1}). The CO stripping experiment was done at a sweep rate of 10 mV s^{-1} and at least two consecutive cyclic voltammogram sweeps were recorded. In the first anodic sweep, oxidation of CO takes place, showing a current signal around 0.6 V. For an accurate determination of the ECSA, the second sweep is carried out as baseline. The integrated peak area between the first and second
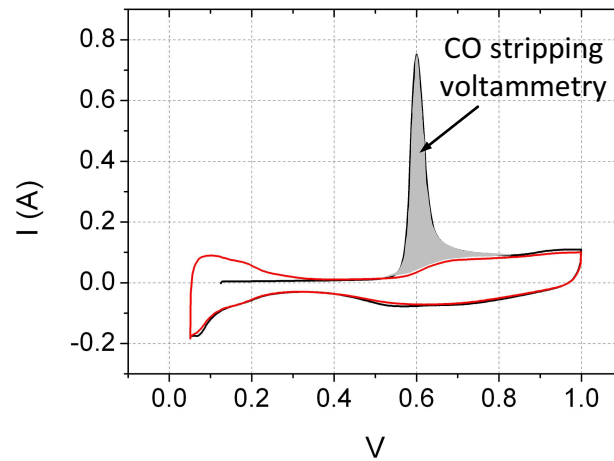
Figure 2.9: Schematic representation of a CO stripping voltammogram. The peak represents the charge exchange during CO oxidation. The shaded region of the voltammogram corresponds to the electrochemically active surface area (ECSA).

anodic sweep corresponds to the ECSA. Assuming that oxidation of CO monomer layer requires $420~\mu C~cm^{-2}$, the ECSA can be calculated [147].

3

Effect of the α-methyl group of MAN

3.1 Grafting of styrene / MAN and styrene / AN into ETFE

Poly(styrene sulfonic acid) (PSSA) composite membranes were used in the early fuel cell applications [13]. However, PSSA is susceptible to addition of OH$\cdot$, which is present in the fuel cell environment, and can subsequently undergo chain scission [48, 62, 64, 104]. This process constitutes a serious threat to the lifetime of a fuel cell membrane based on sulfonated polystyrene. Therefore, membranes consisting of PSSA as protogenic constituent have to be well designed to enhance their longevity and fuel cell performance. A suitable comonomer in the radiation grafting process can be employed together with styrene to improve membrane durability. A combination of styrene and methacrylonitrile (MAN) grafted into a poly(ethylene-alt-tetrafluoroethylene) (ETFE) base film can greatly improve the membrane durability in the fuel cell compared to that of a pure styrene grafted membrane [104]. In a range of other non-related applications, the nitrile group was pointed out to be a desired functional group to be incorporated into polymer materials in order to improve their gas (e.g., O_2, CO_2 and N_2) barrier properties [148–150]. This stimulated research into the understanding of how MAN influences in the stability and the fuel cell relevant properties of the styrene / MAN co-grafted membranes, how the comonomer affects membrane properties, and which functionalities lead to considerable improvement of membrane durability.

To investigate the effect of nitrile containing comonomers on the fuel cell relevant properties, proton conducting membranes were prepared by radiation grafting of styrene and its comonomers into ETFE base films, followed by sulfonation. For this work, two comonomers were used, namely MAN and acrylonitrile (AN). Considering that the only difference in their molecular structure is the substituent at the alpha position of the nitrile comonomers, the effect of the α-methyl group on the relevant membrane properties can be investigated. Detailed kinetics studies were performed and the film compositions were determined using FTIR spectroscopy.

3. EFFECT OF THE α-METHYL GROUP OF MAN

Understanding of the polymerization kinetics of the co-grafted membranes was important to ensure an optimal control of monomer composition in the grafted films. Fuel cell data and hydrolysis results on both membrane types are presented. In addition, the membranes were characterized for their *ex situ* fuel cell relevant properties, namely ion exchange capacity (IEC), water uptake, dimensional stability and proton conductivity.

3.1.1 Grafting kinetics

Grafting of styrene and MAN was conducted in the grafting solution containing the monomer mixture, water and isopropanol. The amount of monomers grafted into the base film is quantified by the graft level. Figure 3.1 shows the graft level of styrene / MAN grafted into pre-irradiated ETFE (1.5 kGy) as a function of the styrene molar fraction in the grafting solution (X_0). The results follow the generally observed grafting behavior, where the graft level increases sharply in the beginning due to chain propagation and then levels off with further increase in the reaction time. The curvature of this kinetic plot is a measure for the lifetime of the radicals in the film [151], whereas the leveling off can be attributed to polymer chain recombination and radical decay, which reduces the overall rate of grafting [152].
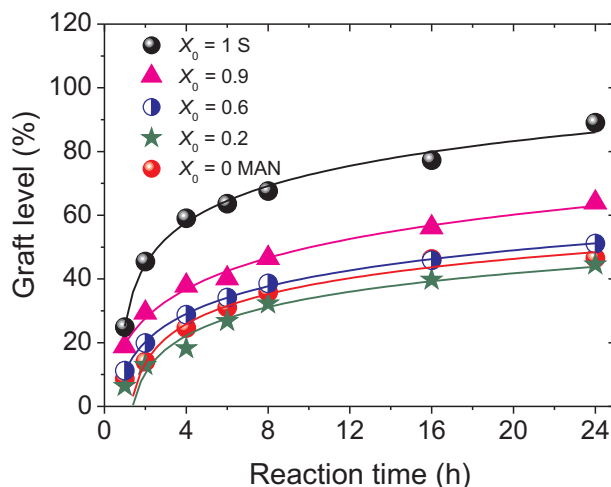
Figure 3.1: Mass based graft level of styrene / MAN grafted films as a function of reaction time and styrene molar fraction in the grafting solution (X_0) containing 20% (v/v) monomer, 70% (v/v) isopropanol and 10% (v/v) water. 1.5 kGy pre-irradiated ETFE with 25 μm thickness film was used as base polymer.

The highest graft level is obtained with pure styrene as the only monomer (X_0=1), while an increase in MAN molar fraction is associated with a decreasing grafting rate except for X_0=0 (grafting of pure MAN), which showed a slightly higher grafting rate than X_0=0.2. This may imply that the chemical compatibility of the base film and monomer plays a role in the grafting behavior.

Grafting of styrene is favored due to its nonpolar nature, which is comparable to that of ETFE. Therefore, styrene can penetrate more easily into the ETFE matrix than the polar MAN. However, in case of X_0=0.2 where MAN is abundant, a large portion of MAN is grafted into the film. This induces the grafted films to become more polar and allows an easier access of MAN, whereas the diffusion of styrene into the ETFE matrix becomes more limiting. As a result, the grafting rate for X_0=0.2 is higher than that for X_0=0.

Significant differences in the graft level can be observed from the grafted films prepared with X_0=1 and 0.9. This may indicate that a small amount of MAN can create substantial difference in the diffusion of the monomers, leading to the change in the environment around the radicals and allowing simultaneous incorporation of both monomers into the ETFE base film.

Yet, the mass based graft level is admittedly somewhat misleading for a system containing more than one monomer, since it neglects the fact that the incorporated monomers do not have the same molar mass. The difference between the mole based graft level of pure styrene and pure MAN is found to be less pronounced than in the case of the mass based graft level (Figure 3.2). This emphasizes that the grafting rate of styrene is indeed higher than that of MAN. Besides the compatibility of the monomer and the base film, the intrinsic kinetics may also play a role in the grafting procedure. The propagation rate constants of styrene polymerization and MAN polymerization in bulk at 60°C are 187 mol l^{-1} s^{-1} and 55 mol l^{-1} s^{-1}, respectively [153]. Therefore, it is not surprising that styrene yields higher grafting rate than MAN. Furthermore, the solvent can also affect the grafting rate [151].
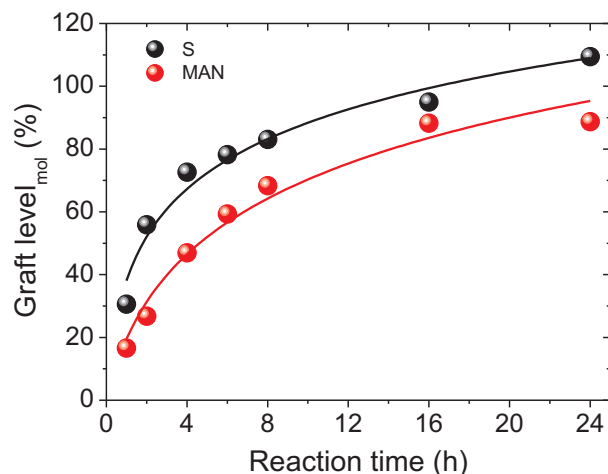
Figure 3.2: Mole based graft level as a function of time of styrene and MAN grafted films (1.5 kGy)

Possibly, grafting proceeds via the grafting front mechanism, where the grafting initially takes place at the film surface and behaves as a grafting front that gradually penetrates through the film [80, 82]. Since the ETFE film barely swells in most of the common solvents [154], grafting

through the film is induced by swelling of the grafted layer in the grafting solution, which allows monomer access to the active centers (radicals) in the film. Pure AN grafted very poorly and a maximum graft level of only 3.6% was obtained (Figure 3.3), assuming that only the surface of the ETFE was grafted. The low graft level of AN could be due to the incompatibility between the monomer and its polymer. Since poly-AN (PAN) is insoluble in its monomer [71, 155], the PAN grafting front may not swell in the grafting solution, which limits the diffusion of AN into the ETFE matrix. However, it was shown that AN can be grafted onto polypropylene fibers under different grafting conditions [28]. Perhaps, there is little diffusion involved in this process.
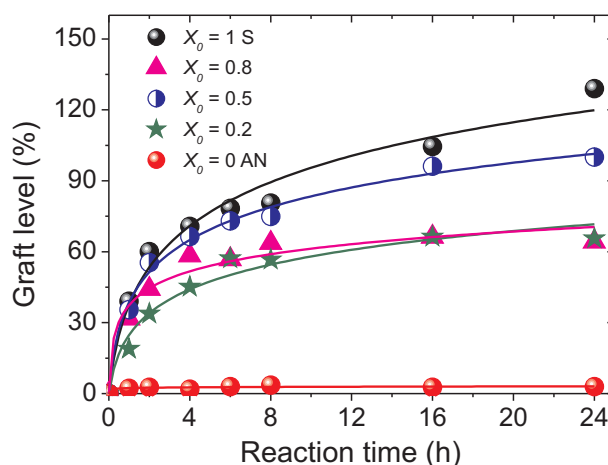
Figure 3.3: Mass based graft level of styrene / AN grafted films as a function of reaction time and styrene molar fraction (X) in the grafting solution containing 20 vol% monomer concentration, 70 vol% isopropanol and 10 vol% water. 3 kGy pre-irradiated ETFE with 25 μm thickness film was used as base polymer.

The grafting rate of styrene / AN is enhanced by increasing the styrene content up to X_0=0.5, while further increase in styrene content to X_0=0.8 showed a grafting curve comparable to that at X_0=0.2. A different trend was found by Becker and colleagues. They reported that when the graft copolymerization was carried out in bulk, grafting of styrene / AN with X_0=0.7 leads to a higher grafting yield than when only styrene is used [103]. This result suggested that the co-grafting kinetics depend greatly on the used grafting conditions.

The graft level analysis addresses the total grafted mass, yet it does not provide information about the content of the different monomer units in the film. To distinguish the amount of the grafted monomers, we carried out compositional analysis using FTIR spectroscopy.

3.1.2 Compositional analysis

The composition of the graft copolymer is an important parameter that determines the membrane properties and ultimately its practical application. Styrene / MAN and styrene / AN

grafted films were characterized by FTIR to investigate their chemical composition (Figure 3.4). A broad absorption at 3200-2800 cm^{-1}, which is characteristic for C-H stretching, changes upon grafting. The band around 1600 cm^{-1} corresponds to one of the aromatic ring-stretching vibrations. The presence of these two bands indicates the presence of an aromatic compound. Closer inspection also shows another aromatic ring-stretching vibration at 1493 cm^{-1}. In addition to these bands, the very strong bands near 770 cm^{-1} and 700 cm^{-1} (not shown here) due to the C-H out-of-plane vibration and a ring out-of-plane deformation also confirm the presence of the monosubstituted aromatic ring of styrene [156]. The C≡N stretching vibration of MAN and AN occurs at around 2234-2241 cm^{-1}. In addition to this band, a small peak around 1390 cm^{-1} due to the symmetric C-H ("umbrella") deformation of the α-methyl group can also be observed for MAN containing films. Furthermore, the grafted films contain typical vibrational bands characteristic of ETFE in the 1480-1430 cm^{-1} region. The peak intensity is determined by the amount
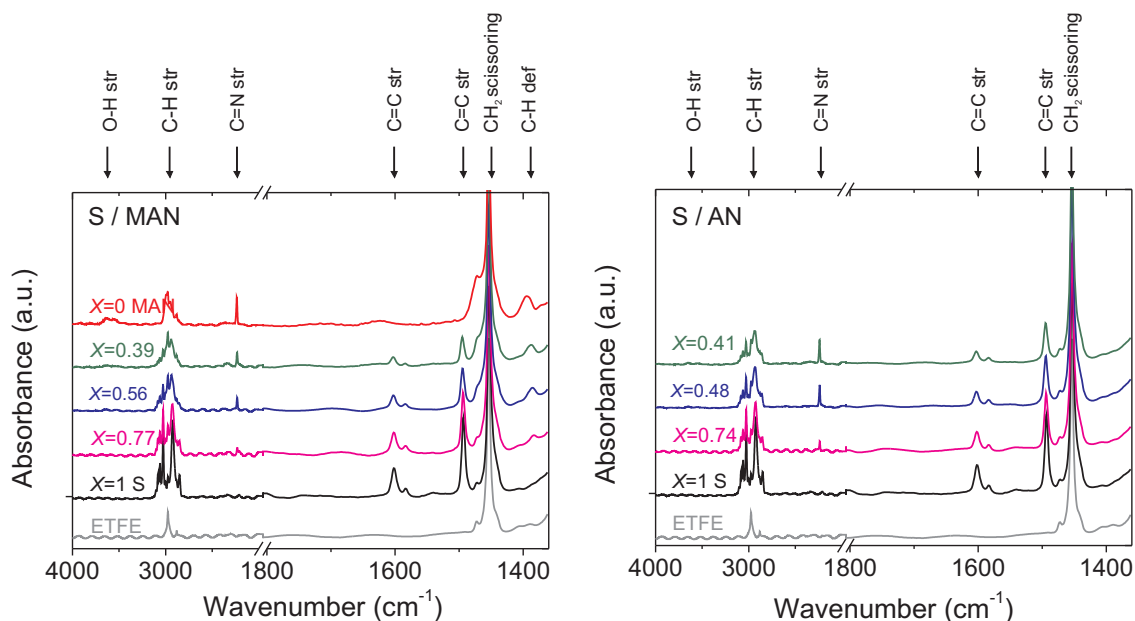
Figure 3.4: FTIR spectra of styrene / MAN and styrene / AN grafted films at fixed graft level (GL~40 %).

of the grafted components and varies with the styrene molar fraction in the grafting solution. However, upon grafting, the introduction of the graft copolymer leads to film expansion and increase in film thickness. The area change leads to the dilution of components and the amount of functional groups can therefore be underestimated if the intensity of the FTIR vibrational bands is directly used for quantification. Our previous study showed a decrease in the intensity of the peak corresponding to ETFE as a result of the dilution effect originating from the increase in the amount of grafted component [135].

3. EFFECT OF THE α-METHYL GROUP OF MAN

Figure 3.5 demonstrates the volume expansion of the film as a result of grafting. The expansion shows a strong dependency on the graft level and is independent of the composition of the grafts and irradiation dose. In addition, we found that the expansion of the film in the machine direction is slightly higher than in the transverse direction. This difference may be attributed to the film processing of ETFE by extrusion of the polymer melt.
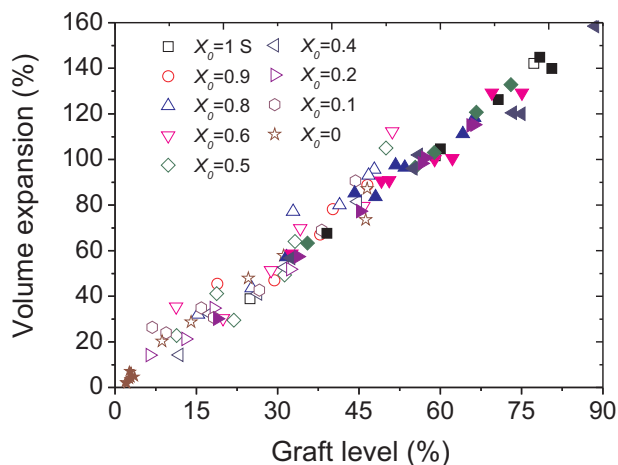
Figure 3.5: Volume expansion of the film with varying styrene molar fraction in the grafting solution as a function of graft level. The open symbols are styrene / MAN grafted into 1.5 kGy pre-irradiated ETFE film, the filled symbols are styrene / AN grafted into 3 kGy pre-irradiated ETFE film.

The fractional graft level of the different monomer units was determined based on the calibration curves of pure styrene and pure MAN grafted films. The calibration was established from the linear relationship between the intensity ratio of the vibrational bands associated with the monomer to that associated with the base polymer and the graft level (Figure 3.6). Since the graft level obtained from pure AN is too low to establish a calibration curve, the content of AN was calculated based on the difference between the overall graft level and the styrene graft level obtained from the FTIR analysis. The FTIR spectra and the film expansion provide supporting evidence that the monomers were grafted into the ETFE film.

The composition of the graft component, based on the peak-fitting of the FTIR spectra, was determined for films prepared using different grafting times (Figure 3.7). A relatively constant composition, expressed as styrene molar fraction X, within the grafted films over the reaction time was observed. The composition of the grafted chain depends on the feed composition and is constant, implying no composition drift in the examined graft level range.

3.1.3 Copolymerization parameters

Copolymerization of styrene and its comonomer leads to two types of propagating species at the chain end, namely styrene and comonomer radicals. The monomer can be added to a radical of
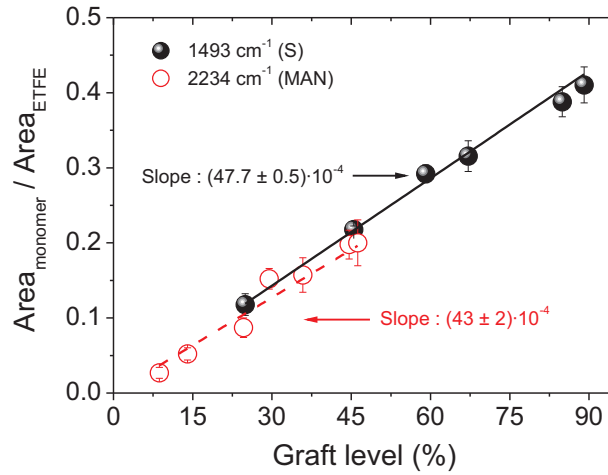
Figure 3.6: Calibration curve used to determine the fractional graft level for styrene and MAN, respectively. The band at 1325 cm^{-1} (characteristic for ETFE) was used to normalize the characteristic peaks.

the same species (self-propagation) or the foreign species (cross-propagation), depending on the chemical reactivity of the radical at the chain end. To determine the composition of the polymer, the terminal model is applied, under the assumption that the reactivity of the propagating species only depends on the identity of the chain end (terminal unit) and is independent of all the monomer units but the terminal one [157]. Four propagation reactions are possible.

$$\sim A \cdot + A \xrightarrow{k_{AA}} \sim AA\cdot \tag{3.1}$$

$$\sim A \cdot + B \xrightarrow{k_{AB}} \sim AB\cdot \tag{3.2}$$

$$\sim B \cdot + A \xrightarrow{k_{BA}} \sim BA\cdot \tag{3.3}$$

$$\sim B \cdot + B \xrightarrow{k_{BB}} \sim BB\cdot \tag{3.4}$$

A and B represent styrene and its comonomer, k_{ij} is the rate constant and the indices i and j indicate the radical type and the propagating species, respectively. Based on the Mayo-Lewis equation, the composition of the growing copolymer chain in the film (X) can be predicted from the known composition in the reaction mixture.

$$X = \frac{(r_A A + B) A}{(r_A A + B) A + (r_B B + A) B} \tag{3.5}$$

55

3. EFFECT OF THE α-METHYL GROUP OF MAN
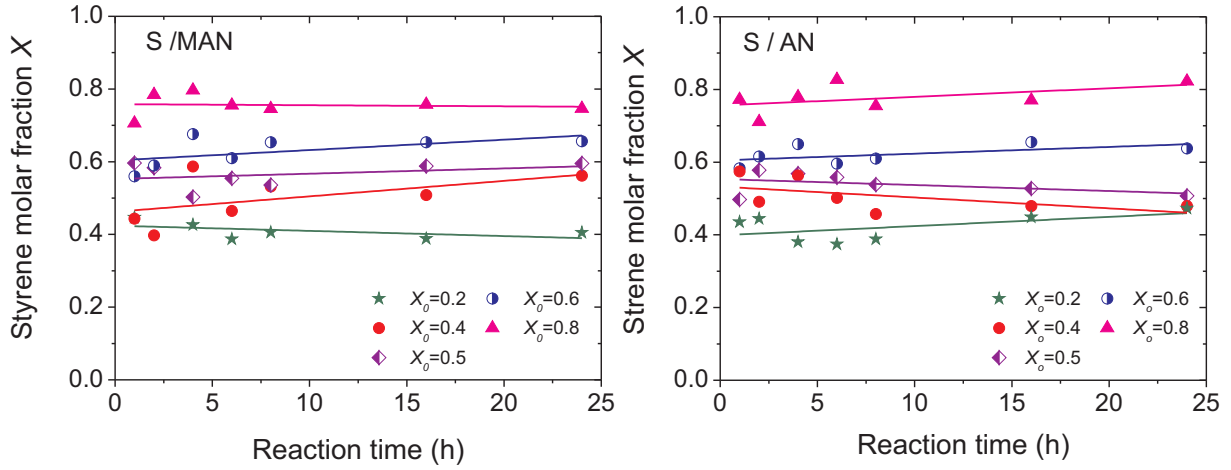
Figure 3.7: Variation of the styrene molar fraction in styrene / MAN and styrene /AN co-grafted films as a function of the grafting time. Composition was determined by FTIR analysis of the various grafted films.

In case of graft copolymerization, X is the molar fraction of styrene in the grafted chain. This relationship can also be expressed in term of molar fractions.

$$X = \frac{(r_A X_A + X_B) X_A}{(r_A X_A + X_B) X_A + (r_B X_B + X_A) X_B} \tag{3.6}$$

where A and B are the number of mol of styrene and the comonomer, and X_A and X_B are the mole fractions of the monomers A and B in the feed, in which the sum of the fractions is unity ($X_A + X_B = 1$). The reactivity ratios (r_A and r_B) are defined as the ratios of the rate constant for self-propagation and the rate constant for cross-propagation.

$$r_A = \frac{k_{AA}}{k_{AB}} \tag{3.7}$$

$$r_B = \frac{k_{BB}}{k_{BA}} \tag{3.8}$$

X_A is equal to styrene molar fraction in the grafting solution X_0 and Equation 3.6 can be expressed as

$$X = \frac{(r_A - 1)X_0^2 + X_0}{(r_A + r_B - 2)X_0^2 + (2 - 2r_B)X_0 + r_B} \tag{3.9}$$

Assuming that the system is supplied with excess monomers and no concentration change is observed throughout the polymerization process, the number of radicals generated is equal to the number of radicals consumed under steady-state conditions. This leads to

$$k_{AB} [A\cdot] [B] = k_{BA} [B\cdot] [A] \tag{3.10}$$

Applying the Mayo-Lewis model, the relation between styrene molar fraction in the film X can be correlated to that in the grafting solution X_0, as shown in Figure 3.8 for styrene / AN and styrene / MAN.
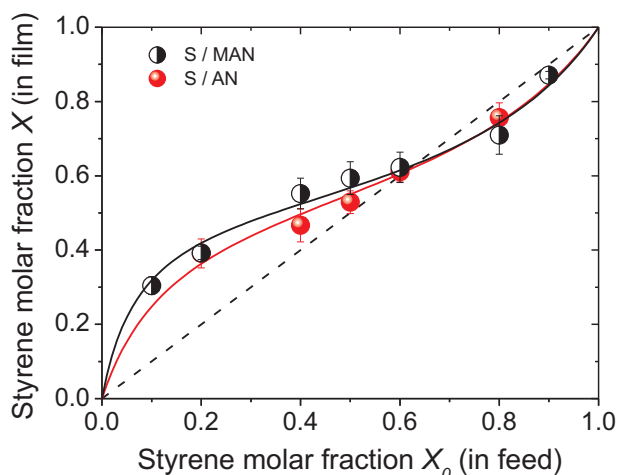
Figure 3.8: Mole fraction of styrene in the grafted film (X) versus mole fraction of styrene in the grafting solution (X_0). The curve is fitted via the weighted non-linear least squares method to determine the reactivity ratios. The graft levels of the films are approximately 40%.

On the left side of the diagram from X_0=0-0.6, the curve predicts that the styrene composition in the film is higher than in the feed, while the opposite is observed for X_0 >0.6. By carrying out a nonlinear fitting procedure, the reactivity ratios can be determined under the steady state assumption. The fitted curves of both systems are similar and the slight difference of the fitted curves is reflected in the reactivity ratios. For both monomer combinations, the reactivity ratios are lower than unity, indicating that the grafting of styrene / MAN and styrene / AN into ETFE shows a tendency of alternating chain formation, which is in agreement with data reported in the literature (Table 3.1). The obtained results are also supported by the feature of the copolymerization composition plot, which is typical for an alternating polymer. Factors such as solvent used, monomer diffusivity into the base film and swelling of base films also play a role in graft copolymerization [29, 43]. The monomer concentration at the grafting sites may vary from the monomer solution as grafting proceeds and the environment inside the polymer matrix may change with time. Furthermore, copolymer formation in the solvent-swollen polymer matrix leads to a change in viscosity, which can affect the monomer diffusion and hence influence the grafting rate [158]. This emphasizes that grafting is a highly complex process compared to bulk and solution polymerization. Under similar polymerization conditions, the reactivity ratios obtained from different research groups are largely in agreement. The most obvious difference in the reactivity ratios is found between grafted styrene / AN copolymer and bulk copolymerization, possibly because of the difficulty of AN to swell an AN-rich graft component.

Table 3.1: Comparison of the reactivity ratios of styrene and its comonomers obtained by various polymerization methods

System	Polymerization conditions	$r_{styrene}$	$r_{comonomer}$	Ref.
Styrene / AN	grafting into ETFE (60°C)	0.52±0.06	0.25±0.05	this study
	grafting into PET	0.05	0.04	[158]
	bulk (60°C)	0.40±0.05	0.04±0.04	[159]
	bulk (60°C)	0.41±0.08	0.04±0.04	[160]
	bulk (70°C)	0.41	0.04	[161]
Styrene / MAN	grafting into ETFE (60°C)	0.50±0.06	0.14±0.03	this study
	in benzene solution (60°C)	0.30±0.10	0.16±0.06	[162]
	in toluene solution (60°C)	0.39±0.07	0.32±0.05	[163]
	in benzyl alcohol solution (60°C)	0.40±0.02	0.16±0.07	[164]
	bulk (60°C)	0.30	0.27	[165]
	bulk (80°C)	0.25±0.02	0.25±0.02	[166]

3.2 Membrane characterization

3.2.1 FTIR analysis

The vital step in membrane preparation is the incorporation of proton conducting sites by sulfonation. Comparison of the FTIR spectra of grafted films (Figure 3.4) and membranes (Figure 3.9) shows some differences resulting from the incorporation of sulfonic acid groups. Although the absorption bands corresponding to the O=S=O vibration of the sulfonic acid group at 1024 cm^{-1} are not visible due to overlap with the ETFE peak, the appearance of a peak around 1412 cm^{-1}, which corresponds to the C=C para-disubstituted benzene vibration, can be observed, confirming the presence of the sulfonic acid group [167]. Although the membranes were exchanged into potassium form and analyzed in nominally dry state, it is unlikely that all water can be removed, especially the water in the first hydration shell, which is strongly bound to the sulfonate groups. The O-H stretching band of water (3000-3700 cm^{-1}) and water scissor vibration (around 1640 cm^{-1}) are clearly visible in the spectra of the membranes [168]. The water sorption in a polymer is thought to depend on the free volume fraction and the presence of a polar group that is capable of forming a hydrogen bond with water [169].

The FTIR spectra show an increase in intensity at around 1700 cm^{-1}, which is attributed to the presence of carbonyl groups. Probably, this is indicative of a hydrolytic process occurring
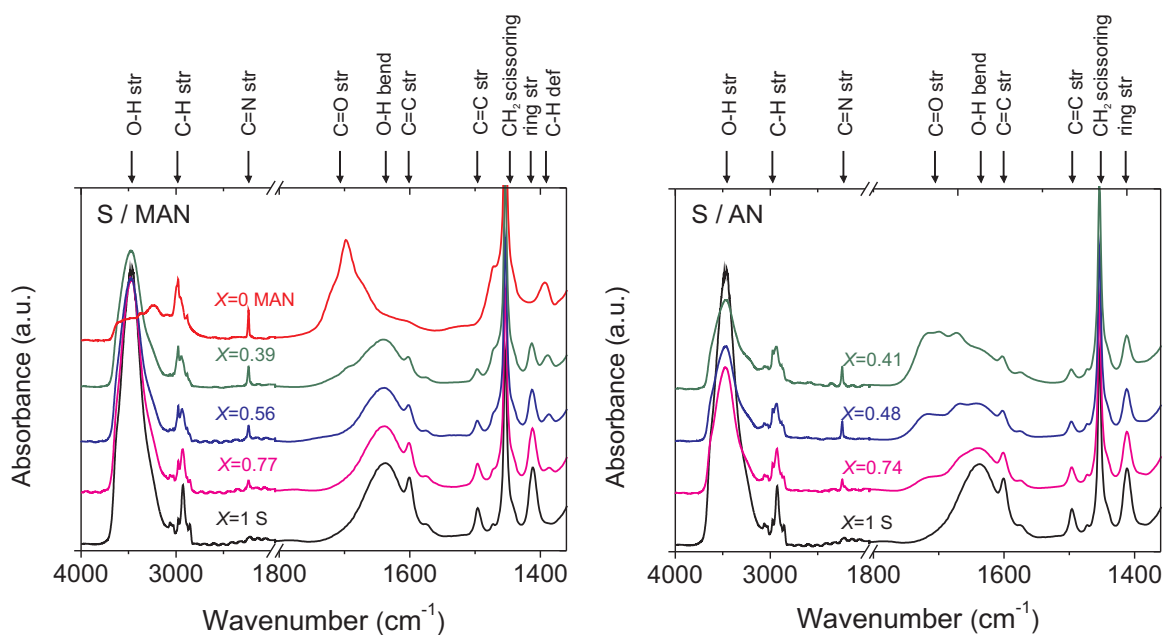
Figure 3.9: FTIR spectra of styrene / MAN and styrene / AN membranes after sulfonation to introduce proton conducting sites.
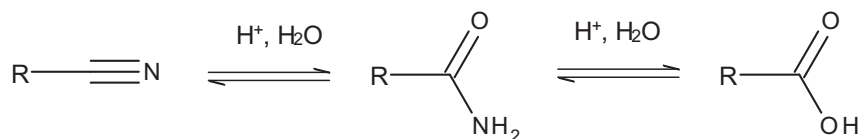
Figure 3.10: Simplified acid-catalyzed hydrolysis reaction of C≡N to form amide and carboxylic acid.

during the membrane preparation and the extent to which the hydrolysis of nitrile takes place correlates with the peak intensity. Membranes with different comonomer content vary markedly in their resistance to hydrolysis.

The hydrolysis of nitrile to amide and carboxylic acid is a nucleophilic addition reaction followed by nucleophilic acyl substitution reaction. In the first step of the acid catalyzed hydrolysis, the nitrogen of the cyano group is protonated to promote the attack of the carbon of the cyano group by water. The partial positive charge on the carbon of the cyano group causes the attack of cyano group by nucleophiles (such as water molecules), resulting in a product which is a protonated amide. The protonated amide can undergo further hydrolysis reaction to form carboxylic acid (Figure 3.10). Hydrolysis of the pure MAN grafted film is believed to occur mostly at the surface of the film because the grafted film does not swell in water. A small absorption band at 3500 cm^{-1}, which is characteristic for water, can be observed. The conversion of nitrile to hydrolyzed products contributes to a more hydrophilic film. The broad band at 1700 cm^{-1} could be assigned to the presence of cyclic dimer of carboxylic acid ($\sim$1700 cm^{-1}) carboxylic

59

acid ($\sim$1720 cm^{-1}) [170] and amide ($\sim$1672 cm^{-1}) (Figure 3.11). A trace of hydrolysis is found for the styrene / MAN membrane with X=0.39. However, with further increase in the styrene molar fraction, the carbonyl peak disappears. In comparison to styrene / MAN membranes, all styrene / AN membranes underwent hydrolysis and a broad carbonyl band at 1720-1600 cm^{-1} is clearly visible.
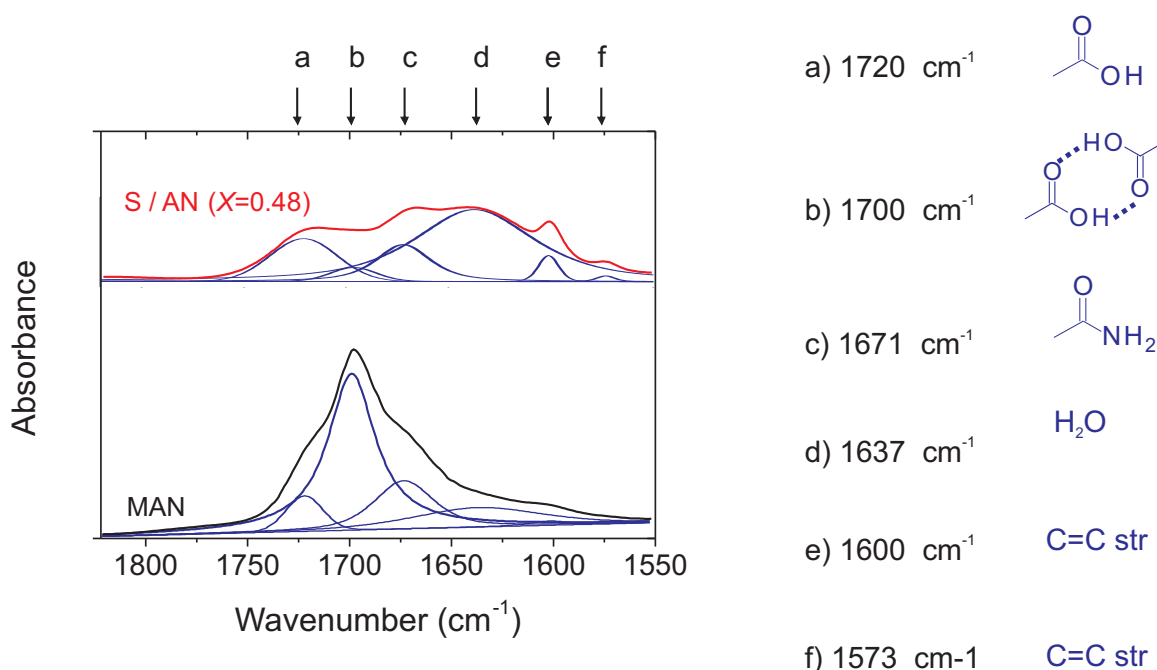
Figure 3.11: FTIR spectra in the carbonyl region of MAN grafted film and styrene / AN co-grafted membrane (X=0.48) after sulfonation.

The extent of nitrile hydrolysis due to sulfonation was determined by FTIR and elemental analysis (Figure 3.12). The precise extent of hydrolysis based on the intensity of the FTIR spectra is difficult to obtain, since the result is associated with high uncertainty of approximately 20%. Based on the intensity of the C≡N peak, the conversion of nitrile to amide of carboxylic is estimated to be 12% for the styrene / MAN membrane with X=0.39. The values are in agreement with the elemental analysis of the same membrane: assuming that the only product of hydrolysis is the carboxylic acid, 8% of nitrile units is hydrolyzed. In analogy, the extent of hydrolysis in styrene / AN membranes was investigated for membranes with different styrene molar fraction. The highest extent of hydrolysis (27%) is found for the S / AN membrane with the lowest investigated styrene content of X=0.41 by elemental analysis. The extent of hydrolysis was found to be lower for membranes with higher styrene content. For a comparable styrene molar fraction, styrene / AN membranes showed a much higher degree of hydrolysis compared to styrene / MAN membranes under the same conditions. This suggests that the presence of the
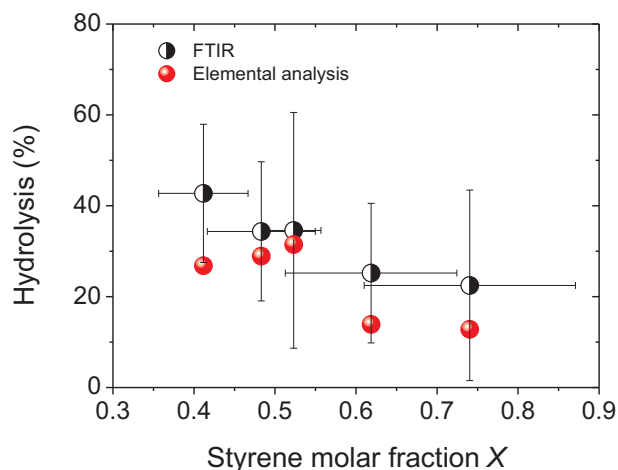
Figure 3.12: Extent of hydrolysis in styrene / AN membranes (GL $\sim$ 40%) with varying monomer content determined by FTIR and elemental analysis.

α-methyl group of MAN significantly decreases the susceptibility to hydrolysis and the reactivity of the nitrile toward hydrolysis can be modified by the substituent at the α-position. The methyl substituent is more electron donating compared to a hydrogen, thereby making the carbon of the nitrile less reactive toward nucleophilic attack by the water molecule compared to that of AN. The presence of α-methyl of methylmethacrylate in the polymer or copolymer with styrene also offers higher resistance to hydrolysis compared to the methyl acrylate analog [171].

The inductive effect of the α-methyl group is also evidenced in the position of the nitrile peak in the FTIR spectra [172]. The stretching frequency of the nitrile peak of MAN and AN was observed at 2234 cm^{-1} and 2241 cm^{-1}, respectively. This difference implies that the C$\equiv$N bond of AN is stronger than that of MAN. The strength of the bond is associated with the bond order between carbon and nitrogen atoms. Considering the difference in electronegativity between carbon and nitrogen, a dipolar resonance form with negative charge on nitrogen and positive charge on carbon can be represented (Figure 3.13). As a consequence, the real structure is between the two resonance structures and the bond is between a double and a triple bond. When the methyl at the α-position donates electrons to the carbon of the cyano group, the carbon becomes less partially positive, which results in a more stable double bond structure. The inductive electron donating effect results in a red shift of the C$\equiv$N bond by 7 cm^{-1} compared to that of AN.
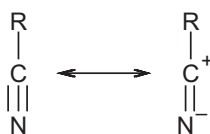
Figure 3.13: Resonance structures of nitrile compound.

3.2.2 Fuel cell relevant properties

To determine the effect of the α-methyl group on the fuel cell relevant properties, a comparison of ion exchange capacity (IEC), water uptake, dimensional stability and proton conductivity was carried out based on styrene / MAN and styrene / AN co-grafted membranes (GL~40%). The ion exchange capacity (IEC) is quantified by the amount of acid (sulfonic acid in this case) per unit mass or volume of water swollen membrane. We used the mass based IEC and the theoretical IEC to determine the degree of sulfonation, which turned out to be more than 95% for styrene / MAN as well as styrene / AN membranes (Figure 3.14). Considering the different densities of the grafted membranes and Nafion, the volumetric IEC (IEC_v) is introduced here to compare styrene / MAN and styrene / AN membranes with the standard Nafion® 212 membrane.

$$IEC_v = \frac{n(H^+)}{V} \tag{3.11}$$

in which, $n(H^+)$ is the number of mol of protons and V is the volume of fully swollen membrane.
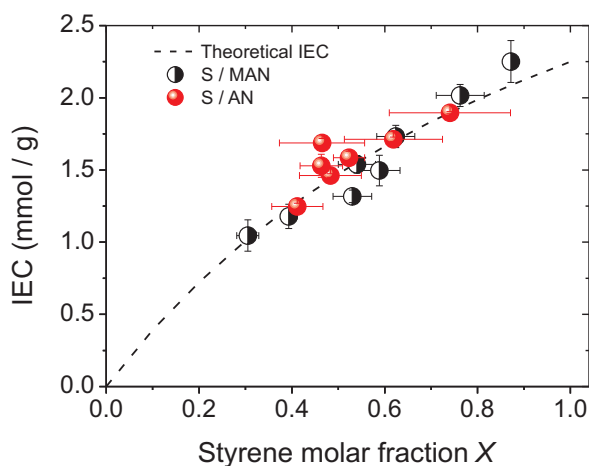
Figure 3.14: Comparison between the ion exchange capacity (IEC) of styrene / MAN and styrene / AN membranes (GL $\sim$ 40%) and the theoretical IEC assuming that each styrene unit carries one sulfonic acid group.

Figure 3.15 shows the relationship between the fuel cell relevant properties and the styrene content in the grafts for membranes with a graft level around 40%. Evidently, the volumetric IEC of both co-grafted membranes increases with the molar fraction of styrene in the grafted component (X). Despite a difference in the molar mass and the susceptibility of nitrile to hydrolysis, which can further increase the water uptake and hence membrane expansion, the volumetric IEC of styrene / MAN and styrene / AN membranes at a given X are comparable.

The water uptake can be measured from the weight change between the dry and water swollen state of the membranes. Although there is no significant effect in the swelling of the
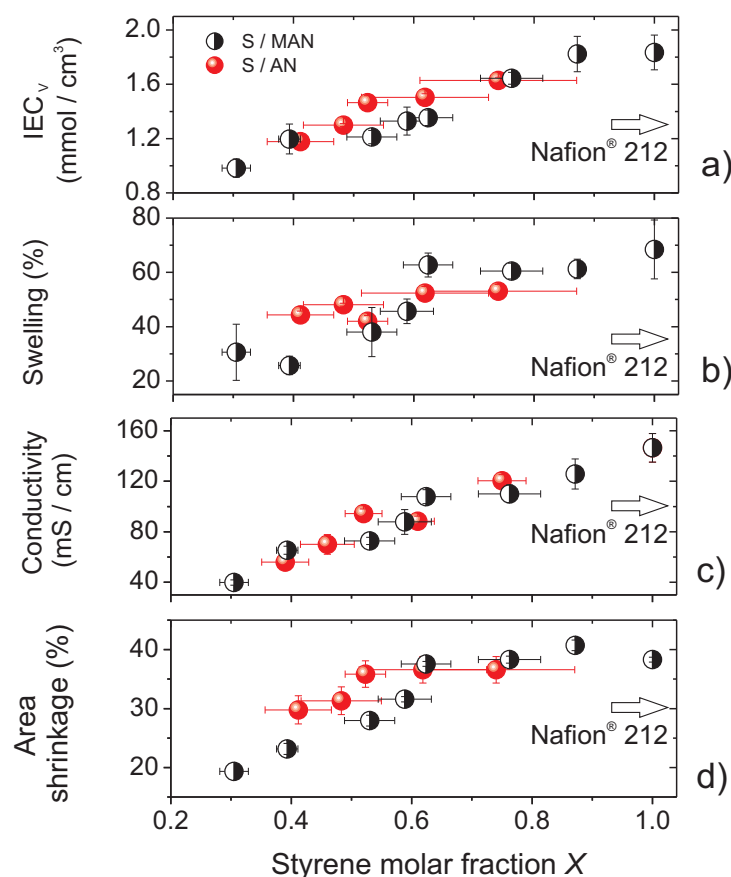
Figure 3.15: *Ex situ* fuel cell relevant properties of styrene / MAN and styrene / AN grafted ETFE based membranes with a graft level of around 40% as function of the styrene molar fraction. a) Volumetric ion exchange capacity (IEC_v), b) Swelling, c) Through-plane conductivity measured in fully swollen state at RT and d) Area shrinkage.

membrane due to the presence of the α-methyl group, we can observe a slight difference in the membrane swelling as a function of the styrene molar fraction. Styrene / MAN membranes show a more pronounced swelling with increasing styrene molar fraction up to X=0.6. A similar trend observed for the water uptake is confirmed by the area shrinkage (wet to dry).

The proton conductivity is predominantly influenced by the water uptake and proton concentration. An increase in the volumetric IEC leads to enhanced proton conductivity in the water swollen state. At comparable volumetric IEC, styrene / MAN and styrene / AN membranes exhibit comparable proton conductivity. The carboxylic acid, a possible result of nitrile hydrolysis, does not contribute to the proton concentration because the acid strength is too weak (pKa $\sim$2-3) [39] compared to the pH in the membrane environment (pH <2). In addition, an increased water uptake of styrene / AN membranes also does not lead to higher proton conductivity. The proton conductivity of the co-grafted membranes is comparable to that of the Nafion® 212 membrane.

3.3 Fuel cell experiment

3.3.1 Fuel cell performance

Despite the notable difference in the extent of nitrile hydrolysis, the *ex situ* properties of styrene / MAN and styrene / AN membranes are quite similar. Such membranes hold some promise in fuel cell application because of their high proton conductivity in water swollen state comparable to that of Nafion. However, it is questioned whether these membranes meet the fuel cell requirements in terms of performance and durability. We carried out preliminary fuel cell experiments using styrene / MAN and styrene / AN co-grafted membranes (X=0.6, GL=40%) and compared with a standard MEA containing a Nafion$^{®}$ 212 membrane. In water swollen state, proton conductivity and volumetric IEC of these membranes are comparable.

The polarization experiments were carried out after conditioning at a current density of 500 mA cm^{-2} to obtain a stable performance. Figure 3.16 shows the polarization curves of the MEAs comprising styrene / MAN and styrene / AN membranes and Nafion$^{®}$ 212. The MEA based on the styrene / MAN co-grafted membrane shows comparable performance to that of the Nafion$^{®}$ 212 membrane, whereas the MEA based on the styrene / AN co-grafted membrane shows lower performance after only 24 hours of operation. The origin for this observation is probably degradation of the styrene / AN membrane, which is supported by a higher rate of HFR increase during cell conditioning compared to that of the styrene / MAN membrane. Degradation of the membrane leads to the loss of ionomer as well as decrease in MEA mechanical integrity. Possibly, the presence of hydrolyzed products leads to inferior lamination quality between the membrane and electrode.

In addition to the fuel cell performance, the hydrogen crossover was evaluated to characterize the mechanical integrity of the MEA [51, 56, 142, 173]. The thicknesses of all the co-grafted membranes are similar and about 1.5 times thinner than Nafion$^{®}$ 212. Yet, the crossover of Nafion$^{®}$ 212 is higher than that of the styrene / AN and styrene / MAN membrane, respectively. In Nafion membranes, the gases permeate through the amorphous phase of the hydrophobic PTFE backbone [174, 175]. This might also be the case for the grafted membranes, in which hydrogen permeates through the amorphous region of ETFE. Possibly, crystallinity of the membranes may be associated with the gas permeability since the crystalline domains exhibit gas barrier properties [176]. The crystallinity of styrene / MAN membranes determined by DSC is approximately 20-25% [177], whereas that of Nafion determined by wide angle X-ray diffraction (WAXD) is around 14-16% [178, 179]. Higher crystallinity of the grafted membranes is likely to suppress the gas crossover. Among the grafted membranes, a possible explanation for higher hydrogen crossover of styrene / AN membranes could be the loss of gas barrier properties of nitrile associated with hydrolysis and membrane degradation during 24 hours conditioning.
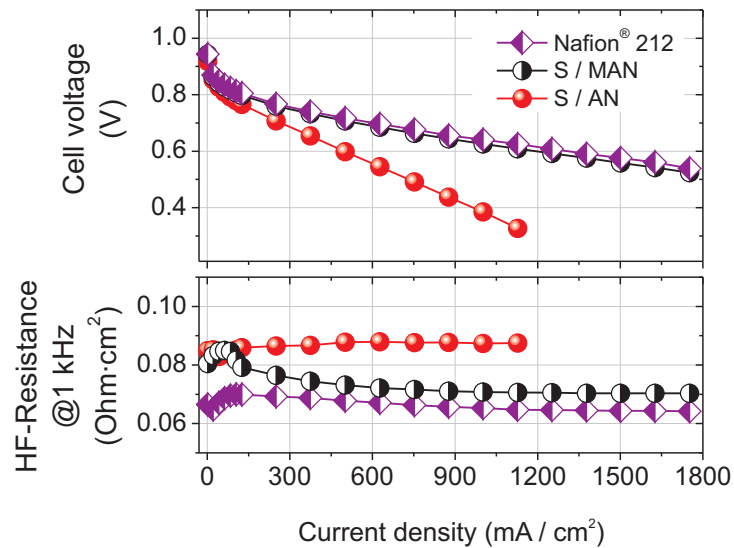
Figure 3.16: Polarization curves of MEAs based on ETFE-*g*-styrene / MAN, ETFE-*g*-styrene / AN based membranes and Nafion® 212 at a cell temperature of 80°C; H_2 / O_2 (1.5 bar_a / 2.0 bar_a) and full humidification at 80°C. High frequency resistance (HFR) measured at 1 kHz for MEAs assembled using JM electrodes (0.4 mg Pt cm^{-2}). The experiments were carried out in collaboration with Dr. H. Ben youcef.

To elucidate the origin of the performance loss, electrochemical impedance spectroscopy (EIS) measurements were performed at 500 mA cm^{-2} (Figure 3.17). The interfacial resistances obtained from the EIS were comparable for the MEAs of styrene / MAN and Nafion® 212, whereas a much higher value was measured in case of the styrene / AN membrane. This suggests that the styrene / AN membrane is less compatible with the ionomer in the electrode compared to the styrene / MAN membrane. Therefore, styrene / AN membranes shows a higher performance loss. In addition, the ohmic resistance of the styrene / AN membrane is slightly higher than that of the other two membranes. Table 3.2 summarizes the results obtained from the *in situ* fuel cell experiments.

Table 3.2: MEA performance characteristics from fuel cell test data of styrene / MAN and styrene / AN co-grafted membranes after 24 hours operating time compared to that of Nafion® 212 membrane.

Membrane	Graft level (%)	Composition of grafts X	Ohmic resistance (mΩ·cm²)	Polarization resistance (mΩ·cm²)	H_2 crossover (mA·cm⁻2)
Nafion® 212	-	-	59	146	0.64
S / MAN	40	0.62±0.04	54	133	0.24
S / AN	40	0.62±0.11	67	534	0.45
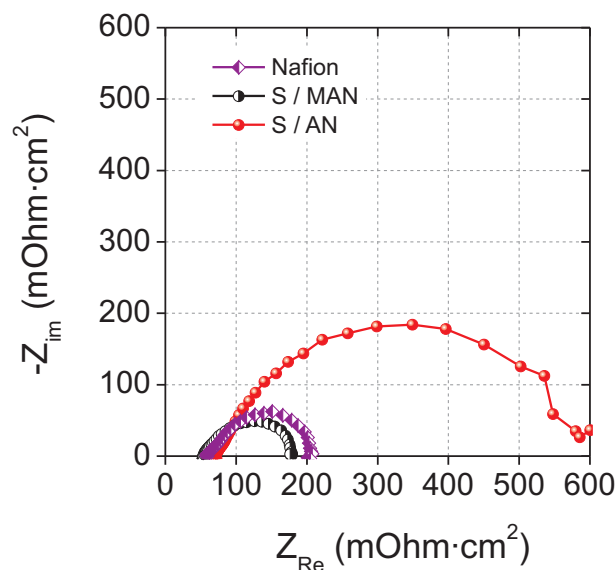
Figure 3.17: AC impedance spectra of MEAs (composing of different membranes) recorded at a constant current of 500 mA·cm^{-2}. The applied frequency range is between 0.1-25 kHz.

3.3.2 Accelerated stress test

In an accelerated stress test, the membrane is subjected to an aggressive environment to accelerate degradation [38]. Membrane degradation is a consequence of the interaction of H_2 and O_2 in the presence of catalyst, leading to polymer attack by radical species, such as HO·, which can result in chain scission (subsubsection 1.4.3.2). The criteria used in the assessment of membrane degradation are concerned with the change in its chemical properties, loss of proton conducting sites and mechanical integrity. These phenomena can be followed by different techniques; spectroscopically in case of the *post mortem* analysis or electrochemically for measuring H_2 crossover. Depending on the degradation mechanism of the membrane, the characterization methods should be well selected. For example, investigation of Nafion degradation has been traditionally carried out by measuring the rate of fluoride emission in the product water [7, 50, 55, 56]. However, this method would not be suitable for radiation grafted membranes containing styrene sulfonic acid groups, since degradation of this membrane type involves loss of styrene sulfonic acids and decomposition products of the comonomer. Therefore, monitoring the change in the loss of sulfonic acid groups in case of radiation grafted membranes is particularly more useful. Büchi *et al.* applied high performance liquid chromatography (HPLC) to analyze the product water of fuel cells comprising radiation grafted membranes, in which monomeric residues were found as a result of ionomer degradation [61].

To evaluate the durability of membranes, accelerated degradation tests at open circuit voltage (OCV) were carried out using cell design 2 (subsection 2.3.1). The decomposition of styrene sulfonic acid can be monitored by an increase in the high frequency resistance. Styrene / MAN

66

and styrene / AN co-grafted membranes with $X \sim 0.5$ (40% graft level) were used without impregnation. Comparison of the open circuit voltage and high frequency resistance (HFR) for MAN and AN containing membranes with similar IEC are shown in Figure 3.18. In the beginning of the test both types of membrane show a dramatic drop in cell voltage, which stabilizes afterwards. Substantial voltage loss in the beginning of OCV hold is a common phenomenon and is usually observed [180, 181]. This loss could be explained by the formation of platinum oxides on the positive electrode. This phenomenon occurs when the electrode potential exceeds the onset potential of platinum oxidation (Equation 3.12 at 0.98 V and Equation 3.13 at 0.88 V). Since the PtO and Pt(OH)$_2$ formation occurs in the range of the OCV values, platinum oxides on the platinum surface can be expected, developing a mixed potential that lowers the OCV accordingly [182].

$$Pt + H_2O \rightleftharpoons PtO + 2H^+ + 2e^- \tag{3.12}$$

$$Pt + 2H_2O \rightleftharpoons Pt(OH)_2 + 2H^+ + 2e^- \tag{3.13}$$
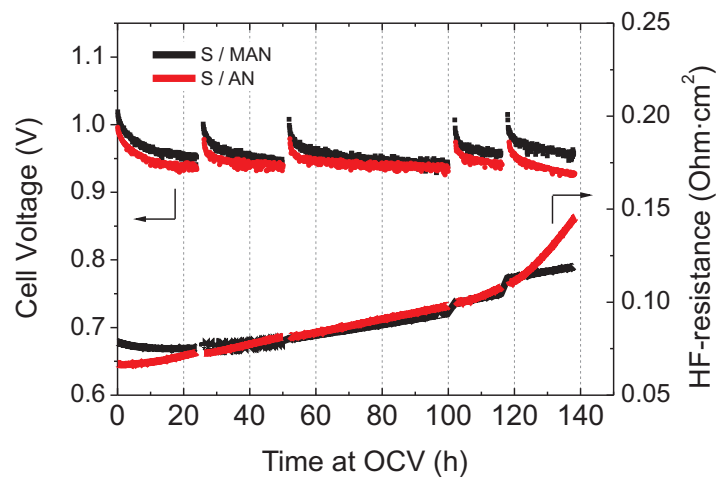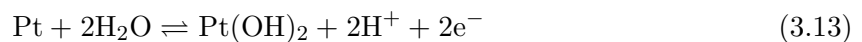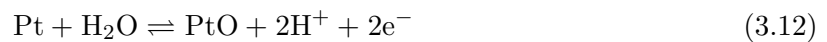
Figure 3.18: Evolution of cell voltage and membrane resistance during an accelerated stressed test of styrene / MAN and styrene / AN co-grafted membrane. The fuel cells were operated under OCV conditions (H$_2$ / O$_2$, 2.5 bar$_a$, 80°C and full humidification). The experiments were carried out in collaboration with Z. Zhang.

The rate of membrane degradation corresponds to the slope of the ohmic resistance. Despite the differences in the nature of the comonomer and extent of hydrolysis, both types of membrane perform quite similar and show a steady increase in ohmic resistance up to $\sim$120 hours (Figure 3.18). After that, there appears to be distinct differences in the extent of degradation between styrene / MAN and styrene / AN co-grafted membranes as observed from an increase in the HFR rate, indicating accelerated membrane degradation in the styrene / AN membrane.

3. EFFECT OF THE α-METHYL GROUP OF MAN

Figure 3.19 shows comparison of H_2 crossover rate of both membrane types. An increase in hydrogen crossover rate corresponds reasonably well with the increase in HFR. The lowest hydrogen crossover current density is found for the pristine membranes and gradually increases with continuing membrane degradation. Since hydrogen crossover and membrane degradation are mutually influential, an increase in hydrogen crossover of the styrene / AN membrane may lead to a higher membrane degradation rate that is observed as an increasing ohmic resistance, and vice versa. In addition, the higher crossover of the styrene / AN membrane comprises an additional contribution to higher cell voltage loss by creating a mixed potential at the electrode compared to its MAN counterpart.
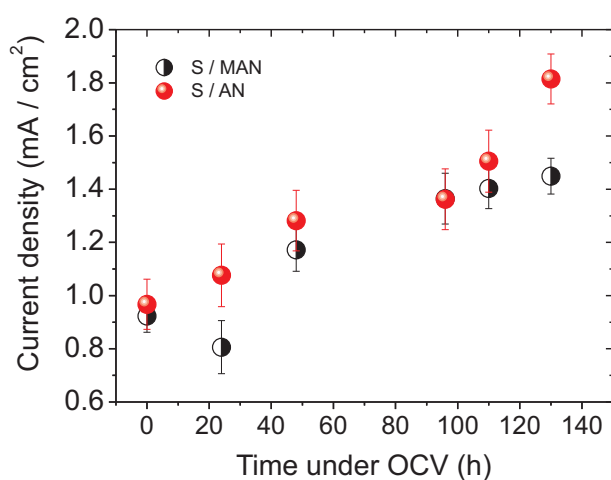
Figure 3.19: H_2 crossover current density of styrene / MAN and styrene / AN co-grafted membranes under OCV conditions (H_2 / O_2, 2.5 bar$_a$, 80°C and full humidification). The experiments were carried out in collaboration with Z. Zhang.

To obtain further insight in membrane degradation, styrene / AN membranes prepared in the same batch were used to investigate the durability of hydrolyzed membranes compared to pristine ones. One styrene / AN membrane was subjected to *in situ* hydrolysis under fully humidified H_2 / N_2 atmosphere at 80°C for 336 h to hydrolyze the nitrile units. The chemical changes were analyzed by FTIR spectroscopy.

It was found that 75% of the nitrile units was lost during the *in situ* hydrolysis treatment, whereas less than 10% of styrene units were degraded. A pristine membrane was hydrolyzed and a subsequent membrane accelerated stress test was performed in an OCV test for 72 hours. For comparison, another OCV test using a styrene / AN membrane without any pretreatment except for conditioning at 500 mA cm^{-2} for approximately 20 hours under H_2 / O_2 was performed. The high frequency resistance (HFR) of the pre-hydrolyzed membrane increased progressively after a few hours under OCV conditions (Figure 3.20), whereas the HFR of the pristine styrene / AN membrane is fairly stable.
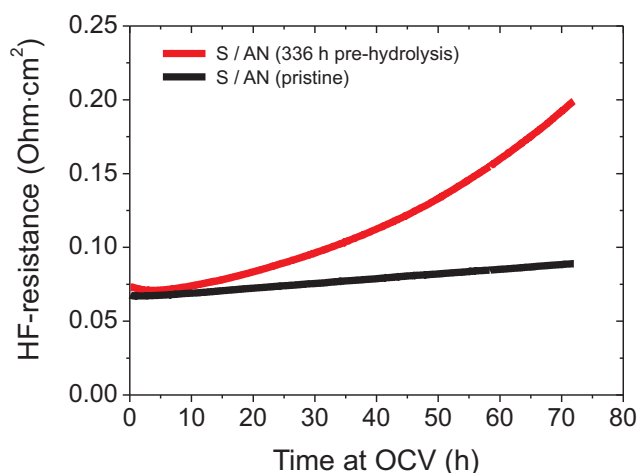
Figure 3.20: High frequency resistance (HFR) measured at 1kHz during the OCV test (H_2 / O_2, 2.5 bar$_a$, 80°C and full humidification) of a pristine and pre-hydrolyzed styrene / AN membrane, respectively. The experiments were carried out in collaboration with Z. Zhang.

It is observed that substitution of nitrile with its hydrolyzed products leads to a significant increase of the rate of membrane degradation. This finding probably explains the results found in Figure 3.18, in which the HFR of the styrene / MAN and styrene / AN membranes are comparable for 130 hours under OCV, at which point the HFR of the styrene / AN membrane starts to increase more rapidly. The primary reason for the premature failure of the styrene / AN membrane is likely to be the loss of nitrile functionality by the hydrolytic process. Yet, the exact degradation mechanism is unknown but of utmost importance to be further investigated to understand the stabilizing effect of nitrile containing membranes.

The difference between the fuel cell properties of styrene / AN and styrene / MAN membranes is likely an effect of the intrinsic properties, since the thickness of both co-grafted membranes is comparable. This considerable change in HFR and hydrogen crossover rate suggests that the type of a comonomer strongly influences the membrane durability. Comparison between gas permeability (O_2, CO_2, N_2 and H_2O vapor) of styrene / MAN and styrene / AN copolymers and the effect on the permeability with varying composition has been reported in the literature [148]. It was found that the increase of nitrile content in the polymer composition reduces the permeability of gases in both systems. The differences between the membrane properties and their degradation during the accelerated stress test can be associated with the loss of nitrile groups by polymer chain degradation due to the attack of radicals or as a consequence of nitrile hydrolysis. To elucidate the effect of hydrolysis, *in situ* hydrolysis of styrene / AN and styrene / MAN is further investigated.

69

3.3.3 *In situ* hydrolysis

A major drawback of the fuel cell experiment is that the effect of membrane degradation and nitrile hydrolysis cannot be separated. To further advance the understanding of the effect of hydrolysis on the durability of the fuel cell, we carried out an *in situ* hydrolysis test in a single cell fixture at 90°C (cell design 3, subsection 2.3.1), yet with fully humidified N_2 on both sides to exclude the effect of the ionomer loss due to the formation of OH· in the presence of H_2 and O_2 [48, 62, 64]. *In situ* H_2 crossover is measured by electrochemical means in H_2 / N_2 mode. Styrene / MAN and styrene / AN co-grafted membranes with $X \sim 0.5$ (40% graft level) were used without impregnation. During the course of the *in situ* hydrolysis experiment, no observable changes in membrane resistance and hydrogen crossover were found (Figure 3.21). This observation may imply that there is no significant change in the composition and morphology of the co-grafted membranes as a result of hydrolysis in the water saturated state. Hydrolysis of nitrile does not lead to an increase in HFR and H_2 crossover of the styrene / AN membrane during the fuel cell test.
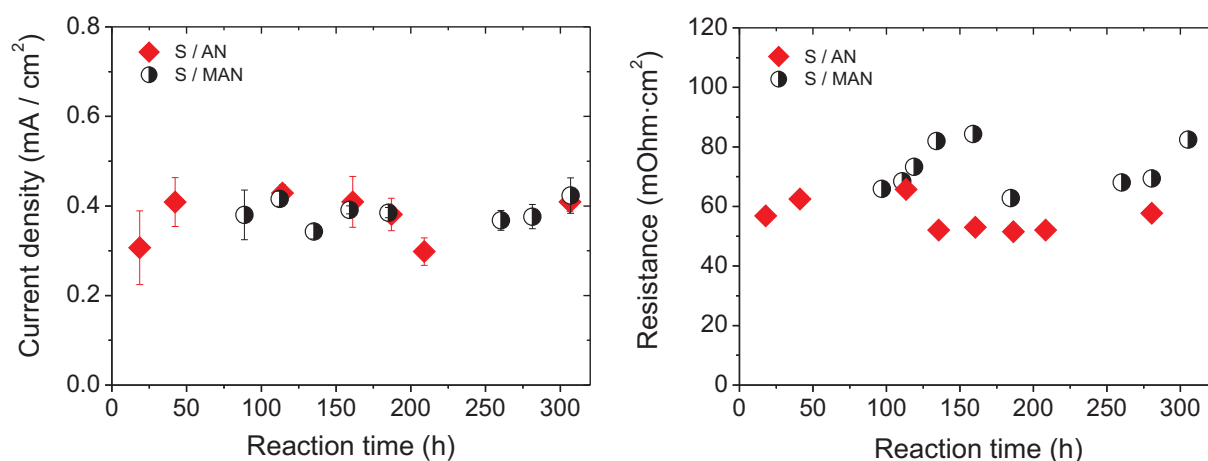
Figure 3.21: H_2 crossover current density (left) and membrane resistance (right) of styrene / MAN and styrene / AN co-grafted membranes with $X \sim 0.5$ measured under fully humidified H_2 / N_2 mode at 90°C and 1 bar$_a$ during the *in situ* hydrolysis experiment.

After the test, the MEAs were disassembled and the composition of the membranes was determined by FTIR spectroscopy (Figure 3.22). The spectra clearly indicate the change in membrane functionalities, with the most noticeable change in the carbonyl region (1700 cm^{-1}). Increase in absorbance in this range implies a further progressing of hydrolysis. In addition, the increase of the broad band intensity around 2500 cm^{-1} and 3200 cm^{-1} (which are characteristic for OH stretching of carboxylic acid and NH stretching of amide, respectively) also indicate that more hydrolysis products were formed.
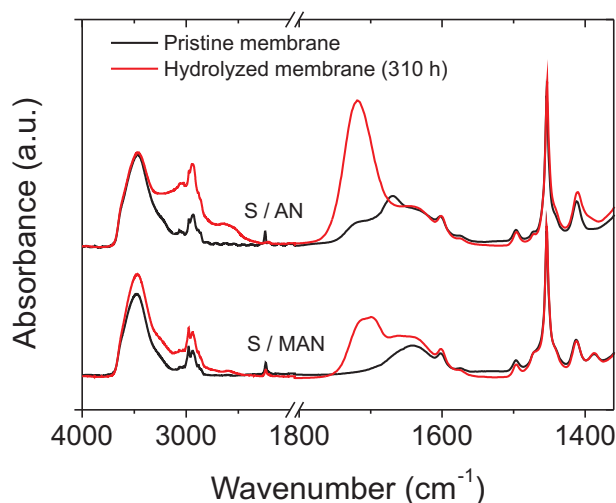
Figure 3.22: Comparison of the FTIR spectra of styrene / MAN and styrene / AN co-grafted membranes with $X \sim 0.5$ before and after *in situ* hydrolysis (total $\sim$310 hours under fully humidified N_2 environment at 90°C and 1 bar$_a$.

Based on the FTIR spectra, the influence of the α-substitution of the nitrile containing comonomers on susceptibility to hydrolysis is further investigated. The nitrile groups of both MAN and AN continue to hydrolyze in fully humidified N_2 atmosphere. However, the styrene / AN membrane is much more sensitive to hydrolysis compared to the styrene / MAN membrane and thus completely hydrolyzed, while only 36±13% of MAN is hydrolyzed after approximately 310 hours under the tested conditions. Therefore, the α-methyl group of MAN significantly inhibits the rate of membrane hydrolysis. In addition, there is no loss of styrene found during the test.

3.3.4 Effect of hydrolysis on fuel cell performance

To investigate the effect of hydrolysis on fuel cell performance, styrene / AN membranes were chosen since they underwent complete hydrolysis during the *in situ* hydrolysis experiment. The performance of the membranes was investigated *in situ*. Membrane degradation during the test is our main concern because the polarization curve is collected in H_2 / O_2 environment, under which radicals can be generated in the presence of catalyst, thereby initiating chemical degradation of the membrane in PEFC.

Prior to the polarization experiment, the fuel cell was exposed to N_2 / N_2 at 90°C for 20 hours similar to the *in situ* hydrolysis experiment and switched to H_2 / O_2 at 60°C for 1 hour to record the fuel cell performance at the beginning of hydrolysis. Then, the fuel cell is exposed to N_2 / N_2 at 90°C before recording the second performance curve at the end of hydrolysis experiment under H_2 / O_2 at 60°C (315 hours total).

71

3. EFFECT OF THE α-METHYL GROUP OF MAN

Figure 3.23 shows the comparison between the fuel cell performance of styrene / AN membrane at the beginning and end of hydrolysis test. A noticeable change was observed in the intermediate current density region, which is governed by the membrane resistance, and at high current density.
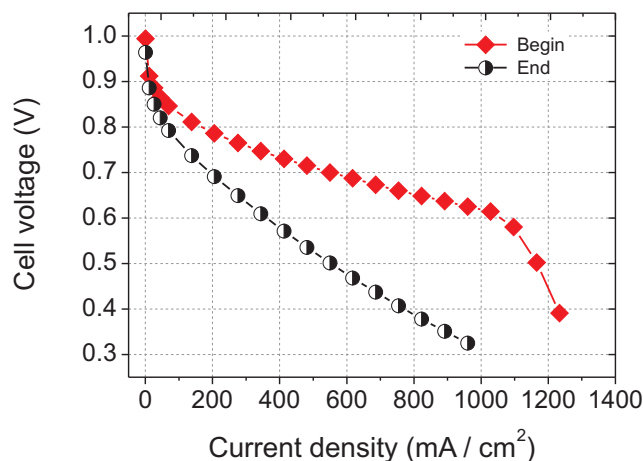
Figure 3.23: Polarization curves of styrene / AN co-grafted membranes at the beginning (29 h) and end of the hydrolysis test (315 h) at a cell temperature of 60°C; H_2 / O_2, 1 bar$_a$ and full humidification.

In addition to the polarization curves, hydrogen permeation and electrochemical impedance spectroscopy (EIS) measurements were carried out to monitor the state of health of the membrane and electrode. A depressed semicircle as shown in Figure 3.24 is generally observed in fuel cell operating on H_2 / O_2 without significant mass transport limitations. The high frequency intercept is mainly determined by the membrane resistance and indicates the loss of proton conductivity, increases from 66 to 147 mOhm cm^2 at the end of hydrolysis experiment. Since the fuel cell is operated under fully humidified condition, membrane drying is unlikely. The increase in ohmic resistance is most likely a result of the degradation of grafts in the membrane and cation contamination as a result of electrode degradation.

The diameter of the distorted semicircle is attributed to the polarization resistance, which increases at the end of test. This increase may be attributed to cumulative effects of different phenomena, e.g., increased apparent charge transfer resistance, mass transport limitations across the ionomer covering the platinum catalyst, and the change of the membrane / electrode interface. Similarly, an increase in polarization resistance has also been observed as a result of catalyst degradation due to start / stop phenomena [183].

The change in the electrochemical surface area (ECSA) is clearly evidenced from the CV and CO stripping experiments (Figure 3.25). The integrated area under the peak near 0.6 V is attributed to CO electrooxidation on the electrode, which corresponds to the ECSA (assuming a specific charge of 420 μC cm^{-2}). After the test, the ECSA is reduced by 27%. In addition, the
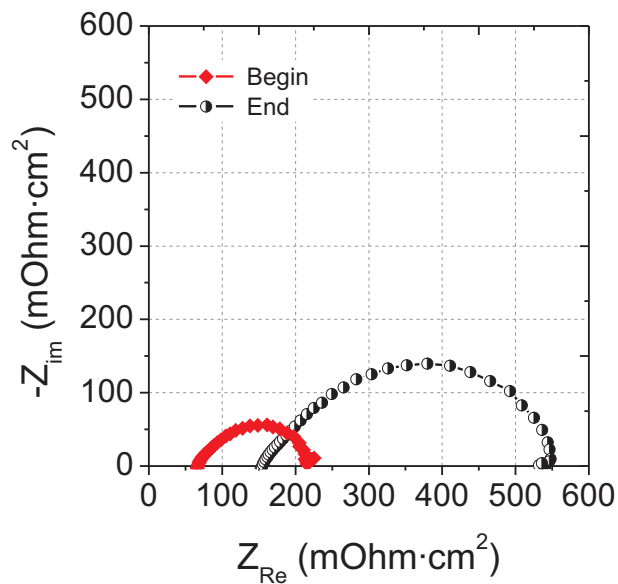
Figure 3.24: AC impedance spectra of an MEA composing of styrene / AN co-grafted membranes recorded at the beginning (29 h) and end of the hydrolysis test (315 h) at constant current of 500 mA·cm^{-2}. The applied frequency range is between 0.1-25 kHz.

peak also shifts slightly to lower potential at the end of the test. According to literature, this is a result of larger platinum particle size [147]. This loss of ECSA implies that the platinum particles are agglomerated. This result is in agreement with the increased polarization resistance as seen in the impedance spectra and the loss of fuel cell performance at the end of the test.
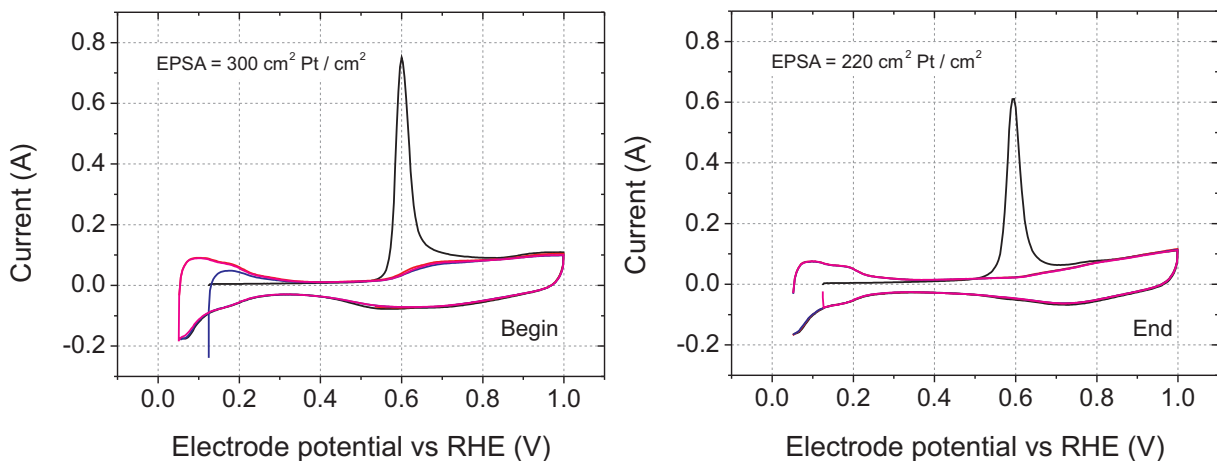
Figure 3.25: CO stripping voltammetry of Pt / carbon electrode (JM ELE162, 0.4 mg Pt / cm^2) before and after the hydrolysis experiments (scan rate 10 mV s^{-1}). The geometrical surface area of the electrodes is 29 cm^2.

As membrane degradation was not observed during the hydrolysis experiment under N$_2$ / N$_2$ atmosphere (Figure 3.21), this emphasizes that an exposure to H$_2$ / O$_2$ even for a short time during the polarization experiment is detrimental to the membrane in the long term. Formation

of H_2O_2 is likely to occur due to gas crossover when the cell is exposed to H_2 / O_2 during the first polarization experiment. When the cell is switched to N_2 / N_2 mode, H_2O_2 can diffuse and still react with the ionic contaminants in the membrane to form OH· radicals. Catalyst degradation may cause platinum dissolution and re-precipitation in the membrane, serving as catalyst for the Fenton reaction. The generated radicals continue to damage the membranes during the progress of hydrolysis under N_2 / N_2, leading to chain scission. The FTIR analysis confirmed that substantial membrane degradation took place during the experiment, in which 84±6% of styrene is decomposed.

Although the membrane started to deteriorate already after the first exposure to H_2 / O_2 and continued to degrade during the hydrolysis experiment, the membrane resistance is rather stable. This implies that there is no severe graft loss before the second exposure to H_2 / O_2 and most of the degraded chain fragments remained entangled in the polymer matrix during the hydrolysis step. During the second exposure to H_2 / O_2, liquid water is produced during the fuel cell operation. This water may be responsible for the graft loss by dissolving the degraded chains and removing them from the polymer matrix, resulting in an increase in membrane resistance (Figure 3.24). The same reasoning may also be put forward regarding the constant hydrogen permeation rate measured during the experiment. Although hydrogen crossover was not measured after the second exposure to H_2 / O_2, the loss of OCV (30 mV) at the end of the test may indicate a higher gas crossover rate.

The results show the limitation of this testing protocol, in which the long term experiment can lead to deterioration of the electrode component. Furthermore, exposure of membranes to H_2 / O_2 for a short time initiates membrane degradation, which continues to occur in N_2 / N_2 atmosphere. Therefore, the performance of the MEA before and after the test cannot be directly compared.

3.4   Conclusions

The effect of the substituent at the α-position of MAN as styrene's comonomer has been investigated using styrene / MAN and styrene / AN co-grafted membranes as model compounds. Co-grafting of styrene with MAN and AN exhibits copolymers with a tendency to alternating monomer sequence. During sulfonation and fuel cell operation, the nitrile group can undergo acid catalyzed hydrolysis, leading to the formation of amide and carboxylic acid. This process is, however, not detrimental to the membrane since the nitrile is not part of the polymer backbone.

Under the same condition, styrene / MAN membranes are more resistant to hydrolysis than styrene / AN membranes, because of the methyl substituent at the α-position and its electron donating nature, which inhibits the nucleophilic attack by water molecules. Ion exchange capacity, water uptake, dimensional stability and proton conductivity in water swollen state of

partially hydrolyzed styrene / AN membranes are comparable to those of styrene / MAN membranes. It was demonstrated based on a hydrolysis experiment in a single cell fixture under inert conditions that during the progress of hydrolysis, hydrogen crossover and membrane resistance remained approximately constant. Yet, the MEA with a partially hydrolyzed styrene / AN membrane displayed inferior fuel cell performance and durability compared styrene / MAN membrane at comparable ion exchange capacity. The reasons for the higher performance loss in case of the partially hydrolyzed styrene / AN membrane could be the poorer membrane / electrode interface, possibly resulting from nitrile hydrolysis and membrane degradation.

To obtain further insight into the stability of membranes, OCV tests were carried out. Hydrogen crossover and ohmic resistance, which are indicators of the membrane's state-of-health, were measured. The increase rate in ohmic resistance agreed with the hydrogen crossover results. Degradation of styrene / MAN and styrene / AN was found to be similar up to ~ 120 hours, after which degradation of styrene / AN is enhanced. Since nitrile groups may play a role in inhibiting gas permeation rate, accelerated degradation of styrene / AN after ~ 120 hours might be due to the loss of nitrile functionality, either by loss of grafts or hydrolysis. The presence of an α-methyl group of MAN reduces the extent of nitrile hydrolysis during membrane preparation and fuel cell test.

4

Structure-property correlations

For the application in the fuel cell, radiation grafted membranes may be prepared using styrene and MAN as comonomers to improve membrane durability [104]. Little is known to date concerning how incorporation of MAN affects the fuel cell relevant properties. As discussed in chapter 3, MAN can undergo hydrolysis during membrane preparation and fuel cell operation, which leads to the loss of the nitrile functionality and can have an impact on the performance, water uptake and durability of the membrane. Therefore, the balance between performance and durability with respect to the monomer composition needs to be optimized.

As a key component in the co-grafted membrane, understanding the role of MAN is at the forefront of this study. To obtain fundamental insight into the properties of styrene / MAN co-grafted membranes and the changes brought about by membrane composition, an in-depth analysis has been carried out to examine the water uptake, proton conductivity, nanoscale structure and durability with varying MAN content.

This chapter is divided into three main parts: membrane synthesis, *ex situ* and *in situ* characterizations. The membranes were prepared such that the ion exchange capacity (IEC) of the membranes containing a different MAN content is kept constant around 1.5 mmol g^{-1}. Membrane characterization and accelerated stress tests were conducted similar to that discussed in the previous chapter. The majority of the results shown is a collaboration with Z. Zhang, Dr. H. Ben youcef, Friederike Lindner and Dr. Sandor Balog.

4.1 Synthesis and characterization

4.1.1 Grafting of styrene / MAN with varying MAN content

The graft level of styrene / MAN in ETFE was determined and described in the previous chapter. The change in the graft level according to the composition of the grafting solution (X_0) suggests the influence of MAN on the grafting kinetics. Since only sulfonated styrene

contributes to the ion exchange capacity (IEC), the IEC of the membranes can be controlled via the amount of styrene present in the grafts. Figure 4.1 shows that the IEC of styrene grafted membranes depends on the graft level and is consistent with the theoretical IEC, implying complete sulfonation.
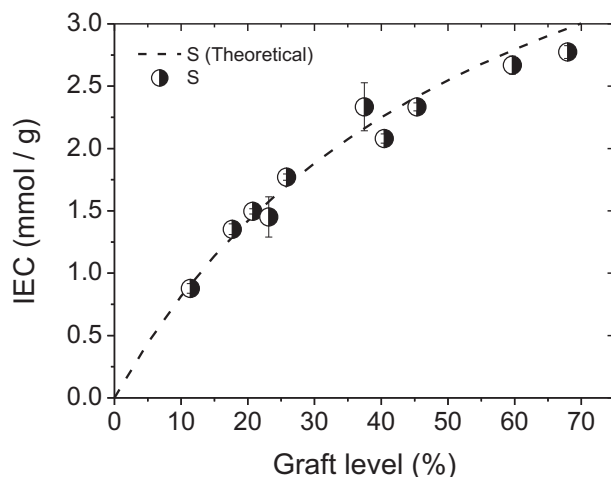
Figure 4.1: The IEC of pure styrene grafted membranes (X=1) as a function of graft level compared to the theoretical IEC, assuming 100% degree of sulfonation of the styrene units.

To determine the influence of MAN on the properties of the membrane, membranes with similar IEC were prepared. The maximum graft level achieved with 1.5 kGy pre-irradiated ETFE for X=0.39 is limited to approximately 40% after 24 hours (Figure 3.1). Therefore, the dose applied for this particular composition is increased to 3 kGy to obtain reasonable grafting time. Since only styrene contributes to the IEC, increasing MAN content requires adjustment to a higher graft level. Figure 4.2 shows the graft level as function of the styrene molar fraction in the membranes (X). Subsequent sulfonation of co-grafted films containing MAN proceeds smoothly and an average 97±4% degree of sulfonation is achieved. At constant IEC of 1.53 ± 0.07 mmol g^{-1}, the graft level of the co-grafted films increases from 23% for pure styrene (X=1) to 63% for X = 0.39. Also shown in the same plot, incorporation of MAN as styrene's comonomer enhances the hydrophilicity of the membrane, resulting in a higher water uptake in the water swollen state.

Although the molecular weight distribution and length of the grafted chains are important factors governing the polymer properties, these parameters have not been explicitly determined. To measure the molecular weight of the grafted chains, the grafts must be cleaved selectively from the base polymer. This can be done by dissolving the grafted copolymer, followed by determination of the molecular weight using size-exclusion chromatograph (SEC) [69]. Yet, this is a tedious (if not impossible) task since ETFE is insoluble in the known solvents. Dargaville *et al.* reported that graft copolymers typically contain longer chains compared to a homopolymer
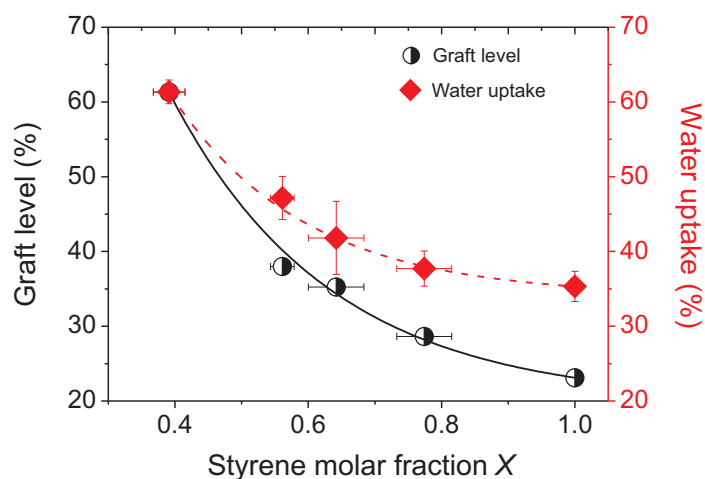
Figure 4.2: Effect of styrene molar fraction (X) on graft level (black semicircle) and water uptake (red diamonds) for styrene / MAN co-grafted membranes with a constant IEC of 1.53 ± 0.07 mmol g^{-1}.

prepared under the same conditions [69]. The radical lifetime in the graft copolymerization is extended due to restriction in chain mobility, resulting in a lower radical recombination rate compared to that of homopolymerization. The graft level increases with grafting time and is accompanied by an increase in grafted chain length [184]. Besides, when more radicals are present in the base polymer, e.g., by increasing irradiation dose, the grafted chains are shorter [69]. Therefore, the radiation grafted films with higher styrene content tend to have shorter grafted chains when the same irradiation dose is applied.

4.1.2 Monomer sequence distribution

An evident drawback of styrene grafted membranes is their intrinsic susceptibility to graft chain degradation under fuel cell operation [104]. The use of MAN as styrene's comonomer in the grafted chain has been shown to improve the durability of styrene based membrane ([104]). Neighboring group effects may play an important role in determining the properties of the co-grafted membrane. For example, the presence of an α-methyl group of MAN may stabilize the α-H of styrene sulfonic acid against radical attack, leading to improved membrane durability. Therefore, an effective means to optimize the chemical stability of the co-grafted membrane is to have an alternating monomer sequence of styrene and MAN in the grafted chain.

The product of the reactivity ratios ($r_A r_B$) is a measure for the alternating tendency in the copolymerization [185]. In an ideal alternating system, the product of the reactivity ratios is zero, while in an ideal random copolymer, is equal to unity ($r_A r_B = 1$). In the previous chapter, the reactivity ratios were determined to be 0.50 ± 0.06 and 0.14 ± 0.03 for styrene and MAN, respectively (Table 3.1). The product of the reactivity ratios is lower than unity ($r_A r_B = 0.07$),

indicating the tendency to form an alternating copolymer.

The degree of alternation is determined by the "run number" (R) [186, 187] as a measure of sequence distribution. It is defined as the average number of uninterrupted monomer sequences (A-A or B-B) in a polymer chain containing 100 monomer units. Figure 4.3 shows a copolymer chain consisting of 10 monomer units and 8 runs (R=80), compared to a perfectly alternating polymer chain (R=100). For an ideal random copolymer, the value R=50 is expected.

Polymer with a tendency to alternate (R =80)
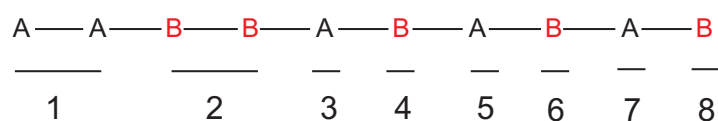
Perfectly alternating polymer (R =100)
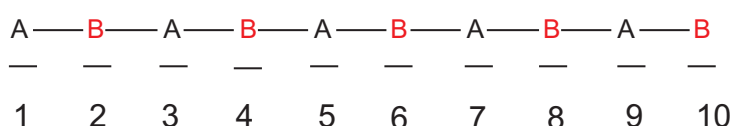
Figure 4.3: Polymer chains consisting of 10 monomer units arranged in 8 runs (top) compared to a perfectly alternating polymer (bottom). The number of runs is underlined.

The run number in a styrene / MAN co-grafted membrane is determined from the styrene molar fraction in the grafting solution (X_0) and the reactivity ratios (r_A and r_B) [187].

$$R = \frac{200}{2 + r_A \frac{X_0}{(1-X_0)} + r_B \frac{(1-X_0)}{X_0}} \tag{4.1}$$

It is apparent that the tendency to alternate in the copolymer chain is most probable when X=0.5. At this composition, $\sim$80% of the styrene / MAN grafted chain took the form of a styrene unit followed by a MAN unit and vice versa (Figure 4.4). The run number decreases when the styrene molar fraction of the copolymer departs from 0.5.

4.1.3 Investigation of styrene / MAN microstructure by FTIR

The molecular composition of the co-grafted films was examined using FTIR spectroscopy, in which two series of styrene / MAN co-grafted films were compared, namely films that yield a constant IEC of ~ 1.5 mmol g^{-1} and films with a constant graft level of $\sim 40\%$ (Figure 4.5). The FTIR spectra of the grafted films reveal that the peak positions of vibrational bands associated with the graft component are influenced by the composition of the graft, irrespective of the graft level.
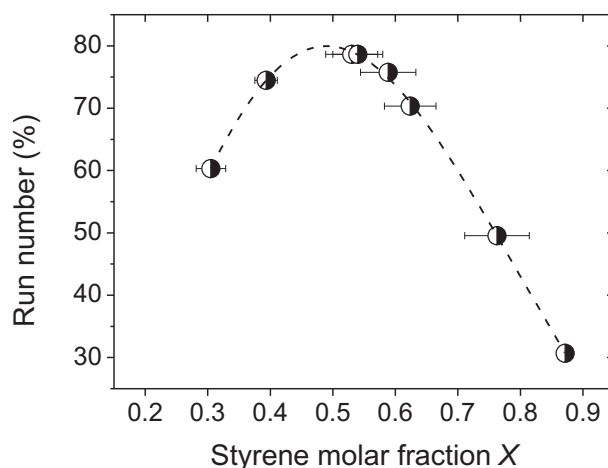
Figure 4.4: Variation of the run numbers in styrene / MAN grafts as a function of styrene molar fraction.

With increasing MAN composition, the C≡N (2231-2236 cm^{-1}) peak shifts to a higher wavenumber with an increase in intensity. This blueshift of the C≡N with increasing MAN content was reported for styrene / MAN copolymers [188]. Interaction between the nitrile groups may induce the change in the environment of the grafted film, resulting in the shift of the nitrile peak position.

According to Dong *et al.*, the orientation and the sequence distribution of MAN can affect the interaction between neighboring nitrile groups [188]. When two neighboring nitrile groups align in parallel, the repulsive forces between the electron-rich nitrogen atoms as well as that between the partially positive carbons of adjacent nitrile groups will restrict the C≡N vibration, hence the blueshift as observed with increasing MAN composition. With increasing styrene content, the repulsion between the adjacent nitriles is likely to be reduced because of the formation of an alternating chain, whereby the C≡N peak will shift towards a lower wavenumber [189]. Furthermore, the grafted chains may adopt a conformation which favors antiparallel alignment of the nitrile and another, distant nitrile group, giving rise to an attractive force yielding a lower C≡N peak position [188].

There is also a detectable shift in the CH_3 symmetric deformation ("umbrella"vibration) and the C=C aromatic vibration associated with styrene to a higher wavenumber as the MAN content increases. This implies that the arrangement of the grafts is sensitive to the environment and is influenced by the graft composition.

Once the grafted films are sulfonated, the hygroscopicity increases significantly by the presence of the sulfonic acid groups rather than the nitrile. Although the nitrile is a polar group (3.5 debye), none of the spectra collected from the grafted films show any traces of water. To confirm this finding, we immersed an MAN grafted film (X=0) with 40% graft level into water at 80°C
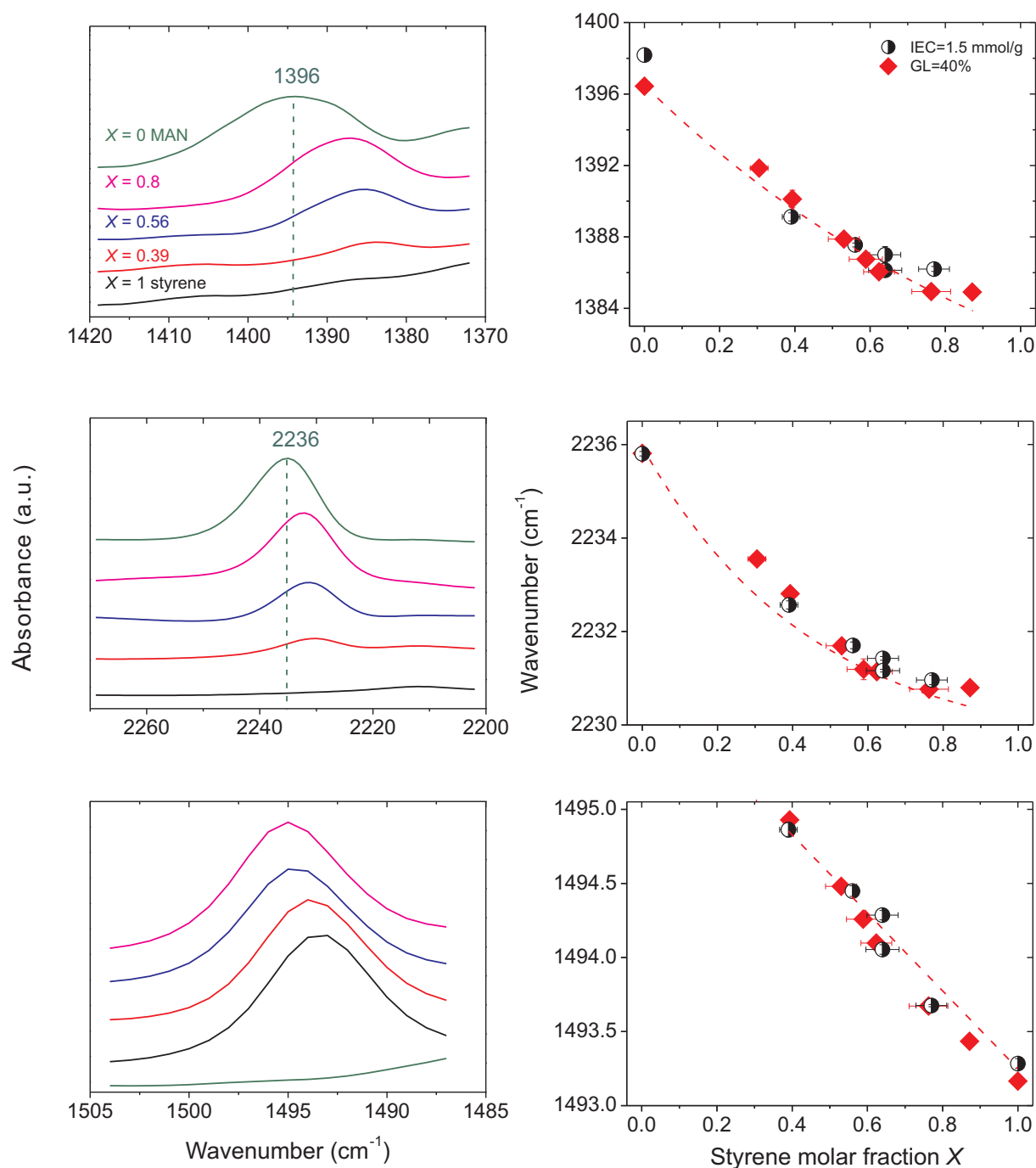
Figure 4.5: FTIR spectra of styrene / MAN co-grafted films. The peaks are characteristic for CH vibration of the α-methyl group around 1381 cm^{-1} (top), C$\equiv$N stretch vibration at $\sim$2231 cm^{-1} (middle) and C=C aromatic vibration around 1493 cm^{-1} (bottom). The plot of the peak position versus the graft composition is shown accordingly. The dashed lines are included as guide to the eyes.

and carried out a dimensional stability test. The dimensional change between fully swollen and dry state should give an indication of the water sorption of the film. However, no swelling and

negligible mass change was found. This supports our hypothesis that MAN cannot absorb the water by its own. The shift observed in the characteristic vibrational bands of the grafted films disappeared after sulfonation, implying that the interaction between the functional groups and the sulfonic acid groups dominates and cancels out the interactions caused by the presence of nitrile.

4.1.4 Proton conductivity in water swollen state

The conductivity is affected by the nature of the ion exchange sites (i.e., the degree of proton dissociation), the concentration of the ion exchange sites in the membrane, the proton mobility, and the structure / morphology of the ion-conducting aqueous domains. The conductivity of pure styrene grafted membranes in water swollen state is determined by the amount of sulfonic acid groups, which correlates to the IEC. With increasing IEC, the membrane becomes more hydrophilic and the proton conductivity increases. When the IEC of styrene / MAN co-grafted membranes is kept constant, the hydration level of the co-grafted membranes can be adjusted by varying the MAN composition in the grafts. An increase in the hydration number corresponds to a higher MAN content. The proton conductivity of styrene / MAN co-grafted membranes with fixed IEC in water swollen state is comparable regardless of the hydration number (Figure 4.6). This can be rationalized in terms of the dilution of the proton concentration, resulting from an
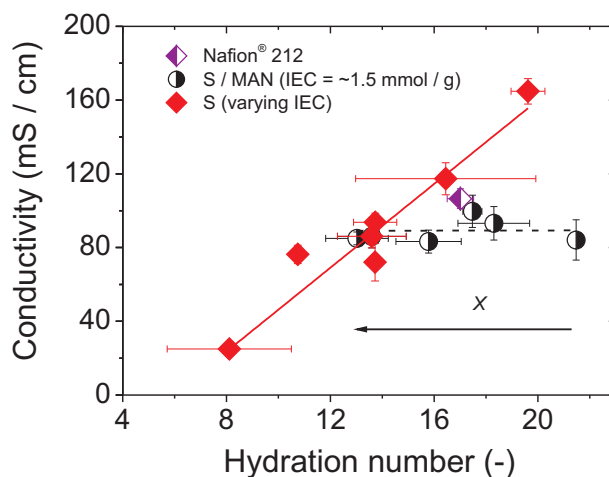
Figure 4.6: Proton conductivity in water swollen state of the co-grafted membranes with fixed IEC as a function of the hydration number (λ). The values for pure styrene grafted membranes and Nafion® 212 are given here for comparison.

increase in the hydration level of the membrane (Figure 4.7). In order to achieve high conductivity in the membranes, the combination of high proton mobility and proton concentration is necessary. Chuy *et al.* have reported that the water uptake due to the presence of AN does not help in assisting the proton conductivity to the same degree as the water around PSSA [190].

4. STRUCTURE-PROPERTY CORRELATIONS

In their study, the poly-AN is incorporated as a polymer backbone with poly(sodium styrene sulfonate) pendant chains.
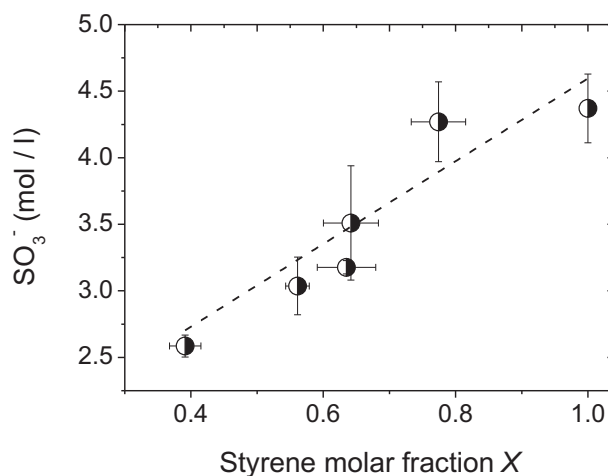
Figure 4.7: The proton concentration (expressed as the number of mol of SO_3^- in water) as a function of styrene molar fraction (X) in styrene / MAN co-grafted membranes with IEC~1.5 mmol g^{-1}.
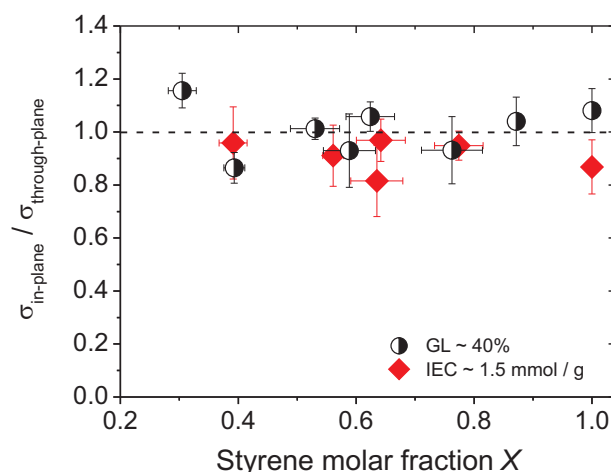
Figure 4.8: The ratios between in-plane and through-plane proton conductivities of styrene / MAN co-grafted membranes with IEC~1.5 mmol g^{-1}. The experiments were carried out at RT in water swollen state. The dashed line is included as an indication when the proton conductivities in both directions are equal, suggesting a homogeneous graft distribution throughout the membrane thickness.

Besides the transport properties, we can obtained the homogeneity information of the membranes from the proton conductivity experiments. The homogeneity of styrene / MAN co-grafted membranes with constant graft level ($\sim 40\%$) and IEC (~ 1.5 mmol g^{-1}) was determined from the proton conductivity measured through-plane and in-plane directions. When the grafted chains have a sufficiently high degree of polymerization, a homogeneous membrane can be obtained and the proton conductivity measured in-plane and through-plane conductivity should

be similar. Figure 4.8 shows that the ratios between the in-plane and through-plane conductivities are close to unity, implying that the membranes are homogeneously grafted. Therefore the conductivity measured from the in-plane mode is directly related to the measurement in the through-plane mode as will be discussed shortly.

4.1.5 Membrane water sorption

Although water is necessary for proton conduction, too much water can lead to extensive membrane expansion and inferior dimensional stability [117]. Therefore, the water uptake of the membrane should be optimized to yield high proton conductivity and minimize dimensional change. The dimensional stability was investigated by measuring the shrinkage of the membranes upon drying. A lower shrinkage of the membrane indicates a better dimensional stability.

Figure 4.9 demonstrates the shrinkage of the co-grafted membranes upon drying with respect to the hydrated state as a function the water uptake. For styrene / MAN co-grafted membranes with constant IEC, the dimensional stability decreases upon addition of MAN. The significant change is observed up to 40% water uptake and stabilizes beyond this level. Although the co-grafted membranes possess higher water uptake, the shrinkage of the co-grafted membranes is less than that of Nafion® 212, indicating higher dimensional stability.
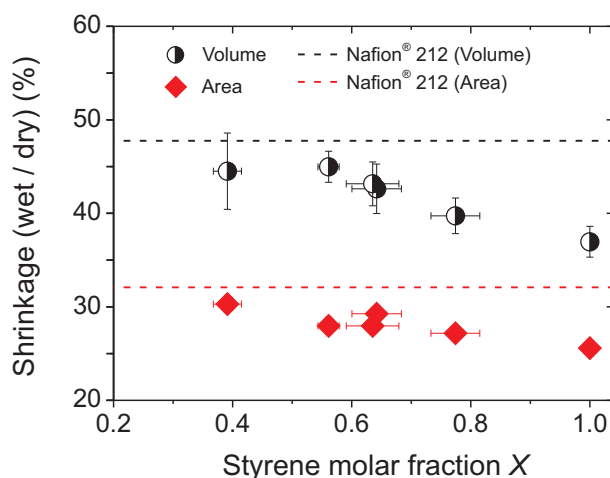
Figure 4.9: The change in the dimensional stability with the water uptake of co-grafted membranes(IEC$\sim$1.5 mmol g^{-1}) compared to Nafion® 212. The higher water uptake corresponds to increasing MAN composition in the grafts.

Upon hydration, the membrane expands in all directions. From the water uptake behavior of different styrene / MAN co-grafted membranes, the relation between water sorption and membrane expansion is investigated. Figure 4.10 shows that the volume expansion of the co-grafted membranes is directly proportional to the amount of absorbed water, corresponding to zero excess volume of mixing (dashed line). Similar trend is observed for all grafted membranes

with varying MAN content. This suggests that the water in the grafted membranes behaves similar to bulk water with the apparent density close to 1 g cm^{-3} and if free volume exists in the membrane, this is not accessible by the absorbed water. In contrast, Nafion® 212 expands more than the volume of absorbed water, which is in agreement with literature [191], indicating a positive excess volume of mixing. The difference between the volume mixing of the grafted membranes and Nafion may be a result from the differences in the membrane structure.
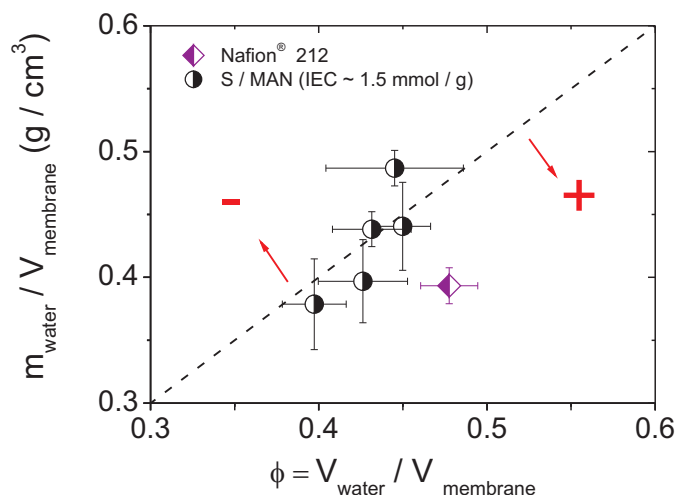
Figure 4.10: The mass of water uptake / volume of wet membrane as a function of the volume of expansion of water / volume of the membrane. The slope of the dashed line is the density of bulk water and indicates zero excess volume of mixing.

4.1.6 Investigation of structural changes by DSC

Incorporation of MAN as styrene's comonomer in the grafts may promote structural changes and result in differences in the membrane properties. DSC analysis was carried out to investigate the effect of MAN on the crystallinity of base films and membranes. The crystallinity of pre-irradiated ETFE with 1.5 and 3 kGy are virtually constant and comparable to that of the pristine film (about 30%), suggesting that the small differences in the dose applied do not lead to significant changes in the base film properties.

In previous works carried out by Schneider and Gürsel, it was reported that upon grafting of styrene into ETFE, the melting temperature of the grafted films remained unchanged while the intrinsic crystallinity slightly decreases with the graft level [192]. For comparison, styrene / MAN co-grafted films were investigated. The melting temperature of the grafted films and ETFE is found to be 262°C and the intrinsic crystallinity of the films remained constant upon grafting up to 60% graft level. This observation indicates that the intrinsic crystallinity of the grafted film is determined by the crystallinity of ETFE. A single recrystallization peak of the grafted films and ETFE is observed at 244°C. The second and third heating cycles suggested

that the crystallinity of the grafted films is slightly lower than that observed after grafting. The results could be explained from the fact that the grafted domains may impede recrystallization of the ETFE crystalline domain.

The results show that two distinct phases exist in the grafted films, namely the crystalline and amorphous phase, of which the latter accommodates the graft components. This observation is well supported by previous studies on different base films [121].
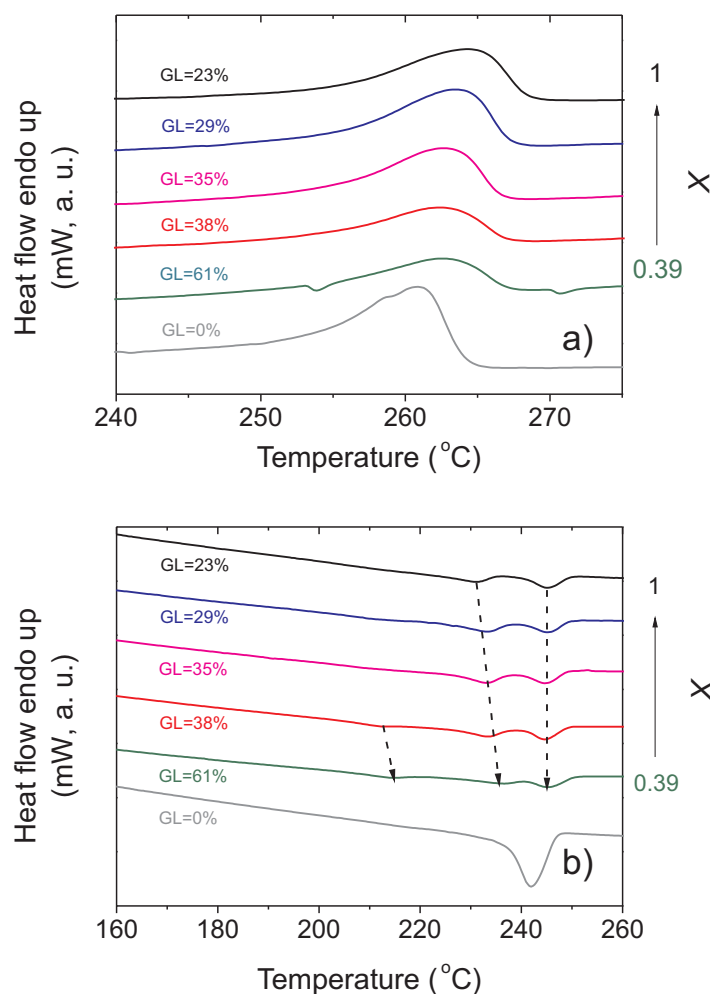
Figure 4.11: DSC heating (a) and cooling (b) thermograms of styrene / MAN co-grafted membranes containing different graft compositions in potassium form.

After sulfonation, a structural change may be observed in the form of a reduction of crystallinity or changes in the melting or recrystallization behavior of the membranes [193]. Figure 4.11a shows DSC melting thermograms of the co-grafted membranes and ETFE base film. A similar shape of endotherms of the styrene / MAN co-grafted membranes (in salt form) and the ungrafted ETFE was obtained. The broad endotherms in DSC experiments as found here are typically observed for semicrystalline polymers. The shift of the melting temperature with MAN

87

composition indicates that the grafts in the amorphous phase induce changes to the crystalline domain of the ETFE base polymer. In addition, the recrystallization thermograms reveal at least two crystallization temperatures at around 230 and 243°C (Figure 4.11b). The former was found to shift to a lower temperature with increasing MAN composition. This may indicate that the formation of ETFE crystallites is induced by the presence of graft composition. Perhaps these ETFE crystallites are originally found at the interface of the crystalline and amorphous domains and are grafted by the monomers. The second crystallization temperature is constant for all co-grafted membranes, which may indicate the crystalline structure of the ETFE base polymer that is not directly grafted. Although not very obvious, the membranes with high MAN composition show a small crystallization peak at around 210°C, which may indicate that the ETFE structure is affected by the presence of high MAN content. This observation suggests that the composition of the graft can cause substantial structural changes in the membrane and could lead to differences in the *ex situ* properties previously discussed.

Considering crystallinity of the grafted membranes, it appears that the intrinsic crystallinity is lower than that of the base film (Figure 4.12). Independent of the composition of the graft component, the intrinsic crystallinity of membranes with comparable IEC (in potassium form) remains almost identical over the entire range of graft levels (23% to 61%). The lower intrinsic crystallinity compared to the base film may be attributed to the presence of sulfonic acid group during sulfonation. Upon swelling of the ionic domains, stress at the interfacial boundary of the hydrophobic crystalline domain of ETFE and amorphous domains containing the grafted chains develops, leading to disruption of crystalline domains of the ETFE. Similar results were also reported on FEP based membranes by Gupta *et al.* [194].
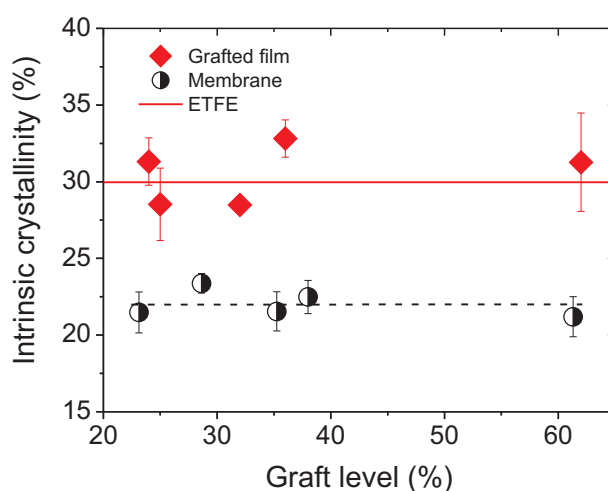
Figure 4.12: The intrinsic crystallinity of styrene / MAN co-grafted membranes with similar IEC in salt form (K$^+$) compared to that of ungrafted ETFE film. The dashed line is given as guide to the eyes.

Since disruption of crystalline domains was not found in the grafted (unsulfonated) film [121], incorporation of MAN through changing the graft level of styrene containing membranes does not affect the intrinsic crystallinity. The result found in this study confirms that the crystallinity of the membrane is determined by the presence of sulfonated groups. Introduction of the sulfonic acid can substantially reduce the degree of crystallinity and may decrease membrane mechanical stability.

4.1.7 Proton conductivity at reduced humidity

The transport of protons in a solid polymer occurs through water swollen channels, which are formed through the phase separation of hydrophobic and hydrophilic domains [134]. When the membrane dehydrates, dissociation of the acid is reduced whereby the proton concentration in the hydrophilic domain decreases. In addition, the proton mobility is limited due to the decrease of the water uptake.

An increase in MAN content in the grafts contributes to the hydration level of the membrane. This was thought to be advantageous for the proton conductivity at reduced humidity by providing necessary water for the proton pathway. Figure 4.13 shows an increase in the hydration level (λ) with relative humidity. Considering the drying procedure, nominally dry membranes may still contain water of the first hydration shell. λ_0 is the hydration number in nominally dry membrane. No significant hysteresis between sorption and desorption has been observed, implying reversible water uptake.
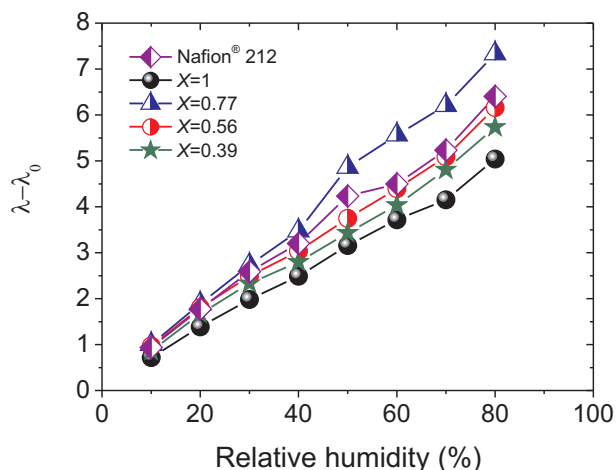
Figure 4.13: Correlation between the hydration level of styrene / MAN co-grafted membranes with different styrene molar fraction (X) and relative humidity (70˚C). The values for Nafion are given for comparison.

Although the water uptake of the co-grafted membranes varies markedly in the water swollen state, the water uptake isotherms in the relative humidity range up to 80% are quite similar.

4. STRUCTURE-PROPERTY CORRELATIONS

This implies that the difference in membrane water uptake due to the presence of MAN is less pronounced at reduced humidity. The hydration level of the co-grafted membranes increases from pure styrene grafted membrane $X=1$ to $X=0.56$, which exhibits similar water content to that with $X=0.39$ and Nafion, while the highest water content is found for $X=0.77$. No significant hysteresis between sorption and desorption was observed, implying reversible water uptake. In general, the water uptake and the water content of the membrane are directly associated with the acid concentration [195]. As the IEC of the co-grafted membranes is kept constant, the hydration level at reduced humidity is comparable.

In comparison to Nafion, the grafted membranes suffer from higher conductivity loss at relative humidity lower than 80% (Figure 4.14). The differences in the proton conductivity between Nafion and grafted membranes may be rationalized in terms of the differences in the acid strength (pKa). Under conditions of minimal water content, the strength of the conjugate base (sulfonate anion) is prevailing and will affect the hydrogen bonding of water molecules, hence the proton transport. Complete proton dissociation from the anion to form a hydronium ion requires a mininum number of water molecules. Paddinson *et al.* reported that three water moleucules are needed to dissociate the proton from CF_3SO_3H (triflic acid) or $CH_3C_6H_4SO_3H$ (p-toluene sulfonic acid), used as model compound for Nafion and sulfonated PEEK, respectively. Proton dissociation from the sulfonate anion takes place as a result of stabilization of the partial positive charge in the H-bond network of the hydronium ion and is different between these model compounds. Likewise, the electron density of the sulfonate anion is delocalized. In trific acid, the electron is withdrawn and stabilized by the high electronegativity of the fluorine atoms, whereas the electron is delocalized over the π-ring of p-toluene sulfonate, leading to a stronger conjugate Lewis base [196]. These interpretation are consistent with a lower pKa of Nafion compared to that of benzene sulfonic acid [116].

Although the proton conductivities of all grafted membranes with comparable IEC are similar at high relative humidity (80-100%), upon drying the conductivity of membranes with increasing MAN content ends up being significantly lower than those with higher styrene molar fraction. This suggests that the presence of MAN can affect the proton conductivity, particularly at low relative humidity. Intuitively, among all grafted membranes the proton transport at reduced humidity is optimized with high styrene content in the grafts. Incorporation of a comonomer may lead to differences in polymer conformation. We may speculate that the presence of MAN may result in a greater separation between the proton conducting sites. Paddinson provided theoretical evidence for DOW perfluorocarbon membranes that the proton dissociation also depends on chain conformation and the distance between neighboring sulfonic acid groups [196]. A close proximity of the sulfonic acid groups allows stronger interaction by electrostatic interaction, hence, larger and purer ionic aggregates can be formed [197]. According to Tsang *et al.*,

increase in the electrostatic forces between the sulfonic acid groups leads to formation of a larger ionic aggregates, favoring high proton conductivity and inhibiting membrane swelling [198].
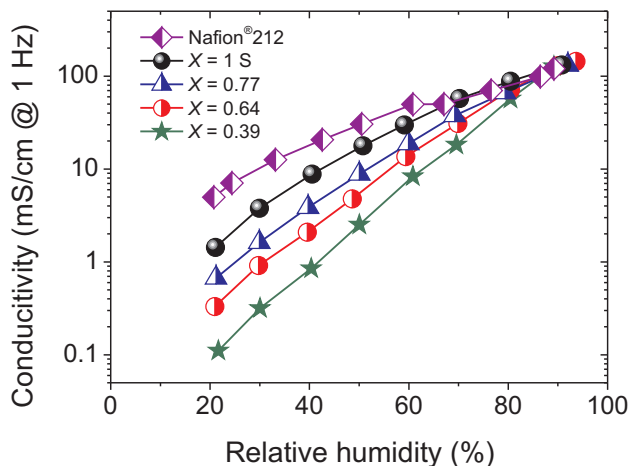
Figure 4.14: Proton conductivity of the co-grafted membranes and Nafion® 212 as a function of relative humidity at 70°C.

The proton conduction in a membrane is an interplay between both chemical and physical properties. With respect to the latter, the structure and morphology on the nanometer scale by small-angle X-rays scattering is investigated to elucidate their connection with the proton conductivity (section 4.3).

4.2 Fuel cell test

Proton conductivity is one of the factors with a direct influence on the fuel cell performance. However, there may be some material related factors that are not accounted for by the conductivity measurement, e.g., the mismatch between membrane and electrode interface leading to loss in fuel cell performance. Fuel cell tests were carried out to understand the behavior of the membranes under fuel cell conditions. The membranes were impregnated with 0.5% Nafion solution to ensure good membrane-electrode contact [41]. The cells were operated at 500 mA cm^{-2} for 24 hours to condition the membranes prior to the polarization measurement. The differences observed in the current-voltage curves can indicate the influence of MAN on performance since all fuel cell components are identical, except the membrane.

4.2.1 Fuel cell performance

Comparison between polarization curves of the radiation grafted membranes with varying styrene molar fractions are shown in Figure 4.15. Nafion was included as a reference of a known material. Despite the fact that the membranes are different in their graft composition and degree of

hydrolysis, the differences in the performances of different co-grafted membranes with constant IEC are rather small and are comparable to that of Nafion® 212. The high frequency resistance (HFR) is mainly determined by the membrane resistance and is comparable for all membranes, confirming that *ex situ* conductivity and the HFR measured *in situ* are related. Further observation shows that the HFR values are not stable in the low current density region (0-150 mA cm^{-2}). The values stabilize at higher current density. It is conceivable that liquid water created at high current density is distributed across the membrane, lowering the membrane resistance and improving the contact between the membrane and the electrodes.
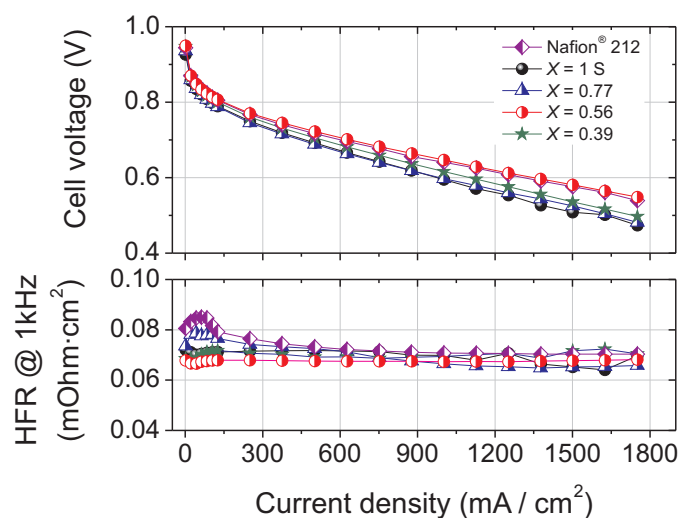
Figure 4.15: Polarization curves and HFR of MEAs based on styrene / MAN co-grafted membranes (IEC ~1.5 mmol g^{-1} with varying monomer content in the grafts and Nafion® 212; H$_2$ / O$_2$ (1.5 bar$_a$ / 2 bar$_a$), 100% relative humidity and 80°C. Experiments were carried out in collaboration with Dr. H. Ben youcef.

The polarization and the ohmic resistances were measured by AC electrochemical impedance spectroscopy to elucidate the origin of the slight discrepancy in the fuel cell performance between the grafted membranes (Figure 4.16). The impedance spectra recorded at 500 mA cm^{-2} revealed no difference in the ohmic resistance of the grafted membranes as a function of the varying monomer content. However, the polarization resistance, which is an indication for the quality of the contact between the membrane and electrodes, seems to increase at intermediate styrene content and stabilizes above $X=0.77$.

Besides the membrane / electrode interface and membrane resistance, gas crossover plays a key role in determining fuel cell efficiency and membrane integrity. As shown in Figure 4.6, an increase in MAN content leads to high water uptake, which may not be desirable as it leads to gas permeation. The influence of MAN on hydrogen permeation rate through the grafted membrane is investigated electrochemically under H$_2$ / N$_2$ conditions. A higher hydrogen permeation is observed with increasing styrene molar fraction in the grafted membranes due to a decrease
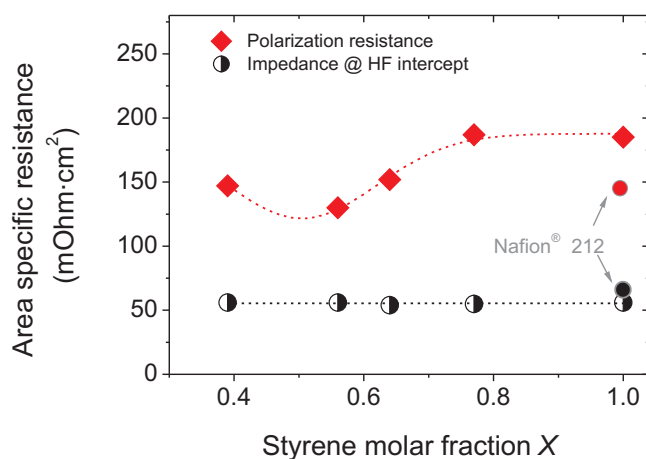
Figure 4.16: Ohmic resistance as determined from the high frequency intercept of the impedance spectra and polarization resistance of MEAs with co-grafted membranes (varying styrene molar fractions) measured at 500 mA cm^{-2}. Experiments were carried out in collaboration with Dr. H. Ben youcef.

in membrane thickness (Figure 4.17). In comparison with the Nafion membrane, all grafted membranes offer a higher resistance to hydrogen crossover, despite the lower thickness.
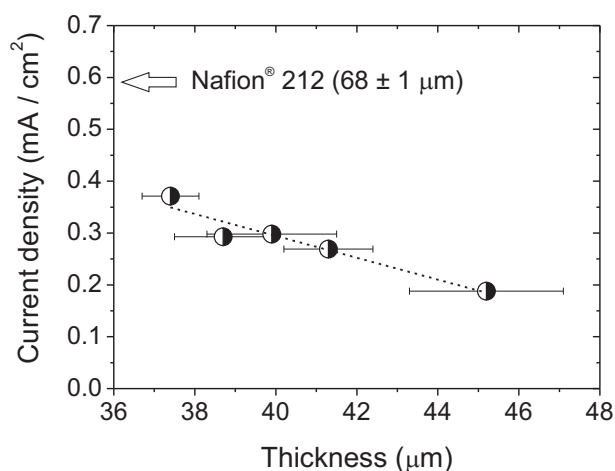
Figure 4.17: H$_2$ crossover current density of styrene / MAN co-grafted membranes with constant IEC of $\sim$1.5 mmol g^{-1}. The thickness of the membranes in water swollen state depends on the styrene molar fraction X. The value for Nafion$^{®}$ 212 is included as a known reference. Experiments were carried out in collaboration with Dr. H. Ben youcef.

The results found in connection with the grafted membranes show that the water uptake of the membrane does not explicitly determine the rate of gas permeation. This observation is also supported by the low solubility of gas, such as oxygen in water [174]. Based on Ogumi [174, 175] and the three phase model of Nafion proposed by Yeager [199], permeation of hydrogen and oxygen through Nafion does not occur through the ion cluster region of the membrane, but

takes place in the amorphous region of Teflon. Therefore, the volume of the amorphous region plays an important role in determining the gas crossover. The polymer crystallinities of styrene / MAN co-grafted membrane with IEC= 1.5 mmol g^{-1} range from 12-16% depending on the graft level, whereas that of Nafion determined by wide-angle X-ray diffraction (WAXD) is reported to be 13.6-14.5 % [178, 200]. Since the effective crystallinities of both types of membrane are comparable, the graft and polymer backbone are expected to have essential impact by limiting gas permeability.
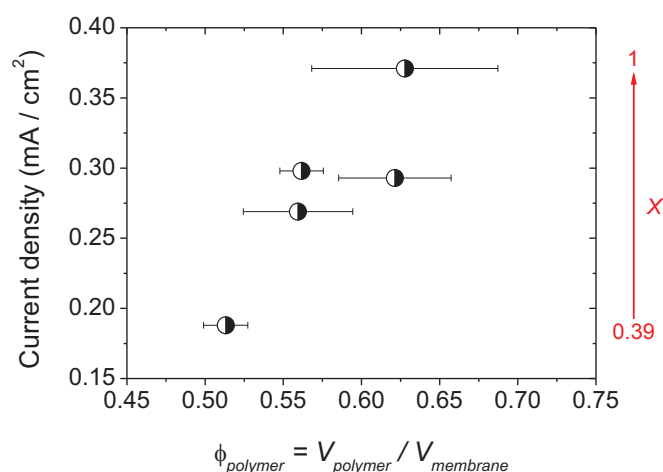
Figure 4.18: H$_2$ crossover current density of styrene / MAN co-grafted membranes with constant IEC of ~1.5 mmol g^{-1} as a function of polymer volume fraction in water swollen membranes. Experiments were carried out in collaboration with Dr. H. Ben youcef.

The hydrogen crossover rate of the radiation grafted membrane increases with the polymer volume fraction (Figure 4.18). This may indicate that gas permeation through the grafted membrane occurs preliminary in the amorphous region of the polymer. When the hydrogen crossover current density is normalized by multiplying with the membrane thickness, a clear trend can be observed (Figure 4.19). With increasing styrene molar fraction, the normalized hydrogen current density increases. The lower intrinsic gas permeation with increasing MAN content is attributed to the gas barrier properties of MAN [149]. Yet it should be noted that the permeation mechanism through ion exchange membranes is still controversially discussed [201, 202].

4.2.2 Accelerated stress test

The loss of sulfonic acid groups owing to membrane degradation is evidenced by an increase in the high frequency resistance (HFR). The OCV hold test was carried out with impregnated membranes using cell design 2 (subsection 2.3.1). Figure 4.20 represents the high frequency resistance of styrene / MAN co-grafted membrane (IEC~1.5 mmol g^{-1}) and Nafion. The HFR
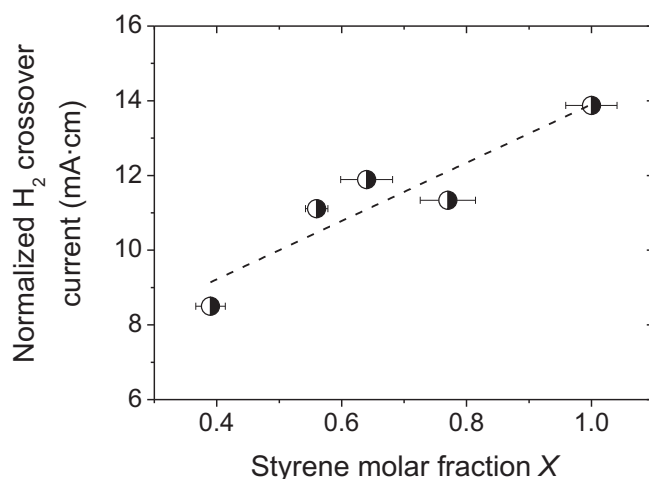
Figure 4.19: H_2 crossover current density normalized by the thickness of styrene / MAN co-grafted membranes with constant IEC of $\sim$1.5 mmol g^{-1}. Experiments were carried out in collaboration with Dr. H. Ben youcef.

of the Nafion membrane does not significantly change during its degradation, because the loss of ionomers is compensated with decrease in membrane thickness, leading to steady membrane resistance.
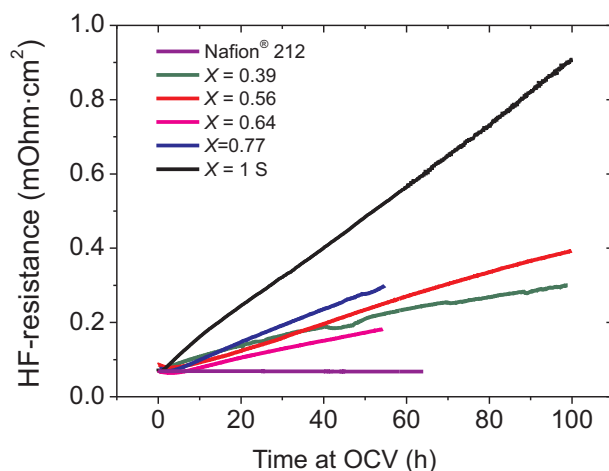
Figure 4.20: Change of high frequency resistance in an accelerated stress test (OCV conditions): H_2 / O_2, 2.5 bar$_a$, 80°C, 100% RH. Experiments were carried out in collaboration with F. Lindner.

Rapid increase in HFR of the pure styrene grafted membrane (X=1) is found after a few hours at OCV and shows the highest increase in HFR among the grafted membranes. This confirms that the pure styrene grafted membrane is more susceptible to degradation under OCV conditions than the co-grafted membranes [104]. If the presence of nitrile would yield a more durable membrane, the membrane with the highest nitrile content should exhibit the lowest rate of HFR increase. Surprisingly, no conclusive trend is found for the HFR behavior of

the co-grafted membranes with varying monomer composition. The data collection for $X=0.64$ and 0.77 was discontinued after 50 hours due to problems with the test stand.

Degradation of nitrile containing membranes is rather complex. Besides the loss of sulfonic acid groups, chemical and structural changes may have occurred during the test, because hydrolysis of nitrile is likely to occur during the OCV test. Although the grafted chain is still intact, the nitrile groups are lost with time while amide and carboxylic acid groups are formed. The presence of these products of hydrolysis during the test may determine the membrane stability and open up new questions regarding membrane properties and durability. A better understanding of the effect of nitrile hydrolysis on membrane durability will be necessary to disentangle the influence of nitrile from amide and carboxylic acid.

Although, the change in HFR is a qualitative means to compare the loss of the ionic groups, it is no direct indication of the quantity of the sulfonic acid loss and how the polymer breaks down or how the graft is released from the matrix. More information may be acquired from the *post mortem* analysis of the membranes by FTIR.

Comparison of the FTIR spectra of the membranes recorded *post mortem* showed that all grafts are lost after 100 hours OCV. The FTIR spectra of the tested membranes are similar to that of ETFE. Also, we found that the impregnation of the membranes with Nafion may accelerate its degradation. The reason for this is currently unknown. Therefore, to investigate the intrinsic property of the membrane, it is recommended to carry out OCV tests without impregnation.

4.3 Nanoscale structure and its connection to proton conductivity

Incorporation of MAN as a comonomer to styrene leads to significant changes in membrane properties. However, there is no clear understanding of how the graft composition of this particular system influences the microstructure as well as proton conductivity. The structure of the co-grafted membranes could be a determining factor to modify mechanical properties or proton transport. In this regard, the nanoscale structure of styrene / MAN co-grafted membranes containing different styrene molar fractions was investigated to elucidate a relationships between structure, morphology and proton conductivity at reduced humidity.

Despite the increasing interest in grafted membranes for fuel cell application, understanding of the structure and morphological effects on the ion rich phase is rather limited [203]. Zhang *et al*. reported the morphological impact of graft length, graft density (mol%) and ionic content in poly(vinylidene fluoride)-*g*-sulfonated polystyrene (PVDF-*g*-PSSA). They carefully controlled the graft length, graft density and ionic content using the ATRP "graft-from" approach, followed

by subsequent sulfonation. The graft copolymer self-assembles into a microphase-separated morphology of the hydrophobic and hydrophilic domains. A cluster-network morphology is found with higher graft density and lower graft length, while lamella and cylinder structures are observed in low graft density and high graft length. Apart from the grafts, they also reported that the molecular weight of the backbone has a significant effect on the water swelling behavior of the membrane [195].

Previously, Holdcroft *et al*. showed that structure and morphology of grafted polymers play a decisive role for proton conductivity [126–128, 204]. Polymers of poly(sodium styrene sulfonate) grafted into polystyrene (PS-*g*-PSSNa) and copolymer of styrene and macromonomer of poly(sodium styrenesulfonate) (PS-*r*-SSNa) served as model systems to investigate the relationship between structure, morphology and conductivity [127]. These copolymers are similar in terms of chemical compositions, yet possess very distinct morphologies as revealed by TEM analysis. The grafted polymer exhibits significantly higher proton conductivity and lower water uptake compared to that of the random copolymer and shows a clear sign of nanophase separation and continuous ionic channels. In contrast, the random copolymer lacks phase separation. They concluded that the grafting process induces phase separation and hence increased proton conductivity.

The same group also reported that the chain length plays a key role in proton conductivity. The grafted membrane based on long grafted chains shows a higher extent of phase separation compared to that with shorter chains. However, nanophase separation is not favorable in low ion content membranes since it leads to isolated ionic domains and therefore hinders proton conduction [126]. The effect of graft length and degree of sulfonation on the nanostructure morphology and properties of membranes containing polystyrene sulfonic acid grafted into P(VDF-*co*-CTFE) was reported [198]. The membranes comprising short graft chains with high degree of sulfonation (closer proximity of sulfonic acid groups) possess larger ionic aggregates due to electrostatic forces and provide higher proton conductivity compared to the longer graft analogues. In addition, the graft copolymer with high graft density and low graft length possess "cluster network"ionic domains, similar to that of Nafion [204].

In our laboratory, the structures of crosslinked and uncrosslinked membranes prepared by radiation grafting of ETFE and FEP with styrene have been investigated using small angle scattering techniques (SAXS and SANS). Radiation grafted membranes contain two distinct phases originating from the base film, namely the crystalline phase and the amorphous phase, which are randomly connected [123]. The amorphous phase hosts graft components and swells upon grafting. This swelling can be reduced by adding crosslinkers, yielding a more dimensionally stable membrane. In addition, the presence of crosslinkers affects the nanostucture of the

ion-rich phase [124]. The structure of the dry membrane has a direct influence on the proton conductivity in water swollen state [203].

Assuming that the structure of the membrane in the dry state resembles that at reduced humidity, the nanostructure of styrene / MAN co-grafted membrane in dry state is investigated. This study is a collaboration project with laboratory of neutron scattering (LNS) using small angle X-ray scattering (SAXS). The SAXS experiments were carried out, analyzed and interpreted by Dr. Sandor Balog [1] and the results will be published [141].

4.3.1 Morphology of crystalline and amorphous domains

To address the influence of the graft composition, SAXS analysis of the co-grafted membranes was carried out in two length scales of approximately 30 nm and 3 nm, respectively (Figure 4.21). The chosen length scales permit studies of polymer morphology in the crystalline-amorphous phase and in the ion-rich phase [195, 198, 204]. Two grafted membrane series with comparable graft level (GL$\sim$40%) and constant ion exchange capacity (IEC$\sim$1.5 mmol g^{-1}) in the acidic and ion exchanged form were studied. *Ex situ* data for these membranes are summarized in Table 4.1.
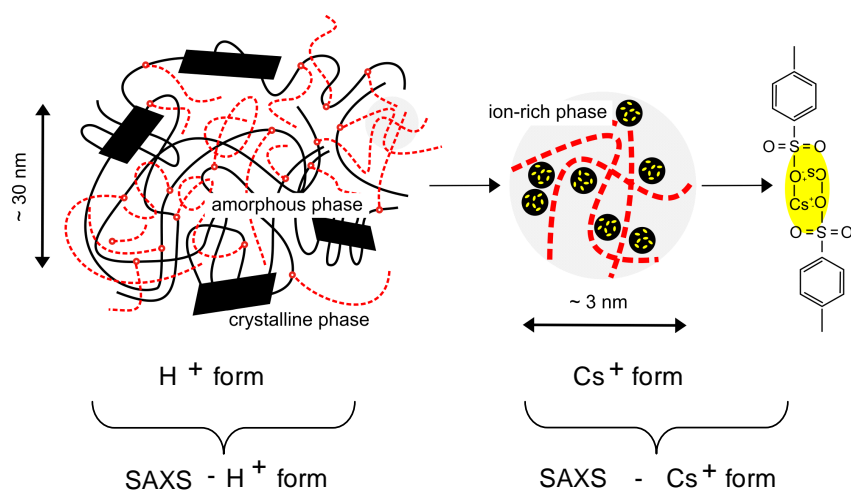
Figure 4.21: Schematic representation of the dominant length scales of heterogeneities in the PEM. Illustration adapted from Dr. S. Balog.

First, the structure of the ETFE base film was determined. In the crystalline phase, the polymer is denser than in the amorphous phase, eventually resulting in phase separation. On the length scale of approximately 30 nm, the anisotropy of the ETFE base film is recognized (Figure 4.22). Based on this scattering pattern, the structure of the ETFE in the machining

[1]current address: Adolphe Merkle Institute, University of Fribourg, 1723 Marly 1, Switzerland

Table 4.1: *Ex situ* properties of grafted membranes and Nafion® 212 membrane. Degree of sulfonation of 100% corresponds to complete sulfonation of each styrene unit. Conductivity (σ) was measured in water swollen state. X is the styrene molar fraction in the membrane, respectively.

Series	GL (%)	X	IEC (mmol / g)[a]	σ at RT (mS / cm)[b]
GL~40%	40.4	0	0	0
	41.8	0.31±0.02	1.05±0.11	40±2
	41.6	0.40±0.02	1.18±0.08	65±3
	38.8	0.53±0.04	1.32±0.04	73±3
	39.8	0.59±0.04	1.50±0.11	88±10
	41.7	0.62±0.04	1.73±0.08	108±6
	41.5	0.76±0.05	2.02±0.08	110±7
	42.4	0.87±0.01	2.25±0.14	126±12
	37.5	1	2.33±0.19	118±9
IEC~1.5	23.1	1	1.54±0.02	86±6
	28.6	0.77±0.04	1.61±0.05	85±3
	34.2	0.66±0.04	1.55±0.01	100±9
	35.2	0.64±0.04	1.47±0.05	83±6
	38.0	0.56±0.02	1.43±0.05	93±9
	61.3	0.39±0.02	1.59±0.03	84±11
Nafion® 212	-	-	1.10±0.02	107±5

[a] Determined by titration
[b] Proton conductivity (through-plane direction)

direction is different from that in the transverse direction as a consequence of the extrusion process during film production [124]. Table 4.2 shows the scattering patterns of the grafted membranes with constant graft level and constant IEC. The membranes with fixed graft level of 40% show similar scattering patterns (ring) and are rather isotropic, unlike that of the pure ETFE base film. In contrast, a slight anisotropic pattern is observed for membranes with $X=0.76$ and 1 (IEC~1.5 mmol g^{-1}), indicating that the anisotropy of ETFE is retained. However, an increase in graft level reduces the anisotropy of the membranes. When the graft level exceeds 28% ($X=0.76$), the grafted membranes show rather isotropic alignment. The azimuthal average of the two dimensional scattering patterns is shown in Figure 4.23. The intensity (I) is given as a function of the scattering vector (q), which corresponds to the length scale in the real space.

The scattering spectra of the co-grafted membranes with constant graft level (proton form) and pure MAN grafted film are practically identical and the scattering is dominated by a low
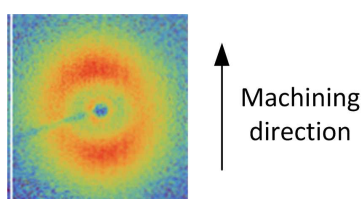
Figure 4.22: Two dimensional scattering pattern of ETFE film (25 μm Tefzel 100-LZ from Dupont). The beam stop is visible and the transverse direction is perpendicular to the machining direction. Experiments were carried out in collaboration with Dr. S. Balog.

Styrene molar fraction (X)	GL=40%	IEC=1.5 mmol/g
1 (pure styrene)		
0.77		
0.64		
0.56		
0.39		
0 (pure MAN)		

Table 4.2: Scattering patterns of ETFE-*g*-styrene / MAN membranes with constant graft level and constant IEC. Experiments were carried out in collaboration with Dr. S. Balog

angle upturn (Figure 4.23a). Even though the co-grafted membranes contain different molar fractions of styrene, the features of the scattering curve of all co-grafted membranes are quite similar. A comparable result is obtained for the grafted membrane with constant IEC (Figure 4.23b). The key finding is that the morphology of the co-grafted membranes in the tens of nanometer range depends largely on the graft level and only weakly on the graft composition.
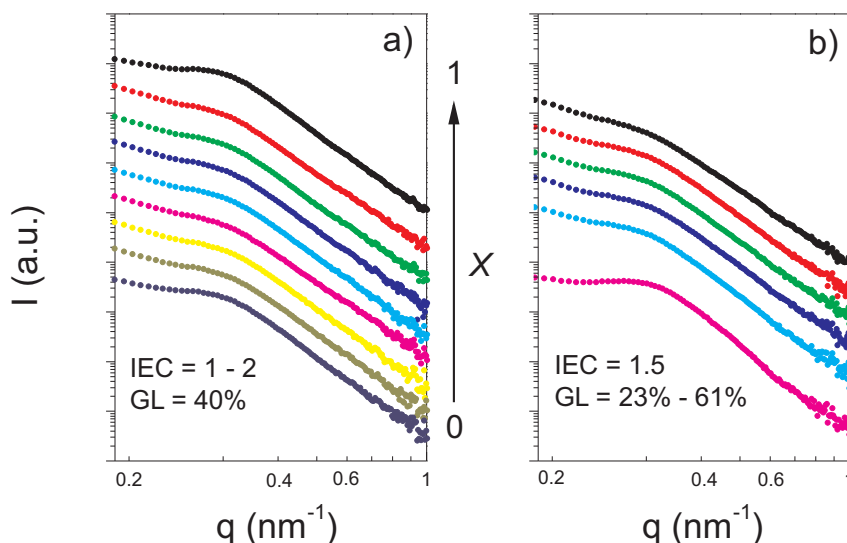
Figure 4.23: Scattering curves of ETFE-*g*-styrene / MAN membranes (proton form) with comparable graft level (∼40%) (a) and constant IEC (∼1.5 mmol g^{-1}) (b) with q ranging from 0.1-1 nm^{-1}, corresponding to morphology on the tens of nanometer scale (crystalline and amorphous phases). Experiments were carried out in collaboration with Dr. S. Balog.

4.3.2 Ionomer peak of membranes with fixed graft level and fixed IEC

In the proton form, the contrast between membranes with different styrene molar fractions is not dominant as shown in Figure 4.23. To enhance the scattering from the ion-rich phase, the membranes were exchanged into Cs^{+} form. The scattering function of the grafted membranes is displayed in Figure 4.24. We are interested in the q-range between 1-10 nm^{-1}, which corresponds to the characteristic length scale of the ionic aggregates [198, 204]. The presence of the ionomer peak at 2-4 nm^{-1} is an evidence for such ionic aggregates and corresponds to a characteristic separation length of 1-3 nm.

The ionic content exists after styrene is functionalized with the sulfonic acid groups and leads to formation of the ionic aggregates that are phase separated from the polymer matrix. In pure MAN grafted film (X=0) or grafted films without sulfonation, there is no ionic content in the film, thus no ionomer peak is observed [203]. The presence of a single scattering peak without higher-order interference peaks implies that the ion-rich clusters lack long range ordering and are randomly distributed within the volume of the membrane with a fluid-like arrangement.

Figure 4.24 shows similar features of the scattering curves for membranes with similar styrene molar fraction. This indicates that the structure of the membrane on the length scale of a few nanometers is dominated by the styrene molar fraction and is not affected by the graft level and IEC. With increasing styrene molar fraction, the peak shifts to a higher q-value and sharpens. The former indicates a shorter characteristic length in the morphology. This characteristic length scale is associated with the distance between the ionic aggregates. Thus, the distance

101
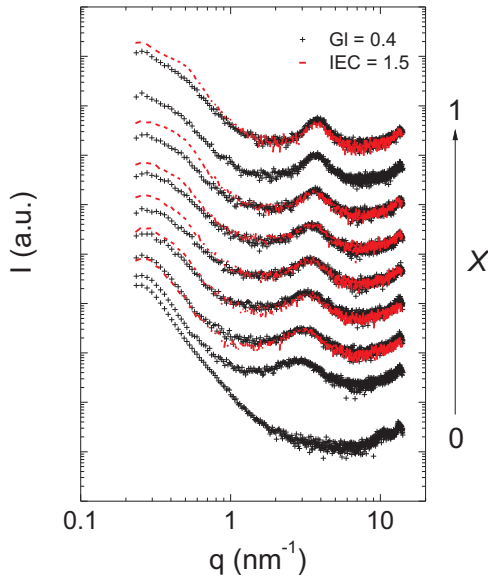
Figure 4.24: Scattering curves of ETFE-*g*-styrene / MAN with constant graft level and constant IEC, respectively. Membranes in proton form and the Cs^+ exchanged form are used to characterize the morphology in the q ranges from 0.1-1 nm^{-1} and 1-10 nm^{-1}, respectively. The peak shifts to a higher q-value with increasing styrene molar fraction X. Experiments were carried out in collaboration with Dr. S. Balog.

between the ionic aggregates of membranes containing lower styrene molar fractions is larger than those with higher styrene molar fractions. Peak sharpening implies that the ionic aggregate is smaller with increasing styrene molar fraction. Furthermore, as a general feature for all the graft copolymers, small angle scattering (an upturn) is observed at $\sim$2 nm^{-1}, indicating an order on a higher length scale. This upturn represents the inhomogeneity of electron density originating from the crystalline and amorphous domains [124, 203] and not from large grafted domains, since it is also present in the ETFE base film. In Nafion, the upturn is also observed at q=0.2 nm^{-1} but with much lower intensity, suggesting more uniformly distributed ionic aggregates.

The differences in the scattering peaks of the co-grafted membranes are small, however, more structural details of the ion rich model can be obtained from models. The model applied here is a hard-sphere-fluid model proposed by Yarusso and Cooper [205], which is based on the assumptions that the system consists of identical spherical ionic aggregates dispersed in the polymer matrix and the ionic aggregates are separated by the polymer matrix. The ionic aggregates are attributed to the ionomer peak with a radius of the core equivalent to R_1 surrounded by a shell of radius R_{ca} (Figure 4.25). This is referred to as a core-shell model, in which the electron density in the core is higher than in the shell. The closest approach distance between two ionic aggregates is equal to $2R_{ca}$. $1/Vp$ is the number density of ionic aggregates (i.e., number of ionic aggregates per unit volume). According to Kinning, the scattering intensity I is given as

a function of R_1, R_{ca} and V_p [206]. The parameters obtained from the model fit as a function of styrene molar fraction are shown in Figure 4.26.
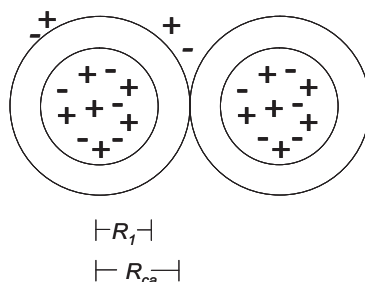
Figure 4.25: Schematic of hard-sphere-fluid model showing a core-shell structure where R_1 represents the radius of the core of the ionic aggregate and R_{ca} is the radius of the shell of the ionic aggregate. The closest approach distance between two ionic aggregates is equal to $2R_{ca}$ [205, 207].

According to Tsang *et al.*, the size of ionic aggregates seems to be related to the proximity of the sulfonic acid groups: the closer they are, the greater electrostatic attractions they experience among each other. This facilitates ion clustering and subsequently leads to larger ionic aggregates [198]. The closest proximity obtained in their work was for an alternating chain of styrene and styrene sulfonic acid. Based on their findings, it was expected that the ionic aggregate size would be largest for the pure styrene grafted membrane (X=1). However, Figure 4.26 reveals that the radius of the core (R_1) and the radius of the shell (R_{ca}) of the ionic aggregates decrease, whilst the number density of ionic aggregates (1/Vp) increases with increased molar fraction of styrene. As shown previously, membranes containing styrene / MAN favor an alternating chain sequence, so most of the styrene sulfonic acid groups are evenly spaced by a MAN unit (subsection 3.1.3). An increase in MAN (X<0.5) interrupts this chain sequence due to the formation of extended MAN sequences, which take up space and result in larger ionic aggregates. In contrast, as the styrene content increases the ionic aggregates are more densely packed. It should be noted that the polymer prepared in this study is less well controlled than the work by Tsang *et al.* [198]. In addition, our synthesis approach is also different. The effect of the size of neighboring groups next to styrene sulfonic acid may influence the chain conformation and steric hindrance, leading to different observations. The parameters obtained from the fit highlight the differences in membrane structure by varying styrene content in the grafts. The structural differences may be used to explain the discrepancy of the proton conductivity of different co-grafted membranes with constant IEC at reduced humidity. An increase in number density with increase in styrene content provides the higher proton conductivity at reduced humidity because the ionic aggregates are closer to each other. Therefore, a more extensive percolation of ionic domains is formed [198], implying less water is necessary to connect the aggregates upon hydration. In addition, this leads to an inherently higher acid concentration. Therefore, the proton conductivity of
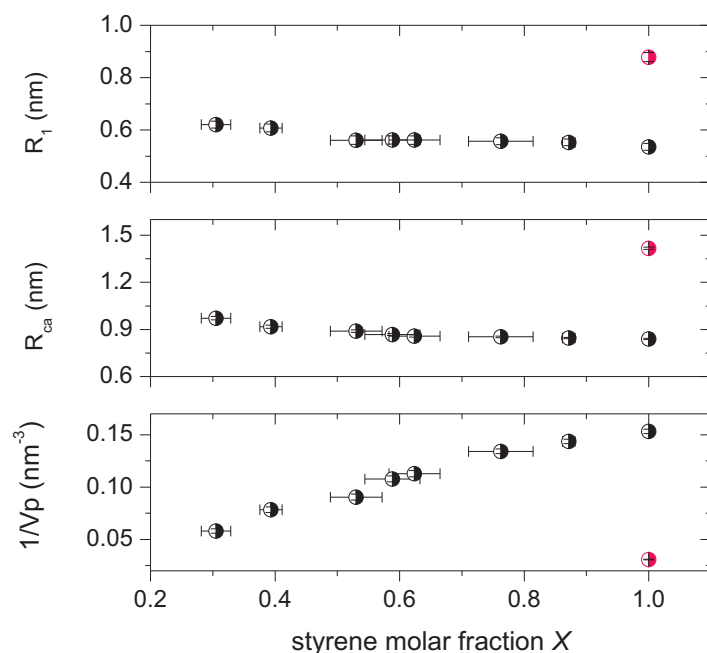
Figure 4.26: Model fit parameters for ETFE-*g*-styrene / MAN membranes with a fixed graft level of 40% as a function of styrene molar fraction. Since the scattering of the membranes with a fixed graft level of 40% and that of a fixed IEC ($\sim$1.5 mmol g^{-1}) is the same, the hard-sphere-fluid model fit would give the same results. The red data point is shown for comparison with the Nafion$^{®}$ membrane. Experiments were carried out in collaboration with Dr. S. Balog.

membranes with similar IEC increases significantly with increasing styrene content at reduced humidity. While the styrene molar fraction is kept constant, an increase in graft level (and IEC accordingly) will lead to larger or more grafted domains. The schematic representation of the co-grafted membrane structure with varying styrene molar fraction and IEC in dry state is given in Figure 4.27. In comparison, the ionic aggregates in the Nafion membrane are larger but fewer than in the co-grafted membranes. This structure is assumed to resemble that at low relative humidity.

The evolution of the conductivity at reduced humidity as proposed by the percolation model based on spherical ionic aggregates [119] is expected to be identical for the co-grafted membranes and Nafion. The dry membrane is represented by isolated ionic aggregates. With increasing relative humidity, the water uptake increases due to the hydrophilic nature of the membranes. The water molecules solvate the sulfonic acid groups and subsequent incorporation of water starts to swell the ionic aggregates and forms a connection with their closest neighbors (intra-domain percolation), resulting in hydrophilic domains. A shorter interaggregate distance indicates that a lower water content is necessary to connect them. At higher water uptake, the hydrophilic domains swell and are connected to form inter-domain percolation. This percolation would result in a significant increase in proton conductivity, which is limited by the maximum separation
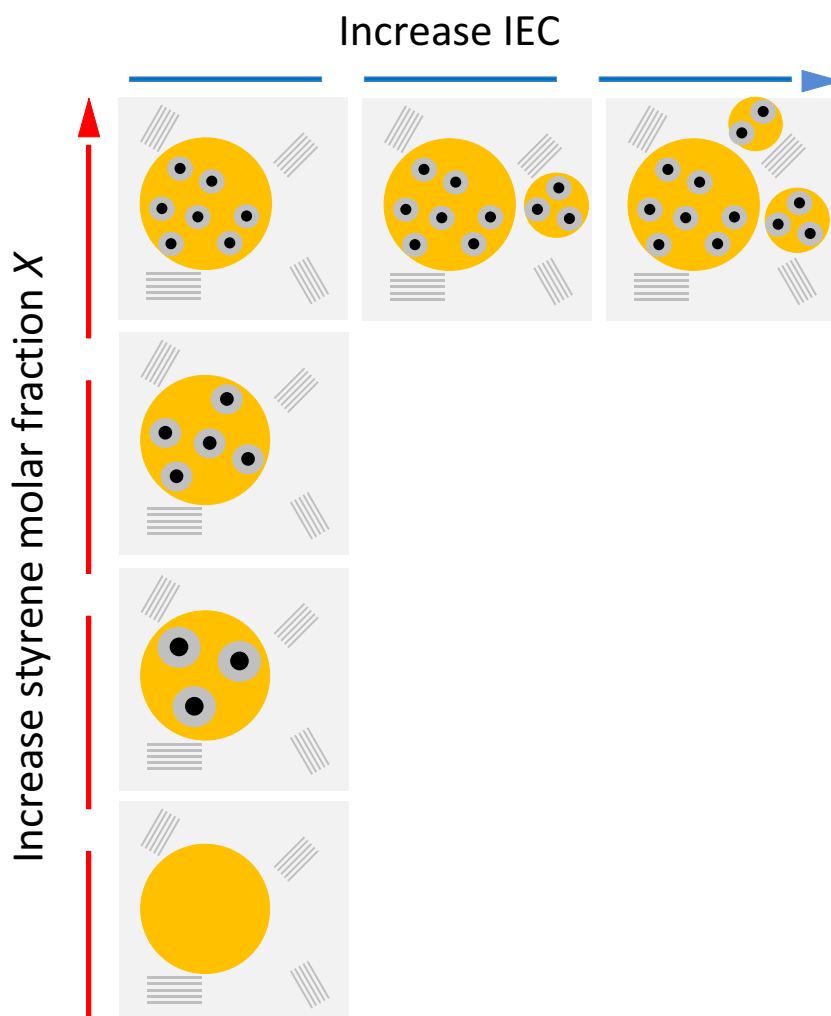
Figure 4.27: Schematic representation for the spatial arrangement of ionic aggregates in dry membranes prepared by radiation grafting based on Yarusso-Cooper model [205, 207]. The density of ionic aggregates increases with increasing styrene molar fraction X but their size decreases (vertical axis). An increase in IEC leads to an increase in the number density (horizontal). The core of the ionic aggregate is given in black surrounded by the shell (light grey). The region in orange are the grafted domains, which can swell upon hydration. The parallel bars in grey are crystalline domains and the light grey area represents the ETFE backbone. Illustration is adapted from Dr. S. Balog.

distance between the hydrophilic domains. Therefore, the conductivity obtained for both types of membrane corresponds to the evolution of percolation. The SAXS results emphasize the differences in the co-grafted membranes and Nafion nanostructures in the dry state. To illustrate the differences between both types of membrane, formation of a percolated ionic network is proposed (Figure 4.28).

Although the co-grafted membranes provide domains richer in ionic aggregates, their proton conductivity at reduced humidity is generally lower than that of Nafion. Given the fact that the

crystallinity is more pronounced in co-grafted membrane than in Nafion, it is possible that the crystalline regions may act as a barrier, inhibiting proton mobility between separated ion rich domains. A greater separation of the ion rich domains due to the presence of crystalline domains in the co-grafted membranes reduces the proton transport. By inference, if the hydrophilic domains are isolated and are surrounded by ungrafted crystalline domains, the percolation between P1 and P2 will be more difficult compared to the case of Nafion, where P1 and P2 are located in the same hydrophilic domain (Figure 4.28). We may conclude that to obtain high proton conductivity, it is preferred to have well distributed and closely spaced ionic aggregates.
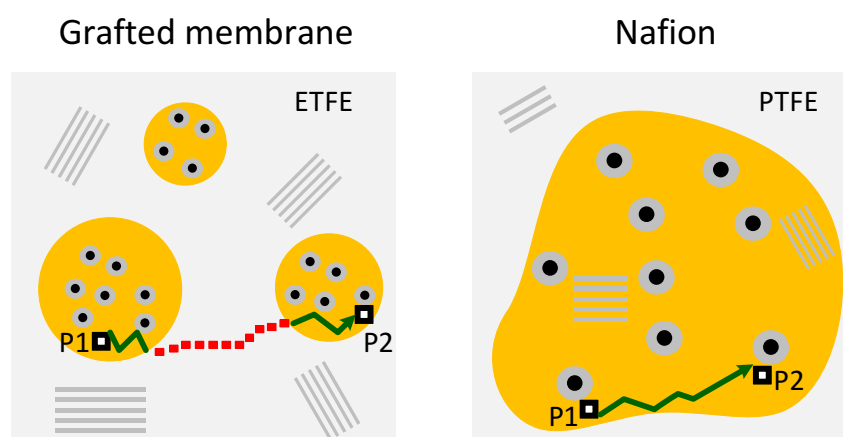
Figure 4.28: Schematic representation for the spatial arrangement of ionic aggregates in dry membranes. The yellow domains are ion rich domains (also known as hydrophilic domains), which can swell upon hydration. In Nafion membranes, the ionic aggregates are homogeneously distributed in the PTFE matrix. The hydrophilic domains of the grafted membranes are more separated, which impedes the percolation between ionic aggregates, e.g. P1 and P2. Illustration adapted from Dr. S. Balog.

4.4 Conclusions

The effects of MAN in styrene / MAN co-grafted films and membranes on molecular structure and *ex situ* relevant properties of fuel cells have been investigated. FTIR measurements were undertaken to quantify the amount of grafted monomers. We found an apparent peak position shift to a higher wavenumber in the co-grafted films with increasing MAN content, especially those corresponding to C≡N, and CH$_3$ vibrations of the MAN. The shift could be associated with the change in the environment due to the presence of MAN. However, the peak shifts were not found in sulfonated samples. This may suggest that the interactions due to the presence of MAN was minimized by the presence of of sulfonic acid groups.

An increase in MAN molar fraction enhances the hydrophilicity of the membrane, resulting in a higher water uptake in water swollen state. Although water is essential for proton transport,

too much water can lead to extensive membrane expansion and inferior dimensional stability.

Incorporation of MAN as styrene's comonomer shows the strong links between conductivity and the MAN content. The styrene / MAN co-grafted membranes with similar IEC exhibited comparable proton conductivity in fully swollen state, regardless the water uptake. However, at reduced humidity (<80%), membranes with a higher MAN content showed a higher conductivity loss. The water absorption of the membranes at reduced humidity (<80%) does not show the same trend as the water uptake in the water swollen state. The differences in proton conductivity of the grafted membranes at low relative humidity were considered to be a consequence of the different membrane structures due to the presence of MAN. Membrane structural analysis by small angle X-ray scattering (SAXS) was carried out to elucidate the origin of these differences.

The SAXS spectra reveal the ionomer peak, which is characteristic for ion containing polymers. Its position and intensity are related to the membrane structure. In the grafted membrane series, the structure of the dry state is directly affected by the graft composition. With an increase in styrene molar fraction, the size of ionic aggregate decreases while their number density increases. This structure results in a more extensive percolation, which leads to a better connectivity between the ionic aggregate domains and therefore yields highest proton conductivity among the co-grafted membranes.

In addition to the ionomer peak, an upturn at very small angle is observed in the grafted membranes, indicating heterogeneity in a larger length scale due to the presence of crystalline and amorphous phases. Although the proton transport occurs in the ion rich domains, the proton conductivity is highly affected by the presence of the crystalline phase. The latter are ion-free non-grafted domains, which are impermeable to water [208] and therefore impede the inter-domain percolation between separated hydrophilic domains. This is in contrast to Nafion where the separation between amorphous and crystalline domains is less dominant and it can be anticipated that the hydrophilic clusters are uniformly distributed. The structure of the co-grafted membranes in the dry state possesses smaller ionic aggregates (~ 2 nm) compared to that of Nafion (~ 3 nm). The size of the former is in good agreement with literature based on grafted polymer containing styrene sulfonic acid [198].

At low water uptake, the distribution of the ion rich domains determines the proton transport since the hydrophilic domains are isolated. The presence of the crystalline regions contributes to more separated hydrophilic domains. In order to form a well-defined network to facilitate proton conduction throughout the membrane, water is necessary to overcome this obstruction. The observations indicate that the crystalline domains are responsible for the lower proton conductivity at reduced humidity of the styrene grafted membranes compared to Nafion.

The work clearly emphasizes that the proton conductivity is an interplay between many factors, i.e. water uptake, IEC and structure. The trend obtained from the proton conductivity

in the water swollen state can not be used to predict the proton transport behavior at reduced humidity.

The membrane degradation rate was investigated in terms of OCV hold tests, where evolution of the high frequency resistance was monitored with increasing OCV time. Results show that the presence of MAN in styrene based membranes leads to an increase in membrane stability. The improvement in membrane stability could be a cumulative effect from the decreased hydrogen crossover as well as the chemical nature of nitrile.

5

Styrene / MMA and styrene / MAA membranes

The previous chapters were orientend toward membranes containing nitrile comonomers, namely MAN and AN. It was found that the proton conductivity and membrane swelling are bottlenecks of styrene / MAN co-grafted membranes. At reduced humidity the proton conductivity is inhibited by the presence of MAN, suggesting that proton conductivity depends not only on the acid content but also on the presence of a comonomer. In addition, the introduction of a comonomer to styrene sulfonic acid may profoundly affect membrane properties and ultimately performance and durability in the fuel cells. Therefore, tuning the comonomer functional group of the grafted membrane is of utmost importance. A major incentive of this chapter is to investigate the effects of nitrile-free comonomers on the proton conductivity and water uptake. Methyl methacrylate (MMA) and methacrylic acid (MAA), containing an ester and carboxylic functional groups, respectively, will be used as model compounds to be grafted with styrene. It should be noted that the functional groups at the end of synthesis route may be different from the original comonomer due to the susceptibility to hydrolysis or other chemical reactions that may induce changes in the membrane structure during sulfonation step.

In the first place, styrene / MMA and styrene / MAA films will be prepared by radiation grafting. The composition of the grafted films was kept constant in order to differentiate the effect of the different functional groups. To obtain an equimolar styrene to comonomer ratio, we carried out a series of experiments using grafting solutions containing different styrene to comonomer ratios. The chemical composition in the grafted films and membranes was determined by FTIR. To ensure that styrene is sulfonated, the ion exchange capacity of the membranes was determined as described in the previous chapters.

To compare the proton conductivity of different grafted membranes in water-saturated state, a series of membranes with varying ionic content was prepared and characterized. The benefits

of a systematic study of proton conductivity may reveal the structure-properties relationships in greater detail.

5.1 Synthesis and characterization

To determine the compositions of co-grafted membranes, a calibration curve of a single monomer needs to be established. Grafting of MMA and MAA into ETFE base film was carried using 1.5 and 15 kGy pre-irradiated ETFE films, respectively. The amount of graft in the polymer matrix is quantified by the graft level (Equation 2.1). The grafting behavior is significantly affected by the grafted monomers. The irradiation dose was adjusted to obtain a reasonable grafting time.

5.1.1 Grafting of styrene / MMA into ETFE

The difference in the grafting behavior of styrene and MAA can be understood based on the compatibility with the ETFE base film (Figure 5.1). For pure MMA grafted into ETFE, the graft level increases slowly in the first four hours, after which it increases rapidly. Such delay in the grafting rate was previously explained as the result of the slow warming of the solution and restricted diffusion of MMA to the grafting sites [151], which in turn lower the local monomer concentration and the grafting rate. The polar nature of MMA may restrict its diffusion into the apolar ETFE film. Based on this observation, a pronounced formation of grafting fronts may be expected. With time, more MMA is introduced into the film and makes the film more polar, allowing more MMA to penetrate into the polymer matrix. This increases the local monomer concentration, yielding a higher grafting rate.

It is evident from the kinetic curves that the graft level of styrene responds differently compared to MMA grafted films, in which the highest grafting rate is found in the beginning of the reaction and levels off already after two hours. The compatibility between styrene and ETFE appears to enhance the diffusion of styrene into ETFE matrix. Therefore, styrene grafts were built up faster than the MMA grafts and caused the film to swell appreciably, allowing access of styrene to the radicals. Leveling off of the kinetics curves implies fast termination of growing chains. Upon increasing graft level of MMA, the mobility of the polymer chains increases, thereby shortening the radical life time.

Subsequently, FTIR analysis of pure MMA grafted films with varying graft level was carried out. To establish a calibration curve, the characteristic vibrational bands of the grafted components normalized to the bands of the ETFE film. The same principle is applied here as shown in subsection 3.1.2.

As a first approximation to prepare styrene / MMA co-grafted membranes with equimolar styrene to MMA, a series of grafted films with varying styrene molar fraction in the grafting
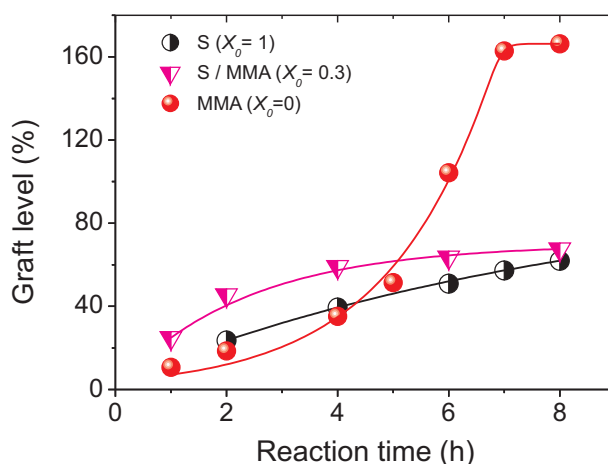
Figure 5.1: Grafting kinetics of styrene / MMA into 25 μm ETFE film (1.5 kGy) at 60°C for different styrene molar fraction in the grafting solution (X_0). The grafting solution contains 2:7:1 (v/v/v) of monomer: isopropanol: water.
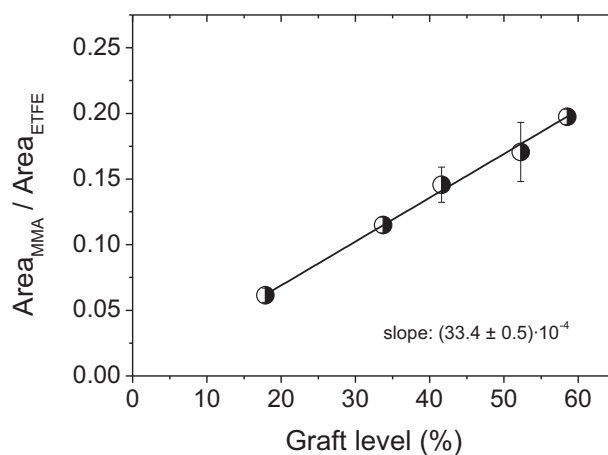
Figure 5.2: Calibration curve for determining the amount of MMA introduced into ETFE base film. The characteristic band chosed for MMA is the C-H deformation (umbrella) vibration of the CH_3 group (1390 cm^{-1}). The characteristic peak is normalized by the intensity of C-H deformation vibration of ETFE band (1325 cm^{-1}).

solution X_0 was prepared. The graft composition of the films was analyzed based on the calibration curve (Figure 5.2). The styrene molar fraction in the film was found to increase with that in the grafting solution. Apparently, to obtain styrene molar fraction of approximately 0.5 in the grafted film, a styrene molar fraction in the grafting solution X_0 of 0.3 should be applied. This indicates that grafting of styrene into ETFE is more favorable than MMA in the bimonomer mixture. The grafting curves of this composition is shown in Figure 5.3 along with the graft composition of the grafted films. The graft composition seems to be unaffected by the grafting time, implying no composition drift up to 8 hours grafting. A tendency of alternating chain sequence of styrene / MMA copolymer can be expected as reported in literature, in which the

reactivity ratios in bulk copolymerization of styrene and MMA are approximately 0.5 [160, 162].
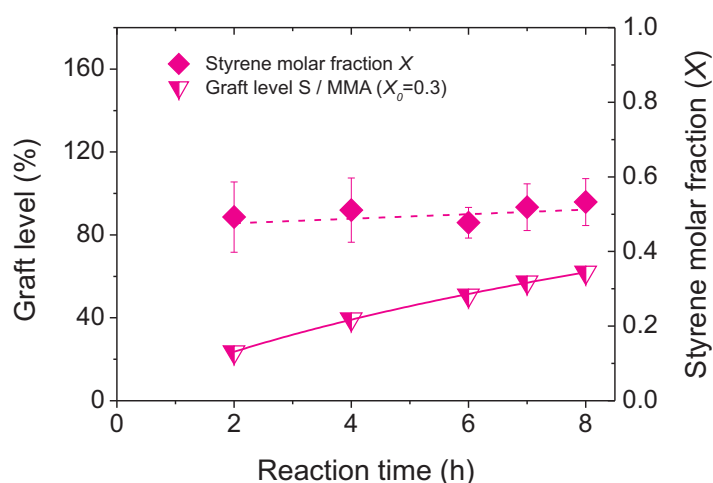
Figure 5.3: Grafting kinetics of styrene / MMA into ETFE base film (styrene molar fraction in the grafting solution X_0=0.3). The amount of styrene grafted into the base film is determined based on the calibration curve.

It appears that the kinetics curve of styrene / MMA follows a similar trend as that of styrene. This suggests that penetration of MMA is less restricted in the presence of styrene. Based on this observation, further analysis was performed to compare the molar based graft level of styrene. Figure 5.4 shows that the amount of styrene introduced into the base film when styrene is the only monomer in the grafting solution is higher than in the styrene / MMA mixture (X_0=0.3). This indicates that the presence of MMA influences grafting of styrene into the base film. Plausible explanations to the lowering of styrene graft level could be the competitive reaction between styrene and MMA with the radicals, different diffusion behavior ands dilution of styrene at the grafting sites.

5.1.2 Grafting of styrene / MAA into ETFE

As a first screening step for potential grafting conditions of MAA, the graft level was determined for 2:8 (v/v) mixtures of MAA with water at 60°C (15 kGy). After 14 hours, the graft level reaches 280% and the membrane became very brittle and difficult to handle. In addition, the grafting solution at the end of the experiment became very viscous, indicating formation of homopolymer. To impede the grafting rate, additional experiments were performed with a lower dose (1.5 kGy). It was found that by lowering the dose, the grafting rate was dramatically inhibited. After 24 hours, the graft level of ETFE-g-MAA was still close to zero. This was thought to be partially attributed to extensive homopolymer formation, and hence lower grafting rate. To minimize homopolymerization in the grafting medium, inhibitors such as Mohr salt
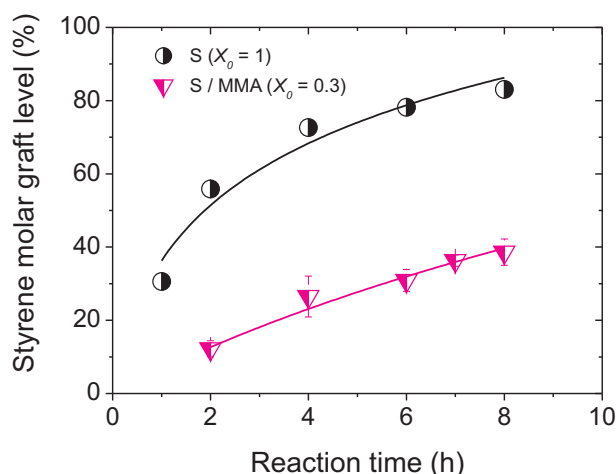
Figure 5.4: Grafting kinetics of styrene and styrene / MMA (X_0=0.3) grafted films expressed in the number of mol of styrene.

$((NH_4)_2Fe(SO_4)_2)\cdot6H_2O)$, $CuSO_4$ or $FeCl_3$ can be applied [209, 210]. Yet, this approach is not favorable for our application because traces of the iron ions may interfere with the crystallite structure and contaminate the grafted films [211]. MAA is hydrophilic in nature and it can be expected that grafting of MAA into ETFE is limited by monomer diffusion due to the differences in their hydrophilicity. Since ETFE does not swell in common solvents, it can be reasonably assumed that grafting proceeds by the grafting front mechanism, in which the grafting begins at the surface and facilitates swelling of the film, allowing monomer diffusion. The faster grafting takes place at the surface, the higher diffusion rate is obtained. At a lower irradiation dose, the initial rate of grafting is lower than at a higher one due to lower radical concentration. Grafting proceeds successfully in higher dose film, indicating that grafting rate at the early stage is vital. In the 1.5 kGy pre-irradiated films, the radical concentration is too low, so when MAA is introduced into the polymer matrix, the amount of grafted monomers is insufficient to the change the hydrophilicity of the films. This inhibit monomer diffusion, and hence results in an unsatisfactory graft level.

To establish a calibration curve, grafting of MAA was carried out in a grafting mixture containing 1:9 (v/v) MAA : water (Figure 5.5). Although it is not very obvious, a delay in grafting at the beginning of the reaction may be expected. Subsequently, the calibration curve for pure MAA grafted film is carried out according to the FTIR analysis (Figure 5.6). The intensity of C-H deformation band of CH_3 (1390 cm^{-1}) normalized by ETFE band (1325 cm^{-1}) have been chosen to correlate the FTIR intensity with the graft level.

Since styrene is not soluble in water, grafting of styrene / MAA was carried out in a grafting solution containing 2:8 (v/v) MAA: ethanol. The graft composition is characterized based on the established calibration curve. It is evident that when X_0 of 0.5 is used, X of approximately
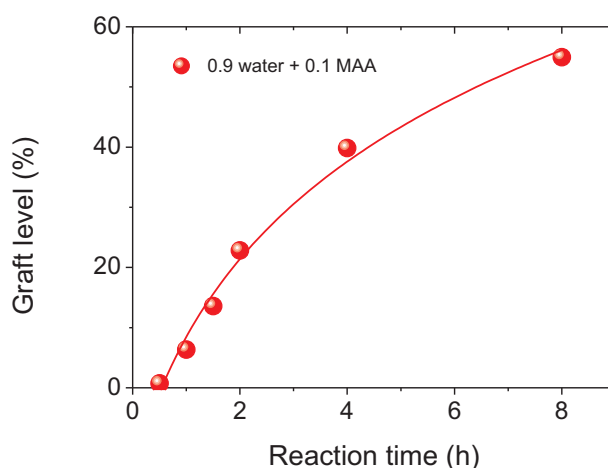
Figure 5.5: Grafting kinetics of MAA into 25 μm ETFE film (15 kGy) at 60°C. The grafting solution contains 1:9 (v/v) of monomer: ethanol.
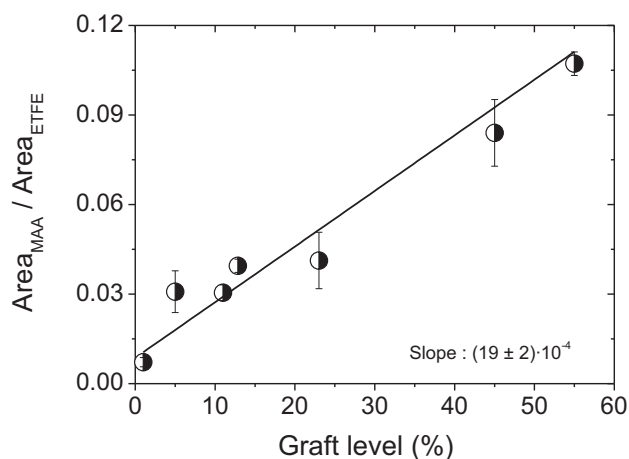
Figure 5.6: Calibration curve for determining the amount of MAA introduced into ETFE base film (15 kGy). The characteristic bands chosen for MAA is the C-H deformation (umbrella) vibration of the CH_3 group (1390 cm^{-1}). The characteristic peak is normalized by the intensity of C-H deformation vibration of ETFE band (1325 cm^{-1}).

0.6 is obtained with only a slight decrease in styrene molar fraction up to 24 hours grafting (Figure 5.7).

5.1.3 FTIR analysis

The appropriate conditions for preparing an equimolar graft composition was determined by adjusting X_0 as described above. After the desired graft composition is obtained, the grafted films were subjected to sulfonation to incorporate sulfonic acid groups. According to the FTIR spectra, a change in pure MMA grafted sample is observed after sulfonation. The reason for this is the nature of ester compound, which is prone to hydrolysis under acidic conditions. It
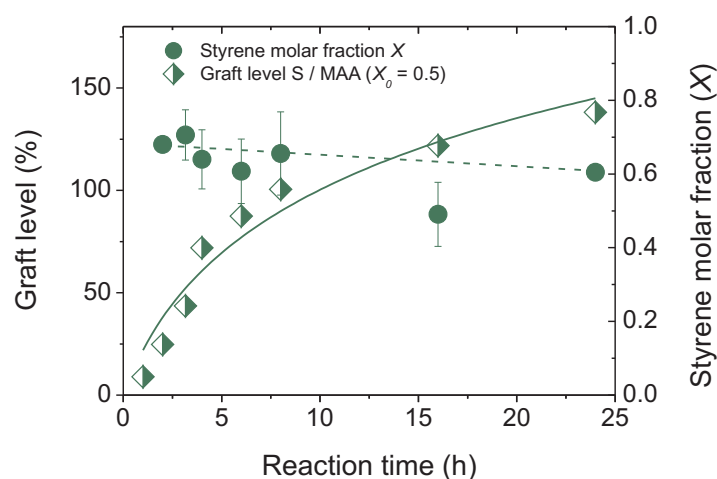
Figure 5.7: Grafting kinetics of styrene / MAA. The styrene molar fraction in the solution is 0.5. Based on the calibration curve, the styrene molar fraction in the grafted films is determined. The lines are given as the guide to the eyes.

is demonstrated that similar peaks are found for sulfonated ETFE-*g*-MAA films, implying that the same reaction seems to occur as in the homopolymer of MMA (Figure 5.8).
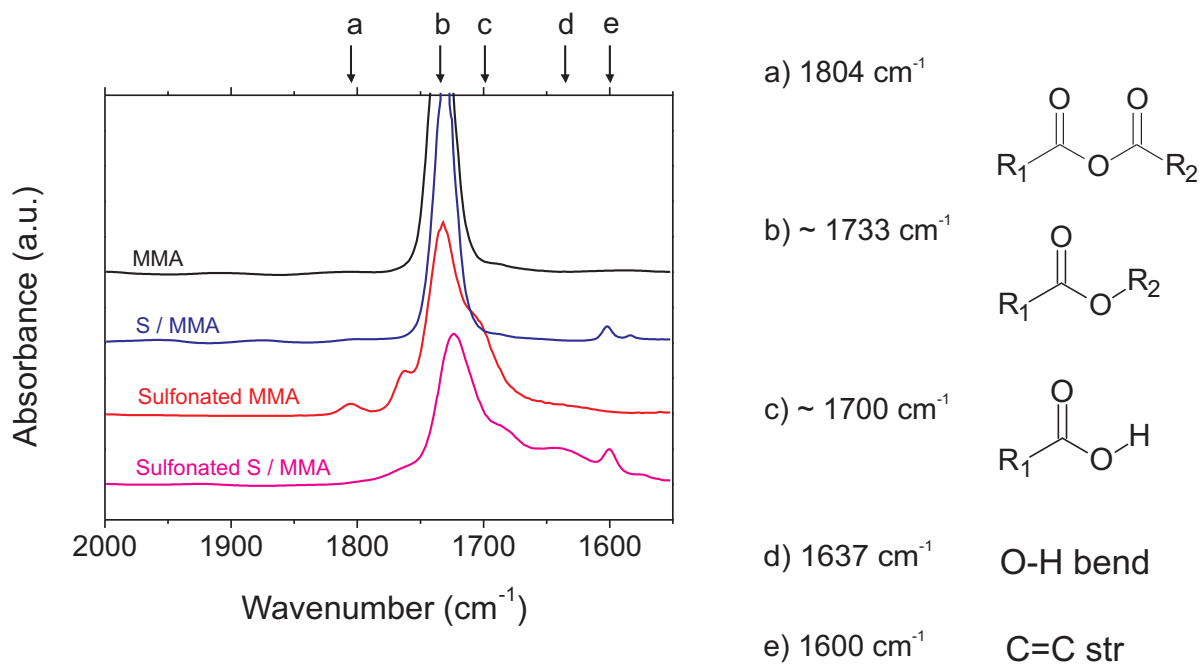
Figure 5.8: FTIR spectra of pristine and sulfonated styrene / MMA ($X \sim 0.5$) and MMA grafted films.

In the carbonyl region (1800-1700 cm^{-1}), the formation of carboxylic acid after our sulfonation procedure is confirmed by the presence of a peak shoulder at 1700 cm^{-1} (-COOH). The adjacent absorption band at 1733 cm^{-1} corresponds to the ester (COOMe). The intensity of this

ester band decreases significantly, which is associated with the dilution of mass because of the membrane expansion. A peak at 1804 cm^{-1} is only found in sulfonated MMA film. This peak is associated with the acid anhydride, which may have been formed by condensation of adjacent carboxylic acid groups during drying [212]. The absence of this peak in the co-grafted membranes indicates that the monomer units in the grafted copolymer have a tendency to alternate, in which the nearest neighbors of MMA are styrene units.

For styrene / MAA, a shift in the carbonyl peak is observed to a lower wavenumber after sulfonation (Figure 5.9). This implies that sulfonation leads to a change in carboxylic acid structure. The redshift in the carbonyl region from 1700 to 1679 cm^{-1} indicates formation of a conjugated ketone [213, 214], suggesting that the carboxylic acid group is predominantly lost during this step. The precise chemical structure is difficult to establish with certainty with only FTIR spectra. A more detailed investigation is carried out in section 6.1.
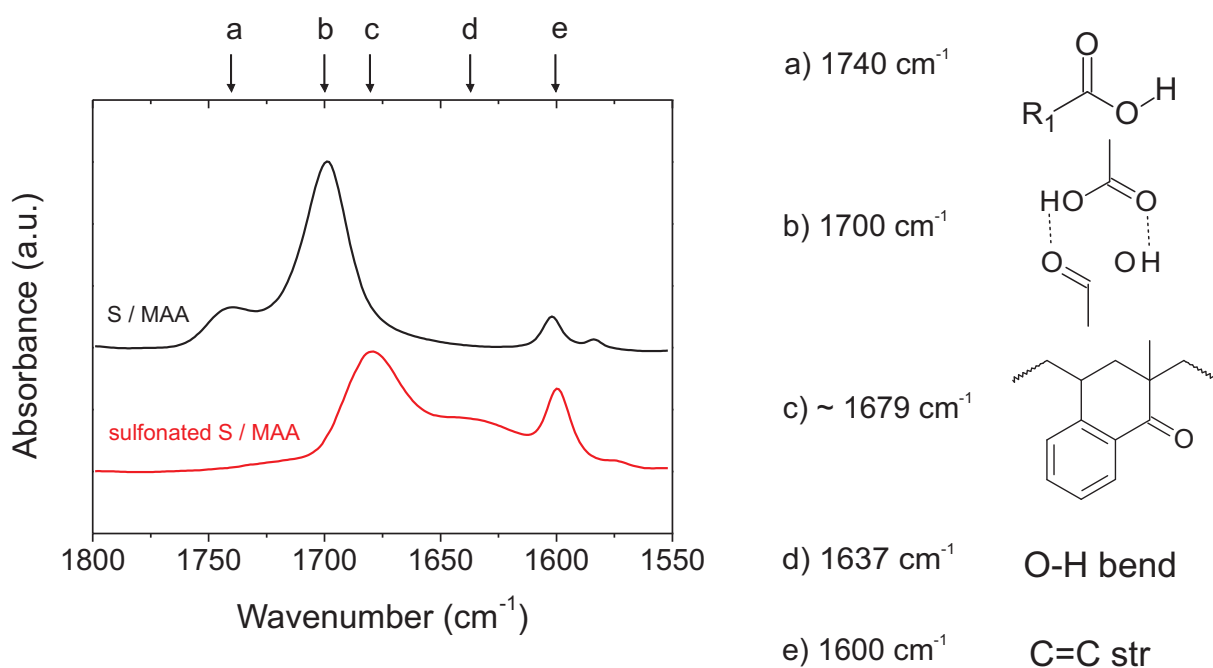
Figure 5.9: FTIR spectra of pristine and sulfonated styrene / MAA films ($X\sim0.6$).

5.1.4 Degree of sulfonation

In addition to the chemical structures, fuel cell relevant properties of the grafted membranes are studied to better understand the structure-property relationships. Figure 5.10 shows the IEC as a function of the graft level of styrene / MMA membranes sulfonated with 2% and 10% chlorosulfonic acid. The theoretical IEC (solid line) is calculated based on the assumption that each styrene units carries one sulfonic acid group. The increase in IEC with graft level confirms the presence of sulfonic acid group, which is a key species for proton transport.
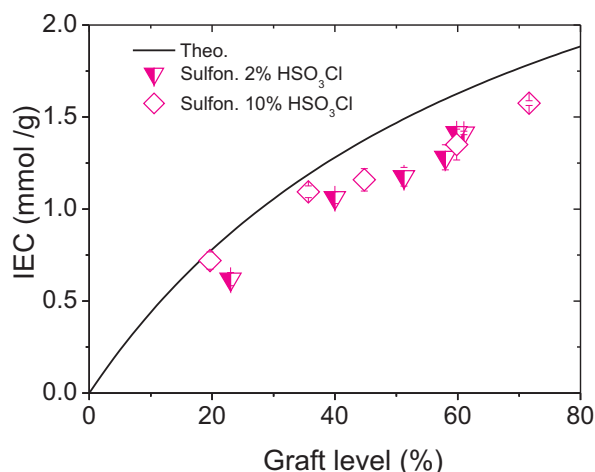
Figure 5.10: Relationship between IEC and the graft level of styrene / MMA membranes. The sulfonation of the films was carried out with 2% and 10% chlorosulfonic acid in dichloromethane at room temperature for 5 hours and subsequent hydrolysis in 80°C water for 8 hours. The theoretical IEC is calculated based on an average styrene molar fraction of 0.51.

The degree of sulfonation is determined from the acid content determined by titration and the calculated theoretical IEC. On average, the degree of sulfonation was found to be close to 80% using 2% chlorosulfonic acid solution in dichloromethane at room temperature. Incomplete sulfonation was initially attributed to the rather mild sulfonation conditions. However, by increasing the concentration of the sulfonating agent to 10%, the average degree of sulfonation is largely unchanged, implying that the concentration of the sulfonating agent does not enhance the rate of sulfonation. It should be pointed out that the sulfonation process of the grafted film is also a diffusion controlled reaction. The presence of a comonomer may restrict swelling of the grafted films compared to styrene grafted film and lower the accessibility of the sulfonating agents to the styrene units. In addition, MMA may reduce the reactivity of the styrene units towards electrophilic substitution by chlorosulfonic acid. This type of behavior is observed in FEP-g-AMS / MAN, where the degree of sulfonation decreases with AMS content, in which it is explained that the susceptibility to sulfonation is affected by steric reasons [215].

The homogeneity of the sulfonic acid distribution was verified by the conductivity measurements in the through-plane and in-plane directions (Figure 5.11). The conductivities in both directions of styrene / MMA membranes (except for that with lowest graft level of 23%) are comparable, implying a homogeneous distribution of the sulfonic acids. For the membrane with lowest graft level of 23%, the conductivity in the in-plane direction is higher than in the through-plane direction. This can be explained by a significant grafting gradient in the thickness direction, in which a higher density of grafts is found on the membrane surface than in the center of the membrane. Over time, the grafting front moves to the center of the films and a homogeneous graft distribution is obtained. This observation emphasizes that it is vital
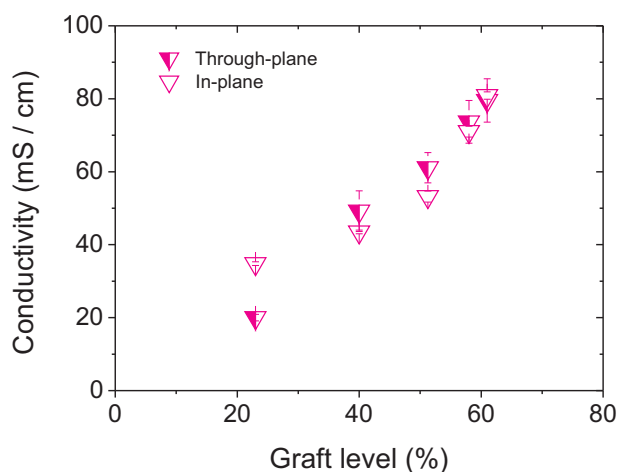
Figure 5.11: Through-plane and in-plane proton conductivity of styrene / MMA membranes ($X{\sim}0.5$) in water swollen state at RT.

that adequate time is allowed for monomer diffusion through the polymer matrix to obtain a homogeneous membrane.
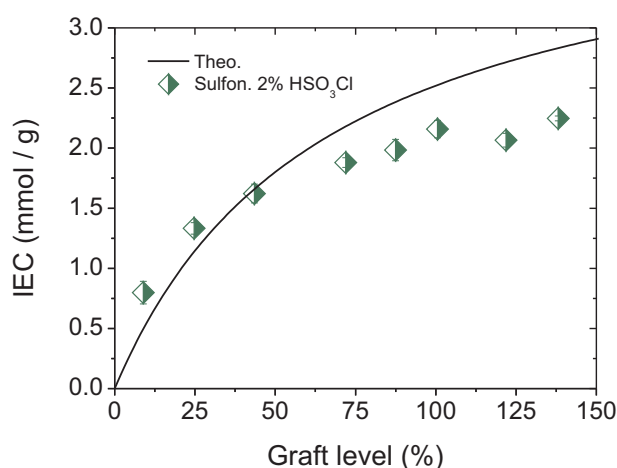
Figure 5.12: Relationship between IEC and the graft level of of styrene / MAA membranes. The films were sulfonated in 2% chlorosulfonic acid in dichloromethane at room temperature for 5 hours and subsequent hydrolysis in 80°C water for 8 hours.

The behavior of styrene / MAA membranes is similar to that of styrene / MMA membranes. Figure 5.12 compares the theoretical IEC calculated from an average styrene molar fraction X of 0.61 and the IEC obtained experimentally by titration of the sulfonic acid groups in the membrane. It seems that at low graft level, the IEC of styrene / MAA membranes are comparable to the theoretical IEC, implying complete sulfonation. When the graft level exceeds 40%, the IEC starts to diverge from the theoretical values with an average degree of sulfonation of 84±4%. As shown previously, an increase in concentration of the sulfonating agent does not lead to further improvement in the degree of sulfonation, therefore only 2% chlorosulfonic acid

in dichloromethane is used. The change in the polymer matrix by increasing the graft level may reduce the susceptibility of styrene towards sulfonation. The precise sulfonation mechanism of the co-grafted films is still unclear and requires further investigation.

The homogeneity of the membranes is further investigated by the conductivity experiments as discussed above. The difference between in-plane and through-plane conductivities of styrene / MAA membranes are not significant over the examined graft level range (Figure 5.13), hence the monomers are grafted homogeneously throughout the membrane.
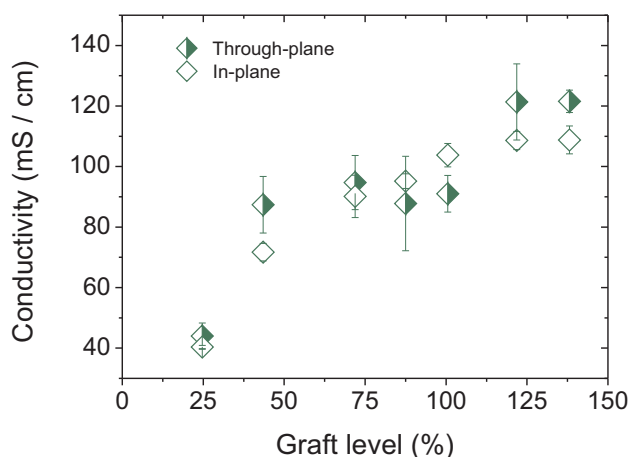
Figure 5.13: Conductivity of water swollen styrene / MAA membranes ($X \sim 0.6$) measured through-plane and in-plane as a function of the graft level.

5.1.5 Water uptake and proton conductivity analysis

The conductivity is the product of proton concentration and mobility, which are coupled with the water uptake. To elucidate the effects of MMA and MAA, the relation between hydration level and IEC was examined (Figure 5.14). For pure styrene grafted membranes, the hydration level increases linearly with the IEC. This observation can be explained by considering the change in membrane structure: incorporation of the sulfonic acid group leads to a partial disruption of the crystallites (subsection 4.1.6), which allows the membrane to swell more and affords a higher water uptake. The result is in agreement with Gupta *et al.* [208].

An approximately linear relationship between hydration number and IEC may be assumed for all grafted membranes with constant graft composition. At a first approximation, it might be expected that the co-grafted membranes with the same IEC should exhibit higher water uptake than the pure styrene grafted membrane, as found for styrene / MAN and styrene / AN membranes (subsection 3.2.2). However, this is not clearly the case. At a constant IEC, incorporation of MMA shows a significant increase in hydration level, while the membrane containing MAA shows a hydration level comparable to styrene grafted membranes. The difference
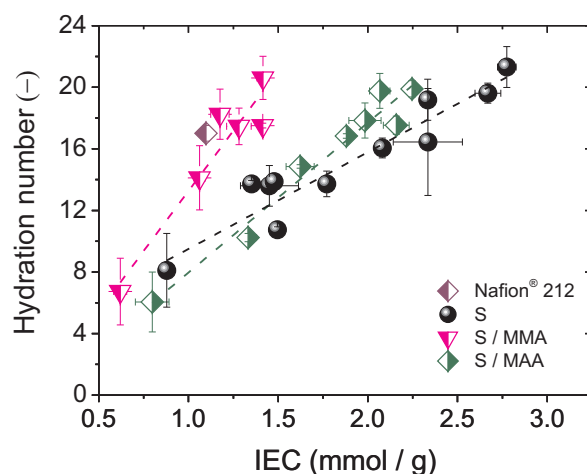
Figure 5.14: Hydration number of styrene, styrene / MMA and styrene / MAA grafted membranes as a function of IEC in water swollen state at RT. The data of Nafion is included for comparison.

may be attributed to the membrane structures: styrene / MAA membranes end up with a dense structure, which does not allow swelling to the same extent as styrene / MMA membranes, and therefore the water uptake is less affected by changes in IEC.

The proton concentration in the water swollen membrane can be determined from the volumetric IEC (IEC_v). As the water content increases, the protons are diluted. In Figure 5.15, the relation between (mass based) IEC and volumetric IEC is displayed. It can be expected that at a given IEC, membranes containing more water would yield a lower volumetric IEC (lower proton concentration). An interesting trend is observed, in which the volumetric IEC seems to increase at low IEC up to approximately 1.5 mmol g^{-1} and then levels off due to proton dilution. This observation confirms the findings that the water uptake increases progressively with increasing IEC, leading to excessive membrane swelling.

To elucidate the effect of proton concentration at room temperature, the proton conductivity through the membrane is plotted as a function of the IEC_v (Figure 5.16). It appears that the conductivity of pure styrene grafted membranes increases with the IEC_v (up to $IEC_v \sim 1.8$ mmol cm^{-3}) and then increases sharply without further change in IEC_v. A similar trend is also observed for styrene / MMA, in which the critical IEC_v is found at around 1.3 mmol cm^{-3}. For styrene / MAA, the data are limited, and it is unclear whether there is a definite trend or not. Yet, it shows that the proton conductivity at IEC_v of approximately 1.5 mmol cm^{-3} varies significantly. This sharp increase in proton conductivity at constant IEC_v is likely due to an increase in proton mobility, implying that the conductivity is less affected by the proton concentration expressed in terms of IEC_v but strongly depends on the water uptake.

By examining the proton mobility, the effects of proton concentration are canceled out and useful information including the extent of acid dissociation, ionic channel tortuosity and spatial
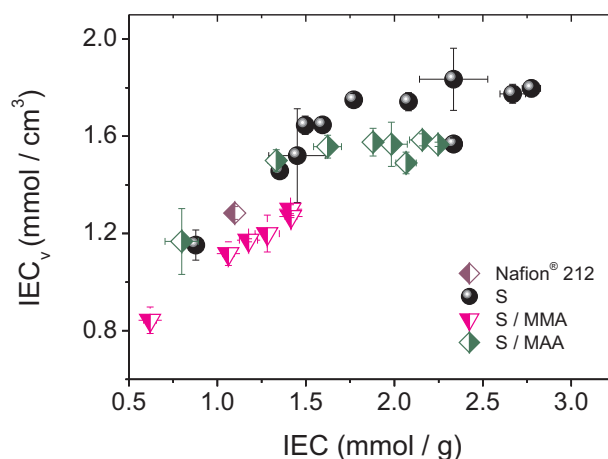
Figure 5.15: Concentration of proton (represented as volumetric IEC in the wet state) of styrene, styrene / MMA and styrene / MAA grafted membranes as a function of (mass based) IEC. The data of Nafion is included for comparison.
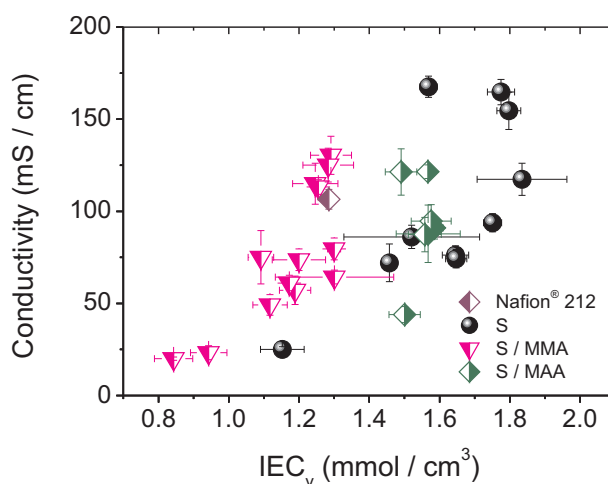
Figure 5.16: Relationship between the (through-plane) conductivity of styrene, styrene / MAA, styrene / MAA membranes and the volumetric IEC in water swollen state at RT. The data of Nafion is included for comparison.

proximity of neighboring acid groups can be obtained [115, 198]. As expected, the proton mobility is higher with increasing water volume fraction (Figure 5.17). Although the data are scatterred, the proton mobility in different types of grafted membranes seems to reflect a trend.

An in-depth analysis to examine the effect of the water content (as represented by the water volume fraction) is carried out. Although the proton conducting sites of all grafted membranes are the same (sulfonic acid groups), the larger distance between the acid groups in the presence of a comonomer may affect the acid strength. This effect could be eliminated by projecting the mobility of different membranes to infinite dilution [198, 216]. Surprisingly, despite the different chemical structures between styrene / MMA and styrene / MAA membranes, the

121

Table 5.1: Proton mobilities at infinite dilution ($\phi_v=1$).

System	$\mu_{eff} \cdot 1000$ at $\phi_v=1$ ($cm^2\ s^{-1}\ V^{-1}$)	Ref.
Styrene / MMA	1.6±0.1	this study
Styrene / MAA	1.7±0.2	this study
Styrene	1.4±0.1	this study
Styrene	2.6±0.2	[216]
Nafion	2.32±0.01	[216]
Free H$^+$ [*]	3.63	[217]

[*] in water at 25°C

proton mobilities at infinite dilution were comparable and slightly higher than that of the pure styrene grafted membrane (Table 5.1). The values obtained from the grafted membranes are significantly lower than the mobility of a free proton in water at 25°C ($3.63 \cdot 10^{-3}\ cm^2\ s^{-1}\ V^{-1}$) and may indicate some tortuosity in the membrane caused by the membrane structure or the presence of bound SO_3^- that restricted the proton pathway [115]. The proton mobility for the pure styrene grafted membranes is lower than that of the ETFE-*g*-styrene polymer reported in literature [216]. The discrepancy may originate from the membrane synthesis method, leading to different membrane structures.
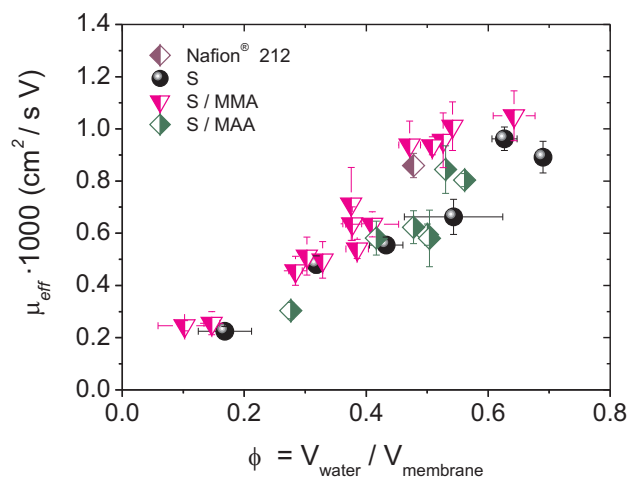
Figure 5.17: Effective proton mobility in styrene, styrene / MMA and styrene / MAA co-grafted membranes in water swollen state at RT as a function of water volume fraction. The data of Nafion is included for comparison.

From the results obtained we can conclude that an increase in IEC may not necessary lead to an increase in proton concentration since it is also associated with higher water uptake and

hence proton dilution. At the same proton concentration (IEC_v), the grafted membranes do not exhibit the same proton conductivity. This can be attributed to different proton mobilities due to varying water uptake and different membrane structures. Figure 5.18 shows that at a constant mass based IEC, the proton mobility is highest in styrene / MMA membranes due to its high water uptake, whereas that of styrene grafted membrane and styrene / MAA membranes are comparable but lower. The ability to absorb water seems advantageous for proton conductivity, yet it is coupled with mechanical deterioration due to membrane swelling.
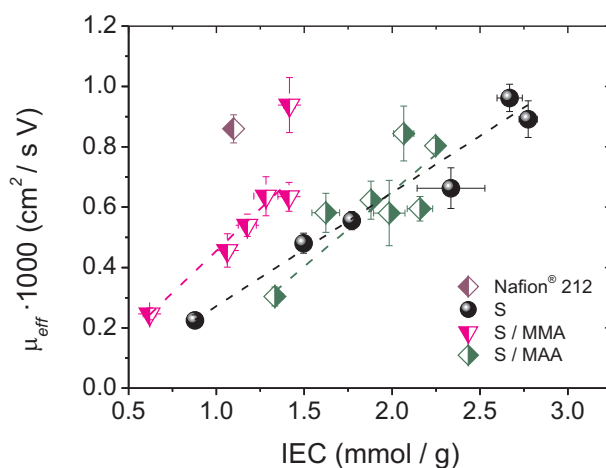
Figure 5.18: Effective proton mobility of styrene, styrene / MMA and styrene / MAA co-grafted membranes in water swollen state at RT as a function of IEC. The data of Nafion is included for comparison.

5.1.6   Membrane durability (styrene / MAA vs styrene / AN)

Although the precise degradation mechanism of the styrene based co-grafted membranes is not fully understood, it is generally accepted that poly(styrene sulfonic acid) is prone to the attack of radicals (HO·, H· and HOO·) that initiates membrane degradation. The reaction of styrene sulfonic acid units with radicals predominantly leads to an OH-adduct with 90% yield, followed by an acid catalyzed water elimination at low pH, in which a short-lived radical cation is formed as an intermediate [64].

The cyclic structure of the styrene / MAA membrane resulting from the internal Friedel-Crafts acylation may inhibit the loss of grafted monomers in the same fashion as a crosslinked membrane. To test this hypothesis, an OCV test was carried out. A styrene / AN membrane is used as a known reference to study the effect of a cyclic structure on membrane durability. The highest OCV was found at the beginning of the OCV test and significantly dropped in the first few hours before reaching a rather stable rate of decay. Further decrease in OCV is an indication of loss of membrane mechanical integrity.

5. STYRENE / MMA AND STYRENE / MAA MEMBRANES

Figure 5.19 shows the OCV with time of styrene / AN ($X\sim0.5$, IEC=1.6 mmol g^{-1}) and a styrene / MAA ($X\sim0.6$, IEC= 1.6 mmo g^{-1}) membranes with comparable *ex situ* conductivity. Prior to the test, both membranes were conditioned at 80°C and 500 mA cm^{-2} for approximately 20 hours.
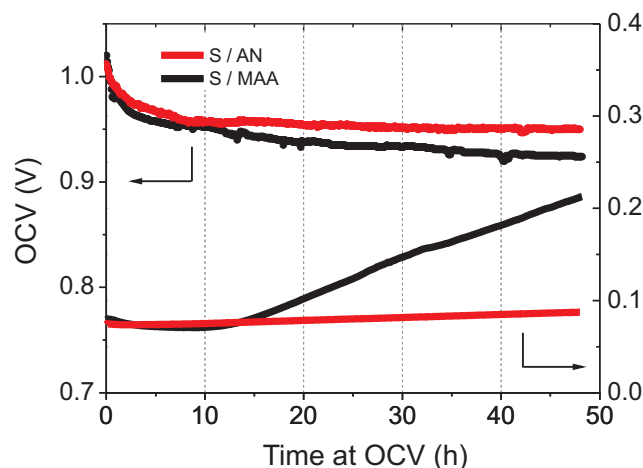
Figure 5.19: Stability of styrene / AN and styrene / MAA membranes in an OCV test. The high frequency resistance (ohmic resistance) is measured at 1 kHz during the course of the test. The experiments were carried out in collaboration with Z. Zhang.

In order to monitor degradation of different membranes, the increase in HFR value of the styrene / MAA membrane was compared to that of the styrene / AN membrane. After approximately 12 hours under OCV conditions, the HFR value of the styrene / MAA membrane increased drastically, while the HFR value of the styrene / AN membrane increased steadily with an observably lower rate. The increase in HFR value indicates that fatal damage of the styrene / MAA membrane could have occurred after 12 hours of OCV conditions. Since there is no change in the fuel cell humidity, the increase in HFR is obviously indicative of a decomposition of the grafted chain, in which styrene sulfonic acid is lost. The average rate for the increase in the HFR of the styrene / MAA membrane is 2.9 mOhm cm^2 h^{-1}, while an approximate loss of 0.3 mOhm cm^2 h^{-1} was found in case of the styrene / AN membrane between 12 to 50 hours OCV test. The cell was stopped after approximately 50 hours OCV conditions due to the dramatic HFR increase of the styrene / MAA membrane.

The change in hydrogen crossover of the two membranes before and after the 50 hours OCV test was determined (Table 5.2). The hydrogen crossover of styrene / MAA membrane after 50 hours OCV significantly increased compared to that of the styrene / AN membrane. This is attributed to higher membrane degradation of the styrene / MAA membrane.

The single cell performance of pristine and tested membranes ($\sim$50 hours, OCV conditions) is shown in Figure 5.20. At the beginning of the test, the performance of the two membranes is

Table 5.2: Hydrogen crossover of styrene / AN and styrene / MAA membranes before and after approximately 50 hours OCV test at 80°C. Measurements were carried out in collaboration with Z. Zhang.

System	H_2 permeation before OCV test (mA cm^2)	H_2 permeation after OCV test (mA cm^2)
S / AN	1.14±0.06	1.32±0.06
S / MAA	1.25±0.03	1.96±0.04

comparable, while after the OCV test a remarkable performance loss was observed for styrene / MAA membrane. The primary reason is membrane degradation, as shown by the significant increase in HFR value.
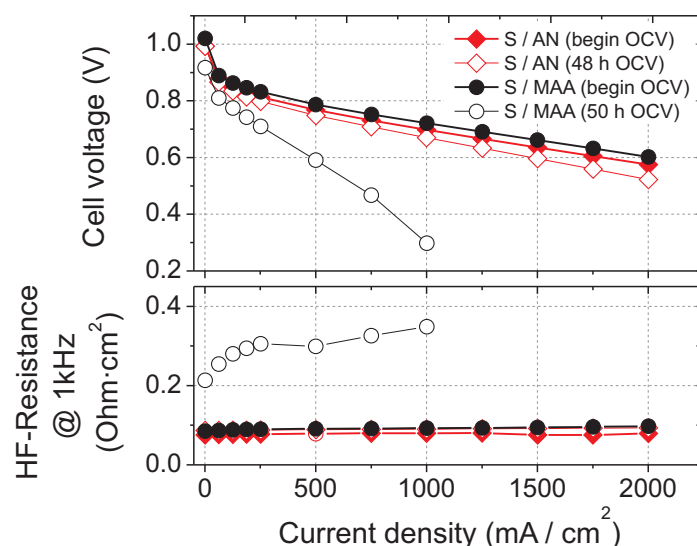
Figure 5.20: Polarization curves comparing styrene / AN and styrene / MAA membranes before and after approximately 50 hours OCV test (H_2 / O_2, 2.5 bar$_a$, 80°C and full humidification). High frequency resistance measured at 1 kHz. The experiments were carried out in collaboration with Z. Zhang.

Post mortem analysis by FTIR spectroscopy shows a decrease in the peak intensities associated with styrene and its comonomer, corresponding to the loss of grafts. The detailed assignment is presented earlier. For styrene / AN membrane, the loss of styrene functionality was estimated to be 35±4% due to membrane degradation, with an additional loss of 59±3% of nitrile accompanied by an increase in the absorbance in the carbonyl region due to nitrile hydrolysis. Such a high extent of graft component loss does not seem to support the HFR values of the styrene / AN membrane measured after 50 hours OCV, since the HFR values at the beginning and after 50 hours OCV are rather similar, implying no significant styrene loss. There

125

are a number of possible reasons for this discrepancy: (i) thinning of the membrane is unknown (ii) detachment of grafted chains may occur in the membrane during the OCV test, but removal of the fragments may only take place when the disassembled membrane is immersed in the salt solution for ion exchange.

In case of the styrene / MAA membrane, a small peak in the carbonyl region of the FTIR spectrum can be observed after the test, whereas the peak associated with styrene disappeared. A comparison of the styrene / MAA membrane before and after the test shows a change in membrane appearance from yellowish (before the test) to transparent in the active area (after the test). This change in the color of the membrane may indicate the loss of grafts and imply that only ETFE base film is left behind at the end of the test.

It can be concluded that the stability of styrene / MAN membrane is higher than that of styrene / AN, styrene / MAA and styrene grafted membranes, respectively. This suggests that the nitrile is a key factor to stabilize the membrane against chemical attack in the fuel cell. An interesting observation is that the presence of styrene's comonomer leads to higher membrane stability compared to a pure styrene grafted membrane.

5.2 Synthesis of membrane containing carboxylic acids

To determine the contribution of carboxylic acid to the fuel cell relevant properties, it is necessary to synthesize membranes containing carboxylic acid groups. However, sulfonation of styrene / MAA films leads to a conjugated ketone structure (subsection 5.1.3). This creates a problem in membrane synthesis to prepare co-grafted membranes with carboxylic acid functionalities. An approach to develop such kind of membrane is based on an *ex situ* hydrolysis of styrene / MAN and styrene / MMA membranes. These membranes were subjected to hot water, acid and alkaline solution at elevated temperature to accelerate the hydrolysis process.

Our first attempt to hydrolyze a styrene / MAN membrane is by immersing the grafted membrane in potassium form in water at 80°C. The hydrolysis during the course of experiment is evaluated from the change in the FTIR intensity of the corresponding nitrile ($2234 \ \mathrm{cm}^{-1}$) and the carbonyl (around $1700 \ \mathrm{cm}^{-1}$) vibrations. One might reasonably assume that reactive oxygen species (ROS) were not generated during the hydrolysis experiment, therefore the product of hydrolysis should retain its original styrene content throughout the hydrolytic process. The significant change should be the conversion of the nitrile groups to amide or carboxylic acid.

Comparison between the FTIR spectra of the pristine and hydrolyzed membranes can give valuable information on membrane degradation. The reduction in peak intensity assigned to a grafted component was recognized as loss of the functional group, presumably because the functional group is chemically modified as a result of hydrolysis. Alternatively or in addition, it may indicate the loss of grafts.

As shown in Figure 5.21, a slight change in the FTIR spectra in the nitrile and carbonyl regions is observed with immersion time. The corresponding nitrile vibration (2234 cm^{-1}) gradually weakened, implying loss of nitrile. Although the decrease of the nitrile peak was not significant, there is evidence for the appearance of hydrolysis products in the carbonyl region around 1700 cm^{-1} (peak b), forming amide and carboxylic acid. However, to fully hydrolyze nitrile groups in a reasonable time a harsher protocol should be applied.
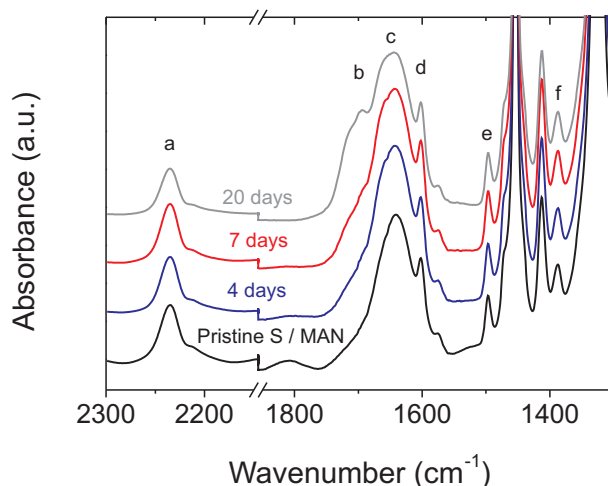
Figure 5.21: FTIR spectra of pristine ETFE-*g*-styrene / MAN membranes, hydrolyzed membranes in acidic aqueous solution between 4-20 days. The decrease in C≡N vibrational band intensity at 2234 cm^{-1} (a) in hydrolysis environment corresponds to the decomposition of nitrile. An increase in C=O stretching vibration at ∼1700 cm^{-1} (b) indicates formation of carbonyl products. Graft relevant peaks: (c) O-H bending (∼1640 cm^{-1}), (d) and (e) C=C stretching vibrations (1600 and 1494 cm^{-1}), (f) C-H deformation (umbrella) vibration of CH$_3$ (∼1390 cm^{-1}).

To accelerate the nitrile hydrolysis, the reaction was carried out at 80°C in 1M HCl. However, only partial hydrolysis of the nitrile was achieved after 7 days (Figure 5.22). The FTIR spectrum of a membrane tested under OCV hold condition is included to provide additional insight with respect to *in situ* nitrile hydrolysis. The results confirmed that when the membrane is hydrolyzed, the products from both *in situ* and *ex situ* hydrolysis experiments are similar.

Hydrolysis experiments of styrene / MMA membranes are analogous to that of styrene / MAN membranes under acidic aqueous conditions. The hydrolytic reaction of MMA leads to the reduction in peak intensity assigned to the ester carbonyl unit (1722 cm^{-1}). This carbonyl peak slightly broadens in the hydrolyzed membranes compared to the pristine one. The ester groups likely underwent hydrolysis to form carboxylic acid as products, which would raise the peak intensity assigned to carboxylic acid (around 1700 cm^{-1}). However, a change in this peak intensity was not clear (Figure 5.23).

Quantitative FTIR analysis revealed that the vibrational bands assigned to the α-methyl group (∼1388 cm^{-1}) and C=C aromatic vibrational band of styrene (1493 cm^{-1}) normalized
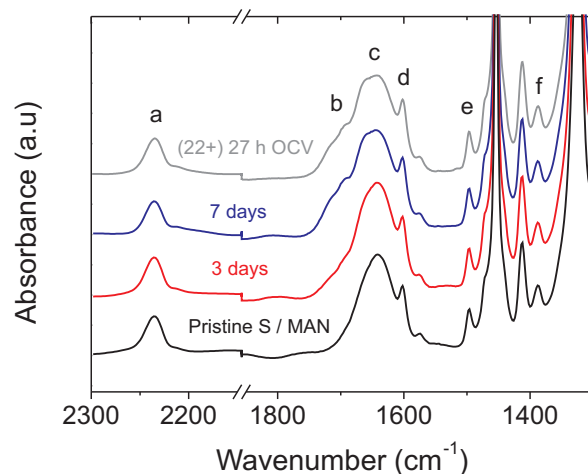
Figure 5.22: FTIR spectra of pristine ETFE-*g*-styrene / MAN membrane, hydrolyzed membranes in acidic aqueous solution after 3 and 7 days and OCV tested membrane. See caption of Figure 5.21 for peak assignment.
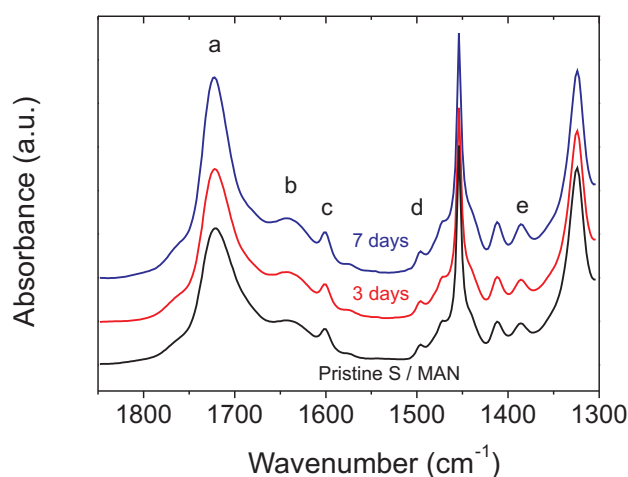
Figure 5.23: FTIR spectra of pristine ETFE-*g*-styrene / MMA membrane and membranes hydrolyzed in acidic aqueous solution at at 80˚C for 3 and 7 days. Graft component relevant peaks: (a) C=O stretching at 1722 $^{-1}$, (b) O-H bending at 1640 cm^{-1}, (c) and (d) C=C stretching vibrations at 1600 and 1494 cm^{-1}, (e) C-H deformation (umbrella) vibration at 1388 cm^{-1}. The decrease in C=O vibrational band corresponds to the loss of ester with the reaction time.

to the ETFE vibrational band (1325 cm^{-1}) change with time. This has raised our concern regarding membrane degradation in fully water swollen state. The loss of monomer units during hydrolysis is calculated from the change in the intensity of the vibrational bands assigned to the monomer compared to the ETFE vibrational band (Equation 2.3).

For styrene / MAN membranes, the MAN content in the grafted membrane was determined from the nitrile vibration at 2234 cm^{-1} and cross-checked with the α-methyl vibration at 1388 cm^{-1}. The change in the styrene content was indicated by the vibrational band assigned for

Table 5.3: Loss of styrene and MAN functional group by immersion of membrane in water and 1 M HCl at 80°C.

System	Hydrolysis conditions	Duration (days)	Loss α-CH$_3$ (%)	Loss of C$\equiv$N (%)	Loss of styrene (C=C str.) (%)
S / MAN	H$_2$O at 80°C	4	-	9±9	9±13
		7	4±4	9±9	8±13
		20	19±7	14±8	20±14
	1 M HCl at 80°C	3	1±10	11±8	2±16
		7	6±8	24±10	16±12
S / MMA	1 M HCl at 80°C	3	25±1	-	22±5
		7	36±1	-	26±3

aromatic C=C (1493 cm^{-1}). The loss of MAN and styrene was observed after immersion in water and 1M HCl at 80°C for a given time (Table 5.3). However, quantitative analysis of the hydrolyzed styrene / MAN co-grafted membrane obtained was unfortunately not conclusive due to high uncertainty. In styrene / MMA, loss of α-methyl (1390 cm^{-1}) and C=C aromatic of styrene were comparable.

The difference between styrene content in the pristine and hydrolyzed membranes may be explained in terms of membrane degradation. In the examined environment, the co-grafted membranes may suffer from detachment of grafted chains. Enomoto *et al.* proposed that chain detachment can occur due to the swelling stress between the hydrophilic PSSA grafts and hydrophobic base film when the membrane is immersed in water, leading to the loss of grafts [218].

An attempt to hydrolyze a styrene / MMA co-grafted membrane in alkaline conditions (1M NaOH) resulted in only partial hydrolysis after 4 days at 80°C (not shown). This emphasized that preparation of ETFE-*g*-styrene / MAA membranes by *ex situ* hydrolysis of styrene / MAN and styrene / MMA membranes is rather complicated and unsatisfactory. In addition, grafts detachment as a consequence of swelling stress is a particularly severe problem. Another possibility to synthesize membranes containing carboxylic acid is to *in situ* hydrolyze membranes containing hydrolyzable groups, as shown in subsection 3.3.3.

5.3 Conclusions

In order to obtain membranes with non-nitrile functional groups, MMA and MAA were used as comonomers to graft with styrene. MMA was particularly chosen as a comonomer since it

contains the carboxylic acid group that represents the product of hydrolyzed MAN. As shown in the previous chapters, MAN is susceptible to hydrolysis to some extent and the change in its chemical structure as a result of hydrolysis may lead to changes in membrane properties as well as stability. Understanding the effect of MAA on membrane properties provides an insight into the role of hydrolysis.

The presence of MMA and MAA as styrene's comonomers hinders the sulfonation reaction. The degree of sulfonation of both membranes was approximately 80%, whereas nearly complete sulfonation of styrene grafted film was obtained. The reason for the incomplete sulfonation could be attributed to the nature of comonomer that changes the susceptibility of styrene towards chlorosulfonic acid. In addition, styrene / MMA co-grafted membranes undergo hydrolysis, whereas styrene / MAA co-grafted membranes undergo internal Friedel-Crafts acylation, leading to a cyclic ketone structure. To obtain further insight into the stability of this membrane, OCV tests were carried out. It was found that incorporation of a comonomer of styrene results in higher membrane durability compared to a pure styrene grafted membrane with comparable IEC. Among the different membranes, the stability is rated according to styrene / MAN > styrene / AN > styrene / MAA > styrene grafted membrane. On one hand, incorporation of a comonomer leads to increased membrane thickness and thus reduces the gas crossover. On the other hand, the presence of a suitable functionality (i.e., nitrile) improves the chemical stability.

Swelling of styrene / MAA co-grafted membranes was comparable to styrene grafted membrane and significantly lower than that of styrene / MMA co-grafted membranes. This suggests that formation of a cyclic structure may be beneficial for the mechanical stability of the membrane by restricting dimensional change upon water absorption. This is however coupled to a lower proton mobility.

By lowering the water volume fraction, the level of tortuosity increases and thereby inhibiting the proton transport. The water volume fraction appears independent of comonomer type and is comparable to those found with styrene grafted membrane with varying the graft length [198].

In order to synthesize membranes containing carboxylic acid groups, the styrene / MAN and styrene / MMA membranes were hydrolyzed by immersion in water, acidic and alkaline aqueous solutions to convert the nitrile of MAN and ester of MMA to carboxylic acid. Under the examined conditions, partial transformation to carboxylic acid occurs, yet also loss of styrene sulfonic acid is observed, indicating membrane degradation. The loss of grafted styrene units is due to chain detachment as a result of swelling stress at the interface between the hydrophilic grafts and the hydrophobic ETFE [218]. This suggested that preparation of the co-grafted membranes containing carboxylic acid groups by *ex situ* hydrolysis is probably not suitable for our application. The effect of hydrolysis on the fuel cell performance and durability of membranes containing different comonomers will be discussed in the next chapter.

6

Effects of comonomer functionalities

Styrene and its derivatives are the most widely used monomers for preparation of radiation grafted proton conducting membranes [61, 85, 219, 220]. Attention was given to styrene owing to its low cost, easy sulfonation and amenability to radiation polymerization. Yet, styrene based membranes are prone to chemical degradation under fuel cell conditions due to the presence of weak α-H [48, 62, 64]. The use of styrene derivatives with a protected α-position [13, 97], such as α,β,β-trifluorostyrene (TFS) in BAM® membranes [95, 96] or α-methyl styrene (AMS) [43], increase membrane durability but suffer from low grafting rate [32–34, 43].

To circumvent these limitations, comonomers are introduced to styrene and its derivatives. Crosslinking monomers such as divinylbenzene (DVB) and diisopropylbenzene (DIPB) are used to improve chemical and mechanical stability of the membranes [98–100]. Although a crosslinker may improve the lifetime, it also lowers proton conductivity and brings along brittleness [40]. A non-crosslinking monomer, methacrylonitrile (MAN) has shown to significantly promote the grafting kinetics of α-methylstyrene [70] and also improve the fuel cell durability of styrene / MAN co-grafted membranes compared to a pure styrene grafted membrane [104]. However, the effect of non-crosslinking comonomers of styrene on fuel cell relevant properties has not been investigated in detail.

To investigate the effect of comonomer functionalities on the proton conductivity of styrene based radiation grafted membranes. Four comonomers with different functional groups, namely MAN, acrylonitrile (AN), methylmethacrylate (MMA) and methacrylic acid (MAA) were grafted with styrene into ETFE base film to form proton conducting membranes. The chemical structure, ion exchange capacity, hydration level and nanostructures of these membranes were investigated and compared against the properties of styrene based membranes.

131

6.1   Chemical changes after sulfonation

The nature of the grafted comonomer affects the membrane preparation in several stages. The differences in reactivity and diffusivity of the monomer into the polymer matrix led to different grafting kinetics. Therefore, the irradiation dose of the base film was adjusted accordingly to obtain a reasonable grafting time.

The composition of the grafted copolymer was determined by FTIR applying an established method [135]. The IR absorption bands at 2234, 1495 and 1388 cm^{-1}, which correspond to C≡N stretching, aromatic ring-stretching, and α-CH$_3$ symmatric bending (umbrella) vibrations, were normalized by the C-H deformation vibration of ETFE at 1325 cm^{-1} to quantify the content of respective grafted monomer units.

After grafting, the grafted films underwent sulfonation to incorporate proton exchange sites. This is a crucial step which determines the properties of the membrane, since the chemical structure of the grafted films can undergo considerable changes during sulfonation [85, 214]. For all grafted membranes, a color change was observed from transparent ETFE to an opaque grafted film. After sulfonation, styrene / MMA and styrene / MAA membranes became yellow, while the color of styrene / MAN, styrene / AN and pure styrene grafted membranes remained unchanged.

The FTIR analysis of the styrene / MAN, styrene / AN and styrene / MMA membranes showed that new peaks appear after sulfonation. An obvious change is observed in the characteristic region of the OH stretching vibration around 3500 and 1620 cm^{-1} and the carbonyl band around 1700 cm^{-1} (Figure 6.1). The former bands are associated with water taken up by the membrane, which is expected from the incorporation of the hydrophilic sulfonic acid. The latter peak is attributed to hydrolysis products from the sulfonation reaction. The nitrile group is well known to undergo hydrolysis under acidic or basic conditions, leading to the formation of amide and carboxylic acid functional groups.

The sulfonation conditions present a strongly acidic environment, facilitating the hydrolysis of styrene / MAN and styrene / AN membranes [221]. Although the chemical structures of MAN and AN are similar, the observed partial hydrolysis of styrene / MAN membranes is minute compared to its styrene / AN counterpart. The broad absorption of the AN containing membrane at 1700 cm^{-1} could be assigned to the presence of a cyclic dimer of carboxylic acid ($\sim$1700 cm^{-1}), unpaired carboxylic acid ($\sim$1720 cm^{-1}) [170], and amide ($\sim$1672 cm^{-1}), which are characteristic for hydrolysis products.

Ester decomposition by sulfonation also occurs in the styrene / MMA membrane. In this case, the sulfonation product is the carboxyl group as confirmed by the presence of a peak shoulder at 1700 cm^{-1}(-COOH). The adjacent absorption band at 1733 cm^{-1} corresponds to
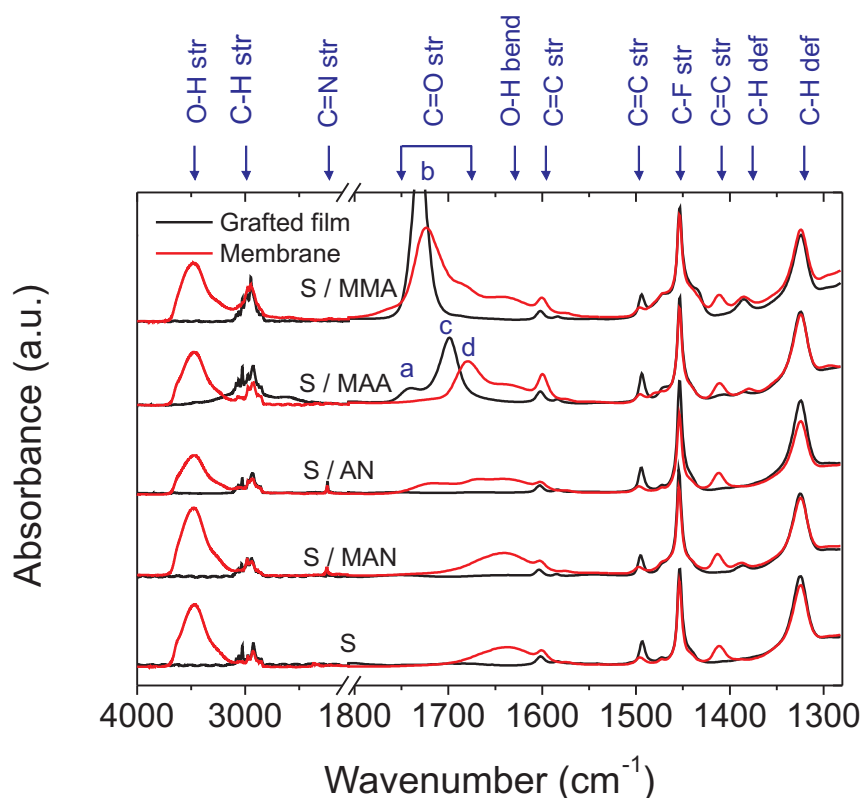
Figure 6.1: Comparison of FTIR spectra of grafted films and membranes containing styrene and its comonomers. Relevant peaks in the carbonyl region ($\sim$1700 cm^{-1}) are (a) unpaired carboxylic acid (1740-1720 cm^{-1}), (b) ester (1733 cm^{-1}) and cyclic dimer of carboxylic acid ($\sim$1700 cm^{-1}), (c) amide (1672 cm^{-1}) and (d) cyclic ketone (1679 cm^{-1}).

the ester (C=OOMe). The intensity of this band decreases significantly, which is associated with carboxylic acid formation by partial hydrolysis. Hydrolysis of nitrile and ester functionalities does not necessarily lead to chain scission because the hydrolyzed group is not part of the polymer backbone.

Interestingly, while MAA is the end product of hydrolysis, a shift in the carbonyl region is observed after sulfonation of the styrene / MAA film. In the latter, we found two characteristic peaks for the carboxyl group at 1740 and 1700 cm^{-1}, corresponding to the dimeric carboxylic and free carboxylic absorption [170, 222]. The formation of a dimeric carboxylic acid by hydrogen bonding could take place between grafted polymers or even within the same chain. The free carboxylic acid can be expected in the copolymer with tendency to form an alternating monomer sequence.

After sulfonation of styrene / MAA grafted films, no free / dimeric carboxylic acid peaks are observed and the absorption redshifted to 1679 cm^{-1}, which is characteristic for a conjugated ketone. A similar result was found for a sulfonated styrene / acrylic acid (AA) co-grafted membrane [214]. During sulfonation, the styrene / AA copolymer is suggested to undergo an

133

internal Friedel-Crafts acylation reaction followed by cyclic dehydration, resulting in a cyclic ketone [213]. Likewise, the carboxyl group in styrene / MAA co-grafted films may be available for cyclization in the same fashion. In addition, this membrane is more brittle compared to other grafted membranes with similar water uptake, which may result from cyclization between adjacent styrene and MAA units, restricting the mobility of the polymer chain.

A possible mechanism of Friedel-Crafts acylation is proposed (Figure 6.2). In the first step, the carboxylic acid group of MAA is activated by a proton during hydrolysis to form an acylium ion ($RC^+=O$), which is an electrophile. This acylium ion can attack the ring of styrene sulfonic acid, resulting in formation of a new C-O bond and a positively charged intermediate. The carbocation of the intermediate is rearranged to give an aromatic substitution product. Finally, a proton is abstracted, yielding intramolecular cyclization of styrene and MAA. This type of reaction is also known as the Harworth reaction [223]. Since posst -sulfonation of styrene / MAA leads to the formation of a conjugate ketone structure, synthesis of sulfonated styrene / MAA membranes without affecting the carboxyl group may be carried out by co-grafting of styrene sulfonate and MAA into base film [224].
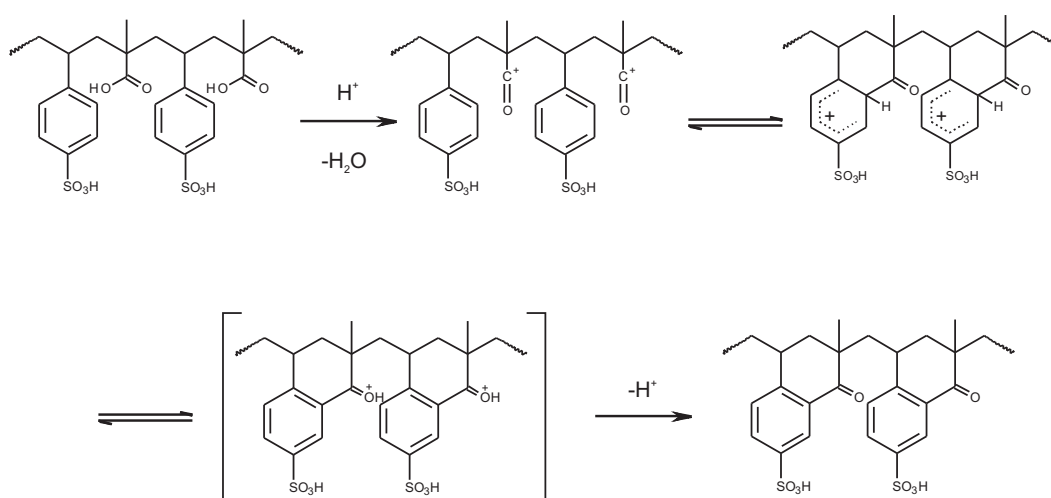
Figure 6.2: Proposed mechanism for the internal Friedel-Crafts acylation in the styrene / MAA co-grafted membrane (adapted from literature [223]).

6.2 Influence of comonomers on fuel cell relevant properties

6.2.1 Proton conductivity and water uptake of co-grafted membranes

The proton conductivity depends on the concentration of free protons and their mobility, which are coupled to the hydration level. An increase in water uptake will eventually lead to free protons and formation of water network, which is necessary for long range proton conduction.

However, excessive water uptake might result in proton dilution, which lowers proton conductivity [111]. Therefore, the water uptake should be well balanced to maintain a high proton conductivity.

The proton conduction of radiation grafted membranes takes place exclusively in the amorphous phase, which accommodates the protogenic groups [78, 121–124]. The presence of sulfonic acid groups makes the membrane hydrophilic. The hydrophilicity is expressed as hydration number (defined as the number of water molecules per sulfonic acid group present in the grafted chain, $\lambda = n(\text{H}_2\text{O}) / n(\text{SO}_3\text{H}))$ of the co-grafted membranes compared to Nafion and styrene grafted membrane, and is presented in Table 6.1. By varying the graft level and styrene molar fraction in the grafting solution, grafted membranes with relatively constant IEC ($\sim$ 1.5 mmol g^{-1}) were synthesized.

Among the radiation grafted membranes, the pure styrene grafted membrane and styrene / MAA co-grafted membrane exhibit the lowest hydration level. An increase in hydrophilicity of the co-grafted membranes compared to styrene grafted membranes with constant IEC may be caused by various factors, including an enhanced interaction with water, polymer free volume and membrane structure. Comonomers containing nitrile and carbonyl groups are able to form hydrogen bonds with water, which may help to facilitate water uptake in the polymer matrix. In addition, the presence of a comonomer may also increase the polymer free volume to accommodate additional water molecules. The flexibility of the grafted chain may also contribute to an increase in water uptake by allowing a higher extent of membrane expansion upon addition of water. This reasoning seems to explain the lowest hydration number of the styrene / MAA membrane among the other co-grafted membranes with comparable IEC, owing to its rigid structure of the graft copolymer. The study carried out with different proton conducting membranes also supports the hypothesis that the more flexible polymer network permits a larger water uptake at high relative humidity [225]. Although not shown here, the water uptake of all membranes increases with the IEC.

A higher hydration level of the co-grafted membranes may confer a higher proton mobility and could adversely dilute the ionic charge carriers and limit the proton conductivity. Additionally, incorporation of a comonomer increases the graft level and results in a thicker membrane, which can also increase membrane resistivity.

Table 6.1: *Ex situ* properties of grafted membranes and Nafion® 212 membrane. Degree of sulfonation of 100% corresponds to complete sulfonation of every styrene unit. Conductivity (σ) was measured in water swollen state. X_0 and X are styrene molar fraction in the grafting solution and in the membrane, respectively.

System	X_0	X	GL (%)	IEC	Degree of sulfonation (%)	λ at RT	σ at RT (mS / cm)[*]
S	1	1	23	1.50±0.06	>95	14±1	86±6
S / MAN	0.4	0.56±0.02	38	1.49±0.06	>95	18±2	85±11
S / AN	0.4	0.46±0.09	41	1.56±0.07	>95	20±1	76±8
S / MMA	0.3	0.56±0.06	60	1.41±0.01	81	17.5±0.2	80±6
S / MAA	0.5	0.62±0.06	44	1.62±0.08	84	14.9±0.1	87±9
Nafion® 212	-	-	-	1.10±0.02	-	17.0±0.5	107±5

[*] Proton conductivity (through-plane direction)

The conductivity of different radiation grafted membranes in water saturated state was measured at room temperature. Figure 6.3 shows an increase in conductivity with increasing IEC. Interestingly, all membranes follow the same master curve. This result may be understood from the fact that the chosen comonomers do not contribute to proton conductivity since they do not possess a sulfonic acid group, and the dissociation constant of carboxylic acid (pKa ~4-6) is too high to allow dissociation under the examined conditions. The results suggest that the presence of the chosen comonomers and their chemical nature do not contribute to the proton conductivity of the co-grafted membranes in fully hydrated state, and the proton conductivity depends primarily on the IEC. In fact, the relationship between IEC and proton conductivity cannot be directly related, since IEC is a dry-state parameter. It is however used a starting point for an analysis.
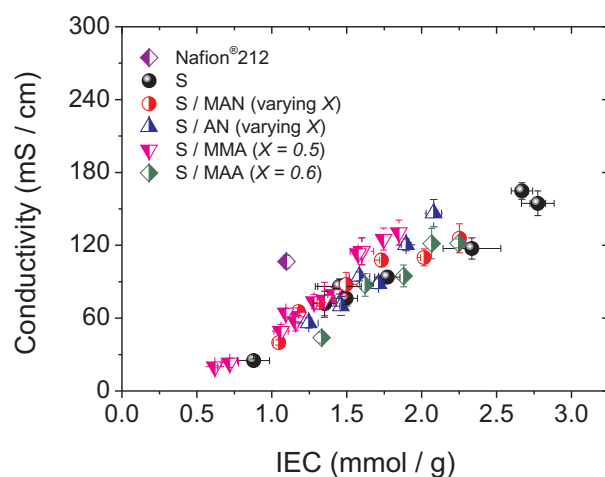
Figure 6.3: Effect of IEC on proton conductivity of different grafted membranes compared to Nafion® 212 in fully hydrated state. The data were obtained at room temperature.

Since the proton conductivity and hydration level are intimately linked, we hypothesized that the membranes containing a comonomer may retain water more strongly than the styrene grafted membrane. This in turn could lead to improved proton conductivity under reduced humidity. Vapor sorption properties of the membrane are particularly interesting for understanding proton conductivity in fuel cell application, because the membrane can face dynamic changes due to changes in relative humidity, which affects the water uptake. For this reason, proton conductivity (measured in-plane) and hydration level of radiation grafted membranes with similar IEC and graft composition ($X \sim 0.5$-0.6) were investigated at 70°C at controlled relative humidity.

6.2.2 Water sorption behavior of co-grafted membranes

The sorption isotherm of a membrane was obtained gravimetrically, by measuring its mass at various relative humidities. Figure 6.4 shows the average λ values obtained from the sorption and

desorption isotherms at various relative humidities (70°C). All membranes show a narrow hysteresis behavior, suggesting a reversible sorption mechanism. The shape of the sorption isotherm provides information on the state of water in the membrane and the interactions between water-water and water-polymer interactions [226]. The sorption behavior of all membranes except styrene / MMA represents a Type II isotherm according to the Brunauer classification [227], which is also characteristic for Nafion and styrene sulfonate ion exchange resin [228, 229]. The isotherm of styrene / MMA shows a Type III isotherm, which is similar to sorption isotherms of poly(2,5-benzimidazole) [230]. Both types of the sorption isotherms are typically observed in hydrophilic polymers, in which Type III isotherm is characteristic of a less hydrophilic polymer (weak interaction with water) [226]. All membranes show a steep increase in the λ value due to formation of water clusters at high relative humidity (RH above 60%). The isotherms of styrene,
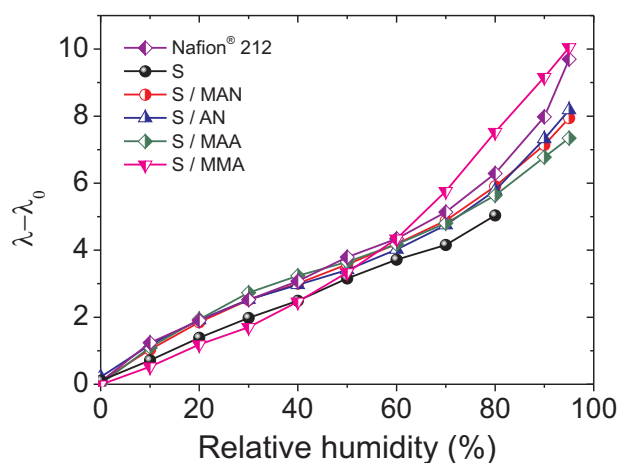
Figure 6.4: Hydration number as a function of relative humidity for various grafted membranes with similar IEC, measured at 70°C. The values for Nafion® 212 are shown for comparison.

styrene / MAN, styerne / AN, styrene / MAA and Nafion indicate two distinct sorption regimes. The first regime corresponds to an approximately linear increase in water sorption, which is observed when $1 < \lambda - \lambda_0 < 5$ due to water molecules filling the primary hydration shell of SO_3H [231, 232]. Since four to six water molecules are necessary to form the first hydration shell of SO_3H [231, 233–235], there could be residual water molecules in the nominally dry membranes (λ_0). To fully remove all water, the membrane should be heated up above its glass transition temperature (T_g) [231], which is around 110 °C for Nafion [236]. Although the T_g of grafted membranes has not been reported so far, it is expected to be in the same range as the T_g of ETFE (104 °C [192]). Further water adsorption takes place in the second regime ($\lambda - \lambda_0 > 5$), contributing significantly to membrane swelling [232].

The sorption isotherm of Nafion lies slightly higher than that of styrene / MAN, styrene / AN and styrene / MAA grafted membranes at high relative humidity (RH>70%). The co-grafted membranes except styrene / MMA show similar water uptake behavior over the entire

relative humidity range. On the other hand, the styrene grafted membrane shows the lowest λ values. The λ values of the styrene / MMA membrane are comparable to those of the pure styrene grafted membrane up to 60% relative humidity. Above that hydration of the co-grafted membrane increases more strongly.

In addition, it is found that the water uptake of the co-grafted membranes increases with temperature, while the results obtained for Nafion® 212 measured at 25 (not shown), 60 and 70°C shows rather small temperature dependence (with only 0.1 m% deviation at each water vapor activity). Similar observation in the temperature effect on Nafion water uptake has been reported [237], although with different values. The reason for the discrepancies between the Nafion results obtained from different laboratories could be attributed to different initial configurations of Nafion due to dissimilar pretreatment [228].

The hydration level of the membranes in vapor phase did not follow the same trend as observed when the membranes are immersed in liquid water. This may be attributed to the difference in water uptake kinetics of the membrane in vapor and liquid phase. In vapor phase, water uptake depends strongly on interfacial mass transport, which is determined by the physical and chemical structure at the membrane surface [232, 238]. Higher vapor absorption of the co-grafted membranes, as observed from sorption isotherms at 70°C compared to the styrene grafted membrane, can be explained by an increased hydrophilicity of the membrane surface or larger surface pore compared to the pure styrene grafted membrane due to the presence of a comonomer. While in liquid water, the water uptake is governed by polymer relaxation dynamics associated with swelling [238].

6.2.3 Effect of comonomers on proton conductivity at reduced RH

As shown in Figure 6.5, the proton conductivity of all membranes is highly sensitive to a change in relative humidity, with the most dramatic effects for the co-grafted membranes. Nafion exhibits a significantly higher proton conductivity than the grafted membranes over the entire RH range. Since the water uptake of Nafion is only slightly higher than that of the grafted membranes, we attribute the high proton conductivity of Nafion to its structure, which facilitates proton mobility [141]. However, the difference in the acid dissociation constant between PFSA membranes such as Nafion (pKa $\sim$ -6) and co-grafted membranes (pKa of benzensulfonic acid $\sim$ -2) should not be excluded [116]. A higher acid dissociation constant (lower pKa) implies easier proton dissociation, hence higher proton concentration.

A comparison between pure styrene and co-grafted membranes with similar IEC shows a clear divergence in proton conductivity towards lower RH levels. This observation shows that the dependence of proton conductivity on IEC (Figure 6.3) may only hold true for non-crosslinked membranes equilibrated in liquid water. Within the series of co-grafted membranes, the proton
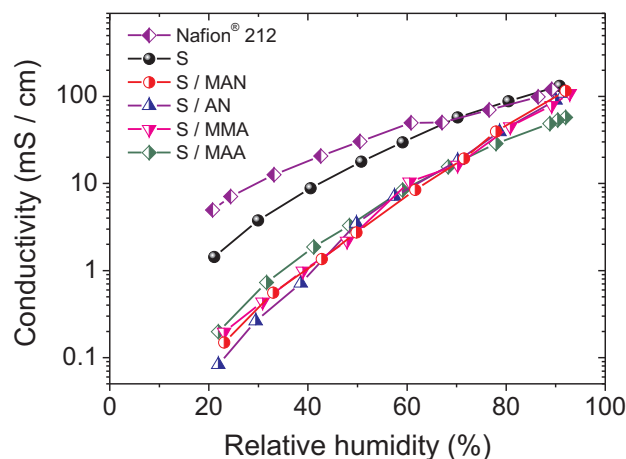
Figure 6.5: Effects of comonomers on proton conductivity of radiation grafted membranes with IEC of approximately 1.5 mmol/g compared to Nafion® 212 at 70°C as a function of relative humidity.

conductivities are consistent almost over the entire RH range, yet all values are lower than that of the pure styrene grafted membrane, despite comparable hydration numbers and IEC. Irrespective of the chemical nature, incorporation of a comonomer with a tendency to form an alternating copolymer with styrene results in reduced proton conductivity of the membrane at reduced humidity.

Further examination reveals that at 80-95% RH, the proton conductivity of styrene / MAA membrane is three times lower than that of the other co-grafted membranes at similar RH. The discrepancy could be due to the greater rigidity of the membrane conferred by the formation of a cyclic structure, which influences the water transport properties. Such a membrane may require a longer time to equilibrate at high RH than the time given during the measurement. Thus, the proton conductivity could be underestimated.

As the hydration level of individual membranes increases by raising the relative humidity, the proton mobility increases. Membranes with most efficient proton conductivity will be those that require the least water to sustain the same proton conductivity. Lowering membrane swelling is of interest to improve its mechanical stability and resistance to drying and swelling induced degradation [239].

The results obtained allow us to correlate the λ-λ_0 values with the proton conductivity by carrying out a fifth order polynomial fit to the water uptake isotherm [240]. As some water is required to form transport pathways for protons, a rapid increase in proton conductivity with water uptake at low water uptake can be expected. Figure 6.6 shows a comparison of proton conductivities and their dependence on the hydration level of the grafted membranes compared to Nafion. The shape of these curves is similar to those in Figure 6.5. The co-grafted membranes,

namely styrene / MAN, styrene / AN and styrene / MAA exhibit similar proton conductivity at comparable λ-λ_0 (and RH), while the proton conductivity of styrene / MMA diverges due to its sorption behaviour.

The styrene grafted membrane reveals a striking feature since it displays significantly higher conductivity than the co-grafted membranes at the same λ-λ_0 values and follows the similar trend as the Nafion membrane. This implies that styrene grafted membrane and Nafion have a lower percolation threshold for the aqueous phase compared to the co-grafted membranes. Such property leads to more efficient proton transport.
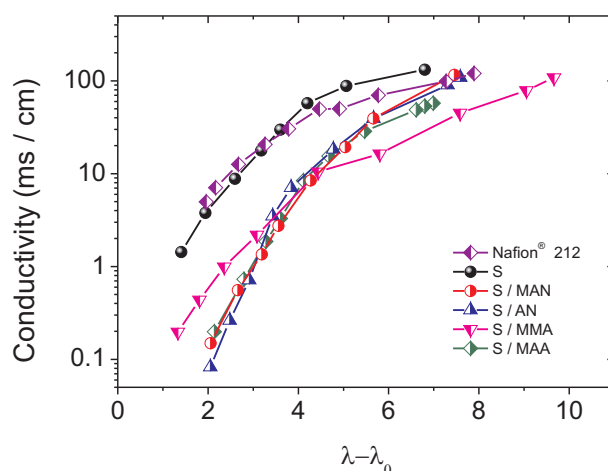
Figure 6.6: Proton conductivity and water sorption of radiation grafted membranes at 70°C with IEC of approximately 1.5 mmol/g compared to Nafion® 212

6.2.4 Effective proton mobility as a function of water content

By examining the water uptake of the co-grafted membranes with different IEC in water swollen state, the general trend, as might be expected, is observed. Increasing water uptake (Figure 6.7a) and water volume fraction (Figure 6.7b) lead to higher proton conductivity. This is mainly due to higher proton concentration with increasing IEC. Further examination is done by breaking down the proton conductivity into its proton mobility to exclude the effect of proton concentration. Despite the differences in IEC, graft composition and comonomer type, the proton mobilities of all grafted membranes are similarly affected by the water volume fraction (Figure 6.7c). An increase in water volume fraction in the membrane leads to a more connected percolation pathways, which increase the proton mobility and hence resulting in a greater proton conductivity.
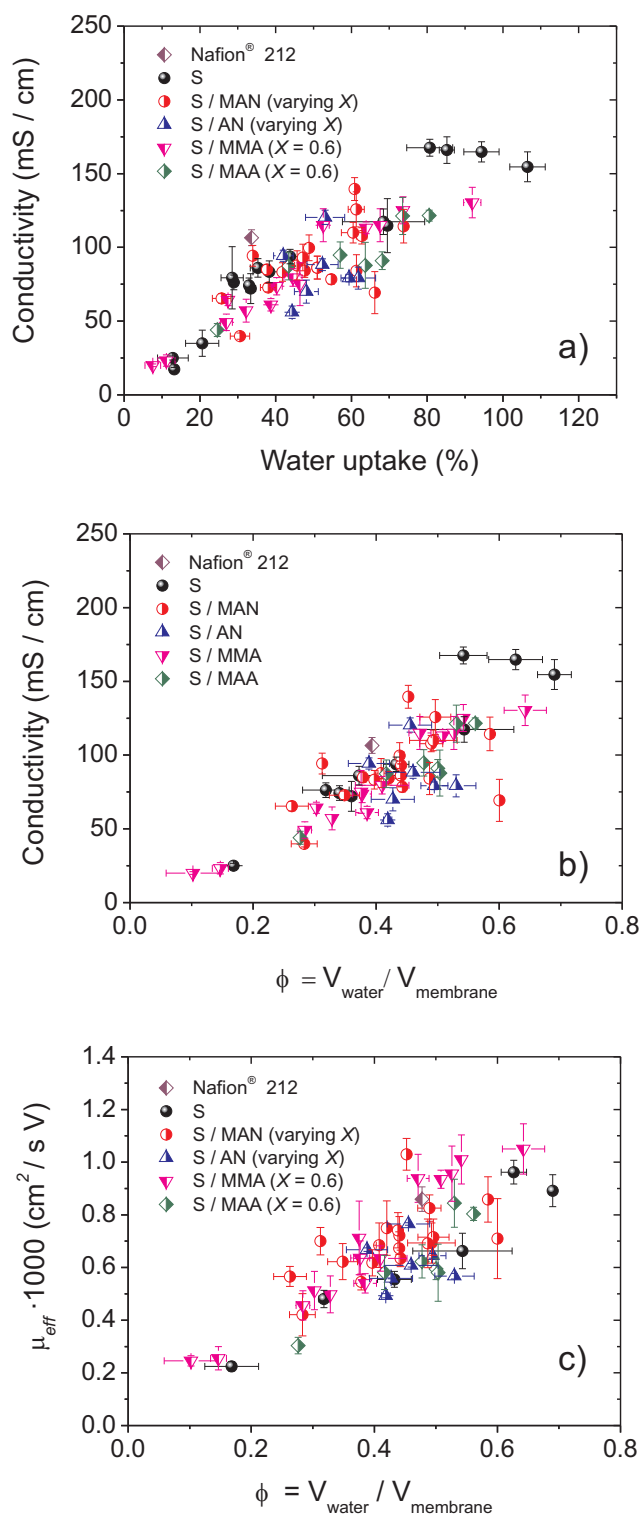
Figure 6.7: Comparison of proton conductivity and proton mobility as a function of water uptake and water volume fraction of various co-grafted membranes in water swollen membrane at RT. The values of Nafion are included as a known reference.

6.2.5 Nanostructure

To get a better insight into the membrane structure, we carried out small-angle X-ray scattering (SAXS) experiments of the grafted membranes and Nafion® 212. The morphology of the membrane in dry state may resemble the morphology of the membrane at reduced humidity [141].
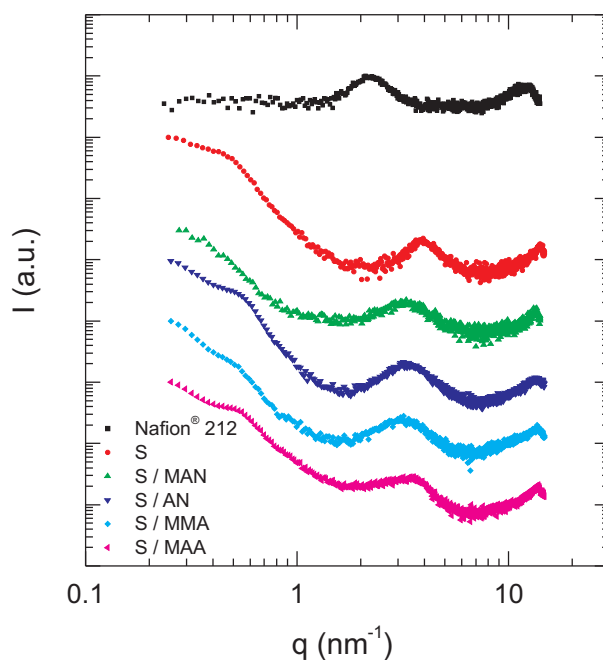
Figure 6.8: Azimuthally integrated SAXS spectra of radiation grafted membranes with IEC of approximately 1.5 mmol/g in cesium form (dry state). The spectra are vertically shifted for the sake of clarity. Experiments were carried out in collaboration with Dr. S. Balog.

Figure 6.8 shows the spectra obtained from SAXS measurements of membranes containing styrene with different comonomers. The center position of the ionomer peak of all co-grafted membranes is shown at $q = 3\,\text{nm}^{-1}$. This peak position corresponds to the distance between ionic aggregates, while the peak broadening of the curve resembles the number density of the aggregates. The consistency in SAXS spectra suggests a similar morphology for co-grafted membranes containing different comonomers with similar styrene molar fraction. These data highlight that the structure of the co-grafted membrane seems to be independent of the type of comonomer and the membrane structure can be adjusted with the styrene molar fraction.

In the hydrated state, we did not observe the ionomer peak by SAXS. This implies that there is no contrast between the ionic domains and the polymer. This is likely to be a result of a more homogenous membrane when it swells in water.

6.3   Conclusions

The effect ofnon-crosslinking comonomers (MAN, AN, MMA and MAA) with styrene (as primary monomer) on the fuel cell relevant properties and membrane structure of radiation grafted membranes was investigated. During sulfonation, grafted films containing nitrile (MAN and AN) and ester (MMA) functional groups undergo partial acid catalyzed hydrolysis, yielding amide and carboxylic acid functionalities. Styrene / MAA grafts undergo an internal Friedel-Crafts acylation during the sulfonation reaction, yielding a conjugated ketone structure.

In water swollen state, the presence of comonomer increases the water uptake of the membrane without contributing to the proton conductivity. The proton conductivity of water swollen membranes is mainly governed by the IEC in the examined range (up to 2.5 mmol g^{-1}). This correlation, however, fails to explain the loss of proton conductivity in the presence of a comonomer towards lower relative humidities. All of the co-grafted membranes exhibit a significantly lower conductivity compared to Nafion and the pure styrene grafted membrane at low relative humidity. The major factor contributing to proton conductivity of the grafted membranes is their ability to absorb water. The proton mobilities of all grafted membranes strongly depends on the water volume fraction.

Analysis of the nanostructure of the membranes using small-angle X-ray scattering (SAXS) technique highlights that the structure of the co-grafted membranes are similar but different from that of the pure styrene grafted membrane. The presence of a comonomer increases the distance between the acidic groups and adversely affect the proton conductivity at low hydration level. Close proximity of acid groups is preferable for better connectivity between hydrophilic domains.

A key challenge in the development of co-grafted membranes is to improve proton conductivity at low RH. Finally, the durability of membranes with different comonomers should be further investigated.

7

Conclusions and outlook

7.1 Conclusions

The PSSA based proton exchange membrane prepared by the radiation grafting method provides high proton conductivity at potentially low cost. However, it also degrades quite rapidly under the PEFC operating conditions as it is susceptible towards oxidative attack in the fuel cell environment. To suppress this degradation, a suitable comonomer such as methacrylonitrile (MAN) can be employed together with styrene [104]. Although it was previously demonstrated that the chemical stability of the membrane can be increased with MAN as styrene's comonomer, there is still a lack of understanding of the mechanism of this improvement in the membrane durability. This immediately raises the questions: how does the comonomer affect membrane properties, and what are the functionalities that lead to considerable improvement of membrane durability?

As a basis for an alternative membrane design, fundamental research was performed to address these questions by investigating the effect of MAN on the fuel cell relevant properties and to identify the functionalities that affect the membrane chemical stability. We prepared proton conducting membranes using radiation grafting, which involves the polymerization of a monomer mixture into an ETFE base film. The attractiveness of this method is that it allows accurate tailoring and tuning of the membrane composition. The method is simple and allows the use of a wide range of monomers and base films. In addition, with regards to commercialization, radiation grafting is a promising process for industrial applications. The molecular structures of grafted membranes prepared in this thesis are shown in Figure 7.1.

Co-grafted membranes with various styrene / MAN compositions were prepared to investigate the role of MAN in the membrane properties. The membranes were synthesized such that the ion exchange capacities (IEC) are similar. Since only sulfonated styrene contributes to the ion exchange capacity, the difference in the membrane properties is due to the MAN content. The composition of the grafted polymer was determined by FTIR spectroscopy.

7. CONCLUSIONS AND OUTLOOK

Comparison of the graft level of the co-grafted membranes with different styrene / MAN composition shows that membranes with a higher MAN molar fraction require a higher graft level to yield the same IEC. An increase in MAN molar fraction enhances the hydrophilicity of the membrane, resulting in a higher water uptake. Although water is essential for proton transport, too much water can lead to extensive membrane expansion and inferior dimensional stability [117].

Increased hydrophilicity and water uptake typically favor proton conductivity, however the styrene / MAN co-grafted membranes with similar IEC exhibited comparable proton conductivity in fully swollen state, regardless of the water uptake. When the relative humidity is reduced to below 80%, discrepancies in the proton conductivity as a function of styrene / MAN composition can be observed. Membranes with a higher MAN molar fraction showed a higher conductivity loss at reduced humidity. This could be due to dehydration and morphological changes, as confirmed by small angle X-ray scattering (SAXS).

Degradation of PSSA membranes is mainly caused by addition of HO· to the aromatic ring, which can lead to subsequent chain fragmentation and degradation of the graft component. To slow down the degradation, the α-position of styrene should be protected. Styrene derivatives such as α-methylstyrene (AMS) or α,β,β-trifluorostyrene (TFS) have already been applied in proton conducting membranes for fuel cells. The protecting groups at the α-position have shown beneficial effects on the chemical stability [13, 39]. Despite their high stability, membranes based on AMS and TFS are difficult to prepare compared to their styrene counterpart because of their poor radical polymerization kinetics. Perhaps, the methyl protected α-position of MAN can improve the membrane stability and constitute a potential use of MAN as styrene's comonomer. In comparison to styrene / MAN, styrene / acrylonitrile (AN) co-grafted membranes were prepared to investigate the effect of the α-methyl group of the comonomer on the membrane properties and durability. The difference in the molecular structure between these two comonomers is the absence of the α-methyl group in AN. Styrene / AN co-grafted membranes led to pronounced hydrolysis during membrane preparation, which converted the nitrile into amide and carboxylic acid in the acidic environment of the hydrated polymer. The styrene / MAN co-grafted membranes were more resistant to hydrolysis, and by tuning the ratio of styrene to comonomer, hydrolysis of styrene / MAN co-grafted membranes in the preparation step can be avoided. Yet, hydrolysis of both membranes takes place gradually during fuel cell operation, albeit with much lower rate in case of MAN.

In addition to high chemical stability, the membrane materials have to retain their gas barrier properties throughout the fuel cell operation. A hydrolysis experiment of styrene / MAN and styrene / AN co-grafted membranes under N_2 environment (100% RH, 90°C) was carried out for approximately 300 hours. Under these conditions, there was no appreciable change in hydrogen

permeation as well as membrane resistance due to hydrolysis. Some of the MAN units were hydrolyzed whilst nearly all of the AN units were converted into amide and carboxylic acid. Hydrolysis of the nitrile is not a direct cause of the polymer chain scission, because the nitrile group is not part of the polymer backbone, but nevertheless, hydrolysis of nitrile contributes to accelerated membrane deterioration.

To determine the role of nitrile in the membrane properties and durability, different co-grafted membranes of styrene and a comonomer containing an α-methyl group were prepared. Methyl methacrylate (MMA) and methacrylic acid (MAA) were chosen for this purpose and compared with those containing MAN and AN as comonomers. Although IEC is a dry state property, it determines the hydrophilicity and water uptake of different co-grafted membranes in fully swollen state. At reduced humidity, the co-grafted membranes have a significant disadvantage compared to pure styrene grafted membrane since they show a more pronounced conductivity loss, regardless of the comonomer type. The preliminary structure investigation by SAXS reveals that the structures of different co-grafted membranes on the nanoscale are comparable and may be used to explain this similar behavior. It is suggested that the pure styrene grafted membrane exhibits a lower percolation threshold and the ionic aggregates are better connected compared to the co-grafted membranes, leading to improved proton conductivity at reduced humidity.

Although proton transport occurs in the hydrophilic regions of the membrane, the hydrophobic base film structure appears to be a critical factor limiting proton conductivity at reduced humidity. The semi-crystalline structure of the base film presents a barrier to the grafted domains. To connect the aqueous pathway throughout the membrane, more water is needed compared to the system with a homogeneous distribution of the hydrophilic domains. Optimizing the structure-property relation of the base film for a better connectivity of the hydrophilic domains while providing adequate mechanical stability is a motivation for further improvement of proton transport in radiation grafted membranes at reduced relative humidity.

The accelerated stress tests show that nitrile containing membranes showed a superior durability in comparison with styrene / MAA co-grafted membranes. There is certainly still much to learn about these phenomena and detailed studies on membrane properties and the degradation mechanism should be carried out to identify the effect of the comonomer's functionalities on the membrane stability. Recommendations for further investigations are given below.

7.2   Outlook

Preliminary results suggest that MAN contributes to membrane stability, in which the electron donating nature of the α-methyl group increases the stability of nitrile towards hydrolysis during sulfonation and fuel cell operation. Substitution of α-hydrogen by an electron donating group can increase the resistance towards hydrolysis, which may also translate to other hydrolyzable

7. CONCLUSIONS AND OUTLOOK
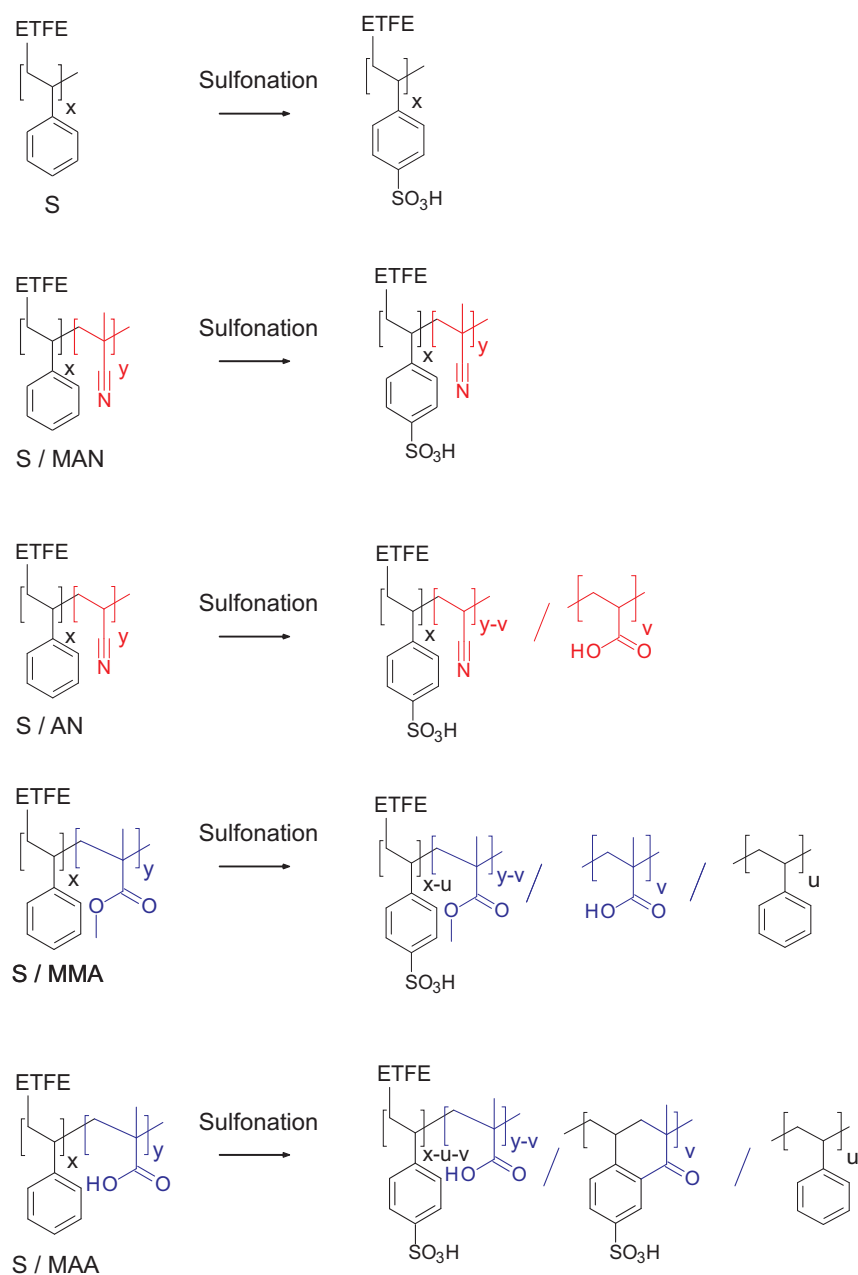
Figure 7.1: Molecular structures of films and coresponding membranes prepared in this study by radiation grafting and subsequent sulfonation.

comonomers. Future work should not be restricted to increase the hydrolytic stability, but also to study of polymer degradation of a model compound using electron paramagnetic resonance (EPR) to identify material weaknesses and yield valuable insight into alternative membrane design. Additionally, further studies are needed to identify the optimum membrane characteristics to meet the lifetime requirements of the fuel cell. Future work can be carried out using different functional groups to investigate the role of chemical functionalities on membrane durability. By examining co-grafted membranes containing amide and hydroxyl groups under accelerated stress

test (OCV conditions), information can be obtained about the influence of these chemical functionalities on the membrane stability. Methacrylamide and dimethyl acrylamide may be used as styrene's comonomers to investigate the role of amide on the chemical stability, as well as to obtain insight into the effect of hydrolysis on membrane properties. Co-grafted membranes containing hydroxyl groups may be synthesized using vinyl acetate as a starting material to graft with styrene. Due to the susceptibility of ester to hydrolysis under acidic conditions, the styrene / vinyl acetate membranes may be subjected to base-catalyzed hydrolysis to convert ester into carboxylic acid and hydroxyl groups. As polyvinyl alcohol is widely used in various applications (including food packaging), the benefit of incorporating the hydroxyl group in the graft may improve the gas barrier properties of the co-grafted membrane.

In a later development stage, further improvements in membrane durability, such as incorporation of radical scavengers or chelating agents can be applied to optimize the membrane lifetime.

Apart from the durability, the fuel cell performance of hydrolyzed membranes is worth exploring since nitrile-containing membranes undergo hydrolysis during fuel cell operation, thereby converting nitrile to hydrolyzed products. Such chemical changes may lead to alteration of membrane properties such as membrane / electrode interface and water transport in the membrane, which can affect the fuel cell performance. Perhaps, one could pre-hydrolyze a styrene / AN membrane in a fully humidified chamber at elevated temperature before assembly in the MEA, and compare its performance with that of the pristine membrane under the same conditions. Another possibility is grafting of styrene sulfonate with MAA and compare its performance with that of a styrene / MAN membrane.

Another critical issue is the severe loss of proton conductivity of the co-grafted membranes at reduced humidity. Such conditions may occur while operating the fuel cell at high temperature, inadequate humidification or at low load when only a small amount of water is generated. All grafted membranes with similar IEC show similar hydration number in the examined temperatue range (up to 70℃), irrespective of the comonomer type. The conductivity of co-grafted membranes drops by several orders of magnitude as the relative humidity decreases below 80%. To facilitate proton conductivity, the membrane should sustain high water uptake particularly under low relative humidity conditions. Since the kinetics of water uptake in the vapor phase are mostly governed by the surface properties [238], this limitation may be resolved by surface modification using e.g. plasma treatment, to incorporate suitable functional groups to improve surface wettability and improve the vapor transport into the membrane. In addition, the advantages of such technique may also include improvement of the membrane / electrode interface and hence reduced polarization resistance and increased fuel cell performance. Preferable functional

groups are those which do not undergo hydrolysis in the fuel cell environment. The relationship between molecular interaction, water uptake and proton transport mechanism needs to be developed.

The knowledge gained in understanding the relationship between nanoscale structure and proton conductivity of the co-grafted membranes are inspiring and of practical relevance. The structural changes in the hydrophilic domains of the membrane upon addition of comonomer were suggested to explain the loss in proton conductivity at low relative humidity. In addition, the base film may play a crucial role in determining the proton pathway. Further evidence for our hypothesis is given by Chen *et al.* [85]. They showed that at the same IEC, membranes prepared from different base films exhibit different proton conductivity. The size and shape of the crystalline domains and the intrinsic crystallinity of the base films are among other important parameters that can influence proton conductivity and water uptake. Therefore, a systematic study of these parameters needs to be performed, ideally with a base film that allows the control over the structure and morphology. Base film modification by, e.g., thermal-mechanical treatment, could be applied to amend base film properties. Stretching, annealing and/or quenching of the base film may be done before irradiating the films to induce crystal alignment in the direction of stretching as well as to control the crystal growth. Probably, decreasing the size of crystalline domains of the base film can be expected to be beneficial for the proton conductivity (though at the expense of membrane integrity).

Important aspects which have not been investigated in this study include the role of the grafted chain (flexibility, hydrophilicity, polymer configuration, length), which may also play a role in determining water content, water distribution and membrane structure, which are essential for design and optimization.

Further research should investigate potential applications of the co-grafted membrane. One of the prime candidates is to use them as membranes in an electrolyzer. Under electrolyzer conditions, the membrane is always exposed to liquid water. Of course, the degradation of such membranes and mechanical stability under electrolyzer environment needs to be performed before it is ready to be used.

Bibliography

[1] I. DINCER, *Energy Sources* **20**, 427 (1998).

[2] J. HANSEN, R. RUEDY, M. SATO, and K. LO, *Rev. Geophys.* **48** (2010).

[3] N. PANWAR, S. KAUSHIK, and S. KOTHARI, *Renew. Sust. Energ. Rev.* **15**, 1513 (2011).

[4] M. M. MENCH, *Fuel cell engines*, John Wiley & Sons, Inc., Hoboken, New Jersey, 2008.

[5] J. LARMINIE and A. DICKS, *Fuel Cell Systems Explained (Second Edition)*, John Wiley & Sons, 2nd edition, 2003.

[6] V. S. BAGOTSKY, *Fuel Cells: Problems and Solutions*, John Wiley & Sons, 2009.

[7] F. A. DE BRUIJN, V. A. T. DAM, and G. J. M. JANSSEN, *Fuel Cells* **8**, 3 (2008).

[8] W. LIU and M. CRUM, *ECS Trans.* **3**, 531 (2006).

[9] S. A. VILEKAR and R. DATTA, *J. Power Sources* **195**, 2241 (2010).

[10] M. RIKUKAWA and K. SANUI, *Prog. Polym. Sci.* **25**, 1463 (2000).

[11] W. T. GRUBB JR., *Fuel cell*, US Patent 2913511, 1959.

[12] G. G. SCHERER, *Ber. Bunsenges. Phys. Chem.* **94**, 1008 (1990).

[13] A. B. LACONTI, M. HAMDAN, and R. C. MCDONALD, Mechanisms of membrane degradation, in *Handbook of Fuel Cells*, edited by W. VIELSTICH, A. LAMM, and H. A. GASTEIGER, pp. 647–662, John Wiley & Sons, Ltd, West Sussex, 2003.

[14] P. KURZWEIL, History: Fuel cells, in *Encyclopedia of Electrochemical Power Sources*, edited by J. GARCHE, C. K. DYER, P. T. MOSELEY, Z. OGUMI, D. A. J. RAND, and B. SCROSATI, Elsevier B. V., Amsterdam, 2009.

[15] C. S. JINZHU WEI and A. E. STECK, Trifluorostyrene and substituted trifluorostyrene copolymeric compositions and ion-exchange membranes formed therefrom, 1995.

BIBLIOGRAPHY

[16] M. Maalouf, *Structure and dynamics influencing proton transport in materials for high temperature (120°C) PEM fuel cells*, PhD thesis, Case Western Reserve University, 2011.

[17] R. Baldwin, M. Pham, A. Leonida, J. McElroy, and T. Nalette, *J. Power Sources* **29**, 399 (1990).

[18] Amir-Al-Ahmed, A. Sultan, and S. Zaidi, Sulfonated Poly(Ether Ether Ketone) (SPEEK): A Promising Membrane Material for Polymer Electrolyte Fuel Cell, in *Ion Exchange Technology I*, edited by I. Dr. and M. Luqman, pp. 437–451, Springer Netherlands, 2012.

[19] Q. Li, J. O. Jensen, R. F. Savinell, and N. J. Bjerrum, *Prog. Polym. Sci.* **34**, 449 (2009).

[20] N. Y. Abu-Thabit, S. A. Ali, and S. J. Zaidi, *J. Membr. Sci.* **360**, 26 (2010).

[21] J. Roziere and D. J. Jones, *Annu. Rev. Mater. Res.* **33**, 503 (2003).

[22] J. A. Kerres, *J. Membr. Sci.* **185**, 3 (2001).

[23] A. J. Berejka, Electron beam grafting of polymers, in *Advances in radiation chemistry of polymers*, pp. 85–89, International Atomic Energy Agency, 2003.

[24] G. G. Scherer, E. Killer, and D. Grman, *Int. J. Hydrogen Energy* **17**, 115 (1992).

[25] A. Elmidaoui, A. T. Cherif, J. Brunea, F. Duclert, T. Cohen, and C. Gavach, *J. Membr. Sci.* **67**, 263 (1992).

[26] R. Ishihara, K. Fujiwara, T. Harayama, Y. Okamura, S. Uchiyama, M. Sugiyama, T. Someya, W. Amakai, S. Umino, T. Ono, A. Nide, Y. Hirayama, T. Baba, T. Kojima, D. Umeno, K. Saito, and S.-T. Asai, Shiho, *J. Nucl. Sci. Technol.* **48**, 1281 (2011).

[27] P. Arora and Z. Zhang, *Chem. Rev.* **104**, 4419 (2004).

[28] K. Makuuchi and S. Cheng, Radiation graft polymerization, in *Radiation Processing of Polymer Materials and its Industrial Applications*, pp. 334–372, John Wiley & Sons, New Jersey, 2012.

[29] W. K. W. Chen, R. B. Mesrobian, D. S. Ballantine, D. J. Metz, and A. Glines, *J. Polym. Sci.* **23**, 903 (1957).

[30] M. M. Nasef, Fuel cell membranes by radiation-induced graft copolymerization: Current status, Challenges, Future directions, in *Polymer Membranes for Fuel Cells*, edited by S. M. J. Zaidi and T. Matsuura, pp. 87–114, Springer Science, New York, 2008.

[31] V. F. D'agostino, J. Y. Lee, and E. H. Cook Jr., *Trifluorostyrene sulfonic acid membranes*, US Patent 4012303, Mar. 15 (1977).

[32] T. Momose, K. Tomiie, I. Ishigaki, and J. Okamoto, *J. Appl. Polym. Sci.* **37**, 2165 (1989).

[33] T. Momose, H. Yoshioka, I. Ishigaki, and J. Okamoto, *J. Appl. Polym. Sci.* **38**, 2091 (1989).

[34] T. Momose, I. Ishigaki, and J. Okamoto, *J. Appl. Polym. Sci.* **36**, 55 (1988).

[35] G. G. Scherer, T. Momose, and K. Tomiie, *J. Electrochem. Soc.* **135**, 3071 (1988).

[36] J. Huslage, T. Rager, B. Schnyder, and A. Tsukada, *Electrochim. Acta* **48**, 247 (2002).

[37] F. N. Büchi, B. Gupta, M. Rouilly, P. Hauser, A. Chapiró, and G. G. Scherer, Radiation grafted and sulfonated (FEP-g-Polystyrene)- An alternative to perflourinated membranes for PEM fuel cells?, Intersociety Energy Conversion Engineering Conference, pp. 3419–3424, 1992.

[38] L. Gubler, S. Alkan-Gürsel, H. B. youcef, F. Wallasch, A. Wokaun, and G. G. Scherer.

[39] L. Gubler, S. Alkan-Gürsel, and G. G. Scherer, *Fuel Cells* **5**, 317 (2005).

[40] L. Gubler, H. Ben youcef, S. Alkan-Gürsel, A. Wokaun, and G. G. Scherer, *J. Electrochem. Soc.* **155**, B921 (2008).

[41] L. Gubler, H. Kuhn, T. Schmidt, G. G. Scherer, H. P. Brack, and K. Simbeck, *Fuel Cells* **4**, 196 (2004).

[42] T. J. Schmidt, K. Simbeck, and G. G. Scherer, *J. Electrochem. Soc.* **152**, A93 (2005).

[43] L. Gubler, M. Slaski, F. Wallasch, A. Wokaun, and G. G. Scherer, *J. Membr. Sci.* **339**, 68 (2009).

[44] M. P. Rodgers, L. J. Bonville, H. R. Kunz, D. K. Slattery, and J. M. Fenton, *Chem. Rev.* **112**, 6075 (2012).

[45] S. Kundu, L. C. Simon, M. Fowler, and S. Grot, *Polymer* **46**, 11707 (2005).

[46] S. Kreitmeier, A. Wokaun, and F. N. Büchi, *ECS Trans.* **50**, 927 (2013).

[47] M. Danilczuk, F. D. Coms, and S. Schlick, *J. Phys. Chem. B* **113**, 8031 (2009).

[48] L. Gubler, S. M. Dockheer, and W. H. Koppenol, *J. Electrochem. Soc.* **158**, B755 (2011).

[49] D. A. Schiraldi, *J. Macromol. Sci., Part C: Polym. Rev.* **46**, 315 (2006).

[50] M. Aoki, H. Uchida, and M. Watanabe, *Electrochem. Commun.* **7**, 1434 (2005).

[51] M. Inaba, T. Kinumoto, M. Kiriake, R. Umebayashi, A. Tasaka, and Z. Ogumi, *Electrochim. Acta* **51**, 5746 (2006).

[52] L. Merlo, A. Ghielmi, L. Cirillo, M. Gebert, and V. Arcella, *J. Power Sources* **171**, 140 (2007).

[53] H. Liu, J. Zhang, F. Coms, W. Gu, B. Litteer, and H. A. Gasteiger, *ECS Trans.* **3**, 493 (2006).

[54] M. Kitazawa, A. Nosaka, and Y. Nosaka, *J. Appl. Electrochem.* **38**, 491 (2008).

[55] H. Liu, F. D. Coms, J. Zhang, H. Gasteiger, and A. LaConti, Chemical Degradation: Correlations Between Electrolyzer and Fuel Cell Findings, in *Polymer Electrolyte Fuel Cell Durability*, edited by F. N. Büchi, M. Inaba, and T. J. Schmidt, pp. 71–118, Springer New York, 2009.

[56] V. O. Mittal, H. R. Kunz, and J. M. Fenton, *J. Electrochem. Soc.* **153**, A1755 (2006).

[57] J. F. Imbalzano and D. L. Kerbow, *Stable tetrafluoroethylene copolymers*, US Patent 4743658, May 10 (1988).

[58] D. E. Curtin, R. D. Lousenberg, T. J. Henry, P. C. Tangeman, and M. E. Tisack, *J. Power Sources* **131**, 41 (2004).

[59] F. D. Coms, *ECS Trans.* **16**, 235 (2008).

[60] V. O. Mittal, H. R. Kunz, and J. M. Fenton, *J. Electrochem. Soc.* **154**, B652 (2007).

[61] F. N. Büchi, B. Gupta, O. Haas, and G. G. Scherer, *Electrochim. Acta* **40**, 345 (1995).

[62] G. Hübner and E. Roduner, *J. Mater. Chem.* **9**, 409 (1999).

[63] M. Yang and Y. Shibasaki, *J. Polym. Sci. Part A: Polym. Chem.* **36**, 2315 (1998).

[64] S. M. Dockheer, L. Gubler, P. L. Bounds, A. S. Domazou, G. G. Scherer, A. Wokaun, and W. H. Koppenol, *Phys. Chem. Chem. Phys.,* **12**, 11609 (2010).

[65] L. Bonorand, G. G. Scherer, and L. Gubler, *PSI Electrochemistry Laboratory - Annual report 2011* , 5 (2012).

[66] N. Walsby, *Preparation and Characterisation of Radiation-Grafted Membranes for Fuel Cells*, PhD thesis, University of Helsinki, 2001.

[67] H. Ben youcef, *Radiation grafted ETFE based membranes for fuel cells: improved mechanical and oxidative stability*, PhD thesis, ETH Zürich, 2009.

[68] J. M. Rosiak, Radiation polymerization in solution, in *Advances in radiation chemistry of polymers*, pp. 41–60, International Atomic Energy Agency, 2003.

[69] T. R. Dargaville, G. A. George, D. J. T. Hill, and A. K. Whittaker, *Prog. Polym. Sci.* **28**, 1355 (2003).

[70] L. Gubler, M. Slaski, A. Wokaun, and G. G. Scherer, *Electrochem. Commun.* **8**, 1215 (2006).

[71] A. Chapiró, *Radiation chemistry of polymeric systems*, volume 15 of *High polymers*, Wiley, New York, 1962.

[72] M. M. Nasef and E. S. Hegazy, *Prog. Polym. Sci.* **29**, 499 (2004).

[73] K. Fujiwara, *Nucl. Instrum. Meth. B* **265**, 150 (2007).

[74] B. Gupta and G. G. Scherer, *Chimia* **48**, 127 (1994).

[75] I. Kamel, S. Machi, and J. Silverman, *J. Polym. Sci. Part A: Polym. Chem.* **10**, 1019 (1972).

[76] M. Lavalle, Nanopolymers and radiation, in *Advances in radiation chemistry of polymers*, pp. 75–78, International Atomic Energy Agency, 2003.

[77] B. Gupta and A. Chapiró, *Eur. Polym. J.* **25**, 1137 (1989).

[78] A. Bhattacharya and B. N. Misra, *Prog. Polym. Sci.* **29**, 767 (2004).

[79] A. Bozzi and A. Chapiró, *Eur. Polym. J.* **23**, 255 (1987).

[80] A. Bozzi and A. Chapiró, *Radiat. Phys. Chem.* **32**, 193 (1988).

[81] X. Zhili, A. Chapiró, and N. Schmitt, *Eur. Polym. J.* **29**, 301 (1993).

[82] J. Dobó, A. Somogyi, and T. Czvikovszky, *J. Polym. Sci. Part C: Polym. Sym.* **4**, 1173 (1963).

[83] S. Alkan-Gürsel, L. Gubler, B. Gupta, and G. Scherer, Fuel Cells I, in *Advances in Polymer Science*, edited by G. Scherer, volume 215, pp. 157–217, Springer Berlin / Heidelberg, 2008.

[84] J. S. Forsythe and D. J. T. Hill, *Prog. Polym. Sci.* **25**, 101 (2000).

[85] J. Chen, M. Asano, Y. Maekawa, and M. Yoshida, *J. Membr. Sci.* **277**, 249 (2006).

[86] M. Senna, H. Aly, Z. Ali, and A. El-Naggar, *Polym. Degrad. Stab.* **71**, 53 (2000).

[87] H. P. Brack, H. G. Bührer, L. Bonorand, and G. G. Scherer, *J. Mater. Chem.* **10**, 1795 (2000).

[88] H. P. Brack, F. N. Büchi, J. Huslage, M. Rota, and G. G. Scherer, Development of Radiation-Grafted Membranes for Fuel Cell Applications Based on Poly(ethylene-*alt*-tetrafluoroethylene), in *Membrane Formation and Modification*, chapter 12, pp. 174–188.

[89] M. M. Nasef and K. Z. M. Dahlan, *Nucl. Instrum. Meth. B* **201**, 604 (2003).

[90] S. Chen, L. Krishnan, S. Srinivasan, J. Benziger, and A. Bocarsly, *J. Membr. Sci.* **243**, 327 (2004).

[91] B. Gupta, F. Büchi, S. G.G., and A. Chapiró, *Solid State Ionics* **61**, 213 (1993).

[92] S. Sugiyama, S. Tsuneda, K. Saito, S. Furusaki, T. Sugo, and K. Makuuchi, *React. Polym.* **21**, 187 (1993).

[93] T. Lehtinen, G. Sundholm, S. Holmberg, F. Sundholm, P. Björnbom, and M. Bursell, *Electrochim. Acta* **43**, 1881 (1998).

[94] M. M. Nasef, H. Saidi, H. M. Nor, K. Z. M. Dahlan, and K. Hashim, *J. Appl. Polym. Sci.* **73**, 2095 (1999).

[95] C. Stone and A. E. Steck, *Graft polymeric membranes and ion-exchange membranes formed therefrom*, US Patent 6359019, Mar. 19 (2002).

[96] C. Stone, A. E. Steck, and B. Choudhury, *Graft polymeric membranes and ion-exchange membranes formed therefrom*, US Patent 6723758, Apr. 20 (2004).

[97] R. A. Assink, C. Arnold Jr., and R. P. Hollandsworth, *J. Membr. Sci.* **56**, 143 (1991).

[98] B. Gupta, F. N. Büchi, G. G. Scherer, and A. Chapiró, *J. Membr. Sci.* **118**, 231 (1996).

[99] H. Ben youcef, S. Alkan-Gürsel, A. Wokaun, and G. G. Scherer, *J. Membr. Sci.* **311**, 208 (2008).

[100] M. Larsen, Y. Ma, P. Lund, and E. Skou, *Appl. Phys. A Mater. Sci. Process.* **96**, 569 (2009).

[101] F. Wallasch, *Investigations on radiation grafted polymer fuel cell membranes: preparation, characterization, application*, PhD thesis, ETH Zürich, 2010.

[102] S. Phadnis, M. Patri, V. R. Hande, S. Roychoudhury, and P. C. Deb, *J. Appl. Polym. Sci.* **92**, 2318 (2004).

[103] W. Becker, M. Bothe, and G. Schmidt-Naake, *Angew. Makromol. Chem.* **273**, 57 (1999).

[104] H. Ben youcef, L. Gubler, S. Alkan-Gürsel, D. Henkensmeier, A. Wokaun, and G. G. Scherer, *Electrochem. Commun.* **11**, 941 (2009).

[105] C. Schmidt, T. Glück, and G. Schmidt-Naake, *Chem. Ing. Tech.* **79**, 137 (2007).

[106] C. Schmidt and G. Schmidt-Naake, *Chem. Ing. Tech.* **80**, 317 (2008).

[107] S. Takahashi, H. Okonogi, T. Hagiwara, and Y. Maekawa, *J. Membr. Sci.* **324**, 173 (2008).

[108] T. T. Hanh, S. Takahashi, J. Chen, S.-i. Sawada, and Y. Maekawa, *J. Appl. Polym. Sci.* **114**, 231 (2009).

[109] J. A. Horsfall and K. V. Lovell, *Polym. Adv. Technol.* **13**, 381 (2002).

[110] H. Zhang and P. K. Shen, *Chem. Rev.* **112**, 2780 (2012).

[111] M. Eikerling, A. Kornyshev, and E. Spohr, *Adv. Polym. Sci.* **215**, 15 (2008).

[112] K. D. Kreuer, S. J. Paddison, E. Spohr, and M. Schuster, *Chem. Rev.* **104**, 4637 (2004).

[113] B. S. Pivovar, *Polymer* **47**, 4194 (2006).

BIBLIOGRAPHY

[114] D. E. MOILANEN, D. B. SPRY, and M. D. FAYER, *Langmuir* **24**, 3690 (2008).

[115] M. R. TIMOTHY J. PECKHAM, JENNIFER SCHMEISSER and S. HOLDCROFT, *J. Mater. Chem.* **17**, 3255 (2007).

[116] J. M. SCHMEISSER, *Proton transport in proton exchange membranes*, PhD thesis, Simon Fraser University, 2007.

[117] T. WEISSBACH, E. M. W. TSANG, A. C. C. YANG, R. NARIMANI, B. J. FRISKEN, and S. HOLDCROFT, *J. Mater. Chem.* **22**, 24348 (2012).

[118] T. D. GIERKE and W. Y. HSU, The Cluster-Network Model of Ion Clustering in Perfluorosulfonated Membranes, in *Perfluorinated Ionomer Membranes*, edited by A. EISENBERG, volume 180 of *ACS Symposium Series*, chapter 14, pp. 283–307, American Chemical Society, Washington D.C., 1982.

[119] G. GEBEL, *Polymer* **41**, 5829 (2000).

[120] R. O'HAYRE, S. CHA, W. COLELLA, and F. B. PRINZ, *Fuel Cell Fundamentals*, John Wiley & Sons, New York, 2006.

[121] B. GUPTA and G. G. SCHERER, *Angew. Makromol. Chem.* **210**, 151 (1993).

[122] M. M. NASEF, *J. Appl. Polym. Sci.* **84**, 1949 (2002).

[123] K. MORTENSEN, U. GASSER, S. ALKAN-GÜRSEL, and G. G. SCHERER, *J. Appl. Polym. Sci.* **46**, 1660 (2008).

[124] S. BALOG, U. GASSER, K. MORTENSEN, L. GUBLER, G. G. SCHERER, and H. BEN YOUCEF, *Macromol. Chem. Phys.* **211**, 635 (2010).

[125] K. JOKELA, R. SERIMAA, M. TORKKELI, M. ELOMAA, F. SUNDHOLM, N. WALSBY, T. KALLIO, and G. SUNDHOLM, *J. Appl. Crystallogr.* **33**, 723 (2000).

[126] J. DING, C. CHUY, and S. HOLDCROFT, *Adv. Funct. Mater.* **12**, 389 (2002).

[127] J. DING, C. CHUY, and S. HOLDCROFT, *Chem. Mater.* **13**, 2231 (2001).

[128] Y. YANG and S. HOLDCROFT, *Fuel Cells* **5**, 309 (2005).

[129] M. A. HICKNER, H. GHASSEMI, Y. S. KIM, B. R. EINSLA, and J. E. MCGRATH, *Chem. Rev.* **104**, 4587 (2004).

[130] B. SMITHA, S. SRIDHAR, and A. KHAN, *J. Membr. Sci.* **259**, 10 (2005).

[131] J. St-Pierre and N. Jia, *J. New Mater. Electrochem. Syst.* **5**, 263 (2002).

[132] J. S. Spendelow and D. C. Papageorgopoulos, *Fuel Cells* **11**, 775 (2011).

[133] F. Zhang, G. Chen, M. A. Hickner, and B. E. Logan, *J. Power Sources* **218**, 100 (2012).

[134] K. D. Kreuer, *J. Membr. Sci.* **185**, 29 (2001).

[135] Y. Buchmüller, K. Jetsrisuparb, and L. Gubler, *PSI Electrochemistry Laboratory - Annual report 2011* , 13 (2012).

[136] www.alvatek.co.uk/fuel-cell-research/membrane-conductivity-testing/in-plane-membrane-conductivity testing.aspx.

[137] C. E. Williams, R. P. May, and A. Guinier, Small-angle scattering of X-rays and neutrons, in *X-ray characterization of materials*, edited by E. Lifshin, chapter 4, pp. 211–254, Wiley, Weinheim, 2007.

[138] B. Hammouda, A tutorial on small-angle neutron scattering from polymers, Technical report, Nationa Institute of standards and technology, 1995.

[139] L. Gubler, Ion-containing membranes for fuel cells, Presentation at Adolphe Merkle Institute, Marly, 2012.

[140] H. Schnablegger and Y. Singh, *The SAXS guide: Getting acquainted with the principles*, Anton Paar GmbH, 2 edition, 2011.

[141] S. Balog, U. Gasser, K. Jetsrisuparb, and L. Gubler, *Polymer* **54**, 4266 (2013).

[142] S. S. Kocha, J. D. Yang, and J. S. Yi, *AIChE J.* **52**, 1916 (2006).

[143] J. Wu, X. Z. Yuan, H. Wang, M. Blanco, J. J. Martin, and J. Zhang, *Int. J. Hydrogen Energy* **33**, 1735 (2008).

[144] R. Kötz, M. Hahn, and R. Gallay, *J. Power Sources* **154**, 550 (2006).

[145] L. Gubler, N. Prost, S. Alkan-Gürsel, and G. G. Scherer, *Solid State Ionics* **176**, 2849 (2005).

[146] X. Yuan, H. Wang, J. C. Sun, and J. Zhang, *Int. J. Hydrogen Energy* **32**, 4365 (2007).

[147] F. Maillard, M. Eikerling, O. V. Cherstiouk, S. Schreier, E. Savinova, and U. Stimming, *Faraday Discuss.* **125**, 357 (2004).

BIBLIOGRAPHY

[148] M. Salame, *J. Polym. Sci. Polm. Symp.* **41**, 1 (1973).

[149] A. E. Barnabeo, W. S. Creasy, and L. M. Robeson, *J. Polym. Sci. Polym. Chem. Ed.* **13**, 1979 (1975).

[150] S. Allen, M. Fujii, V. Stannett, H. Hopfenberg, and J. Williams, *J. Membr. Sci.* **2**, 153 (1977).

[151] T. Rager, *Helv. Chim. Acta* **86**, 1966 (2003).

[152] S. Mitov, G. Hübner, H. P. Brack, G. G. Scherer, and E. Roduner, *J. Polym. Sci. Polym. Phys.* **44**, 3323 (2006).

[153] J. Brandrup, E. H. Immergut, E. A. Grulke, A. Abe, and D. R. Bloch, *Polymer Handbook*, John Wiley & Sons, New York, 4th edition, 1999.

[154] L. I. Sanli and S. Alkan-Gürsel, *J. Appl. Polym. Sci.* **120**, 2313 (2011).

[155] H. M. M. Nizam El-Din, S. M. Badawy, and A. M. Dessouki, *J. Appl. Polym. Sci.* **77**, 1405 (2000).

[156] G. Socrates, *Infrared and Raman Characteristic Group Frequencies: Tables and Charts*, John Wiley & Sons, Ltd., Chichester, 3rd edition, 2004.

[157] F. R. Mayo and F. M. Lewis, *J. Am. Chem. Soc.* **66**, 1594 (1944).

[158] A. El-Naggar, M. Zohdy, S. Sahar, and E. Allam, *Polym. Int.* **50**, 1082 (2001).

[159] K. W. Doak, *J. Am. Chem. Soc.* **72**, 4681 (1950).

[160] F. M. Lewis, F. R. Mayo, and W. F. Hulse, *J. Am. Chem. Soc.* **67**, 1701 (1945).

[161] K. Arita, T. Ohtomo, and Y. Tsurumi, *J. Polym. Sci. Polym. Lett. Ed.* **19**, 211 (1981).

[162] F. M. Lewis, C. Walling, W. Cummings, E. R. Briggs, and F. R. Mayo, *J. Am. Chem. Soc.* **70**, 1519 (1948).

[163] A. Rudin and R. G. Yule, *J. Polym. Sci. Part A: Polym. Chem.* **9**, 3009 (1971).

[164] G. Cameron and G. Esslemont, *Polymer* **13**, 435 (1972).

[165] D. J. T. Hill, L. Dong, and J. H. O'Donnell, *J. Polym. Sci. Part A: Polym. Chem.* **31**, 2951 (1993).

[166] R. G. Fordyce, E. C. Chapin, and G. E. Ham, *J. Am. Chem. Soc.* **70**, 2489 (1948).

[167] S.-H. Hong, S.-A. Lee, J.-D. Nam, Y.-K. Lee, T.-S. Kim, and S. Won, *Macromol. Res.* **16**, 204 (2008).

[168] J. C. Yang, M. J. Jablonsky, and J. W. Mays, *Polymer* **43**, 5125 (2002).

[169] O. Becker, R. J. Varley, and G. P. Simon, *Eur. Polym. J.* **40**, 187 (2004).

[170] J. Dong, Y. Ozaki, and K. Nakashima, *Macromolecules* **30**, 1111 (1997).

[171] F. C. Baines and J. C. Bevington, *J. Polym. Sci. Part A: Polym. Chem.* **6**, 2433 (1968).

[172] J. Coates, Interpretation of Infrared Spectra, A Practical Approach, in *Encyclopedia of Analytical Chemistry*, edited by R. A. Meyers, John Wiley & Sons, Ltd, Chichester, 2006.

[173] S. Cleghorn, D. Mayfield, D. Moore, J. Moore, G. Rusch, T. Sherman, N. Sisofo, and U. Beuscher, *J. Power Sources* **158**, 446 (2006).

[174] Z. Ogumi, Z. Takehara, and S. Yoshizawa, *J. Electrochem. Soc.* **131**, 769 (1984).

[175] Z. Ogumi, T. Kuroe, and Z. Takehara, *J. Electrochem. Soc.* **132**, 2601 (1985).

[176] D. H. Weinkauf and D. R. Paul, Effects of structure order on barrier properties, in *Barrier Polymers and Structures*, edited by W. J. Koros, pp. 60–91, American Chemical Society, Washington, DC, 1990.

[177] K. Jetsrisuparb, H. Ben youcef, G. Scherer, A. Wokaun, and L. Gubler, *PSI Electrochemistry Laboratory - Annual report 2010* , 9 (2011).

[178] J. Lin, P. Wu, R. Wycisk, and P. Pintauro, *ECS Trans.* **16**, 1195 (2008).

[179] Z. Cai, L. Li, L. Su, and Y. Zhang, *Electrochem. Commun.* **14**, 9 (2012).

[180] J. Zhang, B. Litteer, F. Coms, and R. R. Makharia, *ECS Trans.* **41**, 1471 (2011).

[181] H. Xu, R. Borup, E. Brosha, F. Gazon, and B. S. Pivovar, *ECS Trans.* **6**, 51 (2007).

[182] N. Linse, L. Gubler, G. G. Scherer, and A. Wokaun, *Electrochim. Acta* **56**, 7541 (2011).

[183] N. Linse, *Start/stop phenomena in polymer electrolyte fuel cells*, PhD thesis, ETH Zürich, 2011.

BIBLIOGRAPHY

[184] C. Aymes-Chodur, N. Yagoubi, N. Betz, A. Moël, and D. Ferrier, *Chromatographia* **51**, 269 (2000).

[185] K. F. O'Driscoll, T. Higashimura, and S. Okamura, *Makromol. Chem.* **85**, 178 (1965).

[186] H. J. Harwood and W. M. Ritchey, *J. Polym. Sci. Part B Polym. Lett.* **2**, 601 (1964).

[187] H. J. Harwood, *Angew. Chem. Int. Ed.* **4**, 394 (1965).

[188] L. Dong and D. J. T. Hill, *Polym. Bull.* **34**, 323 (1995).

[189] K. Jetsrisuparb, H. Ben youcef, G. Scherer, A. Wokaun, and L. Gubler, *PSI Electrochemistry Laboratory - Annual report 2009* , 9 (2010).

[190] C. Chuy, J. Ding, E. Swanson, S. Holdcroft, J. Horsfall, and K. V. Lovell, *J. Electrochem. Soc.* **150**, E271 (2003).

[191] X. Wu, X. Wang, G. He, and J. Benziger, *J. Polym. Sci. Part B: Polym. Phys.* **49**, 1437 (2011).

[192] J. Schneider, Thermal Characterization of Radiation-Grafted Films and Membranes, Master's thesis, Laboratory for Electrochemistry, Paul Scherrer Institut, General Energy Research, CH-5232 Villigen PSI, 2005.

[193] M. M. Nasef and H. Saidi, *Macromol. Mater. Eng.* **291**, 972 (2006).

[194] B. Gupta, J. G. Highfield, and G. G. Scherer, *J. Appl. Polym. Sci.* **51**, 1659 (1994).

[195] Z. Zhang, E. Chalkova, M. Fedkin, C. Wang, S. N. Lvov, S. Komarneni, and T. C. M. Chung, *Macromolecules* **41**, 9130 (2008).

[196] S. J. Paddinson, *Annu. Rev. Mater. Res.* **33**, 289 (2003).

[197] A. Eisenberg, B. Hird, and R. B. Moore, *Macromolecules* **23**, 4098 (1990).

[198] E. M. W. Tsang, Z. Zhang, A. C. C. Yang, Z. Shi, T. J. Peckham, R. Narimani, B. J. Frisken, and S. Holdcroft, *Macromolecules* **42**, 9467 (2009).

[199] H. L. Yeager and A. Steck, *J. Electrochem. Soc.* **128**, 1880 (1981).

[200] L. Li, L. Su, and Y. Zhang, *Int. J. Hydrogen Energy* **37**, 4439 (2012).

[201] H. F. Mohamed, K. Ito, Y. Kobayashi, N. Takimoto, Y. Takeoka, and A. Ohira, *Polymer* **49**, 3091 (2008).

[202] V. A. Sethuraman, J. W. Weidner, A. T. Haug, S. Motupally, and L. V. Protsailo, *J. Electrochem. Soc.* **155**, B50 (2008).

[203] S. Balog, U. Gasser, K. Mortensen, H. Ben youcef, L. Gubler, and G. G. Scherer, *J. Membr. Sci.* **383**, 50 (2011).

[204] E. M. W. Tsang, Z. Zhang, Z. Shi, T. Soboleva, and S. Holdcroft, *J. Am. Chem. Soc.* **129**, 15106 (2007).

[205] D. Yarusso and S. Cooper, *Macromolecules* **16**, 1871 (1983).

[206] D. J. Kinning and E. L. Thomas, *Macromolecules* **17**, 1712 (1984).

[207] D. Yarusso and S. Cooper, *Polymer* **26**, 371 (1985).

[208] B. Gupta, F. Büchi, G. G. Scherer, and A. Chapiró, *Polym. Adv. Technol.* **5**, 493 (1993).

[209] K. N. Rao, M. H. Rao, P. N. Moorthy, and A. Charlesby, *J. Polym. Sci. Polym. Lett. Ed.* **10**, 893 (1972).

[210] E.-S. A. Hegazy, N. H. Taher, and A. R. Ebaid, *J. Appl. Polym. Sci.* **41**, 2637 (1990).

[211] S. H. Tabaddor, F. Fazilat, and R. Gouloubandi, *J. Macromol. Sci. A Chem.* **13**, 1213 (1979).

[212] C. R. E. Mansur and E. E. C. Monteiro, *J. Appl. Polym. Sci.* **68**, 345 (1998).

[213] A. Mathew and P. C. Deb, *Macromol. Chem. Phys.* **199**, 2527 (1998).

[214] S. Phadnis, M. Patri, V. R. Hande, and P. C. Deb, *J. Appl. Polym. Sci.* **90**, 2572 (2003).

[215] M. Slaski, *Radiation grafted fuel cell membranes with improved oxidative stability*, PhD thesis, ETH Zürich, 2007.

[216] T. J. Peckham, J. Schmeisser, and S. Holdcroft, *J. Phys. Chem. B* **112**, 2848 (2008).

[217] A. A. Adamson, *Textbook of physical chemistry*, Academic press, New York, 1973.

[218] K. Enomoto, S. Takahashi, T. Iwase, T. Yamashita, and Y. Maekawa, *J. Mater. Chem.* **21**, 9343 (2011).

BIBLIOGRAPHY

[219] S. Alkan-Gürsel, Z. Yang, B. Choudhury, M. G. Roelofs, and G. G. Scherer, *J. Electrochem. Soc.* **153**, A1964 (2006).

[220] M. Shen, S. Roy, J. Kuhlmann, K. Scott, K. Lovell, and J. Horsfall, *J. Membr. Sci.* **251**, 121 (2005).

[221] K. Jetsrisuparb, H. B. youcef, A. Wokaun, and L. Gubler, *J. Membr. Sci.* (accepted).

[222] K. ElMiloudi, M. Benygzer, S. Djadoun, N. Sbirrazzuoli, and S. Geribaldi, *Macromol. Symp.* **230**, 39 (2005).

[223] I. Agranat and Y. Shih, *J. Chem. Educ.* **53**, 488 (1976).

[224] J. Zu, M. Wu, J. Zhang, C. Yu, X. Liu, and L. Tong, *J. Appl. Polym. Sci.* **99**, 3401 (2006).

[225] P. M. Mangiagli, C. S. Ewing, K. Xu, Q. Wang, and M. A. Hickner, *Fuel Cells* **9**, 432 (2009).

[226] G. van der Wel and O. Adan, *Prog. Org. Coat.* **37**, 1 (1999).

[227] S. Brunauer, L. S. Deming, W. E. Deming, and E. Teller, *J. Am. Chem. Soc.* **62**, 1723 (1940).

[228] G. Alberti, R. Narducci, and M. Sganappa, *J. Power Sources* **178**, 575 (2008).

[229] G. Alberti, Electrolytes I Polymer, in *Encyclopedia of Electrochemical Power Sources*, edited by J. Garche, C. K. Dyer, P. T. Moseley, Z. Ogumi, D. A. J. Rand, and B. Scrosati, pp. 166–173, Elsevier, Amsterdam, 2009.

[230] L. A. Diaz, G. C. Abuin, and H. R. Corti, *J. Power Sources* **188**, 45 (2009).

[231] M. Escoubes and M. Pineri, Thermodynamic Studies of the Water-Perfluorosulfonated Polymer Interactions, in *Perfluorinated Ionomer Membranes*, edited by A. Eisenberg and H. L. Yeager, volume 180, chapter 3, pp. 9–23, American Chemical Society, 1982.

[232] T. A. Zawodzinski, C. Derouin, S. Radzinski, R. J. Sherman, V. T. Smith, T. E. Springer, and S. Gottesfeld, *J. Electrochem. Soc.* **140**, 1041 (1993).

[233] S. R. Lowry and K. A. Mauritz, *J. Am. Chem. Soc.* **102**, 4665 (1980).

[234] A. Vishnyakov and A. V. Neimark, *J. Phys. Chem. B* **104**, 4471 (2000).

[235] P. D. Beattie, F. P. Orfino, V. I. Basura, K. Zychowska, J. Ding, C. Chuy, J. Schmeisser, and S. Holdcroft, *J. Electroanal. Chem.* **503**, 45 (2001).

[236] S. C. Yeo and A. Eisenberg, *J. Appl. Polym. Sci.* **21**, 875 (1977).

[237] S. Ochi, O. Kamishima, J. Mizusaki, and J. Kawamura, *Solid State Ionics* **180**, 580 (2009).

[238] P. Majsztrik, B. Satterfield, A. Bocarsly, and J. B. Benziger, *ECS Trans.* **11**, 609 (2007).

[239] M. Gross, G. Maier, T. Fuller, S. MacKinnon, and C. Gittleman, Design rules for the improvement of the performance of hydrocarbon-based membranes for proton exchange membrane fuel cells (PEMFC), in *Handbook of Fuel Cells*, edited by W. Vielstich, H. A. Gasteiger, A. Lamm, and H. Yokokawa, pp. 283–299, John Wiley & Sons, 2010.

[240] C. K. Mittelsteadt and J. Staser, *ECS Trans.* **41**, 101 (2011).

List of Tables

List of Figures

Symbols, Indices and Abbreviations

Latin symbols

Symbol	Description	Unit
a	Activity	[-]
A	Active area	[cm^2]
$\widetilde{A}$	Area under FTIR charateristic peak	[-]
C	Crystallinity	
c	Concentration	[mol cm^{-3}]
D	Diffusion coefficient	[cm^2 s^{-1}]
D	Extent of graft loss	[%]
d	Characteristic length	[nm]
ΔG	Standard Gibbs free energy of reaction	[J mol^{-1}]
ΔH	Specific reaction enthalpy	[J mol^{-1}], [J kg^{-1}]
ΔS	Specific reaction entropy	[J mol^{-1}K^{-1}]
E	Electrode potential	[V]
f	Activity coefficient	[-]
I	Current response	[A]
I	Scattering intensity	[-]
j	Current density	[A cm^{-2}]
j_0	Exchange current density	[A cm^{-2}]
k	Correlation coefficient	[-]
p	Pressure	[bar]
Q	Swelling	[%]
R	Area specific resistance	[Ω cm^2]

Symbol	Description	Unit
R	Radius	[nm]
R	Resistance	[Ω]
R_m	Molar ratio of styrene and comonomer	[-]
S	Dimensional change	[%]
SF	Degree of sulfonation	[-]
r	Reactivity ratio	[-]
q	Scattering vector	[nm^{-1}]
T	Temperature	[K]
U	Voltage	[V]
V	Excitation potential	[V]
V_p	Number density	[-]
W	Weight	[g]
X	Styrene molar fraction	[-]
x	Dimension	[cm^2], [cm^3]
Z	Impedance	[Ω]
z	Charge of charge carrier	[-]

Greek symbols

Symbol	Description	Unit
δ	Diffusion distance	[cm]
η	Efficiency	[%]
η	Overpotential	[V], [mV]
λ	Hydration level	[-]
λ	Wavelength	[nm]
μ	Proton mobility	[cm^2 s^{-1} V^{-1}]
ω	Angular frequency	[rad s^{-1}]
ϕ	Azimuth angle	[°]
ϕ	Phase shift	[°]
ϕ	Water volume fraction	[-]
σ	Proton conductivity	[mS cm^{-1}]
θ	Half of the diffraction angle	[°]

Constants

Symbol	Description	Value
F	Faraday constant	96'485 [C mol^{-1}]
R	Universal gas constant	8.3145 [J mol^{-1} K^{-1}]

Indices

Symbol	Description
0	Initial conditions, e.g., in grafting solution or in pre-irradiated film
1	Core size
Ω	Ohmic
A	Anode
C	Cathode
ca	Shell size
CT	Charge transfer
eff	Effective
exp	Experimental
F	Perfluorinated polymer
f	Formation
g	In grafted film
i	Index
ii	Intrinsic
im	Imaginary
lim	Limit
ox	Oxidation
Re	Real
r	Reactant
red	Reduction

Symbol	Description
rev	Reversible
theo	Theoretical
tx	Transport-induced
v	Volumetric

Abbreviations

Abbreviation	Description
AA	Acrylic acid
AC	Alternating current
AFC	Alkaline fuel cell
AMS	α-Methylstyrene
AN	Acrylonitrile
ATRP	Atom transfer radical polymerization
C	Comonomer
CEC	Chlorine Engineers Co.
CHP	Combined heat and power
CTFE	Chlorotrifluoroethylene
DIPB	m-Diisopropenyl benzene
DMFC	Direct methanol fuel cell
DSC	Differential scanning calorimetry
DVB	Divinylbenzene
ECSA	Electrochemical catalyst surface area
EIS	Electrochemical impedance spectroscopy
ETFE	Poly(ethylene-*alt*-tetrafluoroethylene)
EPR	Electron paramagnetic resonance
FEP	Poly(tetrafluoroethylene-*co*-hexafluoropropylene)
FER	Fluoride emission rate
FTIR	Fourier transform infrared
GDL	Gas diffusion layer
GE	General electric

Abbreviation	Description
GL	Graft level
GMA	Glycidyl methacrylate
HFR	High frequency resistance
HOR	Hydrogen oxydation reaction
HPLC	High performance liquid chromatography
IEC	Ion exchange capacity
IR	Infrared
JM	Johnson Matthey
LDPE	Low density polyethylene
M	Solvent
MA	Methyl acrylate
MAA	Methacrylic acid
MAN	Methacrylonitrile
MCFC	Molten carbonate fuel cell
MEA	Membrane electrode assembly
MMA	Methyl methacrylate
OCV	Open circuit voltage
ORR	Oxygen reduction reaction
P	Polymer
PAFC	Phosphoric acid fuel cell
PBI	Polybenzimidazole
PE	Polyethylene
PEEK	Polyether ether ketone
PEFC	Polymer electrolyte fuel cell
PEM	Proton exchange membrane
PEN	Polyethylene naphtalate
PFA	Poly(tetrafluoroethylene-*co*-perfluoropropylvinylether)
PFSA	Perfluorosulfonic acid
PS	Polystyrene
PSI	Paul Scherrer Institut

Abbreviation	Description
PSSA	Polystyrene sulfonic acid
PSU	Polysulfone
PTFE	Polytetrafluoroethylene
PTFSSA	Polytrifluorostyrene sulfonic acid
PVDF	Polyvinylidenefluoride
RH	Relative humidity
RT	Room temperature
S	Styrene
SANS	Small-angle neutron scattering
SAXS	Small-angle X-ray scattering
SEC	Size-exclusion chromatography
SOFC	Solid oxide fuel cell
SPEEK	Sulfonated poly(ether ether ketone)
TEM	Transmission electron microscopy
TFS	Trifluorostyrene
UV	Ultraviolet
VDF	Vinylidene fluoride
WAXD	Wide-angle X-ray diffraction
WAXS	Wide-angle X-ray scattering

Publication list

Peer reviewed papers (as author or co-author)

K. Jetsrisuparb, S. Balog, C. Bas, L. Perrin, Alexander Wokaun, Lorenz Gubler, Proton conducting membranes prepared by radiation grafting of styrene and various co-monomers (in preparation)

Z. Zhang, K. Jetsrisuparb, A. Wokaun and L. Gubler, Study of nitrile-containing proton exchange membranes prepared by radiation grafting: performance and degradation in the polymer electrolyte fuel cell, *J. Power Sources*, **243**, 306-316 (2013)

S. Balog, U. Gasser, K. Jetsrisuparb, L. Gubler, Structure of the hydrophilic phase and its impact on the conductivity of graft copolymer ionomers at low hydration level, *Polymer* **54**, 4266-4275 (2013)

K. Jetsrisuparb, H. Ben youcef, A. Wokaun, L. Gubler, Radiation grafted membranes for fuel cells containing styrene sulfonic acid and nitrile comonomers, *J. Membr. Sci.* (accepted)

Presentations

K. Jetsrisuparb, Z. Zhang, H. Ben youcef, G. G. Scherer, A. Wokaun, L. Gubler
Synthesis and properties of chemically modified membranes by radiation co-grafting of styrene and methacrylonitrile (Oral)
European Material Research Society Spring Meeting 2012, Strasbourg, France, May 14-18, 2012

K. Jetsrisuparb, Z. Zhang, H. Ben youcef, G. G. Scherer, A. Wokaun, L. Gubler
Influence of functional groups on membrane durability (Poster)
European Material Research Society Spring Meeting 2012, Thessaloniki, Greece, September 21-23, 2011

K. Jetsrisuparb, F. Lindner, H. Ben youcef, G. G. Scherer, A. Wokaun, L. Gubler
Modification of proton exchange membranes for fuel cells by radiation induced grafting (Poster)
PolyColl 2011, Geneva, Switzerland, April 29, 2011

K. Jetsrisuparb, H. Ben youcef, G. G. Scherer, A. Wokaun, L. Gubler
The influence of methacrylonitrile (MAN) on fuel cell relevant properties of ETFE-g-styrene / MAN membranes (Poster)
PhD student's symposium 2010, Empa Dübendorf, Switzerland, October 7, 2010

K. Jetsrisuparb, H. Ben youcef, G. G. Scherer, A. Wokaun, L. Gubler
Styrene / methacrylonitrile co-grafted membranes for fuel cells (Poster)
Progress MEA 2010, La Grande Motte, France, September 19-22, 2010

K. Jetsrisuparb, H. Ben youcef, G. G. Scherer, A. Wokaun, L. Gubler
Styrene / methacrylonitrile co-grafted membranes for fuel cells (Poster)
Swiss Chemical Society Fall Meeting 2010, ETHZürich, Switzerland, September 16, 2010

Curriculum Vitae

Personal information

Name	Kaewta Jetsrisuparb
Date of birth	February 15$^{\text{th}}$ 1984
Place of birth	Khon Kaen
Nationality	Thai

Education

2009 - 2013	**Paul Scherrer Institut (PSI) and Swiss Federal Institute of Technology Zürich (ETHZ), Switzerland** Doctoral Thesis Title of the thesis: *Comonomer effects in radiation grafted membranes for polymer electrolyte fuel cells*
2007 - 2009	**Delft University of Technology (TU Delft), The Netherlands** MSc in Chemical Engineering Title of the master thesis: *Co-crystals of Carbamazepine: Screening, phase diagrams and polymorphs (a collaboration project between TU Delft and Tokyo University of Agriculture and Technology (TUAT))*
2003 - 2007	**Delft University of Technology (TU Delft), The Netherlands** BSc in Chemical Engineering and Biochemical Engineering Title of the bachelor thesis: *Design of gas-liquid separator with low back mixing*
1999 - 2002	**High School Diploma** Demonstration school of Khon Kaen University, Khon Kaen, Thailand

Experience

2008   **Industrial internship, Materials Laboratories, Sony Corporation, Atsugi-shi, Japan**
Novel solid electrolyte based on crosslinking polymers for lithium ion battery

Awards and achievements

2012   **Graduate Student Award, 2012 European Materials Research Society Spring Meeting, Strasbourg, France**
Outstanding paper contribution

2002   **Royal Thai Government Scholarship**
Awarded a scholarship to pursue graduate and post graduate studies in Chemical Engineering